Highly Reactive Silver Doped Sol-Gel-Derived Borate Glasses for Wound Healing Applications

Shiva Naseri

Department of Mining and Materials Engineering

McGill University, Montreal, QC, Canada

February 2018

A thesis submitted to McGill University in partial fulfillment of the degree of Doctor of Philosophy

To my parents.

Abstract

Bioactive and soluble glasses exhibit great potential in biomedical applications in both hard and soft tissue engineering. While silicate-, phosphate- and borate-based glasses have been extensively studied for bone repair applications, only recently have these materials been studied in soft tissue applications, such as wound healing. The rate at which these glasses generate a response, or their reactivity, is an important parameter for healing efficacy. Owing to their tetrahedral coordination, silicate-based glasses exhibit slow and incomplete solubility, which limit their application in soft tissue repair. Therefore, there is great interest in developing more soluble and reactive bioactive glass formulations based on the borate network forming oxide, which can be both trigonally and tetrahedrally coordinated. It has been shown that borate-based glasses have higher reactivity than silicate-based glasses attributed to their glass network structure and consequently making them less chemically durable.

Limitations in conventional methods such as the lack of accuracy and consistency and time-consumption to examine reactivity/bioactivity and surface properties of bioactive and soluble glasses have led to an increased interest in finding and investigating new techniques, such as dynamic vapour sorption (DVS) and inverse gas chromatography (IGC). It was demonstrated that DVS has the ability to measure and predict the bioactivity/reactivity of silicate-, phosphate- and borate- based glasses with various specific surface areas/particle sizes or formulations. It was shown that DVS was able to measure and correlate the vapour isotherm values of melt-quench derived Bioglass® 45S5: $(46.1)SiO_2$-$(26.9)CaO$-$(24.4)Na_2O$-$(2.6)P_2O_5$ (mol %) of three different particle sizes (surface areas) with the reactivity, bioactivity and ions release rates of glasses. Higher surface area led to the higher vapour sorption and reactivity. Additionally, IGC was utilized to examine the surface properties of melt-quench derived phosphate glasses (PGs) doped with both SiO_2 and TiO_2 ($50P_2O_5$-$40CaO$-$xSiO_2$-$(10 - x)$ TiO_2, where x = 7, 5, 3, and 0 mol%). It was shown that IGC was more accurate and sensitive than other conventional techniques such as contact angle measurement in determining the effect of silica content on the surface properties of PGs. In conclusion, this dissertation has assessed the potential complementarity of DVS and IGC in the characterization of aqueous reactivity and surface properties of bioactive and soluble glasses.

Moreover, complications in the healing of chronic wounds in patients who are at constant risk of infections have led to a great demand for the development of biomaterial based wound

dressing replacement. Promising biomaterials may be based on soluble glasses due to their ability of release therapeutic ions in biological environments, which can promote the healing process. Borate-based glasses have recently been approved for wound repair which are melt-quench derived, yet borate glasses fabricated through the sol-gel process have the benefits of higher dissolution rate, which could potentially lead to the more rapid wound repair. However, the potential of sol-gel derived borate glasses, in particular, silver doped borate-based glasses (AgBGs) for soft tissue repair has so far not been investigated. In this thesis, anti-bacterial AgBGs in the $B_2O_3Ag_2O$-CaO-P_2O_5 system were fabricated through optimization of sol-gel process and glass composition. The calcined amorphous glasses demonstrated high specific surface areas and porosities. Silver ion release rate and anti-bacterial activity were correlated and demonstrated dose dependent efficacy against *Escherichia coli (E.coli)* or *Staphylococcus aureus* (*S.aureus*) and *Pseudomonas aeruginosa* (*PA14*) bacteria. In addition, AgBGs were systematically examined to determine their effects on cellular functions such as metabolic activity, cell viability and migration through *in vitro* cell culture of human derived keratinocyte (HaCat) and mouse derived fibroblastic (NIH/3T3) cell lines. It was verified that silver release from AgBGs was not toxic to HaCat and NIH/3T3 cells at lower concentrations (<1 ppm) and has the ability to stimulate the HaCat cell migration, *in vitro*. In conclusion, this dissertation has introduced a new class of sol-gel derived silver doped borate-based glasses as promising candidates for wound healing applications.

Résumé

Les verres bioactifs et solubles présentent un grand potentiel dans les applications biomédicales dans l'ingénierie des tissus durs et mous. Alors que les verres à base de silicate, de phosphate et de borate ont été largement étudiés pour des applications de réparation osseuse, ce n'est que récemment que ces matériaux ont été étudiés dans des applications de tissus mous, telles que la cicatrisation. La vitesse à laquelle ces verres génèrent une réponse, ou leur réactivité, est un paramètre important pour la guérison de l'efficacité. En raison de leur coordination tétraédrique, les verres à base de silicate présentent une solubilité lente et incomplète, ce qui limite leur application dans la réparation des tissus mous. Par conséquent, il y a un grand intérêt dans le développement de formulations de verre bioactif plus solubles et réactives basées sur l'oxyde formant un réseau de borate, qui peut être à la fois coordonné trigonalement et tétraédriquement. Il a été démontré que les verres à base de borate ont une réactivité plus élevée que les verres à base de silicate attribués à la structure de leur réseau de verre et, par conséquent, les rendent chimiquement moins durables.

Les limitations des méthodes conventionnelles telles que le manque de précision et de cohérence et la consommation de temps pour examiner la réactivité / bioactivité et les propriétés de surface des verres bioactifs et solubles ont conduit à un intérêt accru pour trouver et étudier de nouvelles techniques telles que la DVS et la chromatographie en phase gazeuse inverse (IGC). Il a été démontré que la DVS a la capacité de mesurer et de prédire la bioactivité / réactivité des verres à base de silicate, de phosphate et de borate avec diverses surfaces spécifiques / tailles de particules ou formulations. Il a été démontré que la DVS était capable de mesurer et de corréler les valeurs isothermes de vapeur de Bioglass® 45S5 dérivé de la fusion-trempe: (46.1) SiO2-(26.9) CaO- (24.4) Na_2O- (2.6) P_2O_5 (mol%) tailles de particules (surfaces) avec la réactivité, la bioactivité et la vitesse de libération des ions des verres. Une surface plus élevée conduit à une sorption de vapeur et une réactivité plus élevées. De plus, la IGC a été utilisée pour examiner les propriétés de surface des verres phosphatés (PG) dérivés de la fusion-fusion dopés à la fois avec SiO_2 et TiO_2 ($50P_2O_5$-40CaO-xSiO_2- (10-x) TiO_2, où x = 7, 5, 3 et 0% en mole). Il a été montré que la IGC était plus précise et sensible que d'autres techniques conventionnelles telles que la mesure de l'angle de contact pour déterminer l'effet de la teneur en silice sur les propriétés de surface des PG. En conclusion, cette dissertation a évalué la complémentarité potentielle de DVS

et IGC dans la caractérisation de la réactivité aqueuse et les propriétés de surface des verres bioactifs et solubles.

De plus, les complications dans la cicatrisation des plaies chroniques chez les patients à risque constant d'infections ont conduit à une forte demande pour le développement d'un remplacement de pansement par des biomatériaux. Les biomatériaux prometteurs peuvent être basés sur des verres solubles en raison de leur capacité à libérer des ions thérapeutiques dans des environnements biologiques, ce qui peut favoriser le processus de guérison. Les verres à base de borate ont récemment été approuvés pour la réparation de plaies qui sont dérivées de la fusion-fusion, mais les verres de borate fabriqués par le procédé sol-gel ont les avantages d'une vitesse de dissolution plus élevée, ce qui pourrait entraîner une réparation plus rapide. Cependant, le potentiel des verres de borate dérivés de sol-gel, en particulier, des verres à base de borate dopés à l'argent (AgBG) pour la réparation des tissus mous n'a pas encore été étudié. Dans cette thèse, des AgBG anti-bactériennes dans le système $B_2O_3Ag_2O$-CaO-P_2O_5 ont été fabriquées grâce à l'optimisation du procédé sol-gel et de la composition du verre. Les verres amorphes calcinés ont présenté des surfaces spécifiques élevées et des porosités élevées. La vitesse de libération des ions argent et l'activité antibactérienne étaient corrélées et démontraient une efficacité dépendante de la dose contre les bactéries *Escherichia coli* (*E.coli*) ou *Staphylococcus aureus* (*S.aureus*) et *Pseudomonas aeruginosa* (*PA14*). En outre, les AgBG ont été systématiquement examinés pour déterminer leurs effets sur les fonctions cellulaires telles que l'activité métabolique, la viabilité cellulaire et la migration par culture cellulaire in vitro de lignées cellulaires de kératinocytes humains dérivés (HaCat) et de lignées fibroblastiques dérivées de souris (NIH / 3T3). Il a été vérifié que la libération d'argent à partir d'AgBG n'était pas toxique pour les cellules HaCat et NIH / 3T3 à des concentrations plus faibles (<1 ppm) et a la capacité de stimuler la migration des cellules HaCat, in vitro. En conclusion, cette dissertation a introduit une nouvelle classe de verres à base de borate dopés à l'argent dérivés de sol-gel en tant que candidats prometteurs pour des applications de cicatrisation.

Acknowledgements

I would like to express my deepest appreciation to my supervisor Prof. Showan Nazhat, for his invaluable guidance, support and encouragement throughout this project. I would like to give special thanks to Prof. Aldo Boccaccini for offering the opportunity to work under his supervision during my master's degree in Erlangen which allowed me to come to McGill.

I would like to give special thanks to my colleague and friend, Will Lepry who showed me the importance of borate-based glasses and to my other colleagues: Gabriele Griffanti, and Hyeree Park.

I would like to extend my sincere gratitude to Barbara Hanley, for her administrative support and to Monique Riendeau and Andrew Golsztajn for their extensive knowledge and suggestions on characterization techniques, Prof. Kristian Waters for allowing the use of DVS and IGC, Prof. Nathalie Tufenkji and Dr. Vimal Maisuria for permitting the use of Biocolloids and Surfaces Laboratory, Prof. Anie Philip, Dr. Kenneth Finnson, and Dr. Meryem Blati for their enlightening discussions on skin repair.

Last but not least, I would like to thank my parents who always boost my self-confidence and my beloved brother, for his full support during my study. At the end, I would like to dedicate this thesis to my parents.

Table of Contents

List of Figures:

List of Tables:

Contributions to Original Knowledge

This thesis describes the *in vitro* analyses of bioactive and soluble silicate-, phosphate-, and borate-based glasses. To better understand the reactivity of glasses and their correlation with the surface and bulk properties, their aqueous interactions, using Dynamic Vapour Sorption (DVS) and Inverse Gas Chromatography (IGC), provided a rapid and more precise technique compared to traditional methods. Chapter 4 describes the potential of DVS in measuring and predicting the reactivity and bioactivity of silicate-based glasses. It was shown that DVS can be utilized to evaluate the potential bioactivity of silicate-based glasses of a range of specific surface areas, with increased precision and accuracy in a shorter time. Chapter 5 highlights the ability of DVS and IGC as complementary techniques for measuring reactivity and surface properties of phosphate-based glasses. The results correlated with the glass properties to better understand the potential of these new techniques comparing the traditional methods.

Furthermore, this thesis describes the fabrication of silver doped borate-based glasses of four and five components with anti-bacterial activity using the sol-gel processing method for the potential application in wound healing. The chemical and structural characterizations of the glasses with the different compositions and range of silver content were performed in order to better understand their impact on the final glass properties. Moreover, *in vitro* analyses such as the aqueous interactions using DVS, the dissolution in deionized water, and anti-bacterial efficacy on *Escherichia coli*, *Staphylococcus aureus* and *Pseudomonas aeruginosa* bacteria has been performed.

Chapter 6 describes the optimization of sol-gel processing parameters, *e.g.,* precursor addition order and composition, as well as silver content in order to develop borate glasses with a homogeneous formation of an amorphous glass structure and controlled silver ion release rate. It was shown that the order of precursor addition and sodium oxide precursor had a direct effect on the silver integration and release. For the first time, silver doped sol-gel derived borate-based glasses with anti-bacterial activity were developed. This study serves as a basis to optimize future glass formulations for potential wound healing applications. Chapter 7 highlights the optimized silver doped sol-gel derived borate-based glasses for wound healing applications. Cellular functions such as metabolic activity, viability, and migration of keratinocytes and fibroblastic cells demonstrated the potential ability of these glasses in accelerating repair of chronic wounds which

are at constant risk of infection and biofilm formation. Chapter 8 reviews and summarizes the studies investigating bioactive and soluble glasses for wound healing applications. Moreover, the most promising methods and results of the field are discussed along with current limitations, including lack of extensive, and standardized, research in this field.

Contribution of Authors

This dissertation is presented as a collection of five published and to-be-submitted manuscripts written by the candidate under the supervision of Prof. Showan N. Nazhat. As the first author of all the manuscripts, I proposed, designed, conducted the majority of the experiments, collected and analyzed all the data, and wrote each manuscript. As the candidate's supervisor, Prof. Nazhat guided me throughout all research activities along with a thorough review of all manuscripts. William C. Lepry assisted with experimental set up and tests examining different bioactive glasses by SEM in Chapter 4, 5 and 6 as well as contributed to Chapter 8. Prof. Kristian E. Waters provided expertise on DVS and IGC in Chapter 4 and 5. Prof. Aldo R. Boccaccini and Wie Li provided the materials (Bioglass® 45S5) and expertise for Chapter 4. Maziar S. Mohammadi provided the Si/Ti doped phosphate-based glass compositional range and data of dissolution rates, glass transition temperature and surface energies as measured by surface contact angle. Prof Nathalie Tufenkji and Dr. Vimal B. Maisuria hosted me in their laboratory and guided me through *in vitro* anti-bacterial characterization studies reported in Chapters 6 and 7. Mr. Gabriele Griffanti assisted with the cell characterizations for the study in Chapter 7. All co-authors reviewed the respective manuscripts and provided significant critical feedback.

1 General Introduction

1.1 Introduction

Bioactive and soluble glasses are a group of materials that can be used for both hard and soft tissue engineering attributable to their wide compositional range and solubility rates, which can be altered according to the desired biological response. Bioactivity, in the context of these glasses, has been defined by their ability to form a hydroxy-carbonate apatite (HCA) surface layer when placed in physiological fluids [1]. The most well-known formulation, Bioglass® 45S5 [(46.1)SiO_2-(26.9)CaO-(24.4)Na_2O-(2.6)P_2O_5 (mol %)], invented by Dr. Larry Hench in 1969 [1], has been extensively demonstrated to be highly biocompatible with host tissues and bonds to bone through HCA formation [1]. Both Bioglass® 45S5 and a second silicate-glass, S53P4 [53SiO_2-20CaO-23Na_2O-4P_2O_5 (mol %)] [2] (BoneAlive, Finland), are currently in clinical use. Attributable to their ability to form HCA, as well as their osteo-conductive and -stimulative properties, these glasses have been used in the repair, augmentation and regeneration of mineralized tissues (bone and teeth), *e.g.*, as filling materials and small implants used in orthopedic and dental applications [2, 3].

Despite successful clinical translation in bone, silicate-glasses exhibit slow and incomplete solubility which limit their wider adoption and therapeutic potential [4]. Therefore, there is significant interest in developing more soluble biomedical glasses based on other network forming oxides; namely phosphates [4] and borates [5]. While the building units of silicates and phosphates are both tetrahedrally coordinated, differences lie in their valence electrons. Silicon, of four valence electrons, forms four single bonds with oxygen, resulting in a very stable glass structure (or high network connectivity). The incorporation of modifying oxides decreases the glass durability by disrupting the network connectivity, thus allowing for easier processing and greater chemical reactivity [5]. In contrast, phosphorus has five valence electrons, forming three single bonds and one terminal double bond with oxygen. This lower network connectivity allows for more flexible orientations of the phosphate tetrahedral and a wider range of glass compositions [6, 7]. Furthermore, pure P_2O_5 is very hygroscopic, and the addition of modifying oxides increases the stability by introducing more hydrolysis resistant bonds, thus tailoring the solubility kinetics [8]. In borate-glasses, the boron ion is typically trigonally coordinated, giving it a pseudo-3D character since the BO_3 network is more planar. However, depending on the amount of modifying oxides present, borate-glasses can also be four coordinated [5]. This combination results in borate-

glasses having lower chemical durability than silicate-glasses, offering higher rates of dissolution and bioactivity [5]. However, the impact of modifying oxide inclusion in borate-glasses, in terms of type and amount, and their potential biomedical applications are still not fully understood. Nevertheless, borate-glasses have recently gained much interest as biomedical glasses attributable to promising *in vivo* data on regenerating mineralized tissues [9], as well as clinical trials on wound healing. More recently (2016), a borate-based glass formulation (MIRRAGEN™, ETS Wound Care LLC, USA) obtained US Food and Drug Administration (FDA) approval as a wound dressing [10].

Bioactive glasses also support various ionic doping applications [11]. Numerous metallic oxides can be incorporated into the glass network as modifiers to adjust their chemical and physical properties. Their subsequent release in ionic form, as a result of glass dissolution in biological contexts, can offer benefits including anti-bacterial effects, *e.g.* Ag, Cu, Ga, Zn, Sr, among others [12]. In fact, inorganic therapeutics offer numerous advantages over organic-based molecules attributable to their low cost and flexibility in processing [11, 12]. However, in designing ion-releasing bioactive glasses, a major challenge is matching their rate of dissolution with that of tissue healing and regeneration as well as ensuring a local therapeutic concentration of ions without systemic toxicity. Therefore, factors such as reactivity, solubility and ionic release rates require precise control.

It is well known that the type of application of bioactive glasses is dictated by their chemical (*e.g.*, composition) and physical (*e.g.*, texture) properties, which directly influence their reactivity and bioactivity [13-15]. Therefore, an initial characterization of the physico-chemical properties of glasses is critical prior to analyzing their biological performance for a specific application. Depending on the application, it might be necessary to modify the glass dissolution properties to control the efficacy of ionic release, cellular responses, as well as any potential toxicity. Traditionally, the mass change or release of ionic species due to glass dissolution are measured over relatively their long-term submersion in aqueous environments [16], which may not be transferable or objective. Furthermore, glass surface properties such hydrophilicity or hydrophobicity are critical parameters for protein adhesion and cellular interactions in biological conditions [17]. Conventionally, the surface properties of glasses have been evaluated by contact angle measurement [18-20], which may lack reliability and accuracy [21, 22]. Therefore, new and more accurate techniques are needed to evaluate and predict the reactivity of glasses in aqueous

environments. Techniques such as dynamic vapour sorption (DVS) has recently been used to investigate glass reactivity and provide correlation with bulk and surface properties of the glass [23, 24]. Furthermore, inverse gas chromatography (IGC), has been used to compare the surface energy of naturally and synthetically derived hydroxyapatite [25]. *To this end a first hypothesis of this PhD research was that DVS and IGC can be utilized to measure and predict the reactivity, surface and bulk properties of bioactive and soluble glasses more rapidly and accurately than classical methods.*

Along with composition, bioactive glasses offer versatility through processing, where physical and topographical properties can be tailored for targeted applications. While the majority of bioactive glasses are processed through melt-quench, the sol-gel technique has demonstrated distinct advantages, including increased surface area, nano-porosity, purity, homogeneity, and reduced processing temperatures [24, 26]. Compared to melt-quench derived equivalents, sol-gel derived glasses have demonstrated better bioactivity and higher dissolution rates attributable to their inherent porosity and increased surface area [24, 26]. Minor alterations in composition or processing routes result in different glass characteristics impacting surface, reactivity and biological properties through dissolution, which can be readily modulated to target an end application. Moreover, due the lower temperature processing required for these materials, ionic doping [27] may be easier to incorporate into the glass network more homogenously, compared to the melt-quench process [28-30], thus allowing for their sustained release during dissolution. Among these, is silver doping, which has been demonstrated to have anti-bacterial protection and used in biomaterial based wound dressings [31]. *Therefore, a second hypothesis of this PhD research is that the addition of silver to sol-gel derived borate-based glasses would increase anti-bacterial efficacy and potentially enhance wound healing rates.*

1.2 Aims and objectives

Based on the above stated hypotheses, there were two specific aims to this PhD research, which were to 1) investigate the potential of DVS and IGC as techniques to evaluate reactivity and surface properties of bioactive and soluble glasses; and 2) fabricate silver-doped sol-gel derived borate-based glasses for wound healing applications.

The objectives for aim (1) were to:

1.1) Characterize glasses via DVS and IGC to analyze their aqueous interactions and surface properties.

1.2) Correlate DVS and IGC generated parameters of reactivity, surface and bulk properties of glasses.

The objectives for aim 2) were to:

2.1) Fabricate and characterize sol-gel derived borate glasses doped with silver for wound healing applications.

2.2) Investigate the efficacy of the silver-doped glass ionic dissolution products against bacteria and biofilm formation.

2.3) Investigate the effect of the silver-doped glass ionic dissolution products on keratinocyte and fibroblastic cellular functions.

To meet objective (1.1), the well characterized melt-quench derived 45S5 bioactive silicate-based glasses with different particle sizes and specific surface areas, were analyzed *via* DVS to correlate the reactivity with bioactivity of glasses through their short-term vapour sorption properties. To satisfy objective (1.2), a recently developed melt-quench derived phosphate-based glasses doped with both SiO_2 and TiO_2 ($50P_2O_5$-40CaO-xSiO_2-(10 − X) TiO_2, where X = 7, 5, 3, and 0 mol%) [21] were characterized using IGC and DVS. The IGC and DVS parameters were correlated with surface and bulk properties of glasses to measure and predict the glass properties as a function of silica content. To meet objective (2.1), a recently reported sol-gel processing route to generate bioactive borate-based glasses [24] was adapted to fabricate silver doped formulations based on a boron substituted 45S5, *i.e.*, B46: $46B_2O_3$-27CaO-(24-X)Na_2O-$3P_2O_5$-XAg_2O where X= 0, 0.15, 0.5 and 1 mol%. The sol-gel processing parameters were also altered to generate a sodium free compositional range, B60: $60B_2O_3$-36CaO-(4-X)P_2O_5-XAg_2O where X= 0.0, 0.3, 0.5 and 1 mol%. The silver doped sol-gel derived borate-based glasses (AgBGs) were characterized to optimize the glass composition for anti-bacterial biomedical applications. To satisfy objectives (2.2 and 2.3), the efficacy of AgBGs were investigated on *Escherichia coli*, *Staphylococcus aureus*, and *Pseudomonas aeruginosa* via the mean viable cell count, bacteria growth curve, disk diffusion method and *in vitro* biofilm formation. Furthermore, keratinocyte and fibroblast cellular functions, *in vitro,* via metabolic activity, cell viability and cell migration were evaluated for potential wound healing applications.

2 Literature Review

This chapter has four sections. The first, second and third sections provide brief overviews on glass structures as well as DVS and IGC as techniques to measure and predict the aqueous reactivity and surface properties of glasses. The fourth section provides an in-depth literature review of bioactive and soluble glasses in wound healing applications, which has been reproduced from a published book chapter by Shiva Naseri and Showan N. Nazhat in "Bioactive Glasses: Materials, Properties and Applications" second edition, edited by Heimo Ylänen, and published by Woodhead Publishing Series in Biomaterials (Elsevier). It is important to note that, Chapter 8 was published prior to Chapter 2. Therefore, Figure 2.10 is cited from the paper in this chapter.

2.1 Glass structure and properties

Glasses are within the ceramics classifications of materials and are distinguished by their amorphous nature, *i.e.,* lacking long range order or crystallinity. According to Shelby, a glass can be defined as "an amorphous solid completely lacking in long-range, periodic atomic structure, and exhibiting a region of glass transformation behavior" [32]. In fact, in order to call a material glass, it must have two characteristics: an amorphous nature and a glass transition temperature (T_g), the temperature above which solid glass begins to behave as a viscoelastic, soft and rubbery material, or when cooling a supercooled liquid, it behaves like a solid [32].

Zachariasen introduced and published the first detailed paper describing the atomic arrangement in glasses as well as the formation and structure of silicate glasses, which were described as having a tetrahedral network, without a periodic or symmetric arrangement in all three dimensions resulting in isotropic behavior [33]. He later developed the random network model (Figure 2.1) to describe the requirements for a glass. Based on this theory, the cations are surrounded by three or four oxygens, the polyhedrals are connected by their corners, and the oxygen atoms are bonded to two cations.

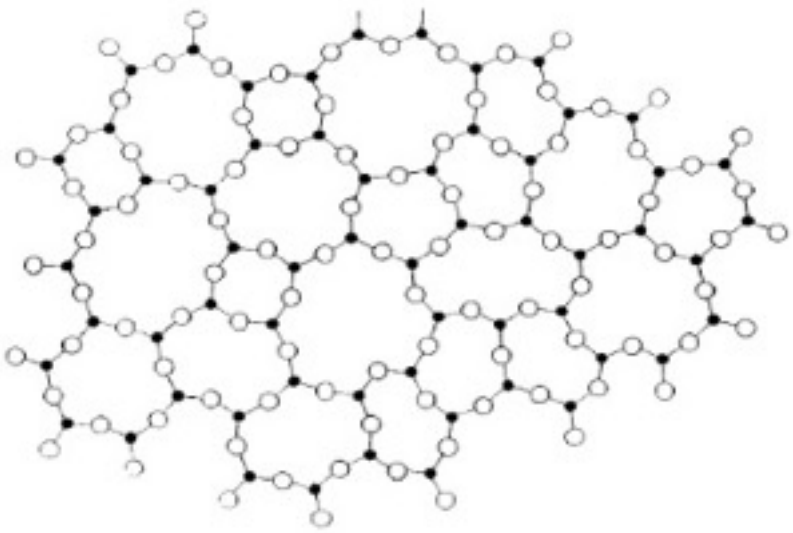

Figure 2. 1: The glass random network model [33].

Additionally, to make a glass, it is necessary to consider the kinetic theory, which concerns the rate at which the material must be cooled in order to prevent crystallization and to maintain an amorphous structure. In fact, the molten glass precursor must maintain its liquid-like structure from the melting point of solid crystals to supercooled liquid and upon further cooling to form a solid [34]. This behavior can be explained by the relationship of enthalpy and temperature (Figure 2.2) [32]. When the molten precursors are slowly cooled from the melting temperature (T_m), there is enough time for the atoms establish long-range and periodic arrangement and transform to a crystalline state. However, upon rapid cooling, a supercooled liquid is obtained below T_m without crystallization. Further cooling results in increased viscosity and rubbery state, which can be used to define T_g, resulting in the formation of an amorphous structure with no periodic atomic arrangement [32].

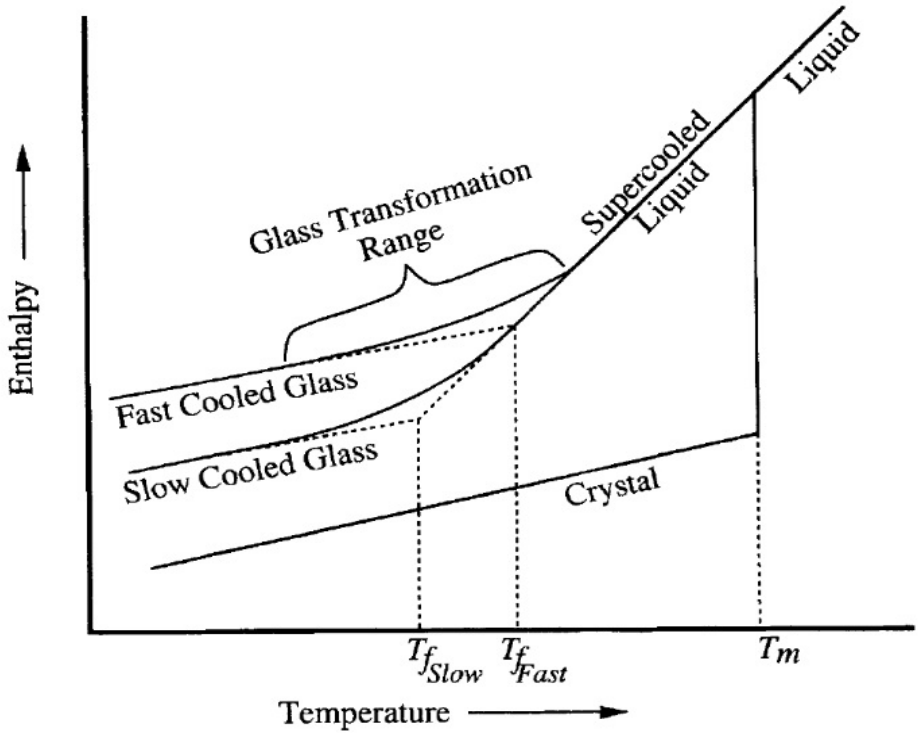

Figure 2. 2: The relationship between Enthalpy and Temperature for glass formation [32].

Glass structure can be defined by the number of oxygens that do not bond to the network polyhedral, i.e, non-bridging oxygens (nbOs) and the number of oxygens that link to the network polyhedral, i.e., bridging oxygens (bOs) [32]. "Q^i notation" is introduced to describe the network forming units of a glass network where "i" represents the number of bO atoms. Q^4 is attributed to the 4-coordination with tetrahedral network such as in pure silica. Disruption of glass network leads to the formation of nbOs and the glass forming units become Q^3, Q^2, Q^1, and Q^0 species [32].

While silica is one of the most abundant mineral and a glass network former, forming SiO_4^{4-} tetrahedron units [26, 35], a problem with pure silica is its high processing temperature (melts at >1700 °C). To this end, glass modifying oxides (metallic oxides) such as CaO or Na_2O are added to the glass network to decrease the processing temperature [32] (Figure 2.3). In fact, the introduction of greater amounts of alkali oxides in the silica glass network leads to a decrease in the Q numbers and generates a less stable glass structure with higher numbers of nbOs. Consequently, this leads to a decrease in T_g and its chemical durability [32].

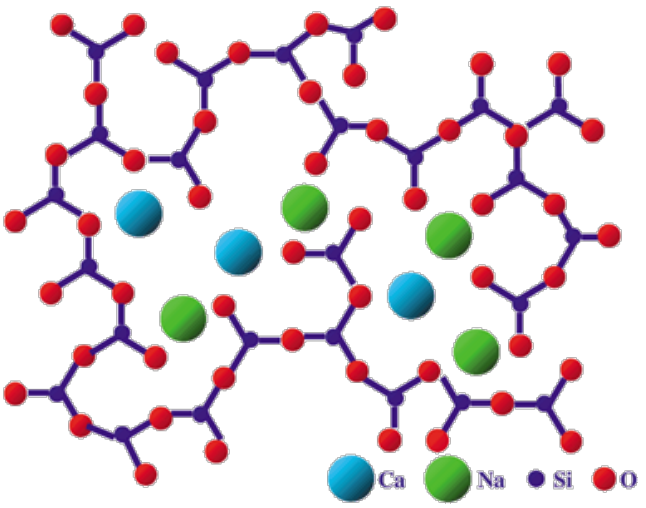

Figure 2. 3: Silicate glass structure consists of NaO_2 and CaO as glass network modifiers [36].

In addition to silicate-based glasses, there are other glass network formers such as phosphates or borates. In case of phosphate-based glasses, the network former is a tetrahedral PO_4^{3-} unit consisting of a double bond of phosphorous with oxygen and two single bonds resulting in formation of Q^3 species and each unit is able to share only three oxygens [37]. Upon addition of glass network modifiers, Q^i species can be decreased to Q^2, Q^1, and Q^0 species [38]. However, in contrast to silicate-based glasses, glass modifiers increase the glass stability by forming P-O-M^+ bonds [39, 40]. The main advantage of phosphate glasses is their flexibility in ionic doping due to their three-coordinated bonds, which allows for a wide range of properties by varying their compositions [41].

Unlike silicate- and phosphate-based glasses, borate glasses possess planar trigonal BO_3 units and a number of boroxol rings, which has been confirmed via neutron diffraction and nuclear magnetic resonance (NMR) spectroscopy data (Figure 2.4) [42, 43]. In fact, boron can bond with three oxygen atoms, and in the presence of alkali oxides it is able to also tetrahedrally bond with four oxygen atoms depending on the amount of glass network modifier utilized [44, 45]. Borate-based glasses are less stable than silicate-based glasses because of the van der Waals bonds within the glass network [44, 45]. This can be verified by a significant low T_g (~ 260 °C) of borate glasses when compared with silicate glasses (~ 1100 °C).

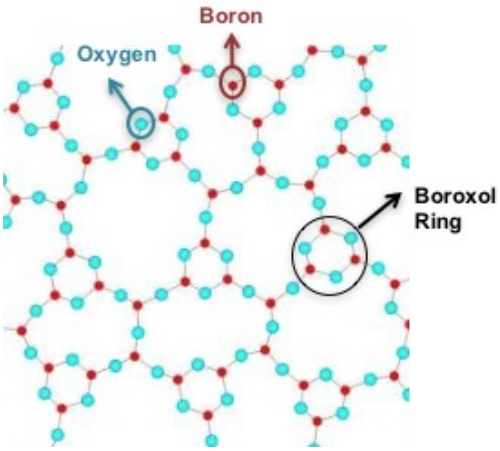

Figure 2. 4: Borate glass consists of trigonal three coordinated borate units and boroxal rings [46].

Furthermore, borate glasses differ from silicate glasses in their response to alkali metal oxide addition into the network. It has been reported that an addition of up to ~20 mol% alkali metal leads to the decrease of boroxol rings and the formation of tetraborate (BO_4 units), leading to more stable glasses [5, 32]. However, upon further addition of alkali metal oxides there is a decrease in tetraborates and the formation of diborates as well as formation of nbOs. Consequently, the glass network becomes less chemically durable [5, 32]. This unique behaviour is termed the boron anomaly (Figure 2.5) [32] and is also reflected in T_g, which initially increases with alkali oxide addition, and then decreases upon further increase in its content [32].

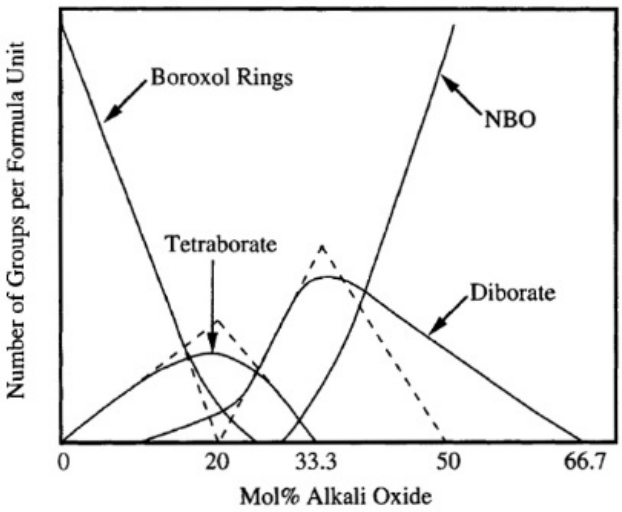

Figure 2. 5: Overview of anomaly model of borate glasses [19].

2.1.1 Sol-gel processing of borate-based glasses

Bioactive glasses can be fabricated by the sol-gel process through the mixing of alkoxides in solution at room temperature. Compared to the traditional high temperature, melt-quench method, the sol-gel approach is advantageous since it can be carried out at room temperature with greater control to adjust the composition, obtain better homogeneity, and producing amorphous, highly porous glasses [47]. The basic approach for making sol-gel glass is gelation of a solution of metallic alkoxides mixed in a solvent such as water or alcohol through hydrolysis and polycondensation reactions followed by ageing, drying, and calcination (typically below 600 °C) [48]. Drying and calcination are crucial stages to remove undesirable organic materials from the final glass, especially for biomedical applications [48].

Until recently, the sol-gel process has been extensively studied for silicate- and to some extent phosphate-based glasses. However, much less has been reported in the case of borate-based glasses due to the difficulty to form a gel and consequently formation of boron ions in solution [49]. This may be due to the bonding nature of borate glass systems of forming three- and four-coordination compared to the four-coordinated silicate glasses [50, 51]. The first sol-gel derived borate glass was fabricated by Tohge and colleagues based on a binary system (80)B_2O_3-(20)Na_2O (mol%) [52]. Recently, in 2015, Lepry and Nazhat fabricated novel sol-gel derived borate-based bioactive glasses with borate content ranging from 36 to 61 mol % with the optimized composition of 46.1 B_2O_3, 26.9 CaO, 24.4 Na_2O and 2.6 P_2O_5 (mol%) [24]. All glasses demonstrated nanoporosity through high specific surface areas and large pore volumes. Additionally, it was shown that the sol-gel derived borate glass had significantly higher surface area compared to its melt-derived equivalent (93.8 ± 8.2 and 0.238 ± 0.017 m^2/g, respectively) resulting in the higher ion release and dissolution rates, reactivity and bioactivity when compared with the melt-derived borate glass. In addition, it was shown that the dissolution and reactivity rates of glasses were composition dependent. An increase in borate content in the glass formulation led to the decrease of dissolution rate and reactivity [24]. Furthermore, the *in vitro* bioactivity of glasses in simulated body fluid (SBF) demonstrated a ~25fold increase in bioactivity rate relative to melt-quench derived borate-based glasses. It was suggested that, the sol-gel derived borate glasses have potential for the repair and augmentation of mineralized tissues [24]. In a follow-up study, Lepry et al also studied the effects of processing parameters such precursor materials and calcination temperature on the structural, textural and bioactivity of the sol-gel derived borate substituted

Bioglass® 45S5 formulation [53]. It was demonstrated that, while the utilization of various precursor materials affected the gelation properties, the glasses maintained their high specific surface areas, porosities and bioactivity. Furthermore, calcination temperature had the dominant effect on the textural properties, where a glass-ceramic was formed at a calcination temperature of 500 °C, with a significantly reduced specific surface area [53]. Lepry also investigated the effect of sodium oxide inclusion and content on the textural properties of the sol-gel derived borate-based glasses [54]. It was shown that lower amounts of sodium oxide increased the specific surface area values and their immediate aqueous interactions. Furthermore, it was shown that sodium oxide did not have any impact on the bioactivity of glasses and complete elimination of sodium oxide from glass formulation did not hinder the rapid HCA conversion [54].

2.2 Dynamic vapor sorption (DVS)

One of the critical parameters of bioactive glasses for biomedical applications is their degradation (or dissolution) rate. Degradation, and therefore ionic release rates from bioactive glasses have direct effects on the rate of tissue regeneration, which has been demonstrated with HCA formation, or bioactivity [55]. The rate of ion release is dependent on various factors including glass composition [1], pH of the external environment, as well as glass surface characteristics [16]. Therefore, an understanding of the short term aqueous interactions of bioactive glasses can potentially be used to tailor their reactivity and degradation rates. Conventionally, the reactivity of bioactive glasses has been determined by measuring the rate of mass change and/or ionic species released when immersed in aqueous environments such as either deionized water [16], SBF [56], (2-Amino-2-hydroxymethyl-propane-1,3-diol) TRIS buffer [57] or non-buffered Dulbecco's Modified Eagle's Medium [58]. However, these methods are typically arbitrary, which is dependent on the source of the solutions, as well as the ratio of glass to solution, amongst other factors [59, 60]. For example, it was shown that, evaluation of bioactivity using SBF, may lead to the false positive or negative result [60]. Alternatively, the glass network connectivity can be calculated and related to the degradation and dissolution rates, but this is a theoretical approach with limitations [61].

DVS is a gravimetric technique that measures the vapour sorption of a material under controlled variable relative humidity values. DVS has been mainly used in the pharmaceutical [62], and food science [63] fields. However, it has recently been used to analyze the reactivity and

aqueous interactions of a compositional range of $50P_2O_5$-30CaO-(20-x)Na_2O-xCuO (x = 0, 1, 5 and 10 mol.%) of melt-quench Cu-doped PGs [23] and various formulations of sol-gel derived bioactive borate glasses [24]. It was shown that the dissolution and ionic release rates of phosphate-based glasses with various dopant amounts could be correlated with mass changes associated with exposure to vapour sorption [23] (Figure 2.6).

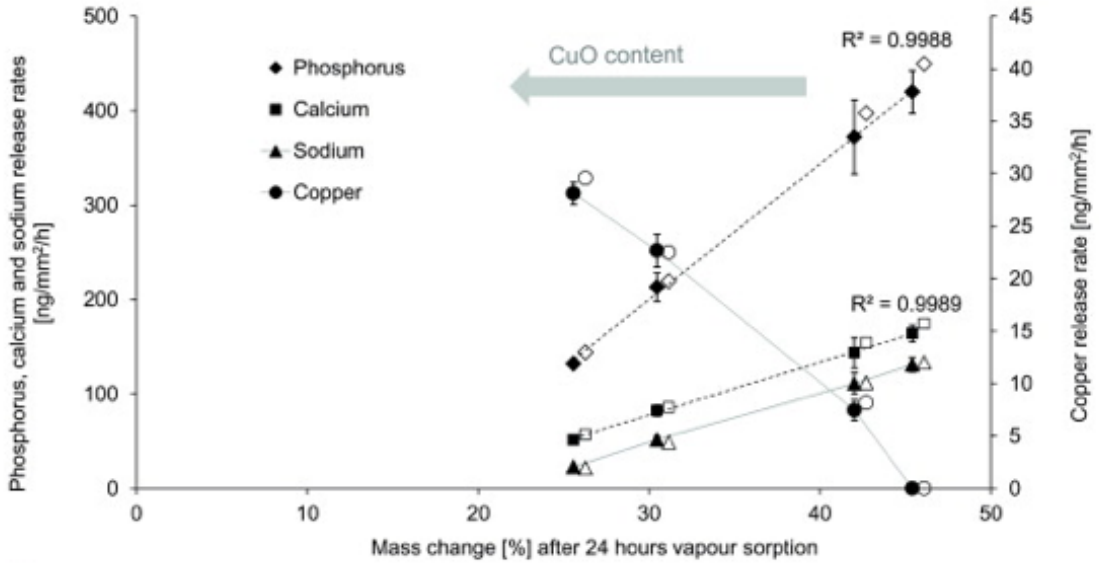

Figure 2. 6: Phosphorus and calcium release rates showed a linear correlation with mass changes after 24 h vapour sorption. All release rates could be predicted (hollow symbols) from estimated dissolution rates using vapour sorption and elemental weight fractions [23].

In the case of the sol-gel borate-based glass compositions with borate content ranging from 36 to 61 mol % and based on a four component melt-derived glass system, 45B5: $(46.1)B_2O_3$−$(26.9)CaO$−$(24.4)Na_2O$−$(2.6)P_2O_5$; mol %, there was an increase in the rate and extent of mass change with lower borate content, which was attributed the lower chemical durability of the glasses as also reflected in their T_g values [24] (Figure 2.7). Additionally, the sorption phase of melt-quench-derived 45B5 demonstrated an initial small increase in mass up to a certain % RH value, which was followed by a sudden increase in percent mass change termed the "inflection point" (Figure 2.7a), similar to that experienced by melt-derived phosphate-based glasses [23]. Furthermore, it was shown that, the direct exposure of 45B5 to 90% RH resulted in ~ 11% mass increase at 6 h, which was substantially less than that of B46 (~ 48%) (Figure 2.7b).

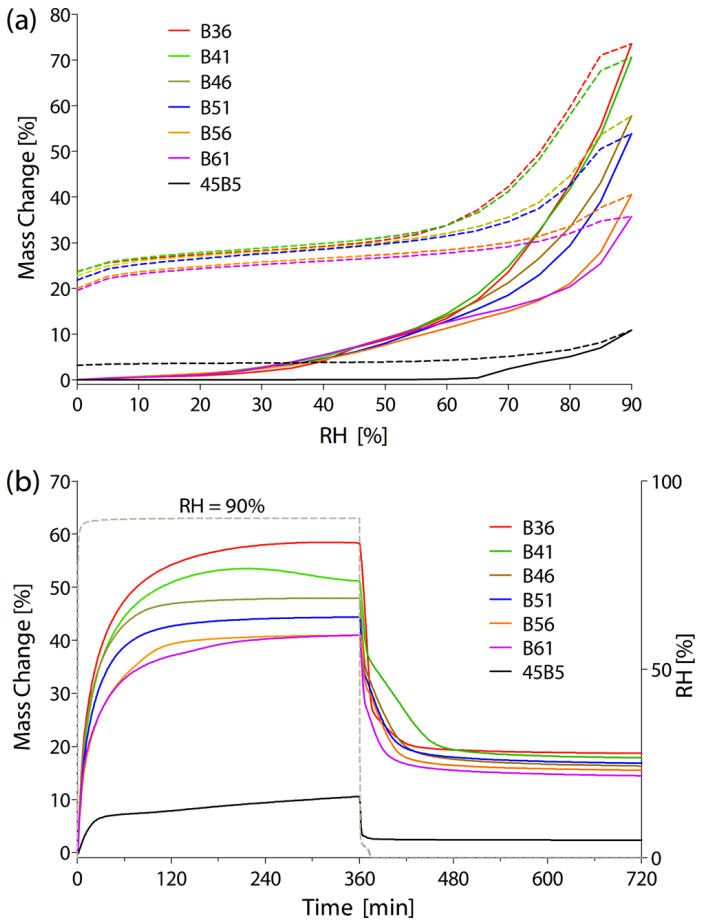

Figure 2. 7: Reactivity through vapor adsorption. (a) Stepwise increase in % RH where the RH was changed by successive steps of 5% over a range of 0 to 90%., with adsorption (solid line) and desorption (dashed line). (b) Direct exposure to 90% RH for a 6 h and subsequently to 0% RH for a further 6 h [24].

Figure 2.8 shows the initial rate of weight increase calculated from the slope of Mass change (%) versus Time (min) during direct exposure to 90% RH and the specific surface area of sol-gel derived boron substituted 45S5 (B46-Sol-gel) and its melt-quench-derived equivalent (45B5-Melt-quench) [24]. It was shown that these glasses, with the same composition, but fabricated though different processing routs resulted in distinct textural properties such as surface area. Consequently, 45B5 demonstrated lower initial rate of weight increase than B46. It was suggested that this was due to the higher surface area and inherent porosity of sol-gel derived glasses compared to their melt-quench-derived equivalents, which resulted in the higher reactivity and dissolution rate of sol-gel derived glasses.

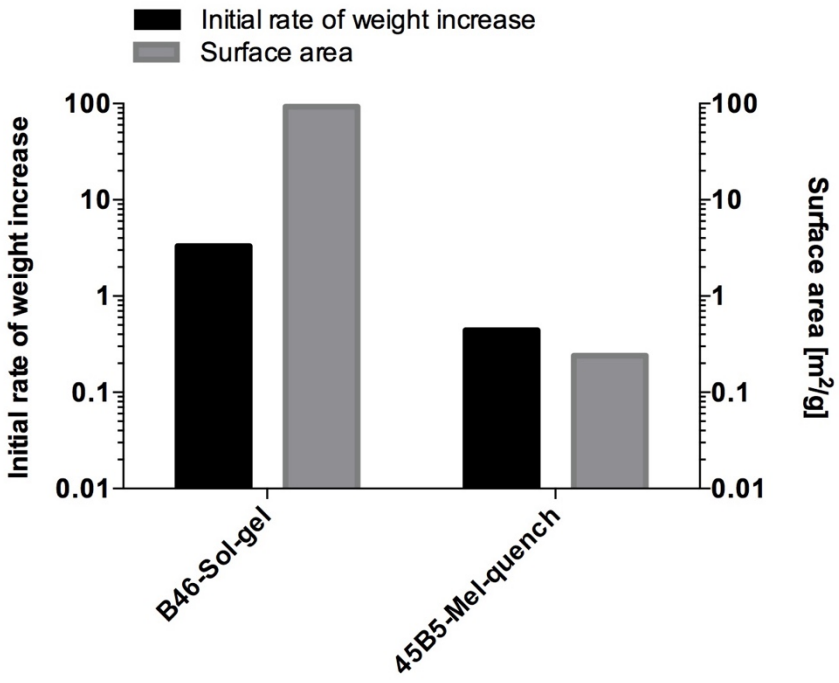

Figure 2. 8: The initial rate of weight increase calculated from the slope of Mass change (%) versus Time (min) during direct exposure to 90% RH (Figure 2.7b) of sol-gel derived boron substituted 45S5 (B46-Sol-gel) and its melt-quench-derived equivalent (45B5-Melt-quench) and their surface area [24].

These studies have demonstrated the ability of DVS in rapidly and accurately determining the immediate aqueous interactions of bioactive and soluble glasses and can be used in predicting their reactivity and potentially bioactivity.

2.3 Inverse gas chromatography (IGC)

Glass composition (e.g., glass modifier and dopant content) and textural properties (e.g., porosity, surface area and particle size) not only affect the bulk properties, but also the surface properties of the glasses [64]. Surface hydrophilicity/hydrophobicity of materials is critical to their solubility as well as their interactions with biological molecules, such as proteins or cells [17]. For example, it has been shown that the surface wettability of alumina and titanium can be enhanced by reducing their particle size leading to better preosteoblast cell attachment and proliferation [65, 66]. Furthermore, it has been suggested that glasses with higher hydrophilicity result in better cell adhesion [17]. A number of studies have shown that, surface energy and wettability of glasses directly affect cell orientation, morphology and cytoskeleton arrangements [67, 68]. The

hydrophilic and hydrophobic nature of glasses is also significant for coating purposes and the quality of interfacial bonding between bioactive glass and the substrate [69].

Surface energy and wetting ability of the glasses are traditionally evaluated with techniques such as contact angle measurement [18-20]. Surface energy is defined as the intermolecular forces at the interface between two media and consists of two main parts: dispersive and polar [70]. This affects the wettability of materials and in order to optimize the adhesion, the attractive forces between the adhesive and bonding surface must be maximized. When the surface energy of an adhesive is lower than the bonding surface, the adhesive will spontaneously wet out the surface. In contrast, if the surface energy of the adhesive is higher than the bonding surface then the adhesive will minimize its contact with the surface. In other words, higher polar surface energy values of a material lead to higher wettability [70].

IGC is a highly sensitive gas phase technique for characterising surface and bulk properties of solid materials by their exposure to a single gas or vapour (probe molecule). A series of IGC measurements with different gas phase probe molecules then allows for the measurement of a wide range of phyisco-chemical properties of the solid sample. This technique has been mainly used to investigate surface and bulk properties of polymers, pharmaceuticals, minerals and nanomaterials [70]. An IGC instrument consists of an oven, column, solute reservoir, detector, mass flow controller and a computer as the processor and controller. In IGC, the stationary phase which is the solid of interest is placed into the column. To analyse the stationary phase, a low concentration of a well characterized volatile single gas or vapour is injected using an inert carrier gas through the stationary phase column. Different probes with different known characteristics such as polarity/non-polarity are used. The retention data of the interaction of a well-defined probe with the stationary phase are used to determine the properties of the stationary phase [70].

In the context of bioceramics, it has been suggested that IGC can be used as a rapid and accurate technique to successfully measure and compare the surface energies of various samples [71]. For example, IGC was utilized to measure the surface energies of rough and porous biosurfaces by comparing synthetic and naturally derived hydroxyapatite samples [25]. It was suggested that, the biological apatite, derived from bovine trabecular bone, has higher surface heterogeneity with high surface energy domains due to the presence of impurities and surface defects in bone mineral. It was proposed that this apatite is more suitable for protein adhesion and cell attachment when compared to the synthetic apatite [25]. The findings of this study suggested

that IGC could be used as a technique to characterize the surface and bulk properties of bioactive and soluble glasses.

2.4 Bioactive and soluble glasses for wound-healing applications

2.4.1 Introduction

Wound-healing forms one of the major challenges in medicine today, especially due to the growing number of diabetic patients. In order to overcome wound-related complications, such as infection, loss of tissue, and scar-tissue formation, various strategies have been developed to accelerate the healing process and control wound infection. However, to date there is no ideal dressing available to fulfill the wound-healing processes.

Recently, it has been demonstrated that the dissolution of bioactive and soluble glasses, doped with various metallic oxides, can controllably release ions to promote the healing process. These ions can be silver (Ag^{+}), copper (Cu^{2+}), zinc (Zn^{2+}), or gallium (Ga^{3+}), among others. This chapter discusses the potential application of bioactive and soluble glasses in wound healing and the role of various ions released through their dissolution on biological responses.

2.4.2 Wound healing

Wound healing encompasses a broad range of clinical applications, including the treatment of skin and oral ulcers; suture, burn, and extraction sites; surgical, traumatic and chronic wounds; as well as clotting, antimicrobial, angiogenic, and anti-inflammatory uses. Skin, in particular, forms the largest surface area organ of the human body with essential roles, such as protection, internal regulation and sensation [72]. Structurally, skin has two major layers; the epidermis (surface layer) and the dermis (deeper layer) [73]. Skin injuries, and the formation of wounds can be caused by various conditions, such as accidents, surgeries and diseases. Based on their healing process, wounds can be classed as either acute or chronic [74]. Acute wounds are injuries with relatively less complications and minimal scar tissue formation that can usually self-heal within 12 weeks. Chronic wounds, on the other hand, are injuries with slower healing rates, often taking longer than 12 weeks, and present more serious conditions [74]. In addition, wounds can be classified according to the depth of skin injuries and include: superficial wounds (injuries to the epidermis); partial thickness wounds (injuries to both layers including sweat glands and blood vessels); and full thickness wounds (injuries of both skin and lower tissues) [75].

Generally, the wound healing process consists of four main phases: haemostasis, inflammation, proliferation and tissue remodelling (Figure 2.9) [76]. Haemostasis occurs as a first step due to the formation of blood clots to stop further bleeding from blood vessels [73, 76]. Inflammation starts with the recruitment of immune cells to reduce infection and stimulate capillary growth [73, 76]. The proliferation phase is initiated through cell growth and new matrix formation [73, 76]. In the latter wound healing stage of tissue remodelling or maturation phase, where granulation tissue is converted to normal skin tissue and healthy extracellular matrix (ECM), a process that can take up to several years [73, 76].

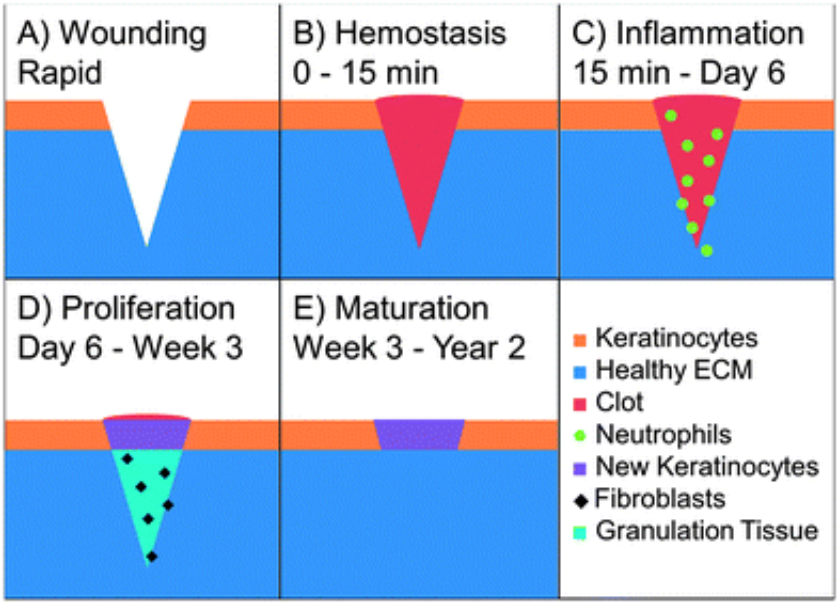

Figure 2. 9: Wound healing processes and timelines: A) wound has occurred. B) Haemostasis stage. C) Inflammation. D) Proliferation. E) Tissue remodelling (Rieger et al. [77]).

When the wound cannot be healed by the body's natural regeneration processes, there is a need to stimulate and accelerate the healing process such as using wound dressing [76]. For example, in compromised patients, numerous factors contribute to wounds with poor healing such as inadequate blood supply, poor glycemic control (e.g., in diabetic patients), immunosuppression (e.g., in transplant recipients), malnutrition, connective tissue disorders, immobility (e.g., stroke or spinal cord injury), heart disease, dementia, cancer, as well as advancing age. In such cases, impaired wound healing results in chronic wounds, e.g., ulcers in diabetic patients, which are constantly at risk of inflammation and infection [76]. Traditionally, wound dressings with high

absorption ability such as cotton wool, lint and gauzes have been used to keep the wound dry and offer protection against bacteria. Polymeric-based dressings offer an alternative approach for accelerating the healing process [78]. However, some of the drawbacks associated with the use of polymers include their hydrophobic nature resulting in poor host-integration as well as their lack of bioactivity [76, 79]. In order to overcome these drawback, recent interest has also focused on developing bioactive and soluble glasses (BGs) that provide controlled release of stimulatory ions, implicated in anti-bacterial, anti-inflammatory or angiogenic properties been proposed as promising materials for wound healing applications (Figure 2.10) [80].

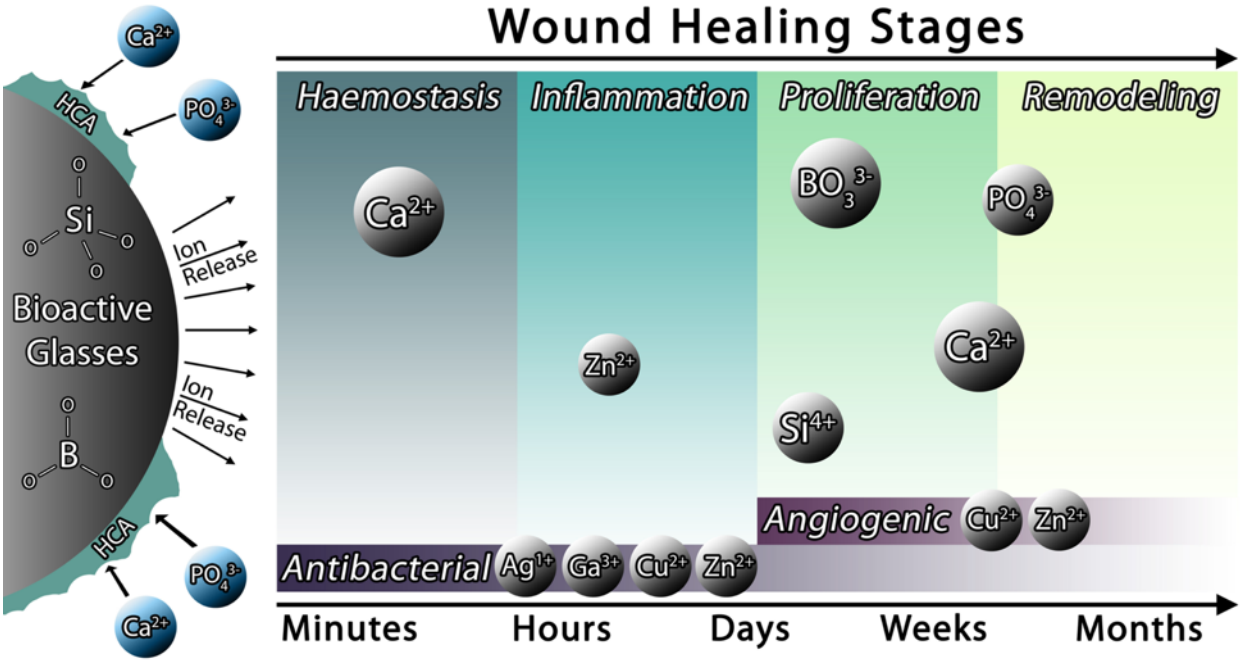

Figure 2. 10: The role of various released ionic species from bioactive glasses on healing mechanisms at various wound healing stages and timelines (Naseri et al. [80]).

2.4.3 Bioactive and soluble glasses

A bioactive material has been defined as one that is induces a specific biological activity (European Society of Biomaterials Consensus; 1987) [81]. Dr. Larry Hench's definition specifies BGs as a category of biomaterials that elicit specific biological responses at the interface with host tissues, which result in the formation of a chemical bond [1, 3]. In particular, certain compositions of BGs have been extensively shown to form surface hydroxy-carbonated apatite (HCA) when in

contact with biological fluid, leading to their bonding to mineralized tissues [82] and in certain formulations to collagenous tissues [1]. While BGs, which can be categorized according to their glass network forming oxides, and be based on either silicate (SiO_2), phosphate (P_2O_5) or borate (B_2O_3) (Figure 2.11), have been extensively studied for bone repair applications [83], these classes of materials have recently generated significant interest in wound healing applications [84]. In fact, in 2016, a borate-based glass microfiber wound dressing (MIRRAGEN™, ETS Wound Care LLC, USA) received FDA approval as a novel wound management for acute and chronic wound healing [10]. It was shown that MIRRAGEN™ wound dressing is able to heal the wounds with no healing under conventional treatment [10].

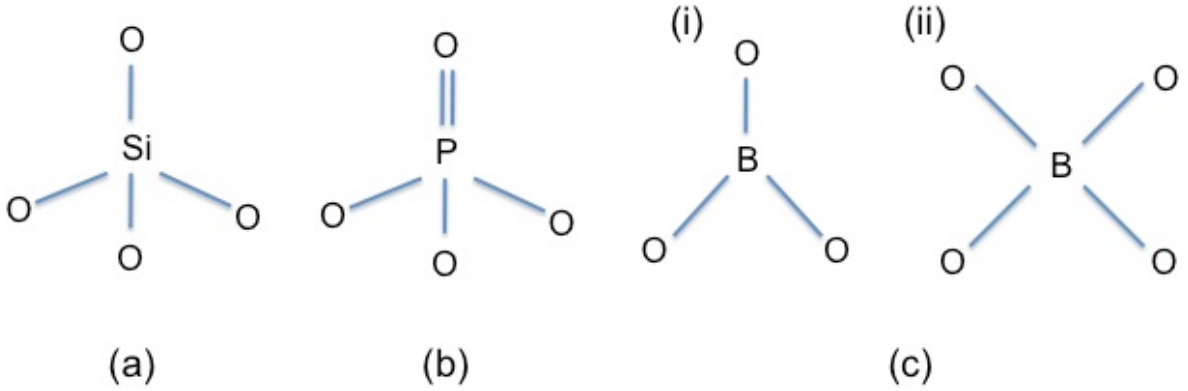

Figure 2. 11: Building units of 3D glass structure. (a) Silicate tetrahedron. (b) Phosphate tetrahedron (reproduced from Abou Neel et al.[8]). (c) (i) three and (ii) four coordinated borate building units (reproduced from Schuch et al.[44]).

2.4.3.1 Silicate-based glasses

Bioactive silicate-based glasses have stimulated much interest in mineralized tissue engineering attributable to a HCA surface layer formation when in contact with biological fluid [85, 86]. The key feature in their bioactivity is their composition, which is based on silica as the glass network former. The basic unit of these glasses is an SiO_4 tetrahedron, and its units form an amorphous 3D glass network (Figure 11a) [26]. High levels of glass network modifiers such as Na_2O, CaO, MgO and K_2O have been demonstrated to have an impact on bioactivity [35]. The ratio of Ca/P is also important in forming a crystalline apatite layer [3]. A clinically applied, and the most extensively investigated composition is Bioglass® 45S5; composed of $46.1SiO_2$-$24.4Na_2O$-$26.9CaO$-$2.6P_2O_5$ (mol%) [8, 35]. Another clinically available formulation is S53P4,

which is composed of $53SiO_2$-$23Na_2O$-$20CaO$-$4P_2O_5$ (mol %) (BonAlive Biomaterials) [2]. The degradation and HCA formation mechanism of silicate-based glasses has been widely investigated, with the following reaction stages have been proposed when immersing silicate-based glasses in physiological fluid [3]:

1) Ion exchange of Na^+ from glass with H^+ from solution/body fluid.
2) Breakage of Si-O-Si bonds and formation of soluble $Si(OH)_4$.
3) Poly-condensation and formation of SiO_2 layer on the surface.
4) Migration of Ca^{2+} and PO_4^{3-} across the SiO_2 layer to the surface and formation of amorphous CaO-P_2O_5.
5) Crystallization of CaO-P_2O_5 and formation of HCA.

2.4.3.2 Phosphate-based glasses

Soluble phosphate-based glasses have P_2O_5 as the network former with a phosphate tetrahedron as the building unit. However, while Si has a valence of 4+ and can form four single bonds with oxygen atoms, P has a valence of 5+ and can form three single bonds with oxygen atoms along with one double bond with an oxygen atom, leading to a different stoichiometry (Figure 11b) [6]. This results in phosphate-based glasses having structural differences from silicate-based glasses and allowing for a wider range of metallic cation incorporation [7].

The degradation rate and solubility of phosphate-based glasses can be tuned and predicted through their composition [87, 88]. The dissolution mechanism of phosphate-based glasses can be divided into two reactions [89, 90]:

1) Hydration reaction: exchange of Na^+ from glass with H^+ in water and the formation of a hydrated layer on the glass surface.
2) Hydrolysis reaction: the breakage of P-O-P due to the presence of water molecules and H^+ that cause the destruction of the glass network.

It has also been shown that the hydration reaction can be controlled by tuning the pH of the media (acid/base reactions) [89].

Generally, phosphate-based glasses have been considered for mineralized tissue engineering due to their high phosphate and calcium content. Indeed, the potential application of these glasses for bone tissue engineering has been widely investigated [4, 8]. However, a different regeneration mechanism has been proposed in the case of these glasses. Instead of promoting

apatite formation, as in the case of silicate-based glasses, phosphate-based glasses have been shown to enhance cell activation for bone growth through Ca^{2+} ion release [4, 91]. However, these glasses can be doped with suitable metallic oxides such as Ga_2O_3 [92-95], Ag_2O [96, 97] and CuO [98-100] to be tuned for wound healing applications.

2.4.3.3 Borate-based glasses

Recently, there has been much growth of interest in borate-based glasses for biomedical applications [55, 101]. The network forming unit of borate is trigonally coordinated with three oxygen atoms, boron can also be tetrahedrally coordinated with four oxygen atoms depending on the amount of alkali metal glass modifier used [44, 45] (Figure 11c i and ii). The combination of trigonal and tetrahedral borate units decreases results in borate-based glasses being less stable than silicate-based glasses [44, 45]. It has been shown that the glass degradation rate can be accelerated by either partially or fully substituting silicate with borate as the building block [102, 103]. Their degradation mechanism is similar to silicate-based glasses, except that they release BO_3^{3-} ions instead of SiO_4^{4-} ions which leads to formation of HCA layer without formation of any silica rich layer [102]. It has been proposed that upon dissolution of the Na^+ and Ca^{2+} ions from the glass, the PO_4^{3-} ions immediately react with the Ca^{2+} ions leading to formation of HCA [102].

2.4.4 Bioactive glass fabrication routes

There are two main routes for glass fabrication; melt-quench and sol-gel processes. In general, the precursors used in melt-quench derived glasses are oxide mixtures that are typically heated to above 1000 °C depending on the glass composition to obtain a melt, which are then quenched rapidly to form an amorphous structure by inhibiting glass crystallization [32]. Heat treatment may be performed slightly above the glass transition temperature to generate a more stable glass through reduction of residual stresses [32]. The fabricated bulk glass can be cast to any monolithic shape, or ground to powders of defined particle size ranges. Since the particles and fully dense, the particle size determines the total specific surface area and result in low surface area (1-2 m^2/g).

Bioactive glasses can also be produced by the sol-gel process through the mixing of alkoxides in solution. The process is initiated by the preparation of the sol from metallic alkoxides in a solvent such as water or alcohol, and is followed by the gelation of the sol through hydrolysis

and polycondensation reactions [48]. Complete gelation is achieved upon an ageing period, and the duration of which depends on the composition. Fabrication is then completed by performing drying and calcination processes (typically below 600 °C) [48]. Sol-gel glasses have nano-porous textures with large surface areas (200-650 m^2/g), which increases their dissolution and potential bioactivity [48]. The sol-gel process has been extensively applied to produce bioactive silicate [26], phosphate [104, 105], and more recently introduced in borate [24, 53] based glasses.

2.4.5 Bioactive glasses and wound healing

In recent years, investigations into the potential application of BGs in soft tissue engineering has gained considerable attention [84]. Prime interest among these has been their use in wound healing applications. In particular, studies have shown that various therapeutic ions released from glasses can accelerate the wound healing process through their control of bacterial microorganisms, blood coagulation and collagen production [83, 106]. Also BGs have been shown to stimulate vascular endothelial growth factor (VEGF) and basic fibroblast growth factor (bFGF), which are essential for angiogenesis and the wound healing processes [1].

Generally, BGs contain CaO as a main network modifier in their structure and it has also been shown that the release of Ca^{2+}, through glass dissolution can promote the migration of epidermal cells and the formation of blood clots [107]. Kawai et al., studied the effects of calcium based nano-particles on wound healing process in mice [108] and observed calcium ions enhanced wound closure and healing rate. It has also been shown that calcium ions increased fibroblast proliferation and caused fibroblast populated collagen lattice contraction [108]. Moreover, BGs have the ability to increase tissue strength at the wound site [109]. Various studies have also demonstrated the haemostatic ability of silicate-based BGs through their increase of blood coagulation rates [110]. On the other hand, it has been shown that hydroxyapatite particles inhibits coagulation activity and decreases clot strength when compared to BGs ($XSiO_2$-(96-X)CaO-$4P_2O_5$ where X=90, 80, 75, 70, 65, 60 in mol%) [111]. In another study, it was reported that BG compositions ($60SiO_2$-$36CaO$-$4P_2O_5$ (mol %)) with higher apatite deposition rates have lower coagulation activities and higher ability for bone growth. In contrast, compositions ($80SiO_2$-$16CaO$-$4P_2O_5$ (mol %)) with lower apatite deposition rates have better coagulation response [110]. Lin et al., studied the effect of different BG compositions incorporated in a commercial ointment, Vaseline® (at 18 wt.%), on full thickness wound healing in normal and diabetic rats [112]. The

glass formulations were sol-gel derived 58S (<53 μm particle size) (58SiO_2-33CaO-9P_2O_5 in wt.%), nano-sized (30 nm) 58S and melt-quench derived Bioglass® 45S5 (<53 μm). In all cases, the addition of BG was shown to enhance and accelerate wound healing and vascularization processes. In addition, sol-gel derived glasses (58S) showed significantly higher healing rates than melt-quench derived Bioglass® 45S5 [112]. Mao et al., studied the effect of incorporating16 wt.% Bioglass® 45S5 and various amounts of Yunnan baiyao (a haemostatic agent, incorporated at 0, 5, 10 and 20 wt.%) into Vaseline® ointments on the healing of chronic wounds in streptozotocin-induced diabetic rats [113]. Additionally, Vaseline® and Vaseline®/Yunnan baiyao ointments were used as control. The effects of these materials on healing, as measured through rate of wound closure, anti-inflammatory response, fibroblasts proliferation rate, granulation tissue formation and angiogenesis were monitored up to 21 days. It was shown that ointment incorporated with 5 wt.% Yunnan baiyao and 16 wt.% Bioglass® 45S5 enhanced the wound healing process yielding higher healing rates [113]. Xie et al., has investigated the role of sol-gel derived BGs on the regulation of fibroblasts cellular behaviour related to the wound healing [114]. A BG composition of 90S (90 SiO_2-6 CaO-4 P_2O_5) in mol% has been fabricated through sol-gel process. In this study, autoclaved glass particles were exposed to the human skin fibroblast cells. It was shown fibroblasts migration enhanced by 90S glass particles. Additionally, it was shown 90S glass particles inhibited the differentiation between fibroblasts and myofibroblasts cells, this was determined by measuring the gene expression of α-SMA (a well-known gene related to the myofibroblastic differentiation). Furthermore, evaluation of the gene expression level of TGF-β indicated TGF-β signaling was inhibited by the 90S glass particles. Also, the gene expressions of collagen type I and collagen type III were down regulated by 90S glass particles. The main difference between cell culture medium with and without BG particle incorporation was the ionic concentration. Medium with 90S BG particles contained Si^{4+} ions which were not present in the control medium. Therefore, it was concluded Si^{4+} ions play a significant role in the regulation of cell behavior in wound healing process to accelerate the healing rate with minimal scaring [114]. Yu et al., reported a bioactive skin graft composed of fibroblast cell sheet cultured with ionic dissolution products of BGs for wound healing. It was shown that the ionic dissolution products stimulated fibroblast cells to secret essential growth factors (VEGF, bFGF and Epidermal Growth Factor (EGF)) for vascularization [115]. An in vivo tested the bioactive skin graft by using a full thickness wound model in a mouse, indicated a significant increase in wound closure and newly formed blood vessels in the fibroblast

cell sheets in the presence of ionic dissolution products [115]. Therefore, an approach to deliver BGs as skin grafts to chronic wounds can be through a composite strategy, via their combination with either natural or synthetic polymers. Zeng et al., showed that a thermosensitive Bioglass® 45S5/agarose–alginate composite hydrogel provided sufficient moisture at the wound site while glass incorporation accelerated angiogenesis and the healing rate [116]. Francis et al., reported a novel composite of Bioglass® 45S5/poly(3-hydroxybutyrate) microsphere films with potential wound healing application [117]. It was demonstrated that incorporation of BG into the polymer increased coagulation rate. Additionally, cell adhesion and proliferation rate of human keratinocyte cells were enhanced when compared to the pure polymer film.

The dissolution of silicate-based glasses leads to an increase in local pH, which have been implicated in having an anti-bacterial effect [118, 119]. To this end, BGs have demonstrated broad anti-bacterial effect on oral and respiratory infection-associated microorganisms [118, 120]. For example, it was has been reported that a BG of the composition 53SiO2-23Na2O-20CaO-4P2O5 (in wt.%), led to the reduction of viability of *Actinomyces naeslundii* within 10 min, and of *Actinobacillus actinomycetemcomitans*, *Porphyromonas gingivalis*, and *Streptococcus mutans* within 60 min [118]. Additionally, BGs had inhibitory effect of *Hamophilus*. *influenza* or *Streptococcus pneumonia* adhesion [120].

Furthermore, the angiogenic ability of Bioglass® 45S5 has been investigated. Day et al., measured the expressions of VEGF and bFGF in human fibroblasts cultured on Bioglass® 45S5-coated polystyrene tissue culture plate surfaces [121]. There was a significant increase in VEGF and bFGF secretion in the presence of Bioglass® 45S5. Additionally, it was shown, that microvascular endothelial had higher proliferation when cultured in medium conditioned by the proteins released from fibroblasts, when compared to non-coated surface [121]. It was concluded that BGs have the ability to stimulate angiogenesis. A number of studies have also demonstrated the angiogenic effect of BGs is highly dependent on concentration, i.e., higher concentrations have been found to lead to no angiogenic response or even cytotoxic effects [122, 123], highlighting the need for precise, therapeutic dose delivery.

In addition, sol-gel derived glasses indicated more rapid wound healing rates compared with melt-quench derived glasses due to the higher surface area and ionic release rates [112]. However, bioactive silicate-based glasses have some limitations such as a low degradation rate [4]. Silica remains in the body and its long-term effects is not well understood [8, 124]. To this

end, attributable to their lower chemical durability compared to silicate-based glasses, borate-based glasses have recently gained noticeable interest for the healing of skin defects. Zhou et al., compared wound dressings composed of Bioglass® 45S5 and bioactive borate glass 13-93B3 ($5.5Na_2O$-$18.5CaO$-$11.1K_2O$-$4.6MgO$-$3.7P_2O_5$-$56.6B_2O_3$ in wt.%) micro-fibres [125] on the healing effects (wound closure and angiogenesis) in a full thickness skin defect model in rats. Initially, it was shown that the ionic dissolution products of both glasses were not toxic to human umbilical vein endothelial cells (HUVECs), in vitro. The follow-up in vivo study indicated that the borate glass resulted in significantly higher rate of blood vessel formation and wound closure, when compared to Bioglass® 45S5 [125].

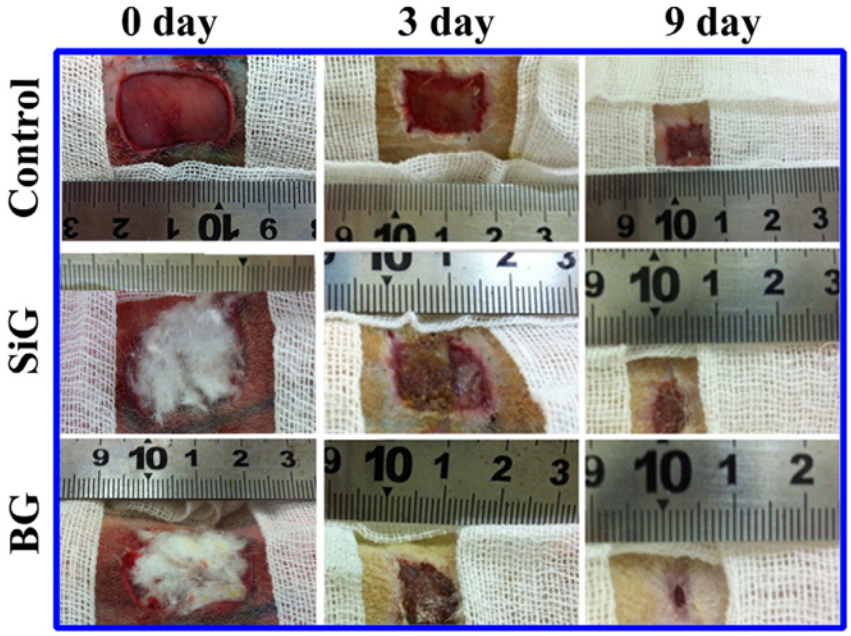

Figure 2. 12: Full-thickness skin defects in rats up to 9 days. Comparison between untreated (top row), silicate glass fibers treated (middle row) and borate glass fibers treated (bottom row), (Zhou et al., [125]).

2.4.6 Ionic doping of bioactive and soluble glasses

In order to expand the potential applications of BGs, such as in wound healing and soft tissue engineering, they have been doped with inorganic-metallic ions (e.g., Ag^+, Zn^{2+}, Cu^{2+}, and Ga^{3+}) [11, 12]. It has been shown that various ionic release through the dissolution of BGs in biological solutions; elicits anti-bacterial, anti-inflammatory and angiogenic effects [11, 12] (Table 2.1). Indeed, the potential of some metallic cations as anti-bacterial agents has been widely studied and may prove useful as an alternative to traditional antibiotic treatments, which are increasingly

associated with bacterial resistance [126]. Since wound infection is a major concern, especially in diabetic patients, the use of an anti-bacterial agent may prevent this and also decrease the inflammation stage of wound healing. However, the rate of release of ions and their concentration in vivo need to be controlled in order to reduce any potential toxic side effects [11, 12].

Table 2. 1: The roles of metallic ions and their biological responses within the various glass compositions: summary of literature.

∗SG: Sol-gel derived glasses, MD: Melt-derived glasses

Ions and their biological response		Ref	Investigated in glass compositions	Findings	Ref
Si^{4+}	- Induces bone tissue calcination. - Stimulates collagen type I formation.	[127] [128]	45**SiO_2**-24.5Na_2O-24.5CaO-6P_2O_5 (wt%)-MD&SG 60**SiO_2**-36CaO-4P_2O_5 (mol %)-SG	- Induced HCA formation. - Enhanced bond to the bone and soft tissue.	[129] [130]
Ca^{2+}	- Enhances osteoblast proliferation, differentiation and ECM mineralization. - Increases the expression of insulin like growth factors. - Promotes the migration and proliferation of epidermal cells. - Accelerates blood-clotting.	[131] [132] [107] [107]	58SiO_2-33**CaO**-9**P_2O_5** (wt%)-SG 45SiO_2-24.5Na_2O-24.5**CaO**-6**P_2O_5** (wt%)-MD 80SiO_2-16**CaO**-4**P_2O_5** (mol%)-SG	- Enhanced wound healing and vascularization processes. - SG glasses showed more rapid wound healing rates compared with MD glasses due to the higher surface area. - Increased blood coagulation rate.	[112] [110]
P^{5+}	- Stimulates the expression of matrix Gla protein (MGP) for bone formation.	[133]			

B^{3+}	- Stimulates vascularization and angiogenesis. - Increases RNA synthesis in fibroblasts.	[134] [137]	5.5Na_2O-11.1K_2O-4.6MgO-18.5CaO-56.6**B_2O_3**-3.7P_2O_5 (wt%)-MD	- Showed higher proliferation and migration rate of human skin fibroblast cells than silicate-based glasses.	[135]
			6Na_2O-8K_2O-8MgO-22CaO-54**B_2O_3**-2P_2O_5 (mol.%)-MD	- Showed high proliferation rate of human endothelia cells. - Enhanced wound closure and vascularization.	[136]
Ag^{+}	- Antibacterial property.	[27]	SiO_2-CaO-P_2O_5-3**Ag_2O** (wt%)-SG	- Demonstrated bacteriostatic effect against *E. coli* bacteria.	[30]
			SiO_2-CaO-P_2O_5-0.02**Ag_2O** (wt%)-SG	- Demonstrated 99% antibacterial rate against *E.coli* bacteria in 12 hrs. - Increased blood coagulation rate.	[138]
			60SiO_2-34CaO-4P_2O_5-2**Ag_2O** (mol%)-SG	- Limited *in vitro* attachment of Staphylococcus epidermis.	[139]
			50P_2O_5-30CaO-(20-x)Na_2O-(x=0,1,2..,15)**Ag_2O** (mol%)-MD	- Glasses containing 3 and 5 mol % Ag were bactericidal for *S.aureus* and *E. coli* and decreased the growth rate of *C.albicans*. - Higher Ag content decreases dissolution rate.	[96]
			45P_2O_5-20CaO-(35-x)Na_2O-(x=0,1,5, 10 and 15)**Ag_2O** (mol%)-MD	- Higher silver content showed higher antibacterial effect with better long term antibacterial effect.	[97]
			6Na_2O-8K_2O-8MgO-22CaO-54B_2O_3-2P_2O_5 (mol%)-0.75,1and 2**Ag_2O** (wt%) MD	- Glasses containing 0.75 and 1 wt% Ag demonstrated antibacterial effect. - Glasses with 2 wt% Ag content were toxic.	[140]
			48.63B_2O_3-22.92Na_2O-22.86CaO-5.59P_2O_5-1,2,4 and 10**Ag_2O** (wt%)-MD	- Demonstrated antibacterial activity. - Metallic silver was formed in glasses containing 10 wt% Ag.	[141]

Zn^{2+}	- Stimulates angiogenesis. - Enhances nerve regeneration. - Anti-inflammatory property. - Enhances wound healing processes. - Increases ATP activity. - Stimulates *in vitro* bone formation.	[142] [144] [145] [146] [11] [11]	$45SiO_2$-$24.5Na_2O$-$24.5CaO$-$6P_2O_5$ -5, 20.2**ZnO** (wt%)-MD	- Higher zinc content decreased degradation rate. - Glasses with 20.02 wt% zinc were toxic on endothelial cells.	[143]
			$6Na_2O$-$12K_2O$-5MgO-20CaO-$51.6B_2O_3$-$4P_2O_5$-0.4CuO-1**ZnO** (wt%)-MD	- Under dynamic flow showed higher proliferation rate of human skin fibroblast cells on zinc doped glasses than undoped glasses.	[135]
Cu^{2+}	- Stimulates angiogenesis. - Demonstrates antibacterial property. - Increases the differentiation of mesenchymal stem cells (MSCs).	[147] [148] [149]	$50P_2O_5$-30CaO-(20-x)Na_2O-(x=0,1,5 and 10)**CuO** (mol%)-MD	- Doping with 10 mol% Cu can kill the *staphylococcus epidermidis* resulting in positive effect on wound healing.	[99]
			$6Na_2O$-$8K_2O$-8MgO-22CaO-$54B_2O_3$-$2P_2O_5$ (mol.%) -0.5,1 and 3**CuO** (wt%)- MD	- Cu doped glasses showed higher newly formed blood vessels and wound closure.	[136]
Ga^{3+}	- Demonstrates antibacterial property.	[94]	$45P_2O_5$-16CaO-(39-x)Na_2O-(x=0,1,3 and 5)**Ga_2O_3** (mol%)-MD	- Showed antibacterial effect on Gram-negative and Gram-positive bacteria.	[94]

2.4.6.1 Silver (Ag^+) ions

2.4.6.1.1 Anti-bacterial activity

While silver is inert in its metallic phase, it can be converted to the highly reactive silver cation (Ag^+) through its contact with wound moisture [27]. Ag^+ ions have both bacteriostatic (i.e., possessing the ability to stop the reproduction of bacteria) and bactericidal (i.e., possessing the ability to kill bacteria) properties. Silver ions can kill bacteria through attachment to their DNA and RNA or to the tissue proteins leading to cell distortion [27]. They have the affinity to attach to the nitrogen and sulfur in DNA and RNA thus stopping their reproduction as well as bind to the thiol and amino groups of tissue proteins [150]. It has also been shown that Ag^+ ions can adhere to cell membranes and inhibit the respiration process of bacteria [27]. Depending on the biological environment, microorganisms and cell type, the effective concentration of silver ions against single-celled organisms (e.g., bacteria, fungi and algae) can vary from 0.1 to 20 mg/L, and their toxic concentrations on eukaryotic cells are around 1 to 10 mg/L [151]. A number of studies have demonstrated the positive anti-bacterial effects of Ag^+ ions on different Gram-negative bacteria including *Escherichia coli* and *Pseudomonas aeruginosa* and Gram-positive bacteria (major cause of surgery infections) *Streptococcus aureus* and *Streptococcus mutans* [152, 153].

Attributable to the anti-bacterial property of Ag^+ ions, there has been extensive research on BGs doped with silver in potential wound healing applications [154-156]. Although the melt-quench process has been used to synthesize silver-doped silicate-based glasses [28], the sol-gel process has been mainly preferred to overcome difficulties in fabricating homogenously distributed silver within the glass network when fabricated through the melt-quench process [29]. Bellantone et al., reported using the sol-gel process to produce a homogenous silver-doped silicate-based ($76SiO_2$-$19CaO$-$2P_2O_5$-$3Ag_2O$; wt.%) glass structure with controllable degradation properties [30]. The incorporation of 3 wt.% silver resulted in a glass of high surface area and demonstrated anti-bacterial effect against Escherichia coli [30]. Moreover, Hu et al., investigated the potential of silver doped nano-sized silicate-based (SiO_2-CaO-P_2O_5-Ag_2O) glass (nBG; of 6 nm particle size and 467 m^2/g surface area) produced using sol-gel process with nano-porous structure for wound healing applications, through in vitro and in vivo haemostatic tests [138]. It was shown that nBG accelerated blood coagulation compared to micron-sized glass particles due to higher ion release rates [138]. The incorporation of 0.02 wt.% silver into nGB significantly enhanced the anti-bacterial efficacy of the glass against Escherichia coli [138]. Silver doped

silicate-based glass coated on polymeric sutures have been reported by Pratten et al. for wound healing applications [139]. Sutures were coated with non-doped melt-derived Bioglass® 45S5 as well as silver doped (at 2 mol.%) sol-gel derived silicate-based glass. Anti-bacterial efficacy was evaluated against Staphylococcus epidermidis with the silver doped glass coated suture having significantly higher anti-bacterial effect when compared with Bioglass® 45S5 coated and uncoated sutures [139].

A number of studies have also shown that phosphate-based glasses have potential applications in wound healing through silver oxide doping [96, 99]. Mulligan et al., evaluated the anti-bacterial effects of melt-quench derived phosphate-based glass doped with silver with using of 0 to 15 mol% against Streptococcus sanguinis bacteria [97], and demonstrated an increase in anti-bacterial efficacy with silver content [97]. Ahmed et al., also demonstrated that silver-doped phosphate-based glasses have the ability to kill Streptococcus aureus, Escherichia coli bacteria, and decrease the growth of Candida albicans [96].

The in vitro cytotoxic effect of silver-doped melt-quench derived borate-glass has been studied using osteoblastic and fibroblastic cells [140]. Borate glasses (13-93B3) were doped with 0.75, 1 and 2 wt% Ag_2O. The incorporation of 0.75 and 1 wt.% Ag_2O indicated no toxic effects, whereas the ionic dissolution products from the glasses with 2 wt% Ag_2O indicated toxic effects [140].

2.4.6.2 Copper (Cu^{2+}) ions

Cu^{2+} ions are naturally present in the body (~1 ppm in blood plasma [157]) with essential metabolic functions. They have anti-bacterial effect and have been shown to promote angiogenesis, stimulate blood vessel formation, endothelial cell proliferation, ECM remodelling, and the differentiation of mesenchymal stem cells [11, 12]. Additionally, Marelli et al., showed that copper ions can crosslink collagen type I with inhibitory effect on fibroblast proliferation [158].

2.4.6.2.1 Anti-bacterial activity

A number of studies have shown that Cu^{2+} has been incorporated into the bioactive and soluble glasses to illicit anti-bacterial effects. Abou Neel et al., has studied anti-bacterial effect of copper doped melt derived phosphate glasses for wound healing application [99]. The effect of

copper on the staphylococcus epidermidis (a common infection in human skin wounds) was evaluated and the result shows doping with 10 mol% copper can kill the bacteria resulting in positive effect on wound healing [99]. Mulligan et al., also demonstrated that Cu-doped phosphate based glasses with 15 mol% CuO content have antibacterial activity do to the Cu^{2+} ions release from glasses [98].

In another study, anti-bacterial activity of sol-gel derived silver and copper doped bioactive silicate-based glasses ($50SiO_2$-$45CaO$-$5P_2O_5$ in mol%) has been investigated [148]. In this study 1, 5 and 10 mol% dopant (Ag_2O and CuO) have been incorporated into the glass structure. It was shown incorporation of 5 mol% Ag_2O has similar anti-bacterial activity as incorporation of 10 mol% CuO. It was also shown Ag-doped glasses have faster initial anti-bacterial effect, however, Cu-doped glasses demonstrated more prolonged ions release. It was concluded that silver ions had stronger anti-bacterial property than copper ions [148].

2.4.6.2.2 Angiogenesis

The development of vasculature is a key process in the tissue growth and repair [159]. When the body lacks the ability to stimulate vascularization in the wound healing process, there is a need to enhance angiogenesis. A recent interesting strategy to induce angiogenesis has been the use of metallic ions such as Cu^{2+} controllably released through the dissolution of ionic-doped bioactive glasses [160, 161]. Metallic doped glasses are less expensive compared to growth factors with a long shelf life.

Copper ions have been shown stimulate angiogenesis via the expression and secretion of VEGF, FGF-1, and interleukin-8 as well as, regulation of hypoxia-inducible factor-1 (HIF-1) [162, 163]. However, the exact mechanisms of copper on angiogenesis stimulation, is not yet fully understood. The effect of copper ions on endothelial cells was discovered by McAuslan et al. who demonstrated an increase in bovine aortal endothelial cell motility through the addition of 2 μM $CuCl_2$ solution in culture [164]. Borkow et al., investigated the healing effects of wound dressing containing copper oxide [165]. It was shown there is significantly higher wound closure in a wound treated by copper containing wound dressing than non-copper wound dressing. Furthermore, the copper containing wound dressing was compared with commercial silver containing wound dressing. The result has demonstrated that copper-treated wounds were treated faster and they exhibited higher formation of new blood vessels compared to silver-treated wound [165]. Kong et

al., investigated the stimulatory effect of combination of both Cu^{2+} and Si^{2+} ions on angiogenesis [166]. In this study angiogenesis activity of Cu-$CaSiO_3$ particles were compared with $CuSO_4$ solution as copper ions control, and $CaSiO_3$ particles as silicon ions control. The vascularization and expression of vascular angiogenic growth factors were evaluated using in vitro culturing of human umbilical vein endothelial cells (HUVECs) and ionic dissolution extracts of particles and ECMatrix™ (contains laminin, collagen type IV, heparin sulfate proteo- glycans, entactin and nidogen). To better characterization of angiogenesis capacity of particles, they were co-cultured in vitro with HUVECs and human dermal fibroblasts (HDFs). The result was shown, Cu-SiO_3 has higher stimulatory effect on angiogenesis and vascularization than only Si^{2+} ions or Cu^{2+} ions [166]. However, recent studies on Cu-doped silicate- and phosphate- based glasses have shown, there is no direct effect of copper ions on the endothelial cells in order to enhance angiogenesis [100]. Staehli et al., investigated the efficacy of Cu^{2+} ions on the endothelial cells metabolic activity using a 3D collagen structure [100, 160]. Network length, connectivity and branching have been examined via confocal laser scanning microscopy image where various concentrations of Cu-doped phosphate glasses (10 mol% CuO) were incorporated into collagen structure seeded by endothelial cells. The result was shown that the higher Cu-doped glasses lead to the higher decrease in network length and cells metabolic activity. However no effect was observed on the network connectivity and branching [100]. The same result was reported on the Cu-doped Bioglass® 45S5 (2.5 wt% CuO) [160].

In terms of borate-based glasses, Zhao et al., investigated the efficacy of wound dressings composed of melt-quench derived microfibres (non-doped and Cu-doped) [136] (Figure 2.13). High proliferation and migration rates of HUVECs on the glasses were reported with no toxicity effects of the released ions [136]. Additionally, the in vivo wound healing effect was evaluated using a wound healing model in the rat. The result showed that significant improvement on the wound healing process was achieved when borate glass fibres used as a wound dressing compared to non-treated wound. Even higher rates of wound closure and vascularization were achieved when using Cu-doped glasses [136].

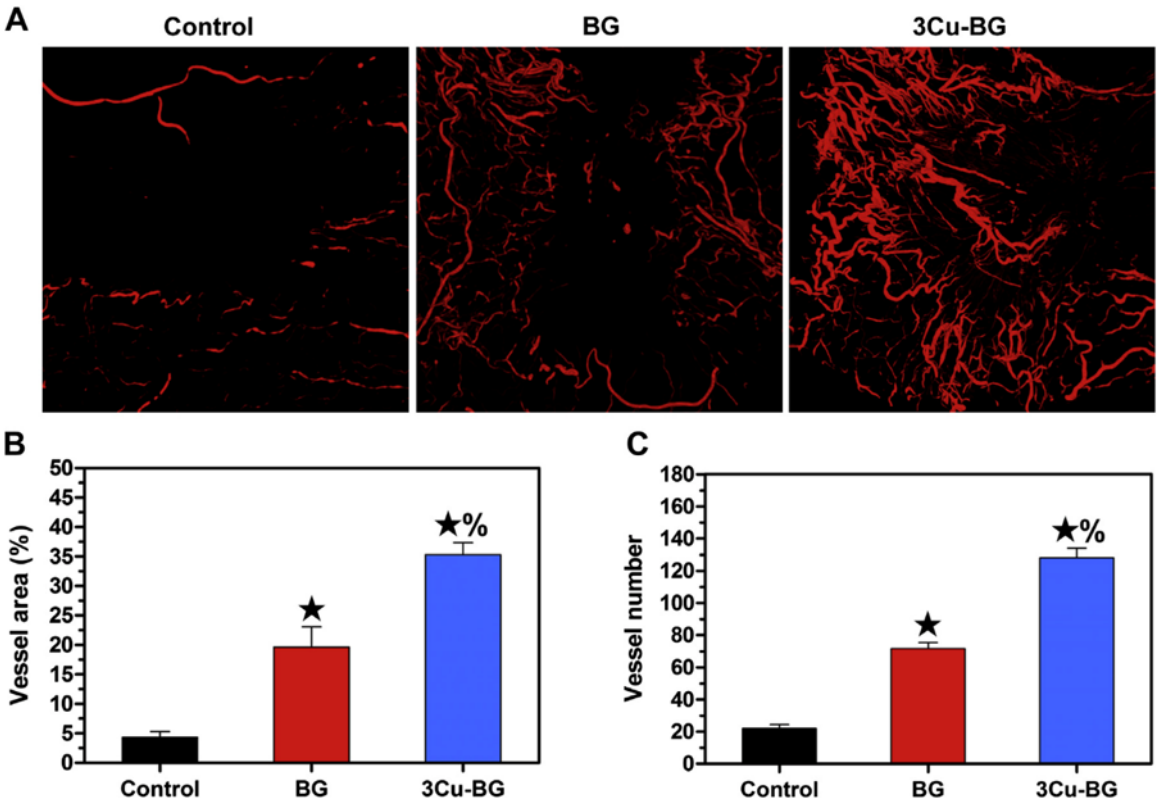

Figure 2. 13: Micro-CT evaluation of blood vessel formation in full-thickness skin defects at 14 days post-surgery. (A) 3D reconstructed images of newly formed blood vessels at non-treated defect (control), defect treated with 13-93B3 borate glass (BG), and defect treated with Cu-doped borate glass (3Cu-BG) microfibers; (B), (C) morphometric analysis of the new blood vessel area percentage and the number of blood vessels (Zhao et al., [136]).

2.4.6.3 Gallium (Ga^{3+}) ions

2.4.6.3.1 Anti-bacterial activity

Ga^{3+} ions are known for their anti-bacterial properties against both Gram-negative and Gram-positive bacteria [94, 167]. A number of studies have reported that Ga^{3+} ions have been controllably released from Ga-doped phosphate-based glasses to effect anti-bacterial properties. Valappil et al., studied the anti-bacterial activity of Ga-doped melt-quench derived phosphate-based glasses of the composition $45P_2O_5$-16CaO-(39-x)Na_2O-xGa_2O_3 (where x is 0, 1, 2 and 3 in mol%) [94]. It was shown that Ga^{3+} ions demonstrated anti-bacterial activities against Pseudomonas aeruginosa, methicillin-resistant, Streptococcus aureus and clostridium difficile growth. It was proposed that Ga^{3+} decreases the Fe^{3+} uptake of bacteria since bacteria cannot distinguish between Ga^{3+} and Fe^{3+} due to their close ionic radius and will uptake Ga^{3+} instead of

Fe^{3+} [167] . It was also shown that, upon the addition of 1 mol% Ga_2O_3, an effective anti-bacterial property can be obtained. Structural characterization of Ga-doped phosphate-based glasses showed that the addition of Ga^{3+} ions led to a stronger glass network [168]. In another study, Valappi et al., reported that the release rate of Ga^{3+} ions can be tuned by varying the calcium content ($xCaO$-$(52\text{-}x)Na_2O$-$45P_2O_5$-$3Ga_2O_3$, in mol%, where x = 14, 15 and 16) [93]. It was shown that an increase in CaO content from 14 to 16 mol%, while maintaining Ga_2O_3 at 3 mol%, led to a decrease in Ga^{3+} ion release rate, 17.6, 13.5 and 7.3 $\mu g\ mm^{-2}\ h^{-1}$, respectively. Pickup et al., reported novel sol-gel derived Ga-doped phosphate-based glasses with anti-bacterial activity against Streptococcus aureus bacteria [95]. However, in this study, sol-gel derived glasses were not compared with their melt-quench derived equivalents.

In another study, gallium- and silver-doped phosphate-based glasses of general composition ($xCaO$-$(47\text{-}x)Na_2O$-$45P_2O_5$-$3Ga_2O_3$-$5Ag_2O$ in mol%, where x = 10, 11 and 12) were developed for potential applications in the treatment of oral cavity infections taking advantage of both anti-bacterial elements [92].

2.4.6.4 Zinc (Zn^{2+}) ions

The human body contains about 1.5 – 2.5 g of zinc, 11% of which is in the skin and liver [169]. At the cellular level, it has been shown the zinc content is in the range of 0.1-0.5 mM [169] and if exceeded may cause cytotoxic effect [169]. Nevertheless, Zn^{2+} ions have been demonstrated to have anti-bacterial and anti-inflammatory properties [170]. Moreover, zinc ions have also been shown to increase adenosine triphosphatase activity, stimulate in vitro bone formation, improve mechanical strength of glasses for hard tissue applications [11, 12] and enhance nerve regeneration and growth [144].

2.4.6.4.1 Anti-bacterial and anti-inflammatory activity

It has been shown that zinc has antibacterial and anti-inflammatory properties. The anti-bacterial effect of zinc has been evaluated in a rat model with chronic bacterial prostatitis where the local injection of zinc inhibited bacterial growth [170]. Lansdown et al., also reported the positive effect of zinc on wound healing application [146]. It has been reported that the local delivery of zinc provides therapeutic advantages in healing of surgical wounds via the stimulation of anti-bacterial effects, reducing necrotic tissue and promotion of epithelialization [146]. Also,

ZnO/ Bioglass® 45S5 has been used as a coating material for anti-bacterial application. It was shown that an increase in ZnO content leads to the increase in anti-bacterial efficacy against Escherichia coli bacteria [171].

Coughlan et al., investigated the synergic effect of silver and zinc ions in glasses of the composition of $56.04SiO_2$-$10.87Na_2O$-$(33.09-X)ZnO$-XAg_2O; where x = 0, 0.33, 0.66 and 0.99 mol%, on anti-bacterial activity against Staphylococcus aureus and Pseudomonas aeruginosa bacteria [172]. It was demonstrated that anti-bacterial activity enhanced by adding silver to the glass, and further enhanced when silver content increased from 0.33 to 0.66 mol%. However, a further increase in silver content (from 0.66 to 0.99 mol%) did not result in further enhancement in anti-bacterial activity. It was concluded that, for this glass formulation, the efficacy of silver on anti-bacterial activity is limited. Additionally, in another study, it was shown, the same glass formulation with 0.33 mol% silver content had inhibitory effect on Pseudomonas aeruginosa biofilm formation [173].

Yang et al., studied the efficacy of the Bioglass® 45S5, 13-93B3 and zinc/copper-doped 1605 ($6Na_2O$-$12K_2O$-$5MgO$-$20CaO$-$51.6B_2O_3$-$4P_2O_5$-$0.4CuO$-$1ZnO$ in wt%)) borate-based glass fibers in wound healing, in vitro [135]. The proliferation and migration rate of CCL-110 human skin fibroblast cells on glasses were measured to evaluate healing effects of the glasses. It was shown that under a dynamic flow rate, there were higher cell proliferation and migration rates with the 13-93B3 and 1605 when compared to Bioglass® 45S5 [135]. Cell proliferation and migration was increased with zinc/copper doped borate-based glasses, also under dynamic flow conditions [135]. Since these two borate glass compositions had significant healing effects on the skin defects, they were used as a wound dressing (DermaFuse, Mo-Sci Corporation, USA) for diabetic patients with chronic, open wounds (candidates for amputation) [174]. In order to perform a small clinical study, wounds were covered with glass fibres, and replaced every 2 to 3, or 5 to 7 days. It was reported that healing capacity of borate glass fibers were similar as current healing approaches such as negative-pressure, but at a reduced cost. It was shown, 13-93B3 formulation has higher collagen production and 1605 composition has higher anti-bacterial activity. On the other hand, DermaFuse did not indicate positive healing effects on the wounds caused by radiation (such as wounds as a result of cancer treatments) [174].

2.4.6.4.2 Angiogenesis

It has been shown that zinc has the ability to enhance angiogenesis. Zinc ions are components of superoxide dismutases (SOD enzyme) that convert the superoxide (O^{2-}) to hydrogen peroxide (H_2O_2) [175]. Also it has been demonstrated that the incorporation of zinc oxide can stimulate angiogenesis [142] as it can chemisorb O^{2-} from oxides and in contact with moisture (water molecule) forming hydrogen peroxide and enhancing wound healing [142]. Based on the previous studies, zinc is highly oxygen reactive and it was shown that it can stimulate endothelial cell proliferation and enhance angiogenesis [142]. Alina et al., studied the effect of melt derived zinc doped Bioglass® 45S5 (with 5 and 20.2 wt% zinc) on endothelial cells [143]. It was shown that the incorporation of zinc in the glass structure decreases the degradation rate resulting in a less increase of pH in the medium. In addition, a high concentration of zinc (20.2 wt%) was found to be toxic, inhibiting cell proliferation [143]. On the other hand, the 5 wt% zinc doped glass was of a lower dissolution rate, when compared to undoped glasses allowing for cell proliferation [143].

2.4.7 Summary

When the body cannot heal the wound by its natural regeneration processes, there is a need to stimulate and accelerate the healing process. The control of infections and ability to vascularize are two crucial factors that contribute to successful wound-healing. Recently BGs (silicate-, phosphate-, and borate-based glasses) have been shown to activate the genes expressed during wound healing such as VEGF for angiogenesis, FGF, fibronectin receptor, and vascular cell adhesion protein. Since BGs generally contain CaO as a glass network modifier in their structure, it has also been shown that Ca^{2+} ion release can promote the migration of epidermal cells and the formation of blood clots. Additionally, the increase of local pH attributable to the dissolution of silicate- and borate-based glasses may contribute to an anti-bacterial effect. More importantly, it has been demonstrated that bioactive and soluble glasses can be doped with various metallic oxides for local and controlled inorganic therapeutic delivery (Ag^{+}, Cu^{2+}, Ga^{3+}, and Zn^{2+}) which have the potential to promote the healing of a wound site. Silver and gallium with anti-bacterial properties against E. coli, S. aureus, and P. aeruginosa (which are associated with wound infections and biofilm formation), zinc with its anti-inflammatory as well as angiogenesis stimulatory abilities, and copper with angiogenesis stimulatory abilities as well as anti-bacterial properties have been investigated for wound healing applications. Also, research has demonstrated that sol-gel–derived

glasses are more effective than their melt-quench-derived equivalents due to their inherent porous structure and higher surface area. In conclusion, ionic doping of bioactive and soluble glasses provides promising opportunities for wound-healing applications.

3 Statement of the Problem

Bioactive glasses exhibit great potential in therapeutic applications by providing a wide compositional range and solubility rates that can be exploited according to the desired biological response. However, it is critical to characterize the physico-chemical properties of glasses prior to analyzing their biological performance for a specific application. Therefore, finding an accurate, reliable and rapid method to evaluate their reactivity is of great interest. Conventional methods, such as measurement of weight loss under long-term immersion in aqueous media lack the ability to consistently, reliably and objectively measure and predict glass reactivity. To overcome these limitations, techniques such as DVS have shown promising results for investigating glass reactivity and bioactivity [24]. In this PhD research, DVS was proposed to investigate the immediate aqueous interaction of glasses as an indicator of reactivity/bioactivity. In addition to reactivity/bioactivity of glasses, another crucial parameter is their hydrophilicity/hydrophobicity, which is traditionally measured by techniques such as contact angle measurements. However, contact angle measurements may not be consistent and sensitive enough to evaluate any slight differences in surface properties of glasses due to the minor changes in their chemistry [21-23]. Therefore, in this thesis, it is also proposed that IGC may be utilized to examine the surface energies of glasses more precisely.

Among the more novel recent therapeutic applications of bioactive glasses has been in the area of wound healing, which encompasses broad clinical scenarios, such as the treatment of skin ulcers, burns, surgical, traumatic and chronic wounds [176]. Under normal conditions, the body can naturally heal acute wounds and regenerate the skin tissue. However, in case of chronic wounds, patients suffer from poor healing and are at constant risk of infections [177]. Therefore, there is a need to help the body stimulate and accelerate the healing process through synthetic wound dressings. Bioactive glasses offer distinct advantages as potential wound dressings as their chemistry can be tuned to have controllable delivery of ions which trigger the body's natural healing mechanisms [11, 12]. Among the investigated compositions, borate-based bioactive glasses show potential attributable to their higher dissolution rate in contact with biological fluid when compared to silicate-based glasses, in particular [84, 178]. Previously, it has been shown that borate glasses can stimulate angiogenesis and enhance the wound healing process, though their mechanisms which are not yet fully understood [84, 178]. In addition, in 2016, a melt-quench derived borate-based glass microfiber wound dressing (MIRRAGEN™, ETS Wound Care LLC,

USA) received Food and Drug Administration approval for acute and chronic wound healing [10]. Extensive research has also demonstrated that sol-gel derived glasses are more effective than their melt-quench derived equivalents in biomedical application due to their nano-porous structure and higher surface area [112]. In addition, since wound infection is a major problem in chronic wounds, the use of an anti-bacterial agent may prevent this, and also decrease the inflammation stage of healing process. While it is widely agreed that silver has an anti-bacterial effect and can kill bacteria through its binding to DNA and RNA, the dose of silver ions and their release rate determine their efficacy in wound healing [179]. For example, elevated concentrations are toxic to mammalian cells [151] and their use in pure silver salt form can cause damage to skin tissues [151]. As a result, by using glass technology, silver toxicity on mammalian cells may be reduced through controlled ion delivery. To meet this goal, novel sol-gel derived borate-based glasses doped with Ag_2O were developed to potentially accelerate the healing of chronic wounds. Thus, this dissertation focused on the fabrication and *in vitro* characterization of novel silver doped sol-gel derived borate glasses for wound healing and skin repair.

4 45S5 Bioactive Glass Reactivity by Dynamic Vapour Sorption

DVS as a relatively new technique requires more studies to evaluate its potential in investigating glass reactivity and bioactivity. Thus, the objective of Chapter 4 is to describe the characterization of BG: Bioglass® 45S5: (46.1)SiO_2-(26.9)CaO-(24.4)Na_2O-(2.6)P_2O_5 (mol %) based with three different average particle sizes and their resultant structural, textural, reactive, and bioactive properties. This work was reported in a manuscript published in the *Journal of Non-Crystalline Solids* and is reproduced below.

45S5 Bioactive Glass Reactivity by Dynamic Vapour Sorption

Shiva Naseri[1], William C Lepry[1], Wei Li[2], Kristian E Waters[1], Aldo R Boccaccini[2], Showan N Nazhat[1]*

[1]Department of Mining and Materials Engineering, McGill University, Montreal, QC, Canada
[2]Institute of Biomaterials, University of Erlangen-Nuremberg, 91058 Erlangen, Germany

*corresponding author showan.nazhat@mcgill.ca

KEYWORDS: DVS (dynamic vapour sorption), Bioglass, Bioactive glass, Bioactivity, Solubility

Abstract:

Reactivity in an aqueous medium is a key parameter for determining the potential bioactivity (*i.e.,* the ability to form a bond to bone) of bioactive and soluble glasses. In this study, dynamic vapour sorption (DVS), a gravimetric technique that measures vapour sorption under controlled relative humidity (RH) and temperature, was used to investigate the short-term aqueous interactions of Bioglass® 45S5 (BG). Specifically, DVS was applied to monitor the sorption characteristics of BG particles of three different sizes exposed to variable RH between 0 and 90%. In addition, the effect of directly exposing these glasses to 90% RH for up to 24 h and its effect on the structural and morphological properties was analysed. Attributable to their larger surface areas, smaller BG particles adsorbed more vapour, and consequently underwent larger total and final mass percent changes as well as greater extent of surface transformation. Precise vapour sorption rates, determined using DVS, were correlated with BG particle surface area and initial rate of ion release when immersed in deionized water, thus demonstrating the ability of DVS to accurately predict reactivity and potential bioactivity.

4.1 Introduction

There is extensive literature on bioactive glasses for potential biomedical applications, however only a few compositions have been approved by the USA Food and Drug Administration (FDA) for clinical use, of which Bioglass® (BG) 45S5 [composition (wt%): $(45)SiO_2$–$(24.5)Na_2O$–$(24.5)CaO$–$(6)P_2O_5$] is considered as the "gold standard" [1, 35, 180]. Since its original conception by Larry Hench, over the past four decades the bioactivity of BG has been extensively studied [26, 83, 181]. Essentially, when BG is placed in physiological fluid, a layer of hydroxy-carbonated apatite (HCA) is formed on the surface, which has been shown to promote bonding to bone tissue [2]. The formation of the HCA layer is initiated (within the first few hours) by the release of ions from the glass through its aqueous interactions. The rate of ion release is dependent on a number of factors, such as the solubility (and composition) of the BG particles [2], the pH of the external environment [16], as well as the glass particle size and surface characteristics. These latter characteristics have been demonstrated to also play important roles as large specific surface areas enhance bioactivity allowing for faster ion release and higher levels of protein adsorption [182]. Nanostructured surface features, on the other hand, are also thought to improve cellular responses and thus better promote quicker tissue integration and regeneration [183-185]. Therefore, the understanding of the short-term aqueous interactions of bioactive glasses is essential in determining, and potentially tailoring their bioactivity towards a desired host response.

Traditionally, the reactivity of BGs is determined by measuring mass change and/or ionic species released when aged in either water [16], simulated body fluid (SBF) [56], TRIS buffer [57], or non-buffered Dulbecco's Modified Eagle's Medium [58], over a period of days to weeks [16]. However, some of these methods (*e.g.,* SBF) have been a source of controversy and considered to be subjective when assessing the bioactivity of a material [60]. In addition, it has recently been shown that the TRIS buffer used to prepare SBF can greatly distort the bioactivity assessment [59]. Alternatively, it has been proposed that the potential reactivity of a glass structure can be determined by calculating its network connectivity [61] where a network connectivity between 2 and 2.6 can be considered as optimal [186], whereas > 2.6 is less optimal due to the resistance to dissolution [187]. With the ability to better model interatomic arrangements, a more recent assessment puts BG network connectivity at 2.12 [187]. However, it is also recognised that network connectivity is just one factor to consider when assessing bioactivity and there are exceptions to these rules.

This current debate in literature opens up opportunities for faster, potentially more accurate routes to determine the reactivity of a bioactive material. Dynamic vapour sorption (DVS) is a gravimetric technique that measures vapour sorption (*i.e.,* change in mass) by a material under controlled variable relative humidity values. DVS, which has mainly been used in the pharmaceutical [62] and food science [63] fields, has recently been used to analyse the reactivity and aqueous interactions of soluble phosphate based glasses [188]. In addition to more accurately measuring mass changes in real-time, DVS is also more rapid than traditional submersion methods [188]. Furthermore, this technique potentially allows for BG-aqueous reactions without the loss of hydrated material that occurs during common reactivity tests, thus enabling the analysis of structural changes occurring at the surface of the glasses.

To this end, this study investigated the potential of DVS in predicting the reactivity BG particles by analysing the short-term aqueous interaction of Bioglass® 45S5. Specifically, DVS was applied to monitor the sorption characteristics of BG particles of three different sizes when exposed to variable relative humidity, from 0 to 90%. In addition, the effect of directly exposing these glasses to 90% RH for up to 24 hours and its effect on the morphological and structural properties were analysed. Finally, the rate of ionic release from the various BG particles in deionized water was correlated with water sorption properties as determined *via* DVS.

4.2 Experimental

4.2.1 Materials

This study investigated the effect of vapour sorption on three different BG samples of distinct particle sizes ("BG-1", "BG-2", "BG-3") prepared from melt-derived Bioglass® 45S5. BG-1 was commercially melt-derived 45S5. BG-2 and BG-3 were prepared from bioactive glass frits of commercial origin as raw materials. First, the 45S5 bioactive glass frits were crushed into granules by jaw crushing (Retsch BB 51, Haan, Germany) by setting a gap width of 0.1 mm. The granules were then sieved into two size fractions (> 32 μm and < 32 μm). Afterwards, the granules of less than 32 μm were milled in a planetary mill machine (Retsch PM 100, Haan, Germany) with ZrO_2 grinding balls in order to further reduce the particle size. After milling, two different particle sizes (BG-2 and BG-3) were generated.

4.2.2 Methods

4.2.2.1 Glass particle size and specific surface area measurements

A particle size distribution analyzer, HORIBA LA-920 (ATS Scientific Ink., Canada) was used to determine the average particle diameter and D_{50} size distribution of the BG samples. The specific surface areas of the glass particles (n = 3) were measured with nitrogen gas adsorption and desorption isotherms collected with a Micrometics TriStar 3000 (Micromeritics Instrument Corporation, USA) gas sorption system. All samples were degassed at 70 °C for 18 h under nitrogen gas to remove contaminants in order to measure accurate mass. The specific surface areas were determined from collected isotherms using the Brunauer–Emmett–Teller (BET) method [189].

4.2.2.2 Vapour sorption

Vapour sorption of the BG particles was examined using a DVS Intrinsic (Surface Measurements Systems Ltd., UK) measuring mass changes (± 0.1 µg) under controlled temperature and humidity. Approximately 50 mg of BG particles was placed in an aluminum pan and inserted into a chamber under atmospheric air and at a constant temperature of 37±0.05 °C. Two methods of analysis were carried out: 1) the RH was increased stepwise at 5% RH up to 90% RH then back down to 0% RH while the relative mass change was measured when equilibrium ($dm/dt < 0.005\%\ min^{-1}$) was reached or after maximum of 4h; 2) the BG particles were immediately exposed to 90% for 24 h, which was then reduced back down to 0% RH for another 24 h. For both methods, the BG particles were dried at 0% RH and 37 °C for 1 h prior to RH increase and each sample was run in duplicate to verify sorption amounts. A Wilcoxon match pair test with 99% confidence confirmed no significant difference between the duplicate runs.

4.2.2.3 Ion release measurements

The release of silicon, calcium, sodium and phosphorous ions from BG particles in deionized water (DIW) was quantified at 37±1 °C, using a constant ratio of 1.5 mg/mL. Measurements were taken in triplicate at 2, 4, and 24 h time points. Aliquots of 10 mL were filtered through a 0.22 µm nylon filter and stored in a 15 mL falcon tube. Silicon release was quantified using atomic absorption with Varian FS240 spectrometer. Ion chromatography (Dionex ICS-5000 chromatograph) was used for calcium and sodium release. An inductively coupled

plasma – optical emission spectrophotometer (Thermo Scientific iCAP 6500) was used to measure phosphorous release. In all measurements, a series of NIST standards were used for calibration values.

4.2.2.4 Scanning electron microscopy (SEM)

SEM was used to analyse the morphological characteristics of the BG particles before and after exposure to vapour sorption. The particles were dried at room temperature for 1 d followed by coating by Au/Pd. An Inspect F50 Field Emission Scanning Electron Microscope (FEI Corporation, USA) was used with an applied voltage of 10 kV.

4.2.2.5 Attenuated total reflectance Fourier transform infrared spectroscopy (ATR-FTIR)

Structural characteristics of the BG particles were examined by ATR-FTIR spectroscopy (Spectrum 400, Perkin-Elmer, USA) before and after exposure to vapour sorption. Post DVS, the particles were analysed after grinding by mortar and pestle. Spectra were collected in a wavenumber range between 4000 and 650 cm^{-1} with a resolution of 4 cm^{-1} using 64 scans per sample. All spectra were baseline corrected and normalized to the total area under absorption bands using Spectrum software (Perkin-Elmer, USA).

4.2.2.6 X-ray diffraction (XRD)

Glass powders were analyzed with a Bruker D8 Discover X-ray diffractometer (Bruker AXSS Inc., USA) equipped with a CuKα (λ = 0.15406 nm) target set to a power level of 40 mV and 40 mA before and after DVS analysis. Using an area detector, 4 frames of 20° were collected from 10 – 80 2 theta (°) and merged in post processing. Phase identification was carried out using X'Pert Highscore Plus (PANalytical, Netherlands).

4.3 Results

4.3.1 BG particle size and surface area measurements

Table 4.1 provides the particle size and surface area values of the different BG samples showing the trend of increasing surface area with smaller particle size.

Table 4. 1: BG particle size and specific surface area measurements.

Sample	BG-1	BG-2	BG-3
Avg. diameter (μm)	5.02 ± 0.14	24.73 ± 1.88	57.37 ± 3.64
D_{50} (μm)	4.94 ± 0.20	19.61 ± 1.24	26.28 ± 0.80
BET surface area (m^2/g)	2.56 ± 0.08	0.68 ± 0.04	0.19 ± 0.06

4.3.2 Exposing the BG particles to different relative humidity percentages

DVS was used to gravimetrically measure the sorption and desorption of water vapour of the BG particles when exposed to different RH values. Figure 4.1a shows the sorption and desorption isotherms of the different sized BG particles when exposed to a systematically increasing and decreasing values of RH. The sorption phase of all three particles sizes were characterised by an initial small increase in mass which at a certain % RH value, termed the inflection point (the % RH when the mass change increased more than 80%), demonstrated a more rapid rate of mass increase when the RH was increased up to a maximum of 90%. However it should be noted that the mass readings for BG-1 from 75 to 90% RH, along with BG-2 and BG-3 from 85% to 90% RH, did not reach to equilibrium after 4 h and therefore do not represent true isotherm values. Nevertheless, BG-1 particles demonstrated the highest level of sorption at 90% RH, an increase of 23.34%, along with the highest final mass change, indicating an increase of 15.24% at the end of desorption cycle. The inflection points for BG-1, -2 and -3 were calculated at 65, 70 and 80% RH, respectively showing an inverse relationship with surface area. Figure 4.1b shows the inflection point %RH values follow a decreasing exponential trend with BG surface areas, where an exponential function with $R^2 = 1$ was fitted to the data. On the other hand, both the mass changes at 90% RH (end of sorption phase) and at 0% RH (end of desorption phase) increase linearly with surface area.

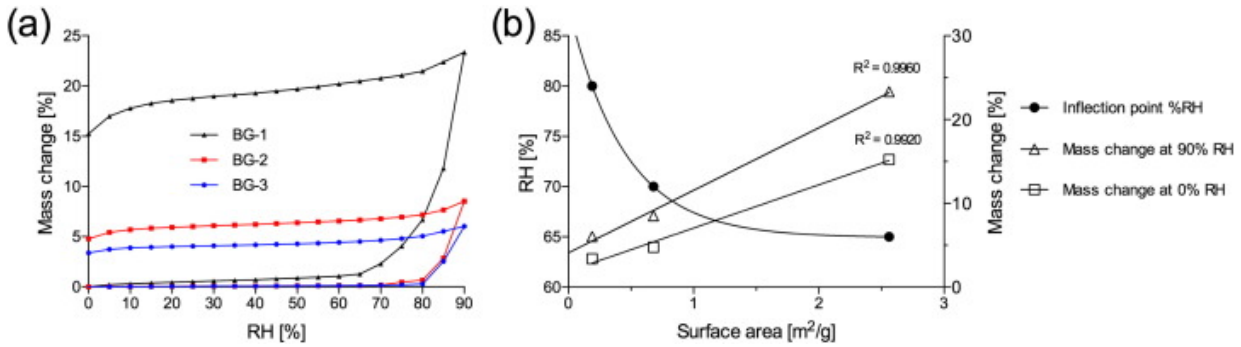

Figure 4. 1: (a) One full vapour sorption and desorption isotherm cycle of the different BG particle sizes exposed to increasing and decreasing %RH where the RH was changed by successive steps of 5% over a range of 0 to 90%. (b) Correlation between BG particle surface area and inflection point %RH as well as % mass change at 90% (end of sorption phase) and 0% (end of desorption phase). There was a decrease and increase in inflection point %RH and mass changes with BG surface area, respectively.

4.3.3 Sorption kinetics at 90% relative humidity

In order to investigate the effect of particle size on the sorption kinetics, the BG samples were directly exposed to 90% RH for 24 hours and followed by exposure to 0% RH for a further 24 hours (Figure 4.2a). The sorption phase of all three particle sizes at 90% RH was characterized by a relatively rapid initial rate of increase in mass, which was followed by a continuous slower rate of increase up to 24 hours. BG-1, with the largest surface area demonstrated the highest rate and percentage increase in mass (>50%). Desorption for 24 hours at 0% RH was characterised by a rapid decrease in mass with all three BG particle sizes approaching equilibrium final mass after 3.5, 1.5, and 1 hours for BG-1, BG-2 and BG-3, respectively and BG-1 with the highest surface areas, demonstrating the greatest increase in final mass. Figure 4.2(b) shows the relationship between BG particle surface area and the initial rate of sorption (calculated as the rate of mass change between 0 and 2 hours of exposure to 90% RH) as well as the static rate of sorption (calculated as the rate of mass change between 12 and 24 hours of exposure to 90% RH).

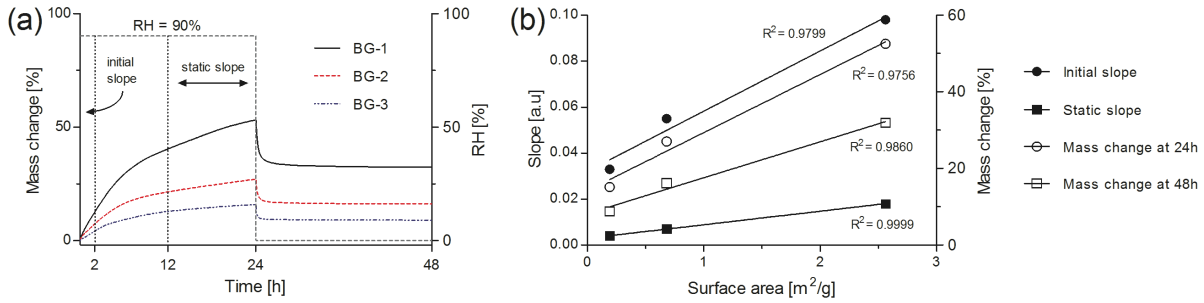

Figure 4. 2: (a) Vapour sorption and desorption curves of the different BG particle sizes directly exposed to 90% and subsequently to 0% RH for a further 24 hours. (b) Correlation between BG particle surface area and initial (calculated between 0 and 2 hours) and static (calculated between 12 and 24 hours) rates of mass change, as well as mass change at 24 hours (end of sorption phase) and 48 h (end of desorption phase). Mass changes after vapour sorption as well as after desorption increased with BG surface area.

4.3.4 Ion release correlated with vapour sorption

Figure 4.3a-d show the release of Si^+, Ca^{2+}, Na^+, and P^- ions, respectively, at 2, 4 and 24 h time points when immersed in DIW. The release profiles of Ca^{2+}, Na^+ and Si^+ were found to be highest for BG-1 when compared to BG-2 and BG-3. In contrast, the release of P^- from BG-1 samples was lower than those of BG-2 and BG-3. In addition, the rate of Na^+ release was greater than that of Ca^{2+}, which were similar to what has been previously reported for Bioglass® [7]. The higher pH values in the presence of BG-1 verify the ion release data where greater extent of ions were released from the smaller particle sized sample, specifically Na^+ [7] but also Ca^{2+} (Figure 4.3e). Figure 4.3f shows that the initial slope of ion release (calculated between 0 and 2 hours) can be correlated with the initial rate of sorption (calculated as the rate of mass change between 0 and 2 hours of exposure to 90% RH), which further confirms the ability of DVS to accurately predict and measure initial reactivity.

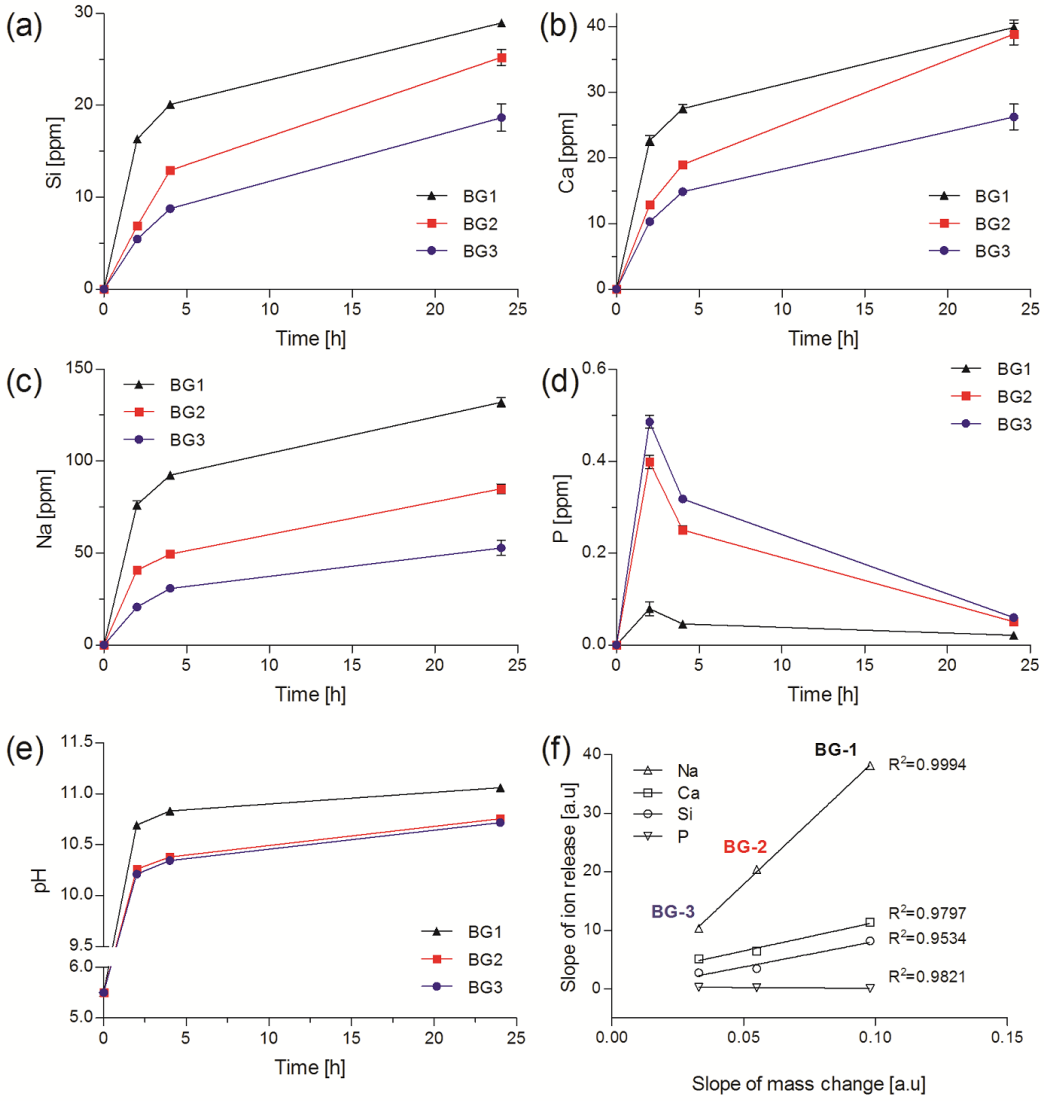

Figure 4. 3: (a) silicon, (b) calcium, (c) sodium, and (d) phosphorus ion release from the BG particles in DIW. (e) pH change as a function of BG dissolution in DIW. (f) Initial ion release (slope calculated between 0 and 2 hours in (a), (b) and (c)) versus initial rates of mass change (calculated between 0 and 2 hours at 90% RH in DVS).

4.3.5 Morphological analysis

Figure 4.4 details SEM micrographs of the BG-1, -2, and -3 particles before and after vapour sorption (24 hours at 90% RH), respectively. Figure 4.4a-c show the glasses with well distributed particle sizes and defined surfaces prior to exposure to vapour sorption. After exposure to 90%RH (Figures 4.4d-f), the glass particles become more rounded suggesting a surface

transformation had taken place. In addition, there was a noticeable level of particle agglomeration which commonly occurs to particles in humid environments [190].

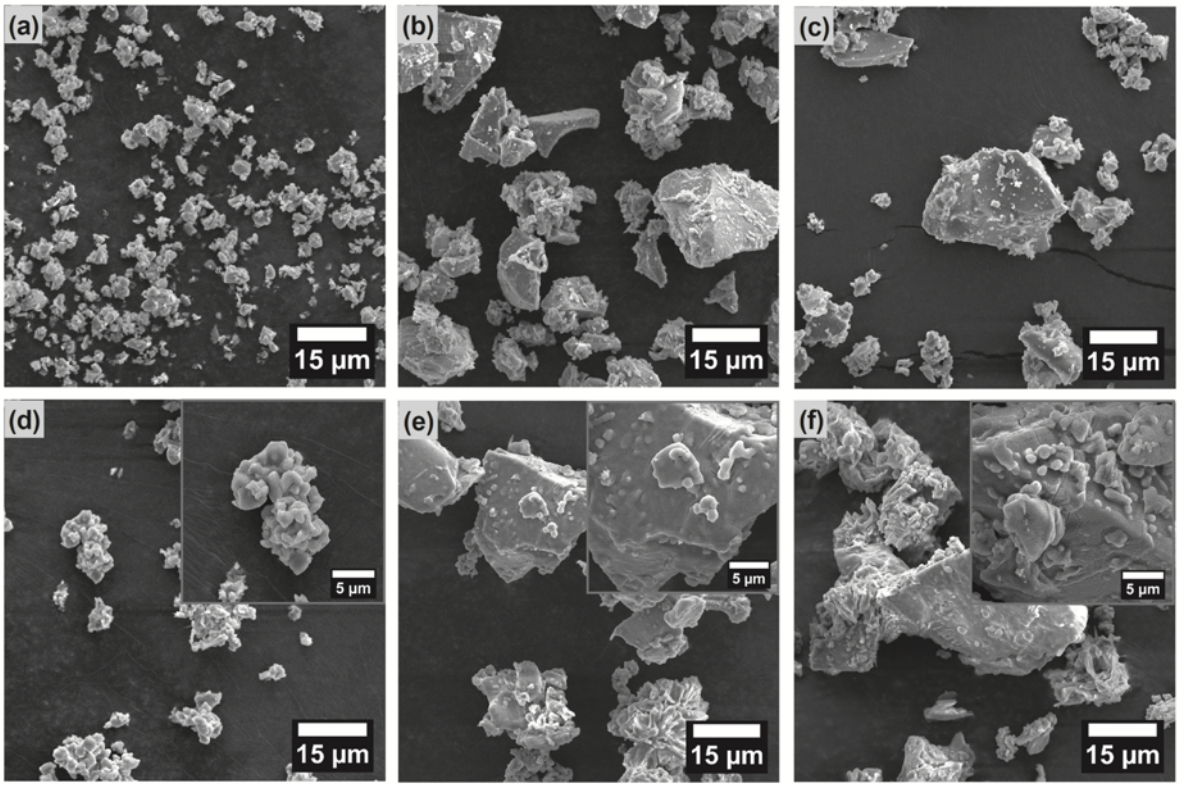

Figure 4. 4: SEM micrographs of the different BG particle sizes before (a, b, and c for BG-1, BG-2, and BG-3, respectively) and after vapour sorption (d, e, and f for BG-1, BG-2, and BG-3, respectively. Insets showing higher magnification).

4.3.6 Chemical analysis

Figure 4.5a&b show the ATR-FTIR spectra of the various BG particles before and after exposure to vapour sorption (24 h at 90% RH), respectively. All as-made BG particles showed typical peaks associated with Bioglass® with carbonate ν_3 and ν_2 bands at 1454 and 867 cm^{-1}, respectively while absorbance of phosphate and silicate groups was present at 998 cm^{-1} [7]. The presence of a carbonate ν_3 band may be attributed to the reaction of Ca^{2+} from the particle surface with atmospheric CO_2 [7]. The vibration at 906 cm^{-1} is attributed to Si-O nonbonding oxygen peak and a weak peak at 740 cm^{-1} is attributable to the absorbance of Si-O-Si δ bond [191, 192]. Figure 4.5b shows FTIR spectra of BG particles after exposure to vapour sorption. The development of

two broad peaks centering at 3400 cm^{-1} (in the range of 3000 to 3800 cm^{-1}) and 1660 cm^{-1} can be attributed to the absorption of water molecules (OH-group) during conditioning at 90% RH [193]. In addition, the appearance of double carbonate peaks at 1415 and 1460 cm^{-1} indicates the crystallization of the carbonate [194]. Furthermore, the formation and growth of the carbonate ν2 at 872 cm^{-1} has been previously reported when Bioglass® was aged in DIW [16]. The absorbance of phosphate peaks is increased (sharper peak), mainly for BG-1 particles, suggesting its increased reactivity attributable to the higher specific surface area. On the other hand, the presence of Si-O-Si δ bond at 740 cm^{-1} and weak Si-O-Si ν1 peak at 1110 cm^{-1} indicates that part of silica is turned to the silica reach layer [192].

Figure 4.5c&d show the XRD patterns of the BG particles before and after vapour sorption (24h, 90% RH), respectively. The broad humps in Figure 4.5c verify the amorphous nature of the staring material. While the amorphous characteristics remained dominant post 24 hours of exposure to 90 %RH, the XRD patterns indicated the onset of crystallization (Figure 4.5d). Phase identification indicated the formation of $CaSiO_4$ (JCPDS 6-0476 and 36-0642) and NaP (JCPDS 04-004-2805) for BG-1. BG-2 indicated the formation of $Ca_{10}Na(PO_4)_7$ (JCPDS 045-0339) and CaP (JCPDS 04-007-3786). Similar to BG-2, BG-3 also showed the formation of $Ca_{10}Na(PO_4)_7$ (JCPDS 045-0339) along with $NaCaPO_4$ (JCPDS 29-113) and CaP (JCPDS 04-004-2805). However, not all peaks could be identified.

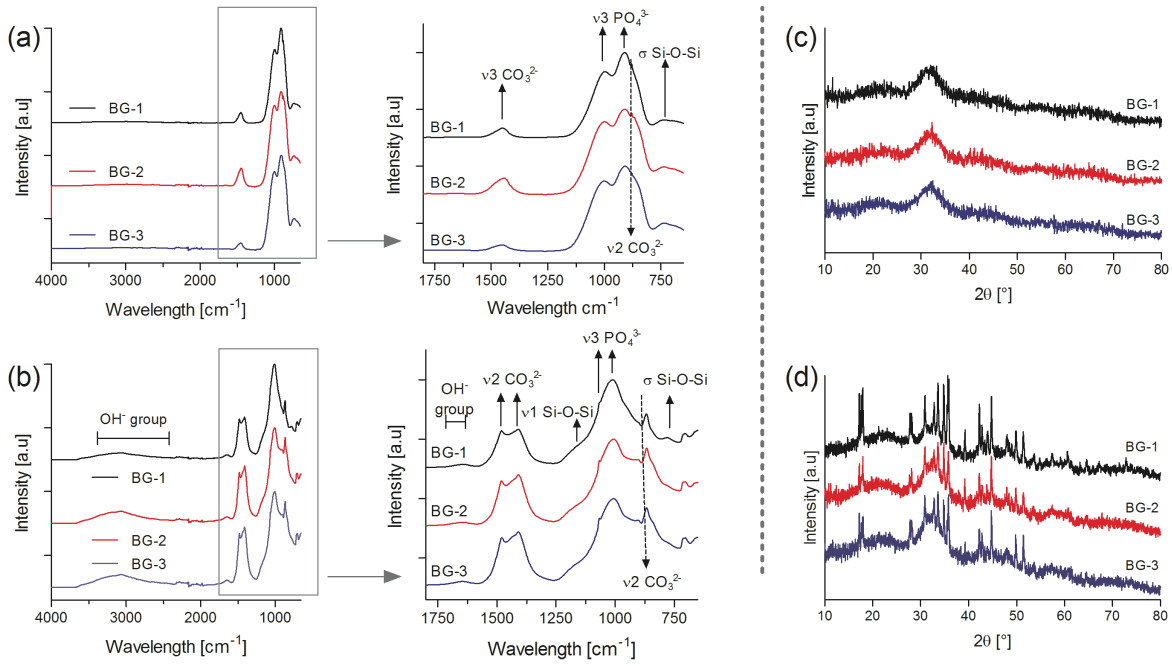

Figure 4. 5: FTIR spectra and XRD patterns of the different BG particles before and after vapour sorption. (a) FTIR before vapour sorption and (b) after 24h at 90%RH and followed by 24h at 0% RH, (c) before vapour sorption, d) after 24h at 90% RH followed by 24h at 0% RH.

4.4 Discussion

Understanding the immediate aqueous interactions of BG particles has an important role in predicting their reactivity and bioactivity. The aqueous interactions of Bioglass® has been well described [181], where initially there is rapid ion exchange between Na^+ from glass and H^+ from solution. This is followed by soluble SiO_2 release into the solution that forms Si-OH groups at the glass surface and allows for polycondensation reactions of Si-OH to form a silica rich layer on the surface [181]. Then, a calcium-phosphate layer is formed by migration of Ca^{2+} and PO_4^{3-} ions to the silica rich surface layer of the glass. The growth and crystallization of the calcium-phosphate layer is controlled by the Ca^{2+}, PO_4^{3-}, OH^- and CO_3^{2-} from solution [181]. In this study, the combination of water vapour and atmospheric CO_2 through the DVS technique, along with the release of ions from the BG particles, contributed to the formation of the different phases on the BG surface.

In this work BG particles were characterized with DVS as a precise method for calculation of vapour sorption isotherms in order to evaluate the kinetics of aqueous reactions of BGs of different particle sizes. During the initial adsorption phase, the total water content adsorbed up to 60% RH for BG-1, BG-2 and BG-3 were 0.5488, 0.0650 and 0.0671 mg water, respectively, indicating that the BG-1 particles adsorbed approximately 8 times more water over the same period. Furthermore, the significant increase in mass change above the inflection point can be attributed to deliquescence. It has been shown for crystalline salts that a sudden dissolution occurs above the deliquescence RH, whereas in amorphous materials, deliquescence takes place more gradually [195, 196]. However, recent work has demonstrated a dramatic increase in mass change in vapour sorption isotherm with phosphate-based glasses. It was proposed that this was due to deliquescence and the formation of a saturated layer at the surface of dissolution products of glasses [188]. In this study, a similar trend was observed with the BG samples and thus the inflection point can be attributed to the deliquescence RH of BG of distinct surface areas.

To better understand the vapour sorption kinetics of BGs, the glasses were examined by direct exposure to 90% RH for 24 hours followed by 24 hours at 0% RH. The initial and static rates of sorption, calculated for BG-1, were almost three times greater than those of BG-3. Similar correlations were demonstrated when considering the mass changes after vapour sorption as well as after desorption, which increased with BG surface area. This linear regression demonstrated the ability of the DVS technique in accurately correlating the sorption rate and mass change with surface area of a BG particle which is known to be critical in determining reactivity, especially in shorter time frames [185, 197].

Ion release rates were measured in DIW to investigate any possible correlations with mass changes via DVS. The ion release rates were increased with a decrease in particle size, except for phosphorous, which decreased and may be attributed to the formation of calcium-phosphate precipitate [16]. The linear relationship between ion release rates and sorption rates showed the ability of DVS in predicting the reactivity of BG particles, as has been previously described for phosphate-based glasses [188].

Structural and chemical characterizations indicated alterations on the surface of BG particles after vapour sorption. FTIR spectroscopy after vapour sorption showed the formation of O-H groups, which remained even after conditioning at 0% RH for 24 hours. XRD diffractograms also indicated changes in the amorphous/crystalline structure of the BGs after vapour sorption.

Furthermore, these peaks appeared to be sharper for BG-1 particles which suggested greater extent of crystallization, and thus potentially more rapid surface transformation [193, 198].

4.5 Conclusions

In this study, dynamic vapour sorption was used to analyse the short term aqueous interactions of Bioglass® 45S5 particles of different sizes. Smaller particles adsorbed more vapour due to their larger surface areas, and consequently underwent larger total and final, mass percent changes. Precise rates of sorption, as determined by dynamic vapour sorption were correlated with particle surface area and the initial ion release data from the Bioglass® samples immersed in deionized water; demonstrating the potential of this technique in accurately predicting the kinetics and mechanisms of aqueous interaction of bioactive glass particles of distinct surface areas.

Acknowledgements

This study was supported by the Canadian Natural Sciences and Engineering Research Council, Canada Foundation for Innovation, Québec Ministère de l'Enseignement supérieur, de la Recherche, de la Science et de la Technologie (MESRST) and McGill University Faculty of Engineering Hatch Faculty Fellowship for S.N.N. Partial funding from the Bavarian-Québec-Project "Mesenchymal stem cell seeded nanocomposite constructs for bone tissue engineering" through the Québec MESRST and the Bavarian Research Alliance is gratefully acknowledged. W. C. L. is supported by the McGill Engineering Doctoral Award and S.N. is supported by Werner Graupe International Fellowships as a part of McGill Engineering Doctoral Award. In addition, the Canada Foundation for Innovation (CFI) is acknowledged for the support in purchasing the DVS Intrinsic, through the Leadership Opportunity Fund (#26517).

5 Surface Properties and Reactivity of Phosphate-based Glasses by Inverse Gas Chromatography and Dynamic Vapour Sorption

IGC and DVS as new techniques require more investigation to examine their potential to characterize glass reactivity and surface properties. Thus, the objective of Chapter 5 is to describe the characterization of four PGs doped with both SiO_2 and TiO_2 ($50P_2O_5$-$40CaO$-$xSiO_2$-$(10 - x)$ TiO_2, where x = 7, 5, 3, and 0 mol%) and the effect of silica content on the surface and bulk properties of PGs.

Surface Properties and Reactivity of Phosphate-based Glasses by Inverse Gas Chromatography and Dynamic Vapour Sorption

Shiva Naseri, William C. Lepry, Maziar Shah Mohammadi, Kristian E. Waters, Showan N. Nazhat*

Department of Mining and Materials Engineering, McGill University, Montreal, QC, Canada

*Corresponding author showan.nazhat@mcgill.ca

KEYWORDS: Phosphate-based glasses, Solubility, DVS (dynamic vapour sorption), IGC (inverse gas chromatography)

Abstract:

The chemical durability of phosphate-based glasses (PGs) in an aqueous environment is a key parameter in determining their properties such as dissolution and ion release rates as well as their ultimate performance *in vivo*. In this study, inverse gas chromatography (IGC) and dynamic vapour sorption (DVS) were used to investigate the short-term aqueous interactions of PGs doped with both SiO_2 and TiO_2 ($50P_2O_5$-40CaO-xSiO_2-(10 − x) TiO_2, where x = 7, 5, 3, and 0 mol%). Specifically, IGC was used to evaluate the surface properties of the PGs by measuring the solubility parameter and surface energy. Good correlation between the polar parts of both the solubility parameter and surface energy with glass transition temperature (T_g) and dissolution rates demonstrated the potential of IGC in predicting the bulk and surface properties of the PGs. Additionally, DVS was applied to monitor the sorption characteristics of the PG particles when exposed to incrementally increasing RH between 0 and 90%. All compositions indicated two different regions of sorption, an initial small increase in mass up to approximately 65 % RH and a second dramatic increase in mass up to 90%. The %RH value at the transition in the sorption behaviour was termed as the inflection point and believed to be associated with deliquescence phenomena. The rate and extent of mass change in the glasses was also measured when directly exposed to 90% RH for up to 24 h. A correlation was found between the inflection point and rate and extent of mass change in the PGs with T_g and dissolution rates. An increase in glass silica content resulted in greater vapour sorption rates, as well as extent of mass change. NMR data of the PGs post exposure to vapour demonstrated that increased SiO_2 content disrupted the glass network and formed protonated phosphate species. FTIR-ATR verified the presence of non-reacted water molecules in the PGs depending on SiO_2 content. Moreover, there was a good correlation between the polar parts of both the solubility parameter and surface energy (as measured through IGC) and inflection points (as measured through DVS), demonstrating the ability of both techniques in predicting the dissolution properties of PGs as consequence of alterations in their chemistry and durability.

5.1 Introduction

Phosphate-based glasses (PGs) have been studied for a wide range of potential biomedical applications since their degradation and ion release rates can be controlled through their chemistry [8]. These glasses have been investigated for bone regeneration [4], repairing damaged nerves [199, 200], angiogenesis and cell differentiation [201], anti-bacterial and wound healing [94, 96, 99] as well as for helping engineer human craniofacial muscle [202]. PG dissolution occurs by an initial ionic exchange process between the glass and aqueous solution to form a hydrated layer on the glass surface, which is followed by the breakage of P-O-P bonds due to the presence of water molecules and H^+ resulting in the degradation of the glass network [89, 90]. The dissolution rate depends on the chemical durability, which is dictated by a number of factors including bulk composition, surface and textural properties (*e.g.,* specific surface area and porosity) [13-15]. Determination of dissolution rate in glasses often occurs via submersion in an aqueous solution, *e.g.,* deionized water (DIW) [16], cell culture medium [58], or simulated body fluid (SBF) [56] for predetermined time points at which the glasses are removed and weighed to measure the rate of weight loss.

The main network former of PGs is P_2O_5 consisting of a phosphate tetrahedron as the building unit. Since phosphorous has a valence of 5^+ its tetrahedron unit has three single oxygen bonds and one double bonded oxygen [6]. Thus, understanding the effect network modifiers is of great importance as this will affect the glass bonding and thus influence the chemical durability and degradation properties.

Glass transition temperature (T_g) is a parameter used to indicate chemical durability in which higher T_g values suggest an increase in glass cross-linking density as well as higher volumetric density leading to a more durable glass. In general, incorporation of cationic oxides (*e.g.,* CaO, CuO, TiO_2 and Fe_2O_3) into PGs increases the glass durability as well as T_g due to their cross-linking effect [4, 21, 22, 89]. These in turn have been shown to decrease the degradation rates, control ionic release through dissolution and subsequently enhance biological responses in the context of osteoblastic cell proliferation as well as antibacterial [99] and potential angiogenic properties [4, 89]. In contrast, the effect of SiO_2 incorporation into PGs is not yet fully understood. For example, while it has been shown that an increase in silica content in PGs ($50P_2O_5$-30CaO-$(15 - x)NaO_2$-$5Fe_2O_3$-$xSiO_2$, where x = 0, 1, 3, and 5 mol%) increases their T_g and the degradation rates [203, 204]. In contrast, previous work has also shown that, substituting Fe_2O_3 with SiO_2 in

the glass composition ($50P_2O_5$-40CaO-xFe_2O_3-(10-x)SiO_2, where x = 0, 5 and 10 mol%), decreased T_g and volumetric density of PGs and consequently their chemical durability which led to a higher dissolution rate in DIW and phosphate buffered saline (PBS) [205]. Similar findings were reported by substituting TiO_2 with SiO_2 in the glass compositional range ($50P_2O_5$-40CaO-$xSiO_2$-(10 − x) TiO_2, where x = 10, 7, 5, 3, and 0 mol%) which led to a less stable glass structure and higher degradation rate [21]. It was shown that SiO_2 incorporation into PGs decreases the glass chemical durability by disrupting the glass network, and decreases the formation of strong P-O-Ti bonds, which have a direct effect on T_g [206, 207].

Network modifying oxides not only control the bulk properties, but also the surface properties of PGs [64]. Surface energy and the hydrophilic/hydrophobic nature of glasses are traditionally measured *via* contact angle measurements [18-20], which may not be sensitive enough to measure changes in surface properties due to slight changes in glass chemistry [21, 22]. For example, while the substitution of TiO_2 with SiO_2 in PGs led to a decrease in T_g and density, and an increase in glass dissolution, no significant difference was reported between the contact angle measured polar surface energy of the glasses with small incremental increases in SiO_2 content [21]. It was shown that only glasses with highest silica content (up to 10 mol% SiO_2) and no TiO_2 exhibited the highest polar surface energy, which was attributed to the formation of Si-OH groups [21]. To this end, there is a need to better understand and evaluate the capability of the other techniques to overcome the limitations of conventional methods of evaluating the surface properties of PGs.

This study explored the potential of inverse gas chromatography (IGC) as a technique to investigate the surface properties of PGs. IGC is a technique that has been mainly used to characterize the solubility parameters, surface and bulk properties of polymers, pharmaceuticals, minerals and nanomaterials [70]. In the context of bioceramics, it has been suggested that IGC can be used as a rapid and accurate technique to successfully measure and compare the surface energies of various particles and porous, textured morphologies [71]. For example, IGC was utilized to measure the surface energies of rough and porous biosurfaces by comparing synthetic and naturally derived hydroxyapatite samples [25]. It was suggested that biological apatite, derived from bovine trabecular bone, has higher surface heterogeneity with high surface energy domains due to the presence of impurities and surface defects. It was proposed that this apatite is more suitable for protein adhesion and cell attachment when compared to synthetic apatite [25]. The findings of this current study suggested that IGC could be used as a technique to characterize the surface and bulk

properties of bioactive and soluble glass particles. Therefore, the solubility parameter and surface energy of PGs of four different formulations in the compositional range of ($50P_2O_5$-40CaO-xSiO_2-(10 − x) TiO_2, where x = 7, 5, 3, and 0 mol%) were determined via IGC to evaluate the effect of SiO_2 and TiO_2 incorporation into PGs on their chemical durability, solubility and surface properties. The surface property parameters were correlated with T_g and dissolution rates in DIW [21] as well as sorption parameters, used to define their immediate aqueous interaction and determined by dynamic vapour sorption (DVS). DVS, which is a gravimetric technique that measures vapour sorption under controlled variable relative humidity (RH) values, has recently been used to characterize the aqueous interactions of soluble and bioactive glasses [23, 24, 208]. Therefore, the aim of this work was to provide an insight into using the complementary IGC and DVS techniques in predicting the surface properties and reactivity of PGs.

5.2 Materials and methods

5.2.1 PG production

Four different compositions of the melt-quench derived PGs ($50P_2O_5$-40CaO-xSiO_2-(10 − x)TiO_2, where x = 7, 5, 3, and 0 mol%) were produced, as previously reported [21]. Briefly, P_2O_5, $CaHPO_4$, SiO_2 (Alfa Aesar, Canada), and TiO_2 (Sigma-Aldrich, Canada) precursors were dry blended at 350 ºC for 20 min. The precursors were then melted in a platinum crucible, cast in a pre-heated mould, and annealed to remove residual stresses [21]. Melt-derived glass rods were pulverized by mortar and pestle. Afterwards, particles were sieved in the 38 and 45 μm with the specific surface area of 0.124±0.001 m^2/g (for Si7Ti3, n=3), which was measured by a Micromeritics TriStar 3000 (Micromeritics Instrument Corporation, USA) using the Brunauer–Emmet–Teller nitrogen adsorption method [189]. These sieved particles underwent analysis through IGC, DVS, scanning electron microscopy, Fourier transform infrared spectroscopy and x-ray diffraction, as described below. T_g and dissolution data were taken from a previously reported study [21].

5.2.2 IGC

Inverse gas chromatography experiments were conducted in a Surface Energy Analyser, SEA (Surface Measurement Systems Ltd, UK), in which the solubility parameter [209] and surface energy [210, 211] of the various glass compositions were investigated. Approximately 1 g of PG particles (n=2) was loaded into a glass column and all measurements were performed at 37±1°C. Helium was used as a carrier gas with the flow rate of 5 mL/min. Different types of probe molecules, hexane, heptane, octane, ethanol, 1-butanol, 1-propanol, dichloromethane, toluene and acetonitrile (Sigma-Aldrich, Canada) were injected to calculate the dispersive, H-bond and polar part of the solubility parameter analyzed using the SMS-iGC advanced software (SMS Ltd, UK). The retention volume of each probe molecule was measured to calculate the Flory-Huggins interaction parameter. Then, by varying the probe molecule, the solubility parameter (δ), a measure of the square root of the cohesive energy density, was determined from the calculated Flory-Huggins interaction parameter (SMS-iGC Advanced Software performed all calculations) [212, 213]. By choosing different types of probe molecule (non-polar, polar and H-bond), different components of the solubility parameter were also calculated. Additionally, the SEA was utilized to examine surface energy of PG particles (n=3) at 50% surface coverage. The retention volumes were calculated from the retention times from the peak maximum to determine the surface energies. The Schultz method was applied for the dispersive components, and the Della Volpe scale for the specific (polar) components.

5.2.3 Vapour sorption

The interaction of the various PG particles with vapour sorption was analyzed using a DVS Intrinsic (SMS Ltd., UK) by measuring mass changes (± 0.1 μg) under controlled temperature and humidity. Approximately 50 mg of PG particles was placed in an aluminum pan and inserted into a chamber with a constant temperature of 37 ± 0.05 °C. Two methods of analysis were carried out: 1) the RH was increased stepwise at 5% RH up to 90% RH then back down to 0% RH while the relative mass change was measured when equilibrium ($dm/dt < 0.002\%\ min^{-1}$) was reached or after maximum of 4h; 2) the PG particles were immediately exposed to 90% RH for 24 h, which was then reduced back down to 0% RH for another 24 h. For both methods, the PG particles were dried at 0% RH and 37 °C for 1 h prior to RH increase.

5.2.4 Scanning electron microscopy (SEM)

An Inspect F50 Field Emission Scanning Electron Microscope (FEI Corporation, USA) was used to analyse the morphological characteristics of the PG particles before and after exposure to vapour sorption with an applied voltage of 10 kV.

5.2.5 X-ray diffraction (XRD)

Glass particles were analyzed with a Bruker D8 Discover X-ray diffractometer (Bruker AXSS Inc., USA) equipped with a CuKα (λ = 0.15406 nm) target set to a power level of 40 mV and 40 mA before and after DVS analysis. Using an area detector, 3 frames of 23° were collected from 10 – 80 2 theta (°).

5.2.6 Attenuated total reflectance - Fourier transform infrared spectroscopy (ATR-FTIR)

A Spectrum 400 (PerkinElmer, Waltham, MA) in the attenuated total reflection (ATR) mode was used. Spectra were generated with 4 cm^{-1} resolution in the 4000-650 cm^{-1} wavenumber range with 64 scans for each sample.

5.2.7 Nuclear magnetic resonance (NMR)

^{31}P magic angle spinning nuclear magnetic resonance (MAS NMR) spectra were obtained at a radiofrequency of 161.8 MHz on a Varian VNMRS400 spectrometer. Samples were placed in 4 mm rotors. At 180-360° a pulse was applied and 256 scans were accumulated with decoupling of 1H during acquisition to observe protonated phosphate groups.

5.2.8 Statistical analysis

Statistical significance of the solubility parameters between sample means was determined using a Student's t-test at a significance level of $p < 0.05$.

5.3 Results

5.3.1 Surface and solubility properties as measured through IGC

The solubility parameter and surface energy of the various PG compositions were evaluated using IGC to characterize their reactivity (Table 5.1).

Table 5. 1: Solubility parameter and surface energy as determined through IGC. Dispersive part of the solubility parameter (δ_{dis}) as measured by hexane, heptane and octane, polar part of the solubility parameter (δ_{polar}) as measured by toluene, DCM and acetonitrile, H-bond of the solubility parameter (δ_H) part as measured by ethanol, propanol and butanol, and the total solubility parameter (δ_{total}). Dispersive part of the surface energy (SE_{dis}(IGC)), and Polar part of the surface energy (SE_{polar} (IGC)).

Sample	δ_{dis} [(MPa)^0.5]	δ_{polar} [(MPa)^0.5]	δ_H [(MPa)^0.5]	δ_{total} [(MPa)^0.5]	SE_{dis} [mN/m]	SE_{polar} [mN/m]
Si0Ti10	28.21±1.21	13.11±0.26	14.85±0.61	34.49±0.66	32.12±0.17	3.88±0.27
Si3Ti7	25.04±1.67	17.20±0.90*	43.99±4.15*	53.49±4.01*	31.03±2.14	4.65±0.32*
Si5Ti5	23.69±1.43	17.31±0.75*	43.41±1.53*	52.42±1.31*	33.26±0.79	5.13±0.45*
Si7Ti3	29.91±0.95	19.05±0.56*	45.50±4.75*	57.75±3.86*	34.47±0.25	5.37±0.21*

* Statistically significant compared to the Si0Ti10 ($p < 0.05$).

The dispersive component of the solubility parameter did not indicate a specific trend or any statistically significant differences ($P > 0.05$). In contrast, the polar and H-bond components of the solubility parameter of the silica containing PG particles were statistically significant ($P < 0.05$) when compared to that of the Si0Ti10 PG particles. Additionally, the dispersive component of the surface energy did not show any statistically significant difference ($P > 0.05$). However, the polar part of the surface energy of the silica containing glasses was significantly different ($P < 0.05$) when compared to that of Si0Ti10 PG. Figure 5.1 correlates the polar part of the solubility parameter and polar surface energy with T_g (Figure 5.1 a&b) and dissolution rate (Figure 5.1 c&d) of the PG particles [21].

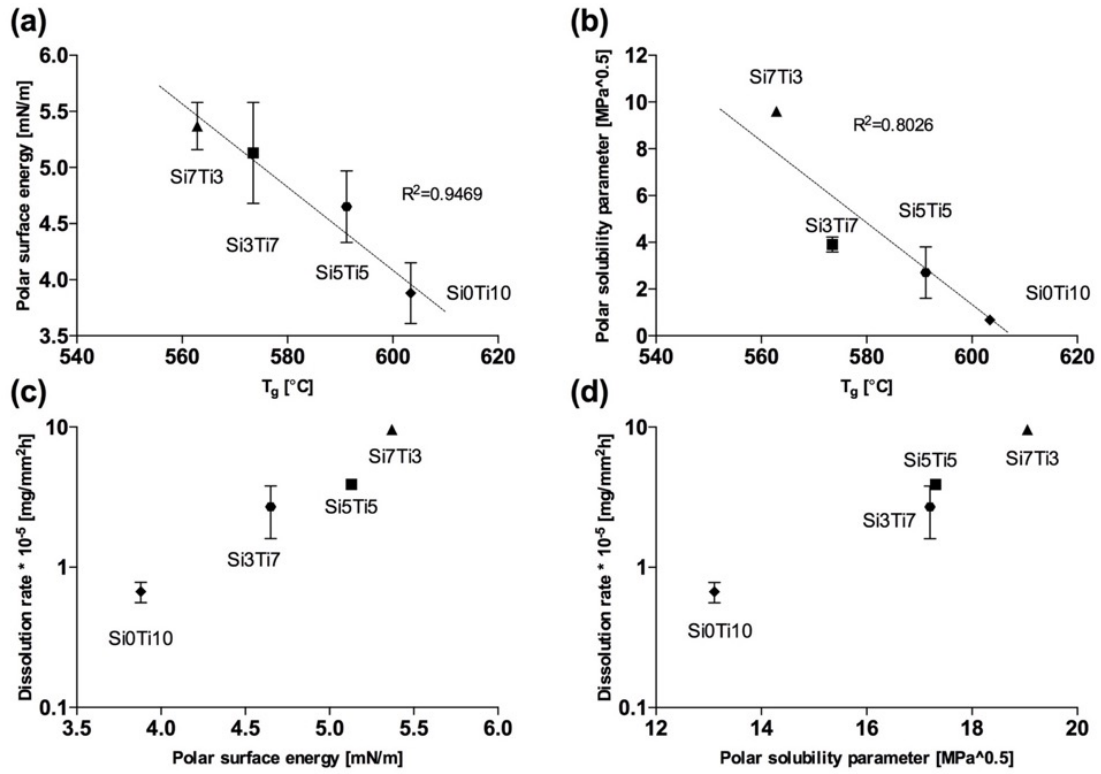

Figure 5. 1: (a) Correlation between the polar part of the surface energy as measured by IGC and glass transition temperature (T_g) [21]. (b) Correlation between the polar part of the solubility parameter as measured by IGC and glass transition temperature (T_g) [21]. (c) Correlation between the glass dissolution rate [21] and the polar part of the surface energy as measured by IGC. (d) Correlation between the glass dissolution rate [21] and the polar part of the solubility parameter measured by IGC.

5.3.2 Vapour sorption

5.3.2.1 Exposing PG particles to different relative humidity percentages

DVS was used to gravimetrically measure the sorption and desorption of water vapour of the PG particles after exposure to different RH values. Figure 5.2(a) shows one full cycle of sorption and desorption isotherms of the four PG compositions with different amounts of silica (0, 3, 5 and 7 mol%) exposed to the variable RH values in the range of 0-90 % RH with a 5 % step size of increase/decrease. The sorption phase of all compositions indicated two different regions; first, an initial small increase in mass up to approximately 65 % RH; secondly, a dramatic increase in mass up to 90%. This sudden inflection point increase was determined as the specific % RH value in which the mass change increased by more than 70% compared to the previous RH% and can be explained by deliquescence phenomena [195, 196]. However, it should be noted that the calculated isotherms do not show a true isotherm since the mass change from 75 to 90% RH

(except for Si0Ti10) did not reach equilibrium after 4 h. The total water content adsorbed up to 60% RH for Si0Ti10, Si3Ti7, Si5Ti5 and Si7Ti3 were 0.016, 0.018, 0.053 and 0.119 mg of water, respectively. The Si7Ti3 particles exhibited the highest total sorption at 90% RH (17.42% mass change). Figure 5.2(b) shows a linear relationship between the inflection point with T_g and glass dissolution rate [21]. Along with T_g, an increase in silica content decreased the inflection point, while it increased the PG dissolution rate. A linear regression (R^2=0.9879) between inflection point and T_g of PGs with different silica contents demonstrated the ability of DVS to provide complementary information on glass durability.

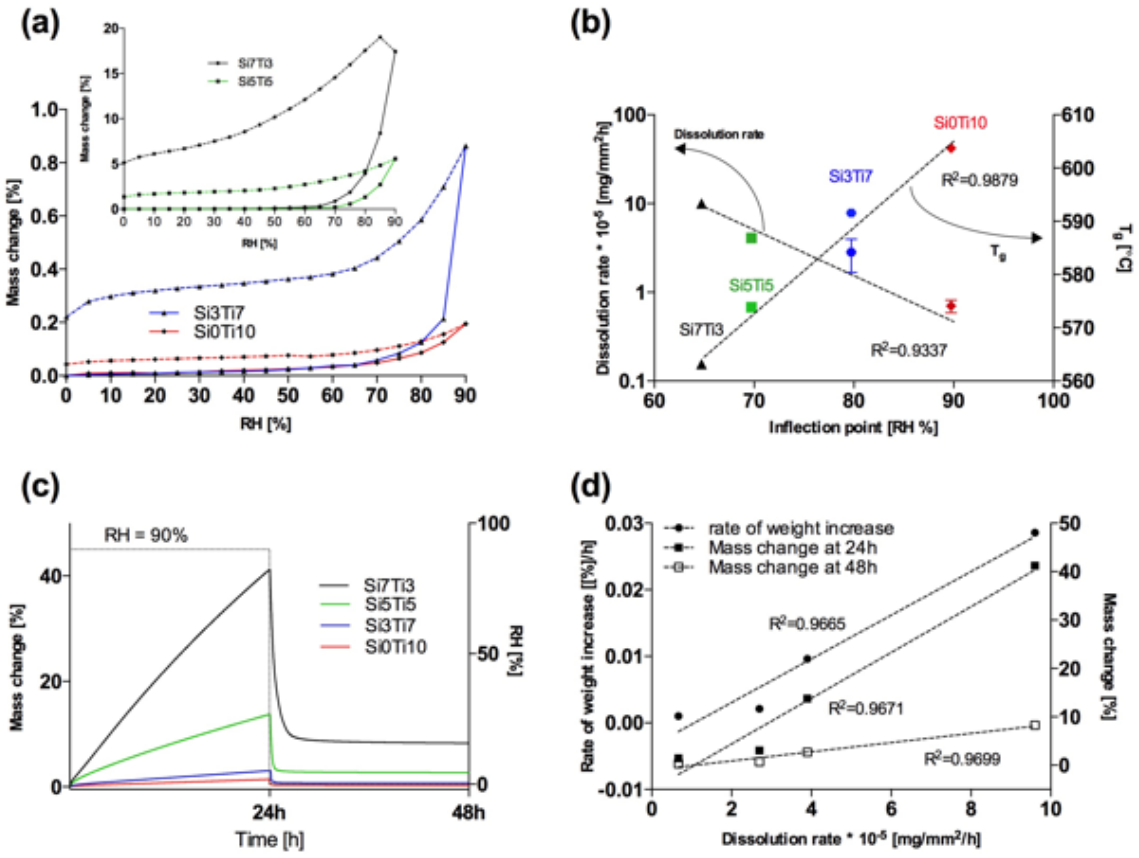

Figure 5. 2: (a) One full vapour sorption and desorption isotherm cycle of the different PG compositions exposed to increasing and decreasing RH% where the RH was changed by successive steps of 5% over a range of 0 to 90%. (b) Correlation between the inflection point and glass dissolution rate [21] and glass transition temperature (T_g) [21]. (c) Vapour sorption and desorption curves of the different PG compositions directly exposed to 90% for a 24 h period and subsequently to 0% RH for a further 24 h. (d) Correlation between glass dissolution rate [21] and rates of weight increase, as well as mass change at 24 h (end of sorption phase) and 48 h (end of desorption phase).

5.3.2.2 Sorption kinetics at 90% RH

PG particles were directly exposed to 90% RH for 24 h in order to investigate the effect of silica content on glass sorption kinetics (Figure 5.2c). The sorption phase of all four compositions at 90% RH was characterized by a linear increase in mass up to 24 h. It can be observed that PG particles with the highest silica content (Si7Ti3) showed the highest rate and percentage increase in mass. Desorption for 24 h at 0% RH was characterized by a rapid decrease in mass and reached equilibrium after approximately 0.5, 1, 2 and 5 h for Si0Ti10, Si3Ti7, Si5Ti5 and Si7Ti3, respectively. Figure 5.2(d) show a linear relationship between glass dissolution rate with the rate of sorption up to 24 h of exposure to 90% RH and the percentage of mass change at 24 h and 48 h. There was an increase in the sorption rate and the mass changes and dissolution rates with an increase in silica content.

The polar parts of both the solubility parameter and surface energy (as measured through IGC) were correlated with the inflection points (as measured through DVS) of the various PG compositions to verify the ability of both techniques in predicting the dissolution properties of PGs (Figure 5.3).

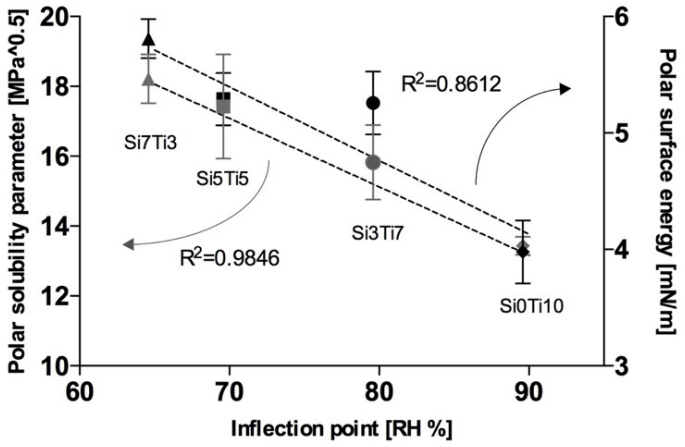

Figure 5. 3: Correlation between solubility parameter (SP) and polar part of the surface energy as measured by IGC (SE(IGC)-Polar) with the inflection point as measured via DVS.

5.3.3 Morphological and chemical analysis pre and post vapour sorption

The sieved PG particles were characterized in terms of morphology and structure before and after exposure to vapour sorption (water molecules) through SEM, FTIR, XRD and NMR. Figure 4 shows the SEM micrographs of the PG particles before and after vapour sorption (24 h at 90% RH), respectively. Figures 5.4a-c show the glass particles with particle sizes in the range of 38-45 μm. There was a smoother surface appearance in the glass particles post exposure to 90% RH (Figures 5.4d-f). Figure 4i&j show the XRD patterns of the PG particles before and after vapour sorption (24h, 90% RH), respectively. The broad humps before and after exposure to vapour (90% RH up to 24) verified that the amorphous nature of the materials was maintained [214].

Figure 5.5a&b show the ATR-FTIR spectra of the PG particles with different compositions before and after exposure to vapour sorption (24 h at 90% RH), respectively. All as-made PG particles showed the various phosphate peaks associated with PGs. In all spectra six phosphate peaks of stretching modes of vibration can be observed including the PO_2 asymmetric stretch at 1250 cm^{-1}, two $P\text{-}O^-$ stretching mode bonds at 1000 and 1100 cm^{-1}, an asymmetric stretching mode peak at 900 cm^{-1} and double symmetric stretching mode peaks in the range of 700-800 cm^{-1} attributed to (P-O-P) bond [215-217]. ATR-FTIR showed that there is a small shift of asymmetric (P-O-P) peak to the higher wavelength with increasing Si^{4+} [216]. Further, PG particles with higher amount of silica (7 mol % Si) shows sharper peak due to the stretching of ionic $P\text{-}O^-$ bond at 1000 cm^{-1} [218]. Figure 5.5b shows ATR-FTIR spectra of PG particles after exposure to vapour sorption. The appearance of a broad peak in the range of 3000 to 3800 cm^{-1} and presence of another peak at 1660 cm^{-1} can be attributed to the sorption of water molecules (OH-group) during conditioning at 90% RH [218], which was more pronounced with increased with silica content led to more pronounced OH-group peaks.

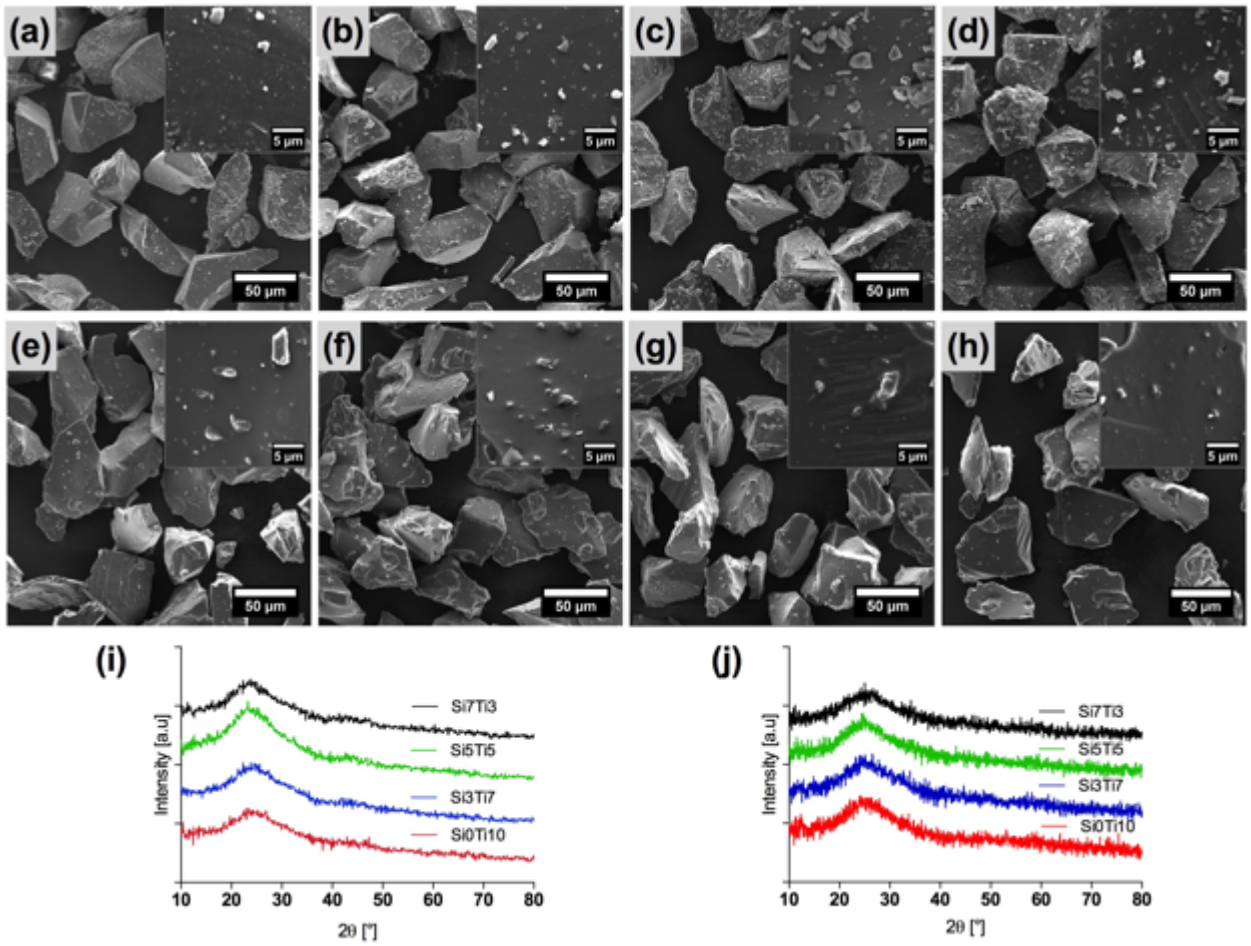

Figure 5. 4: SEM micrographs of the different PG particle compositions before (a, b, c and d for Si0Ti10, Si3Ti7, Si5Ti5, and Si7Ti3, respectively) and after vapour sorption (e, f, g and h for Si0Ti10, Si3Ti7, Si5Ti5, and Si7Ti3, respectively). (Insets showing higher magnifications). XRD patterns of the different PG particles pre (i) and post (j) vapour sorption after 24h at 90% RH followed by 24h at 0% RH.

^{31}P MAS NMR spectroscopy was used to investigate the structure of the PG particles. Figure 5.5 shows the NMR spectra of the different PGs compositions before and after vapour sorption (24 h at 90% RH). In Figure 5.5c&d, a main peak at a chemical shift of -27 ppm shows Q^2 phosphate species (two bridging oxygen atoms in the phosphate tetrahedron) [219, 220]. This Q^2 phosphate structure is expected for a metaphosphate composition due to the 50 mol% P_2O_5 content [221]. Post exposure to vapour, structural changes can be observed for Si5Ti5 and Si7Ti3, where two new peaks were observed at chemical shifts of approximately -1 ppm (attributed to Q^0(1H)) and -11 ppm (attributed to Q^1(1H)) [222, 223] (Figure 5.5d). The presence of these new

chemical shifts after exposure to vapour sorption can be explained by water molecule interactions with PGs particles and the formation of protonated phosphate species due to the hydrolysis of the phosphate unit or from the hydration of existing chain endings [23].

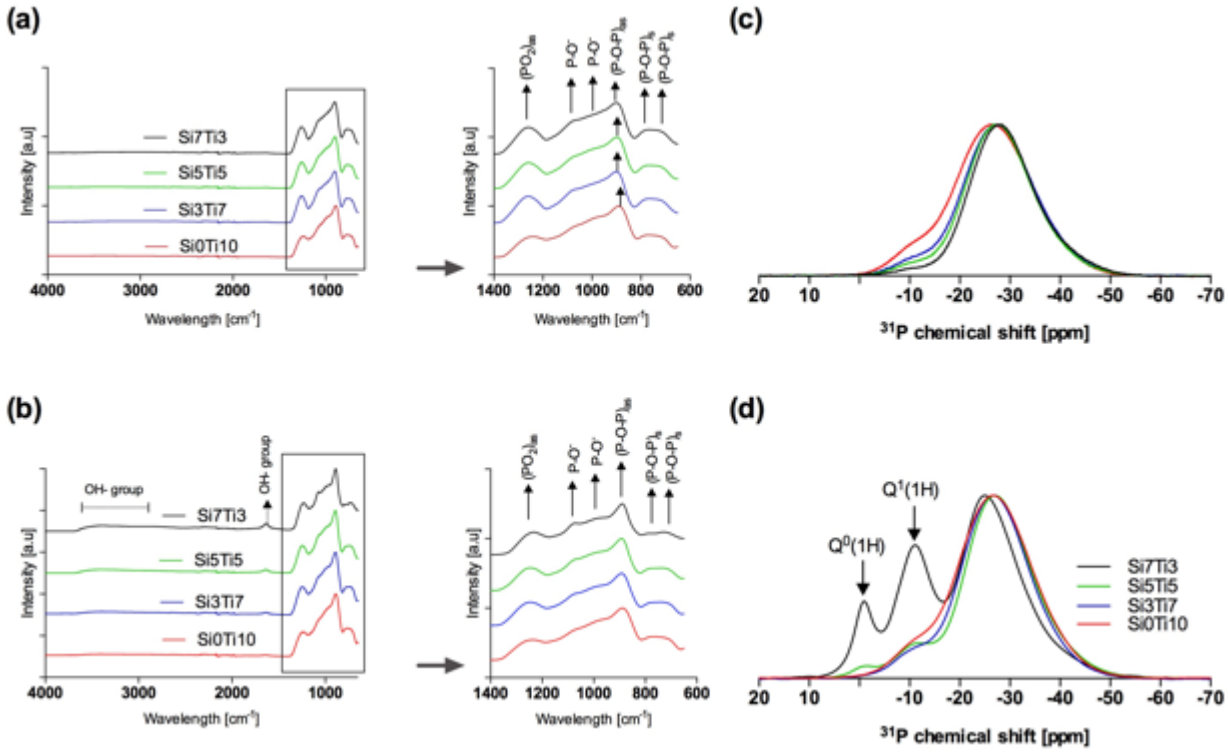

Figure 5. 5: (a and b) ATR-FTIR spectra of the different PG particles pre and post (24h at 90%RH and followed by 24h at 0% RH) exposure to vapour sorption. (c and d) ^{31}P MAS NMR spectra before and after exposure to vapour sorption.

5.4 Discussion

F inding new approaches to evaluate the dissolution characteristics of PGs is of great interest in determining their potential biological and therapeutic properties, *in vivo*. The most applied methods to correlate solubility and surface properties of PGs are through conventional methods such as long-term immersion in DIW, weight loss and ion release rate determination, and contact angle measurements all of which may lack reliability, objectivity and accuracy [21, 22]. Additionally, T_g has been used as an indicator of glass cross-linking density and chemical durability which has generally been shown to inversely correlate with glass dissolution rate [206, 207].

In this study, IGC was used to investigate the effect of substituting TiO_2 with SiO_2 on the solubility parameter and surface energy of a PG compositional range ($50P_2O_5$-40CaO-xSiO_2-(10 − x) TiO_2, where x = 7, 5, 3, and 0 mol%). Previously, it was shown that the substitution of TiO_2 with SiO_2 in PGs led to a decrease in glass density and T_g and thus an increase in glass dissolution and ionic release rates [21]. From a biological response perspective, it was shown that, when compared to glasses with 0 and 3% SiO_2 content, the ionic dissolution products from PGs with 5 and 7 mol% SiO_2 led to an increase in alkaline phosphatase activity of MC 3T3-E1 pre-osteoblast cells, *in vitro* [21]. Consequently, the solubility and degradation characteristics of these PGs can be modified by their doping with different amount of silica and titania for a particular cellular response. It has also been demonstrated that the addition of SiO_2 to PGs leads to the disruption of the phosphate glass network and leads to an increase in degradation and ion release rates [203]. In addition to the disruption of the glass network, silica incorporation into PGs also leads to the formation of surface Si-OH bonds, which contributes to their polar surface parameters [203]. However, regardless of this PG network modifying effect of SiO_2 on T_g and dissolution rates, contact angle measurements showed no significant effect on the glass surface energies [21]. This lack of sensitivity reflected similar findings on the effect of other dopants on the surface properties of PG, such as Fe_2O_3 [22] and CuO [23], when evaluated through contact angle measurements.

According to IGC measurements, it was found that the dispersive (non-polar) properties of the PG particles were not affected by the incorporation of TiO_2 or SiO_2, whereas substituting TiO_2 with SiO_2 increased the polar and H-bond parts therefore increasing polarity. It is known that the polar nature of PGs originates from P-O-P bond [22], and the addition of TiO_2 into the glass network results in reduced polar characteristics [206] due to the formation of the less hydrolysable P-O-Ti bonds. The substitution of TiO_2 with SiO_2 in the glass structure results in more hydroxyl groups (Si-OH) at the surface of the PG particles leading to an increase in polar properties [21, 224]. This alteration in the polar properties of PGs was detected via IGC, which was more sensitive comparing to contact angle measurements, which did not fully distinguish between the small changes in glass polar properties [21]. Furthermore, the correlation between solubility parameter or surface energy and T_g of the PG particles suggested the potential of IGC in predicting the bulk properties of PGs along with their surface properties. This result also suggested that IGC can be a more sensitive technique than contact angle measurement, which enables a more precise calculation of the different components of solubility and surface energy.

DVS has been used to predict the reactivity and solubility of PGs by gravimetrically measuring their immediate aqueous interactions [23]. In this study, DVS was applied to determine the sorption isotherms of the SiO_2 and TiO_2 doped PG particles, when exposed to a relative humidity range between 0 to 90% at 5% intervals and when directly exposed to 90% RH for up to 24 h, which was used to approximate the aqueous environment. In the first approach, all compositions indicated two different regions of sorption, an initial small increase in mass up to approximately 65 % RH and a second dramatic increase in mass up to 90%. The %RH value at this dramatic increase in mass termed as the inflection point and can be explained by deliquescence phenomena [195, 196]. A good linear correlation between the inflection point with T_g and dissolution rate of PGs with different silica contents indicated the ability of DVS to provide complementary information on glass durability. Furthermore, a good correlation between the rate and extent of mass change with T_g and glass dissolution rates when the glasses were directly exposed to 90% RH, verified the ability of DVS to measure glass reactivity. It is expected that by replacing of titania with silica, the PG network disruption leads to a less chemically durable glass, which is more reactive with water vapour molecules [21] as aided by the formation of surface Si-OH bonds [225]. Moreover, there was a good correlation between the polar parts of both the solubility parameter and surface energy (as measured through IGC) and inflection points (as measured through DVS), showing the potential ability of both techniques in predicting the dissolution properties of PGs as consequence of alterations in their chemistry.

Morphological characterization of the PGs post exposure to vapour sorption, indicated their surface interaction with water molecules, which led to the formation of a smooth layer on their surface. The surface transformation has been observed in previous work where phosphate- and silicate-based glasses were exposed to vapour sorption using DVS [23, 208]. NMR showed that with increasing SiO_2 content, there was a chemical shift to the more negative frequencies and a slight decrease in the peak width [21], which can be attributed to the presence of more linear chain segments of P-O-P bonds and is responsible for the polar nature of PGs [89, 203]. Additionally, after vapour sorption, the presence of new chemical shifts can be attributed to the interaction of water with phosphate network [23]. The PGs retained a fraction of non-reacted water molecule, as supported by the ATR-FTIR absorption band at 1630 cm^{-1} [226, 227], which increased with silica content. In PGs with higher silica content (Si5Ti5 and Si7Ti3), a fraction of water caused the hydrolysis of the phosphate units as supported by NMR peaks at -1 and -11 ppm [222, 223]. It can

be concluded, that only non-reacted water molecules are trapped into the glass network when substituting TiO_2 with only up to 3 mol% SiO_2. Increasing silica content to 5 and 7 mol% results in the presence of both non-reacted and reacted water molecules, which is in the form of hydrolyzed phosphate units. The greater presence of hydrolyzed phosphate units in Ti5Si5 and Ti3Si7 is likely to increase the glass dissolution and ionic release rates [21]. Along with PO_4^{3-} it is known that the dissolution of phosphate glasses leads to release of a range of polyphosphates [228], including $P_2O_7^{4-}$, which is responsible for the upregulation in alkaline phosphatase in osteoblastic cells, including those found in MC3T3-E1 cells [21].

5.5 Conclusions

IGC and DVS were used to analyse the surface and short-term aqueous interactions of PG particles doped with either TiO_2 and SiO_2. Good correlation between solubility parameter and surface energy with dissolution rates in DIW demonstrated that IGC is a precise technique in accurately determining surface properties of PG particles when compared with conventional methods such as contact angle measurement. Furthermore, DVS analysis correlated with T_g and dissolution in DIW. PGs with higher silica content showed an increase in the rate and extent of mass change. These results demonstrate that IGC and DVS can be complementary techniques in evaluating the physico-chemical properties of PG particles and be used to correlate their potential biological responses.

Acknowledgements

S.N. is supported by Werner Graupe International Fellowships as a part of McGill Engineering Doctoral Award and W. C. L. is supported by the McGill Engineering Innovation Fellowship.

6 Development and Characterization of Sodium-free, Silver-Doped Sol-Gel-Derived Borate Glasses with Anti-Bacterial Efficacy

Borate glasses have recently gained much interest in wound healing applications since they have higher degradation rate and reactivity than silicate-based glasses, in particular. It is also well known that the sol-gel process can increase glass homogeneity as well as the rate of tissue healing [229]. While sol-gel borate glasses have been previously fabricated [24], there are no studies on incorporating silver into the borate glass using this approach. Therefore, the objective of Chapter 6 is to describe the sol-gel processing of silver doped sol-gel derived borate-based glasses (AgBGs) and their resultant structural and textural properties as well as investigating ion release rate from AgBGs and their correlation with their anti-bacterial efficacy.

Development and Characterization of Sodium-free, Silver-Doped Sol-Gel-Derived Borate Glasses with Anti-Bacterial Efficacy

Shiva Naseri[1], William C. Lepry[1], Vimal B. Maisuria[2], Nathalie Tufenkji[2] and Showan N. Nazhat[1]*

[1]Department of Mining and Materials Engineering, McGill University, Montreal, QC, Canada
[2]Department of Chemical Engineering, McGill University, Montreal, QC, Canada
*corresponding author showan.nazhat@mcgill.ca

KEYWORDS: Borate-based glass, Sol-gel process, Silver, Anti-bacterial efficacy

Abstract:

Borate glasses have gained much interest in wound healing applications attributable to their lower chemical durability when compared to silicate glasses, thus allowing for increased degradation rates and potentially accelerated positive effects on the healing process. Recently, a sol-gel processing route was used to fabricate borate glasses with higher specific surface areas (SSAs) leading to rapid dissolution and reactivity rates when compared to their melt-quench derived equivalents. In this study, silver doped sol-gel derived borate glasses (AgBGs) of the compositional range (60)B_2O_3-(36)CaO-(4-X)P_2O_5-(X)Ag_2O where X= 0.0, 0.3, 0.5 and 1 (mol%) were developed to induce anti-bacterial properties thus offering promising treatment of chronic and infected wounds. Glass composition and sol-gel-processing route were initially optimized to enhance silver incorporation and subsequent ion release rate, which was correlated with anti-bacterial activity. AgBGs with varying silver content were fabricated with high SSA (24-300 m^2/g) and small pore width (31-379 Å). XRD and ATR-FTIR were used to verify the amorphous nature of the glasses and the presence of BO_3 and BO_4 units as the glass network former, respectively. Ion release of AgBG dissolution products in deionized water verified that silver ion release was dependent on glass composition. Additionally, the anti-bacterial efficacy of AgBGs against the Gram-positive *E. coli* and Gram-negative *S. aureus* bacteria was correlated with silver ion release. To the best of our knowledge, this is the first report demonstrating the potential use of anti-bacterial AgBGs for biomedical applications.

6.1 Introduction

According to classical theory, the wound healing process consists of four main phases: hemostasis, inflammation, cell proliferation, and extracellular matrix remodeling [76]. However, in the case of chronic and infected wounds, the inflammation phase fails to reduce infection through the body's immune cells [73, 76]. Therefore, there is a need to help the body overcome infection, reduce inflammation, and thus accelerate the healing process [76]. To this end, ongoing research has focused on biomaterial based wound dressings to accelerate the healing rate. One recent approach has been based on developing bioactive and soluble glasses due to their controlled release of stimulatory ions for anti-bacterial, anti-inflammatory and/or angiogenic properties [80].

Bioactive glasses have the ability to bond to hard and soft tissues through the formation of a surface hydroxy-carbonate apatite (HCA) layer [3]. In 1969, Dr. Larry Hench and his colleagues developed silicate-based bioactive glasses for mineralized tissue repair (*e.g.,* bones and teeth) [1, 3]. The most well-known and clinically used formulation is Bioglass® "45S5" [(46.1)SiO_2-(26.9)CaO-(24.4)Na_2O-(2.6)P_2O_5 (mol %)] which has been used in clinical applications such as fillings or grafts in bone [26] and dental tissues [83]. This particular glass formulation was initially used in studies that indicated their potential in wound healing applications [84, 230]. However, due to their slow and incomplete dissolution, there is significant interest in more readily soluble glasses, such as phosphates [8], and borates [231]. In particular, borate-based glasses have recently gained noticeable attention for biomedical applications [232] as they degrade more rapidly and are more reactive due to their lower chemical durability [102]. These unique properties have led to borate glasses being investigated for soft tissue engineering applications, in particular wound healing [84]. For example, *in vitro* and *in vivo* studies have shown boron to enhance vascularization through stimulation of vascular endothelial growth factor (VEGF) and basic fibroblast growth factor (bFGF), which are essential for angiogenesis and wound healing processes [103, 134]. These, and other findings, have recently led to a melt-derived borate-based glass microfiber wound matrix (MIRRAGEN™, ETS Wound Care LLC, USA) receiving Food and Drug Administration approval as a novel wound dressing [10]. In clinical trials, MIRRAGEN™ wound dressing was shown to heal chronic wounds [10].

Since the potential of infection increases with wounds, silver is often incorporated into a biomaterial, such as glasses or wound healing dressings [233], attributable to its anti-bacterial properties [151, 154, 156]. A number of studies have also shown that silver has anti-inflammatory

activity [234] and can facilitate the migration of fibroblasts [235, 236]. However, there have only been a limited number of studies on silver doped borate glasses for medical applications, which have manly been focused on bone repair [140, 141, 237, 238]. For example, Kamal demonstrated the potential of silver doped melt-quench-derived borate glasses (through complete substitution of silicate with borate in a 45S5 bioactive glass formulation) for bone regeneration and anti-bacterial applications through *in vitro* immersion in simulated body fluid (SBF) [141]. In addition, borate glasses of the composition $6Na_2O$-$8K_2O$-8MgO-22CaO-$54B_2O_3$-$2P_2O_5$ (mol%) doped with 0.75, 1 and 2 wt% Ag_2O, were reported by Luo et al. [140]. It was reported that the incorporation of 0.75 and 1 wt% Ag_2O, had non-toxic effects against mouse osteoblasts and fibroblasts, *in vitro*, while those doped with 2 wt% Ag_2O were found to be toxic. This study also speculated that the glasses may have anti-bacterial potential for soft tissue applications [140]. Furthermore, silver doped melt-quench-derived borosilicate glasses of the composition $6Na_2O$-$8K_2O$-8MgO-22CaO-$36B_2O_3$-$18SiO_2$-$2P_2O_5$ (mol%) doped with 0.05, 0.5 and 1 wt% Ag_2O with anti-bacterial efficacy against *Escherichia coli (E.coli)* and *Staphylococcus aureus* (*S.aureus*) and $6Na_2O$-$8K_2O$-8MgO-16CaO-$2P_2O_5$-6SrO-$36B_2O_3$-$18SiO_2$; mol%) doped with 0, 0.75, or 1.0 wt% Ag2O with anti-bacterial efficacy against *methicillin-resistant S. aureus* for bone fracture fixation and bone infection have been developed [237, 238].

Compared the melt-quench methods, the sol-gel process can produce glasses with higher bioactivity and dissolution rates, as well as a broader range of compositions due to the lower processing temperatures [26]. Recently, Lepry and Nazhat reported on a series of sol-gel derived borate glasses based on a boron substituted 45S5 bioactive glass (B46: $(46.1)B_2O_3$-(26.9)CaO-$(24.4)Na_2O$-$(2.6)P_2O_5$; mol %) formulation [24]. It was demonstrated that sol-gel derived borate glasses were more reactive compared to their melt-quench equivalents due to their enhanced textural properties. It has also been reported that the sol-gel method is the preferred processing route for the silver doping of glasses as it generates a more homogenous distribution of silver within a glass network [28-30]. Therefore, in this study, the processability of silver doped sol-gel derived borate glasses (AgBGs) for potential applications in wound healing, was investigated. The incorporation and integration of silver into two borate glass formulations was investigated initially by its partial substitution of sodium in the B46 composition, and its release was compared to that released from a sodium-free compositional range based on 60 mol% borate content. The effects of the sol-gel processing and composition on the glass properties, as well as their aqueous interactions

were evaluated. Furthermore, the anti-bacterial efficacy of the optimized glasses was investigated and correlated with glass silver content and release.

6.2 Experimental

6.2.1 Materials and methods

Table 6.1 provides a summary of the different compositions and processing procedures investigated in this study. AgBG-1, sequence #1: Silver doped borate-based glasses (AgBGs) of the compositional range (46)B_2O_3-(27)CaO-(24-X)Na_2O-(3)P_2O_5-(X)Ag_2O where X = 0, 0.15, 0.5 and 1 (mol%) were produced based off a previous sol-gel process [24]. Boric acid (Sigma Aldrich), calcium methoxyethoxide (20% in methoxyethanol) (Gelest), sodium methoxide (25% in methanol) (Sigma Aldrich), triethyl phosphate (99%, Sigma Aldrich) and silver nitrate (Fisher Scientific) were used as precursors. Initially, boric acid was mixed with ethanol based on the solubility of boric acid (≈ 11.2 %) into a Teflon beaker covered by a Teflon cap and magnetically stirred at ~40 °C for 30 min or until clear. Next, triethyl phosphate, calcium methoxyethoxide, silver nitrate, and sodium methoxide were added at 30 min intervals with an additional 30 min of stirring after the sodium addition. Afterwards, the sol was transferred into plastic vials to gel and aged for 5 days at 37 °C. At the end of the ageing period, the gels were initially dried in a fume hood at room temperature for 2 days while covered with a non-transparent box to protect them from exposure to light (since silver can undergo photo-reduction of Ag^+ ion into Ag metal), and then followed by further drying at 120 °C for 48 h. The dried as-made powders were then calcined at 400 °C for 2 h.

AgBG-2, sequence #2: similar AgBGs, of the compositional range (46)B_2O_3-(27)CaO-(24-X)Na_2O-(3)P_2O_5-(X)Ag_2O where X= 0, 0.5 (mol%) were fabricated as in AgBG-1 however, precursor addition was modified. The calcium and silver addition were reversed from process #1 (*i.e.,* silver nitrate was added before calcium methoxyethoxide). These glasses underwent the same casting, ageing, drying, and calcination steps as described for AgBG-1.

AgBG-3, sequence #2: Silver doped, sodium free borate-based glasses of the compositional range (60)B_2O_3-(36)CaO-(4-X)P_2O_5-(X)Ag_2O where X= 0.0, 0.3, 0.5 and 1 (mol%) were produced by the sol-gel process as described in process #2 without the addition of sodium. These glasses underwent the same casting, ageing, drying, and calcination steps as described for AgBG-1.

After calcination, all glass particles were ground and sieved to 25 – 75 μm particle size fraction and stored in a desiccator until further use.

Table 6. 1: Overview of the sol–gel processing routes and compositions investigated in this study.

Glass	**ID**	**Composition (mol%)**				
		B_2O_3	**P_2O_5**	**CaO**	**Ag_2O**	**Na_2O**
AgBG-1 (Seq. #1)	B46	46	3	27	0	24
	B46-0.15Ag				0.15	23.85
	B46-0.5Ag				0.5	23.5
	B46-1 Ag				1	23
AgBG-2 (Seq.#2)	B46-0.5 Ag	46	3	27	0.5	23.5
AgBG-3 (Seq#2)	B60	60	4	36	0	-
	B60-0.3 Ag		3.7		0.3	-
	B60-0.5 Ag		3.5		0.5	-
	B60-1 Ag		3		1	-

6.2.2 Particle characterization

The average particle size of the sieved glass powders was determined using a Horiba LA-920 (ATS Scientific Ink., Canada). The specific surface area of each powders (n=3) sieved to 25 – 75 μm was measured with nitrogen gas adsorption and desorption isotherms collected with a Micromeritics TriStar 3000 (Micromeritics Instrument Corporation, USA) gas sorption system. Specific surface area values were determined using the Brunauer–Emmett–Teller (BET) method [189] while the Barrett–Joyner–Halenda (BJH) method [239], using the desorption isotherms, provided the average pore width and pore volume.

6.2.3 X-ray diffraction

X-ray diffraction (XRD) diffractograms of the glasses were analyzed with a Bruker D8 Discover X-ray diffractometer (Bruker AXSS Inc., USA) equipped with a CuKα ($\lambda = 0.15406$ nm) target set to a power level of 40 mV and 40 mA. Using an area detector, three frames of 25° were

collected from 15 – 75 2 theta (°) and merged in post processing. Phase identification was carried out using X'Pert Highscore Plus (PANalytical, Netherlands).

6.2.4 Attenuated total reflectance-Fourier transform infrared spectroscopy

Attenuated total reflectance-Fourier transform infrared (ATR-FTIR) spectroscopy was carried out using a Spectrum 400 (Perkin-Elmer, USA) between 4000 and 650 cm^{-1} with a resolution of 4 cm^{-1} using 64 scans per sample. All spectra were baseline corrected and normalized to the total area surface area under absorption bands using Spectrum software (Perkin-Elmer, USA).

6.2.5 Dynamic vapour sorption (DVS)

Vapor sorption of AgBG particles with 4 different compositions was measured using a DVS Intrinsic (SMS Ltd., UK) measuring mass changes (± 0.1 μg) under controlled temperature and humidity. Approximately 5 mg of AgBG particles was placed in an aluminum pan and inserted into a chamber with a constant temperature of 37 ± 0.05 °C. The AgBG particles were immediately exposed to 90% RH for 2 h, which was then reduced back down to 0% RH for another 2 h.

6.2.6 Inductively coupled plasma optical emission spectrometry

Release of silver, boron, calcium, and phosphorus ions from glass powders in deionized water (DIW) at a 1.5 mg/mL ratio, were quantified using an inductively coupled plasma–optical emission spectrophotometer (ICP-OES, Thermo Scientific iCAP 6500, USA). Aliquots of 2 mL were filtered through a 0.2 μm nylon filter and stored in a 15 mL falcon tube to which 4% (w/v) nitric acid (Fisher Scientific, Canada) was added.

6.2.7 Anti-bacterial assessment

6.2.7.1 Mean viable cell counts

The anti-bacterial activity of glasses was examined using the viable cell count method. An overnight grown culture of *E. coli* D21 or *S. aureus* ATCC 25923 bacteria, was diluted in Mueller Hinton Broth 2 (MHB-II, Oxoid; Fisher Scientific Canada) to 0.05 $OD_{600\ nm}$. AgBGs at various concentrations (0.375, 0.75, 1.5 and 3 mg/mL) were mixed with diluted bacterial suspension in MHB-II. Bacterial cultures exposed to AgBGs were serially diluted in phosphate-buffered saline

(PBS) and plated on the surface of Luria broth agar plate. The number of colonies was counted after 20 h of incubation at 37 °C. All measurements were done in triplicate on different days.

6.2.7.2 Bacteria growth curves

Bacteria growth was analyzed by directly exposing the glass particles to bacteria suspensions in MHB-II with AgBG particles (0.375 and 0. 75 mg/mL) with an initial bacterium cell density of 0.05 $OD_{600\ nm}$. Their $OD_{600\ nm}$ value was then measured up to 24 h at 37 °C using Tecan Infinite M200 microplate reader (Tecan group Ltd., Switzerland). All measurements were done in triplicate.

6.2.7.3 Agar-disk diffusion

A plate containing an agar medium (nutrient for bacteria) overlaid with 1:1000 diluted bacterial culture of *E. coli* or *S. aureus* was exposed to 1 mg of AgBGs, which was placed on the surface of the agar. The zone of inhibition (clear zone) was measured after 18 h incubation at 37 °C to evaluate anti-bacterial efficacy. All measurements were done in duplicate.

6.3 Results and discussion

6.3.1 Effect of addition order of precursors on the silver integration

Figure 6.1 provides an overview of the processing of sol-gel derived AgBGs based on B46 and B60. Initially, for B46-based AgBG-1 and sequence #1, the silver precursor ($AgNO_3$) was added after the addition of the calcium precursor and before that of the sodium precursor where the pH of the solution was ~ 10. The XRD patterns of the resultant AgBG-1 particles with 0 and 0.15 mol% silver verified the amorphous structure of the glasses as indicated by two broad humps [24] (Figure 6.2a). However, in the case of 0.5 mol% silver, there was some indication of a metallic silver phase (JCPDS No 04-0783) due to the presence of a small peak at around 38° 2θ. Furthermore, upon addition of 1 mol% silver, this metallic silver phase was more prominent, which also precipitated during the sol preparation (Figure 6.2a). While this was the first attempt to generate a sol-gel derived AgBG, a number of reports in literature have shown that increasing the amount of silver dopant can lead to the formation of metallic silver within phosphosilicate glasses [240-242]. For example, Simon et al., reported that the doping of melt-derived calcium phosphate glasses with more than 3 mol% silver, leads to the formation of precipitated metallic silver particles

[240]. In another study, Delben et al., showed that sol-gel derived phosphosilicate glasses with more than 3 mol% silver contained metallic silver phases within the glass matrix [241]. However, Vulpoi et al., reported that even 2 mol% silver causes the formation of metallic silver phase in sol-gel derived phosphosilicate glasses, and suggested that silver oxide can decompose at around 485 °C, which is above the 400 °C calcination temperature applied in this study [242].

Figure 6. 1: An overview of the sol-gel process; B46 (AgBG-1 and AgBG-2) and B60 (AgBG-3).

ATR-FTIR spectroscopy allowed for the examination of the bonding regions in AgBG-1 (Figure 6.2b). In all spectra, the presence of a peak at 720 cm^{-1} can be observed attributable to the B-O-B bending linkage of the BO_3 units in the borate network [243]. The B-O stretching of the boroxoal ring leads to the formation of a shoulder at 870 cm^{-1} [243]. Peaks in the range 1200-1600 cm^{-1} (1393 and 1264 cm^{-1}) and 800-1200 cm^{-1} (870, 942 and 1017 cm^{-1}) can be attributed to the B-O stretching of the BO_3 structural units and B-O stretching of BO_4 structural units, respectively [243]. The presence of both BO_3 and BO_4 units verified that the majority of boron formed a typical trigonal planar coordination with a fraction of four coordination formation [45] as also reported for sol-gel derived borate glasses [24].

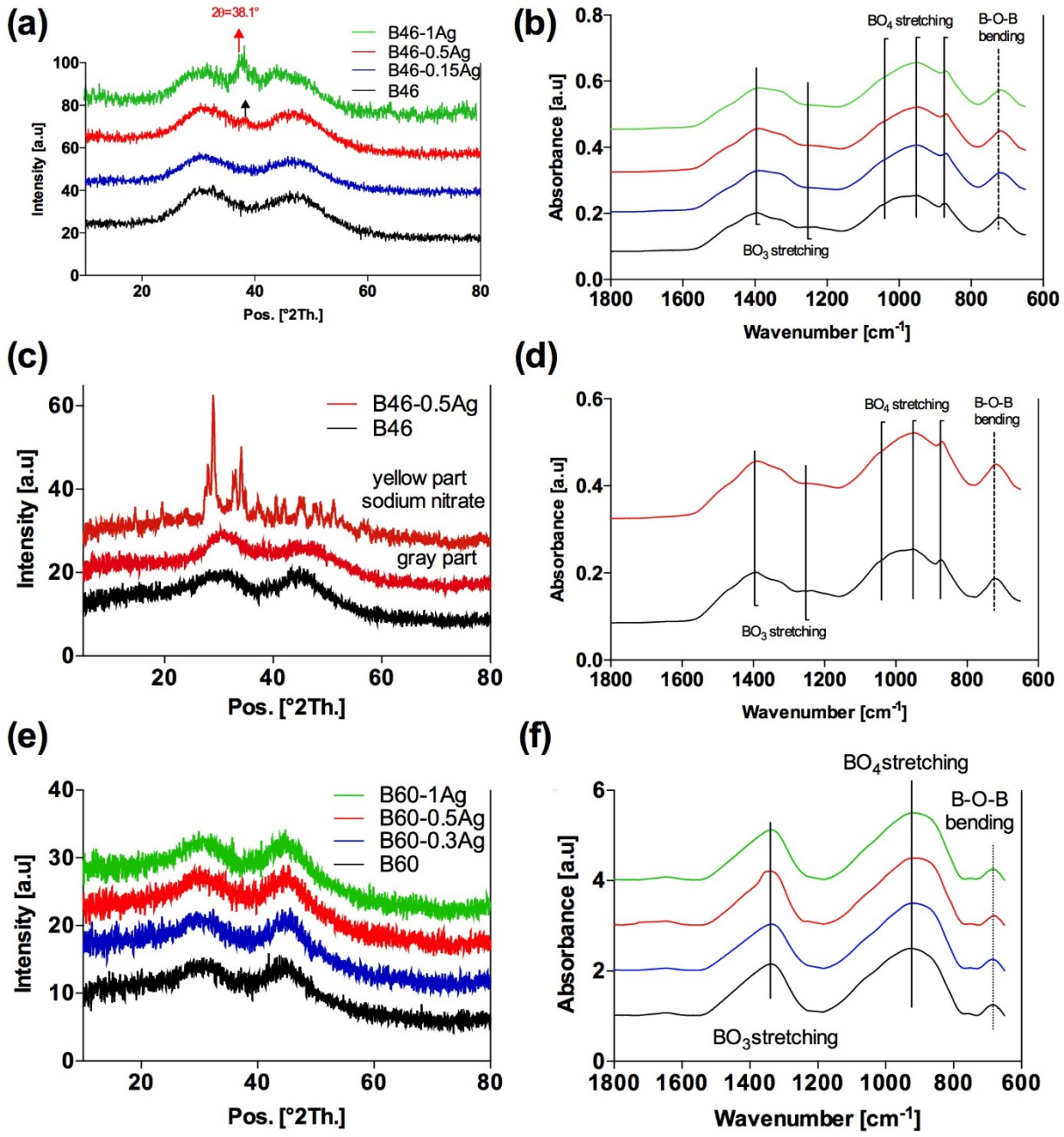

Figure 6. 2: Effect of addition order of precursors on silver incorporation and structure of AgBGs. Left panel, XRD diffractograms of calcined glasses indicating (a) the presence of a metallic silver phase in glasses containing 1 mol% silver (AgBG-1) (c) the formation of a semi-crystalline sodium nitrate phase within the glass structure (AgBG-2), (e) the amorphous characteristics by the presence of two broad humps (AgBG-3). Right panel, ATR-FTIR spectra of (b) AgBG-1, (d) AgBG-2 and (f) AgBG-3. All spectra indicated typical borate bonding modes.

It is well accepted that the sol-gel processing conditions such as pH, type of precursors, and temperature have a direct effect on each step of the processing route, as well as the final product,

and change the pH of the solution depending on the type and ratio of the reactants [244, 245]. In an attempt to eliminate the precipitation and formation of the metallic silver phase and synthesize a more homogenous glass structure, the addition order of the silver precursor during the sol preparation was modified. Therefore, in the B46-based AgBG-2 and sequence #2, the silver precursor was added after that of the phosphorus precursor in which the pH of the solution was ~ 4. Although this modification led to the formation of homogenous sol without any precipitated phase, upon calcination at 400 °C, a non-homogenous appearance of glass particles was observed, with yellow and dark gray fractions (Figure 6.1). XRD patterns were carried out on the separated fractions and while the pattern of the gray fraction indicated an amorphous structure, that of the yellow fraction indicated that a semi-crystalline sodium nitrate phase was formed (Figure 6.2c). Although, there are a limited number of studies reporting on silver doped sol-gel derived glasses containing sodium oxide [153, 246], in these studies, the amount of silver or sodium oxide was significantly low in comparison to the other components, such as in the NaO_2-CaO-SiO_2 composition doped with only 0.5 wt% silver oxide [153] or (58.6)SiO2-(7.2)P_2O_5 7.2 –(4.2)Al_2O_3–(24.9)CaO–(2.1)Na_2O–(3)K_2O(wt%)) with only 2.1 wt% sodium oxide [246]. Although these studies did not state the reasons for the low silver or sodium contents, it may be that the sol-gel reaction is more difficult to control in the presence of a sodium precursor due to its high reactivity rates [247]. In this study, the XRD patterns suggested that the interaction of sodium and silver precursors led to sodium nitrate formation [247]. A similar finding has been reported in sodium acetate formation, confirming the high reactivity rate of the sodium precursor [247]. Figure 6.2d shows the ATR-FTIR spectra of AgBG-2 glasses. In all spectra, the presence of the three main regions associated with borate-based glasses was verified [243] and was in agreement with the bonding regions identified for AgBG-1 glasses (Figure 7.2b).

In order to develop a homogenous glass structure, the addition of the sodium precursor was eliminated from the sol-gel processing route, while maintaining sequence #2. The resultant B60-based sodium free sol-gel derived borate glasses (AgBG-3) was approximately similar to that previously reported by Lepry [61B_2O_3-35.6CaO-3.4P_2O_5 (mol%)] [54]. Figure 6.2e&f show the XRD patterns and ATR-FTIR spectra of AgBG-3 with 0, 0.3, 0.5, and 1 mol% silver content, respectively. XRD demonstrated that all glass formulations were amorphous [29]. ATR-FTIR spectra verified the presence of the three main regions associated with borate-based glasses at 800 – 1200 cm^{-1} (B–O stretching of BO_4 units), 1200 – 1600 cm^{-1} (B–O stretching of BO_3 units), and

a peak at ~720 cm^{-1} attributable to the B–O–B bending of BO_3 units [243]. Furthermore, an increase in glass borate content from 46 to 60 mol%, led to the elimination of a shoulder peak at ~870 cm^{-1}, which is characteristic of the B–O stretching of boroxol rings as observed in the B46 [24].

6.3.2 Particle textural properties

A summary of the average glass particle size, BET specific surface area, pore width and volume values are given in Table 6.2. All glass particles showed a similar range of particle size with an average diameter of approximately 50 μm. Specific surface area values significantly increased with the elimination of sodium (AgBG-3), while those of the pore width and volume values decreased [54]. In general, sodium is a network modifier that disrupts the glass structure, and lowers the glass network connectivity by creating non-bridging oxygens [248]. Previously, in silicate-based glass system it was demonstrated that higher glass network connectivity leads to increased surface area and reduced pore width values [48]. However, there was no correlation found between silver content and specific surface area.

Table 6. 2: Glass particle textural properties: average particle size, BET surface area, average pore volume and average pore width indicating the effect of sodium in borate glass composition on textural properties. (n = 3):

Glass	ID	Particle size (μm)	BET surface area (m^2/g)	pore volume (cm^3/g)	pore width (Å)
AgBG-1	**B46**	48.4±1.1	75.0±1.2	0.69±0.01	241.6±0.6
	B46-0.15Ag	33.8±1.8	53.9±1.4	0.69±0.05	379.9±1.2
	B46-0.5 Ag	33.2±2.5	24.7±0.3	0.59±0.01	332.0±9.7
AgBG-2	**B46-0.5 Ag**	34.1±1.7	28.2±0.3	0.61±0.01	329.2±8.6
AgBG-3	**B60**	48.3±0.4	240.2±2.7	0.23±0.0	35.3±0.03
	B60-0.3 Ag	45.7±0.6	237.7±26.0	0.23±0.01	44.6±0.2
	B60-0.5 Ag	51.1±0.6	300.2±25.6	0.34±0.02	33.9±0.2
	B60-1 Ag	47.5±0.6	238.3±42.8	0.25±0.01	31.3±0.02

6.3.3 Reactivity through DVS

In order to better understand the effect of composition and surface area on the reactivity of the AgBGs, DVS was used to characterize their immediate aqueous interactions. DVS, which has previously been used to examine the reactivity of bioactive glasses, is a gravimetric technique measuring mass changes under controlled temperature and humidity [23, 24, 208]. Figure 6.3 shows the water vapour sorption and desorption profiles of the various glass formulations during direct exposure to 90% RH for 2 h, followed by a further 2 h at 0% RH. The B46 compositional range generating AgBG-1 and AgBG-2 glasses demonstrated an increase in mass for the 2 h duration. However, the B60 range (AgBG-3 glasses) demonstrated an increase in mass only within the first 10 mins, which then reached a plateau. As previously reported for sol-gel derived borate glasses, in this study, it was found that the rate and extent of mass change after 2 h was more dependent on the composition rather than on glass specific surface area [24]. Glasses without sodium had significantly lower values of total mass change. The mass change was independent of the specific surface area values, *e.g.,* at the end of sorption at 90% RH, B46-0.5Ag (AgBG-1) particles of 24.7 m^2/g underwent a mass change of ~85%, and B60-0.5Ag (AgBG-3) particles of 300.2 m^2/g experienced a mass change of ~ 20%. Lowering the RH to 0% caused a rapid decrease in mass with AgBG-1 and AgBG-2 glasses experiencing a greater extent of mass loss. Additionally, there was no effect of glass silver content on their vapour sorption reactivity, confirming that the atomic and molecular structures have dominant roles on the chemical durability of multicomponent glasses [26, 249]. In particular, the effect of sodium on the reactivity of AgBGs can be attributed to a greater presence of non-bridging oxygens and OH groups in the glass structure resulting in their lower chemical durability [26, 250]. Additionally, the sorption and desorption isotherms of the AgBG-3 particles with various silver content, were measured by exposure to systematically increasing and decreasing values of RH (Figure S6.1, supporting information). The sorption isotherms of all glass particles were characterized by continuous increase in mass unlike those observed for melt-quench-derived phosphate-, silicate- and borate-based glass systems [23, 24, 208]. Vapour sorption isotherm of these glasses are generally characterized by a sudden exponential increase in mass at a certain % RH value when the RH is increased up to a maximum of 90% [23, 24, 208]. This difference in behavior of sol-gel derived borate-glasses may be attributed to difference in their processing route, which results in the

formation of highly porous glass particles, however, further structural analysis would be needed to confirm this.

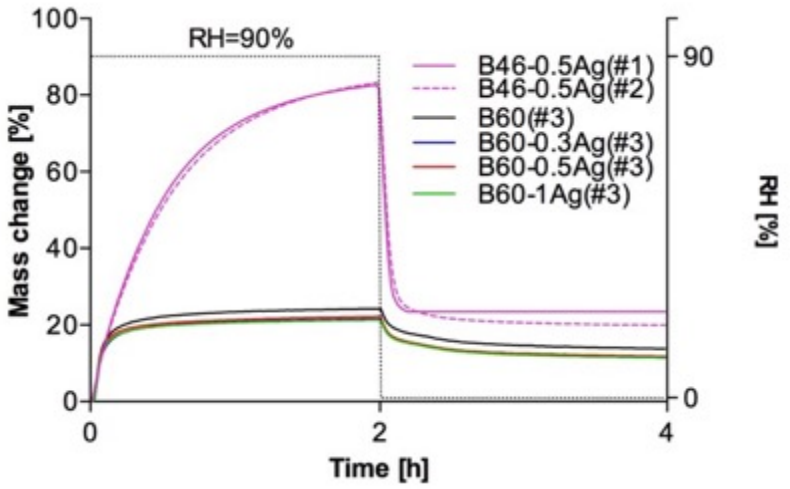

Figure 6. 3: Immediate aqueous interaction of AgBGs as measured through DVS. Average glass particle ~50 µm.

6.3.4 Dissolution and ion release measurements in deionized water

ICP-OES data at 24 h in DIW indicated that only ~ 0.05 and 0.15 ppm silver ion was released from AgBG-1 with 0.15 and 0.5 mol% silver content, respectively (Figure 6.4a). Furthermore, silver ion release from AgBG-2 with 0.5 mol% silver content was below detection limit (data not shown), which corroborated the structural analysis of the B46 compositional range, *i.e.,* the non-homogenous formation of the glass structure. In contrast, silver ion release from the B60 compositional range was significantly higher, *e.g.,* ~ 3.5 ppm silver ion was released from B60-0.5Ag (AgBG-3) (Figure 6.4b). ICP-OES data from the B60 compositional range (AgBG-3) in DIW demonstrated the release of all three components of the base formulation (B60) (Figure 6.4 c-e). There were rapid rates of release of boron and calcium ions, which were almost independent of silver content. The phosphorus ion release from AgBGs was found to decrease over time which may be due to the the formation of a calcium-phosphate precipitate [16]. The ion release profiles from AgBGs were in line with those of the previously reported sol-gel derived borate glasses [24]. Figure 6.4f shows the effect of ionic dissolution production on the pH of DIW through the dissolution of AgBG-3 glasses, which increased to ~ 9.

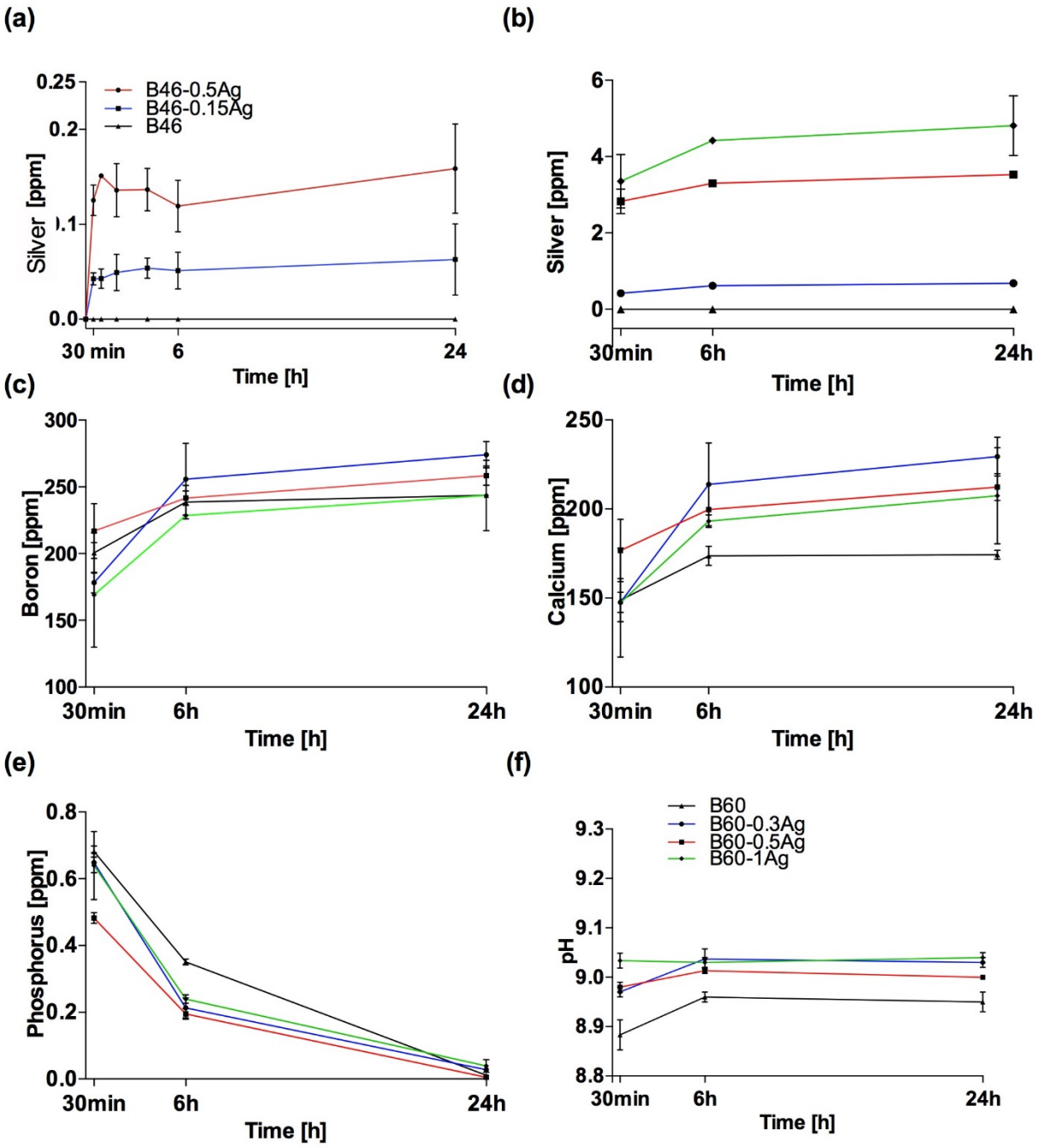

Figure 6. 4: Glass dissolution in DIW. (a&b) ICP-OES data showing silver ion release from AgBG-1 and AgBG-3, respectively. The results indicated significantly higher silver ion release in the absence of sodium in glass composition. (c-e) ICP-OES data showing boron, calcium, and phosphorus ion release, respectively, from AgBG-3. (f) pH changes of DIW at 30 min, and 6 and 24 h as a consequence of AgBG-3 dissolution (Error bars: Standard deviation: SD, n = 3).

As a result, sodium free AgBGs (AgBG-3) demonstrated higher levels of silver ion release and a homogenous glass structure with no tendency to form a precipitated metallic silver phase. AgBG-1 and AgBG-3 glasses were chosen for further characterizations to evaluate their potential anti-bacterial efficacy.

6.3.5 Anti-bacterial efficacy of AgBGs

Based on the silver ion release data, anti-bacterial efficacy of the B60 (AgBG-3) compositional range was assessed on viability and growth of *E.coli* and *S.aureus* through the viable cell count and growth methods (Figure 6.5a&b). In terms of the viable cell count for both strains, there was a dose dependent response to the silver doped glasses. It was also observed that the B60-1Ag was 100% effective against both bacteria, while B60-0.5Ag and B60-0.3Ag were less effective at lower concentrations. Additionally, the result suggests that AgBGs were more effective against *E.coli* than *S.aureus.* It has been reported that silver ion is less effective against *S.aureus* due to the presence of a thick peptidoglycan layer, which can limit the action of silver through the bacterial cell wall [150, 251]. Furthermore, the viable cell count method was also used to examine if B46 (AgBG-1) compositional range had any anti-bacterial efficacy. AgBG-1 glasses doped with 0.5 mol% silver was compared to non-doped glasses (Figure S6.2, supporting information). The result showed that a concentration of 3.2 mg/mL of B46-0.5Ag was needed to have an effect on both bacteria strains. Interestingly, at a higher concentration of 6.4 mg/mL, both formulations demonstrated some level of anti-bacterial efficacy, which may be attributed to the increase of local pH [118, 120].

To further evaluate the anti-bacterial efficacy of the B60 compositional range, the planktonic growth of each bacterial strain was measured in presence of these glasses (Figure 6.5c-f). At a glass concentration of 0.375 mg/mL, both the non-doped and B60-0.3Ag glasses did not inhibit the growth curve of *E.coli* (Figure 6.5c). However, at 0.75 mg/mL of AgBGs, all silver containing glass formulations were found to be effective against this bacterial strain (Figure 6.5d). In case of *S.aureus,* both concentrations of B60-1Ag glasses were effective in stopping the production of this bacterial strain (Figure 6.5e&f). However, at a lower level of silver doping and glass concentrations, the glasses were less effective against *S.aureus*. A number of studies have been reported on the efficacy of silver doped silicate- and phosphate-based glasses against *E.coli* and *S.aure*us [30, 96]. For example, Bellantone et al., reported that the incorporation of 3 wt% silver

into silicate-based glass generated a glass with antimicrobial effect against *E. coli* [30]. Ahmed et al., also demonstrated that silver-doped phosphate-based glasses have the ability to kill *S.aureus* and *E.coli* bacteria [96].

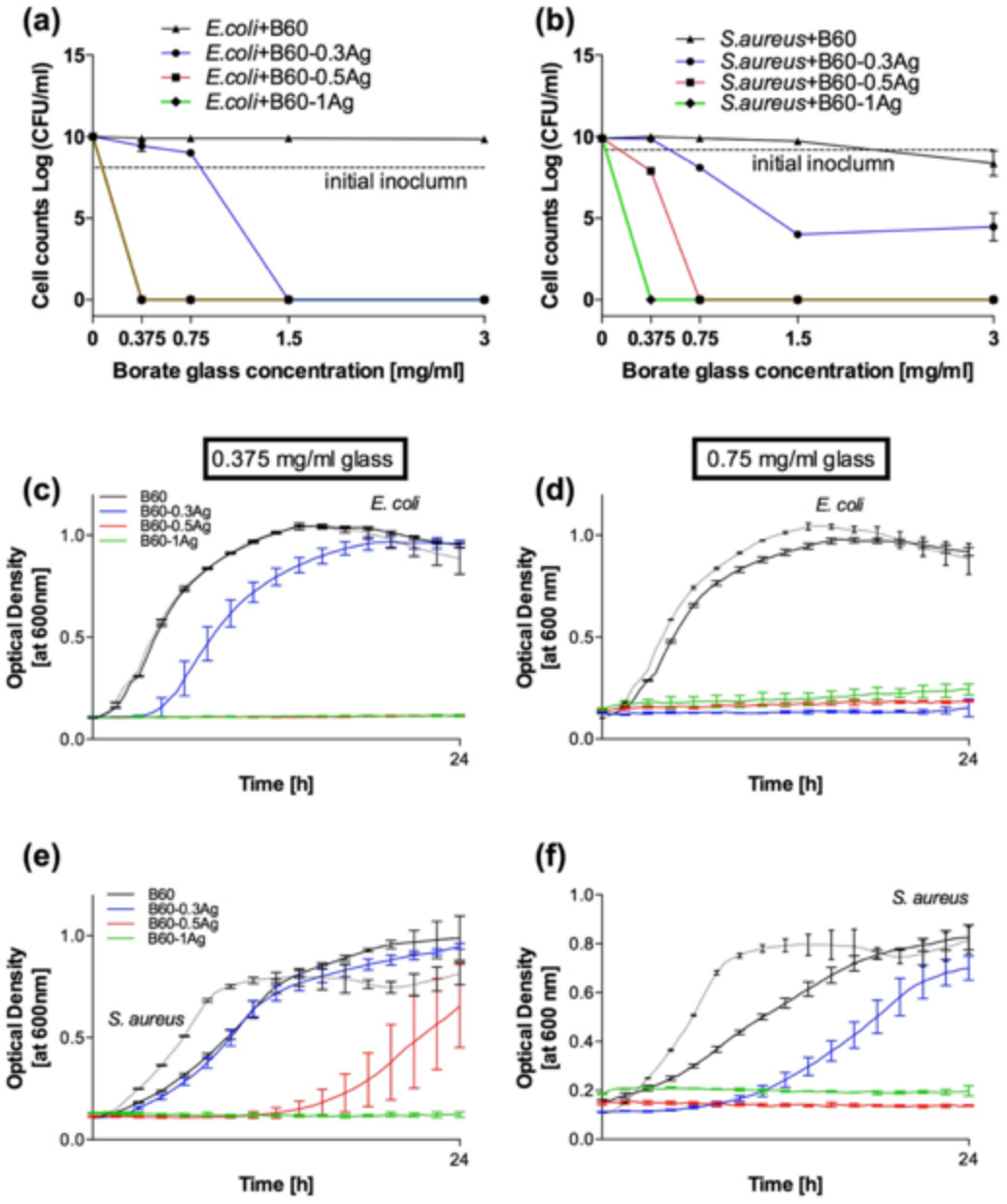

Figure 6. 5: Anti-bacterial efficacy of the B60 AgBG compositional range. (a&b) Viable cell count of *E.coli* and *S.aureus*, respectively, as a function of silver content and glass concentration. (c&d) Growth curve of *E.coli* at a glass concentrations of 0.375 and 0.75 mg/mL, respectively. (e&f) Growth curve of *S.aureus* at a glass concentrations of 0.375 and 0.75 mg/mL, respectively.(Error bars: SD, n = 3).

The disk diffusion assay was also utilized to further evaluate the anti-bacterial efficacy of the B60 compositional range, by measuring the zone of growth inhibition of both bacteria in the presence of glass particles (Figure 6.6). Images indicated that larger diameters of inhibition zone for both bacteria were achieved in the presence of AgBGs with higher silver content. A plot of the diameter of inhibition zone versus silver ion release (from ICP-OES data) indicated a linear correlation with R^2=0.9521 and R^2=0.8989 for *E.coli* and *S.aureus*, respectively.

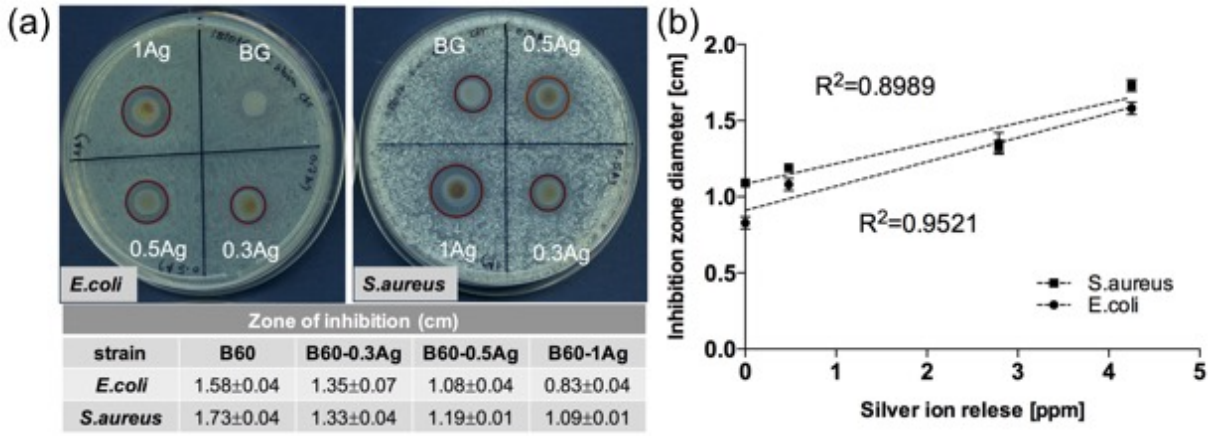

Zone of inhibition (cm)

strain	B60	B60-0.3Ag	B60-0.5Ag	B60-1Ag
E.coli	1.58±0.04	1.35±0.07	1.08±0.04	0.83±0.04
S.aureus	1.73±0.04	1.33±0.04	1.19±0.01	1.09±0.01

Figure 6. 6: Anti-bacterial efficacy of AgBG through the agar-disc diffusion assay. (a) Images of agar plates showing effect of different silver content (0, 0.3, 0.5 and 1 mol%) on *E.coli* and *S.aureus*. (b) Correlation between silver ion release and diameter of zone of inhibition (Error bars: SD, n = 2).

These anti-bacterial results have demonstrated that the B60 AgBGs inhibit the growth of wound associated bacteria [152, 153] in a dose dependent manner, which can be correlated with silver ion release. The results also confirm the efficacy of silver ions against both Gram-negative (*E.coli*) and Gram-positive (*S.aureu*) bacteria [152, 153]. It has been reported that silver ion can kill bacteria through various possible mechanisms, such as by attaching to their DNA and RNA, binding to the tissue proteins [27], and by attaching to cell membranes and inhibiting the respiration process of bacteria [27]. Based on literature, effective concentrations of silver ion against bacteria can vary from 0.1 to 20 ppm depending on the biological condition and bacteria type [151]. This reported range is in line with the concentrations of silver ion released from the B60 AgBG compositional range fabricated in this study, which holds promise for wound healing applications. Further studies will assess the efficacy of these glasses against chronic wound-related

biofilms [252], and evaluate the effects of ionic dissolution products released from AgBGs on cellular processes in wound healing.

6.4 Conclusions

Amorphous, homogenous, and anti-bacterial silver doped borate-based glasses with a promising ability to accelerate wound healing have been created using a novel sol-gel processing route. Aqueous reactivity and silver ion release from the sol-gel derived glasses were found to be composition dependent. Furthermore, anti-bacterial activity of AgBGs against *E.coli* and *S. aureus* indicated that AgBGs are effective against both Gram-positive and Gram-negative bacteria resulting in dose dependent efficacy and correlated with silver ion release through glass dissolution. Future work will investigate their efficacy against wound related-infection and their effect on mammalian cells for would healing applications.

Acknowledgements

This study was supported by Canada NSERC, CFI and McGill University Faculty of Engineering Hatch Faculty Fellowship for S.N.N. S.N. is supported by the McGill Engineering Doctoral Award.

6.5 Supporting information

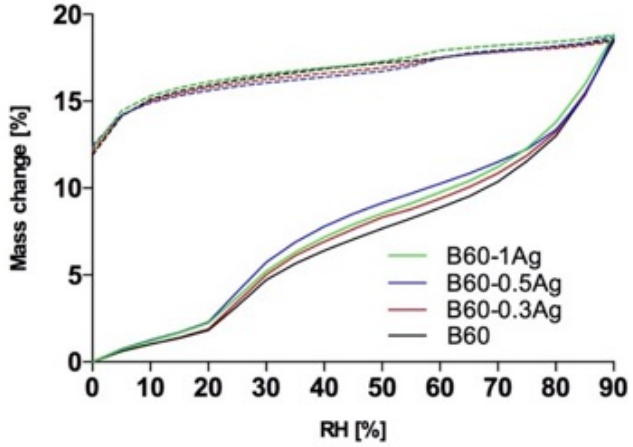

Figure S6. 1: Aqueous interactions of AgBG-3 with various silver content of 0, 0.3, 0.5 and 1 mol% through stepwise increase in RH% at 5% RH up to 90% RH (solid line) then back down to 0% RH (dashed line). The relative mass change was measured when equilibrium (dm/dt < 0.005% min-1) was reached or after maximum of 4h. The sorption phase of all glass particles was characterized by continuous increase in mass when the RH was increased up to a maximum of 90%.

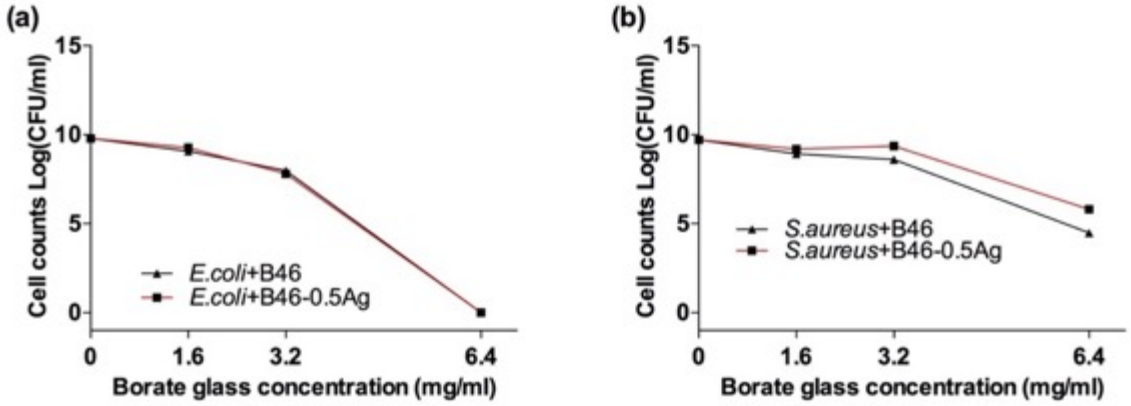

Figure S6. 2: Anti-bacterial efficacy of the B46: AgBG-1 compositional range with 0 and 0.5 mol% silver content at various concentrations of 1.6, 3.2 and 6.4 mg/mL. (a&b) Viable cell count of *E.coli* and *S.aureus*, as a function of glass concentration, respectively. Both glass compositions did not indicate efficacy against *E.coli* and *S.aureus* (Error bars: SD, n = 3).

7 Assessment of Anti-Bacterial Efficacy of and Cellular Responses to Silver-Doped Sol-Gel-Derived Borate Glasses for Wound Healing Applications

In Chapter 6, for the first time, silver doped sol-gel derived borate glasses were reported with anti-bacterial efficacy. The objective of Chapter 7 is to describe the effect of ions released from AgBGs on *in vitro* anti-bacterial efficacy and on keratinocyte and fibroblast cellular functions for chronic wound repair application.

Assessment of Anti-Bacterial Efficacy and Cellular Responses to Silver-Doped Sol-Gel-Derived Borate Glasses for Wound Healing Applications

Shiva Naseri[1], Gabriele Griffanti[1], Vimal B. Maisuria[2], Nathalie Tufenkji[2] and Showan N. Nazhat[1]*

[1]Department of Mining and Materials Engineering, McGill University, Montreal, QC, Canada
[2]Department of Chemical Engineering, McGill University, Montreal, QC, Canada
*corresponding author showan.nazhat@mcgill.ca

KEYWORDS: Borate-based glasses, Wound healing, Biofilm, Keratinocyte

Abstract:

In the case of chronic wounds, healing is complicated by the threat of infection and biofilm formation, which adversely affect the inflammation phase. Recently, borate-based glasses have gained much interest in wound healing applications. The doping of glasses enhances their chemical properties, and their dissolution leads to controlled ionic release with potentially beneficial biological properties. Among these, silver has been demonstrated to be effective against a wide range of bacteria, yet at high concentrations, its cytotoxicity against mammalian cells highlights the need for controlled delivery. In this study, the anti-bacterial efficacy of and keratinocyte and fibroblastic cellular responses to silver-doped sol-gel derived borate glasses (AgBGs) of the compositional range $(60)B_2O_3$-$(36)CaO$-$(4\text{-}X)P_2O_5$-$(X)Ag_2O$ where X = 0.0, 0.3, 0.5 and 1 (mol%) were investigated, *in vitro*. The dose dependent anti-bacterial activity of AgBGs was demonstrated against *Pseudomonas aeruginosa* under planktonic conditions and on their pre-formed biofilms with up to 99.66% reduction in bacterial cell counts. Furthermore, ionic dissolution products from AgBGs were found not to be toxic on keratinocyte and fibroblastic cells at lower concentrations and stimulated the migration of keratinocytes in a dose dependent manner. In sum, a therapeutic borate glass with promising ability to accelerate the healing process has been developed.

7.1 Introduction

The healing of full-thickness skin lesions is a significant clinical challenge, in particular, for diabetic patients with chronic and infected wounds [253]. Current treatments based on the utilization of autografts, allografts, xenografts and bioengineered skin tissue substitutes involve a wide range of limitations, such as lack of bioactivity, possibility of disease transmission and limited availability [254, 255]. For this reason, bioactive glass-based wound dressings have received noticeable research interest as a promising solution for wound repair [35, 80]. While silicate-based bioactive glasses (*e.g.,* Bioglass® 45S5) have been extensively studied and clinically applied in bone and hard tissue engineering [26, 256, 257], more recently, the relatively less durable borate-based glasses have received considerable interest for their wound repair properties [9, 84]. Borate-based bioactive glasses demonstrate higher dissolution rates and greater extent of reactivity [102, 103], and their ionic release through dissolution have been implicated in healing mechanisms, such as anti-bacterial activity [35, 80] and various cellular responses, such as increasing their proliferation and migration as well as stimulating angiogenesis [125]. In both *in vitro* and *in vivo* studies, borate-based glasses have demonstrated significantly higher wound closure and healing rates when compared to silicate-based glasses [35, 80]. For example, in a full thickness skin defect model in rats, *Zhou et al.*, demonstrated that a wound dressing composed of melt-quench-derived borate glass micro-fibers of the composition $(56.6)B_2O$-$(5.5)Na_2O$-$(18.5)CaO$-$(11.1)K_2O$-$(4.6)MgO$-$(3.7)P_2O_5$ (wt.%) had significantly higher blood vessel formation and wound closure rates than 45S5 glass microfibers, which was attributed to the presence of boron and its angiogenetic ability [125]. Using a similar model in rats, *Zhao et al.*, showed that the utilization of melt-quench-derived borate glass fibers of the composition $(56.6)B_2O$-$(5.5)Na_2O$-$(18.5)CaO$-$(11.1)K_2O$-$(4.6)MgO$-$(3.7)P_2O_5$ (wt.%) doped with 0–3.0 wt.% CuO led to significantly higher rates of wound closure and blood vessel formation when compared to non-treated wounds [136]. More recently, it was reported that melt-quench-derived borate bioactive glass microfibers had the capacity to heal skin defects in humans [174, 258] along with a formulation (MIRRAGEN™, ETS Wound Care LLC, USA) obtaining US Food and Drug Administration (FDA) approval as a matrix for acute and chronic wound healing [10].

Chronic wounds suffer from repeated tissue insults and infection, which adversely affect the inflammation phase of the healing process [253]. In fact, due to the potential formation of

antibiotic resistant biofilms, it is critical to eliminate any infection to accelerate the healing process [259]. Thus, inorganic anti-bacterial therapeutics such as Ag^+ ion are of interest attributable to their low cost, and no bacterial resistance when compared to antibiotics [27]. Silver ion has been demonstrated to be anti-bacterial [150] with anti-inflammation properties [260] and to have the ability of stimulating the migration of fibroblast cells to a wound site [261].

Using a recently reported novel route, the sol-gel processing of silver doped borate glasses (AgBGs) of the compositional range $(60)B_2O_3$-$(36)CaO$-$(4\text{-}X)P_2O_5$-$(X)Ag_2O$ where X= 0.0, 0.3, 0.5 and 1 (mol%), glasses with promising anti-bacterial efficacy against Gram-positive and Gram-negative bacteria have been developed (Chapter 6). However, it is also known that at high dosages, silver ion can be toxic to cells. Depending on the biological environment and cell type, the toxic concentration of silver ion on mammalian cells has been reported to be in the range of 1 to 10 ppm [151]. Given that silver-based biomaterials do not discriminate between healthy cells involved in wound healing and pathogenic bacteria [179], it is imperative to evaluate both cytotoxicity and anti-bacterial efficacy to better understand the effects of silver ion on the healing process. Therefore, the objective of this study was to evaluate an optimum glass composition and concentration that demonstrates anti-bacterial efficacy, yet at the same time enhances the cellular functions, *in vitro*. For this, the anti-bacterial efficacy of these glasses was evaluated against *Pseudomonas aeruginosa* (*PA14*), an opportunistic pathogen in chronic wounds with the ability to form resistant biofilms [259]. Furthermore, the dose effect of the ionic dissolution products of AgBGs on keratinocyte and fibroblastic cells were investigated to assess their potential in accelerating the healing of chronic wounds.

7.2 Experimental

7.2.1 Materials and methods

Silver doped, sodium free borate-based glasses of the compositional range $(60)B_2O_3$-$(36)CaO$-$(4\text{-}X)P_2O_5$-$(X)Ag_2O$ where X= 0.0, 0.3, 0.5 and 1 (mol%) were produced, by the sol-gel process. Boric acid (Sigma Aldrich), calcium methoxyethoxide (Gelest), triethyl phosphate (Sigma Aldrich) and silver nitrate (Fisher Scientific) were used as precursors. Initially, boric acid was mixed with ethanol based on the solubility of boric acid (~11.2 %) into a Teflon beaker covered by a Teflon cap and magnetically stirred at ~40 °C for 30 min. Triethyl phosphate was then added

and the mixture was stirred further for 30 min, followed by the addition of silver nitrate into the resultant sol and stirred for another 30 min. Calcium methoxyethoxide was then added and the sol was stirred for a final 30 min. Afterwards, the sol was transferred into plastic vials and aged for 5 days at 37 °C. The aged sols were initially dried in a fume hood at room temperature for 2 days while covered with a non-transparent box to protect them from exposure to light and then followed by further drying at 120 °C for 2 days. The dried as-made powders were then calcined at 400 °C for 2 h. All glass particles were ground and sieved to 25 – 75 μm particle size fraction and stored in a desiccator until analysis.

7.2.2 Scanning electron microscopy (SEM)

An Inspect F50 Field Emission Scanning Electron Microscope (FEI Corporation, USA) was used to analyse the morphological characteristics of the AgBG particles with an applied voltage of 5 kV.

7.2.3 Inductively coupled plasma optical emission spectrometry

Release of silver, boron, calcium, and phosphorus ions from glass powders in Dulbecco's modified Eagle's medium (DMEM; Sigma) at a concentration of 1.5 mg/mL, were quantified using an inductively coupled plasma–optical emission spectrophotometer (ICP-OES, Thermo Scientific iCAP 6500, USA). Aliquots of were filtered through a 0.2 μm nylon filter and stored in a 15 mL falcon tube to which 4% (w/v) nitric acid (Fisher Scientific, Canada) was added.

7.2.4 Anti-bacterial assessment

7.2.4.1 Mean viable cell counts

The anti-bacterial activity of glasses was examined using the viable cell count method. An overnight culture of 3 ml of *Pseudomonas aeruginosa* (*PA14*), was diluted in Mueller Hinton Broth 2 (MHB-II, Oxoid; Fisher Scientific Canada) to 0.05 optical density (OD) value at 600 nm. AgBGs at various concentrations (0.375, 0.75, 1.5 and 3 mg/mL) were mixed with *Pseudomonas aeruginosa* (*PA14*) bacteria suspension in MHB-II. Serially dilutions in phosphate-buffered saline (PBS) were undertaken to quantitate effectively, which were placed on the surface of LB agar plate. Then after 20 h incubation at 37 °C the number of colonies was counted. All measurements were done in triplicate on different days.

7.2.4.2 Bacteria growth curves

Bacteria growth curves were measured by directly exposing the glass particles to bacteria suspensions of *P. aeruginosa* PA14 in MHB-II (0.375 and 0. 75 mg/mL) with an initial bacterial cell density of 0.05 OD_{600nm}. Their OD_{600nm} value was then measured up to 72 h at 37 °C using Tecan Infinite M2000 microplate reader (Tecan group Ltd., Switzerland). All measurements were done in triplicate on different days.

7.2.4.3 Efficacy of AgBGs against *PA14* biofilms

A biofilm was formed by placing glass discs (1cm diameter) into 24-well plates containing inoculum of *PA14* in MHB-II and incubated overnight at 37 °C. Then, the discs were washed gently using sterile PBS to remove non-adherent cells. After washing, discs were placed in a fresh 24-well plate containing 500 µl of ionic dissolution products of silver doped borate glasses with silver content in the range of (0, 0.3, 0.5 and 1 mol%) and glass concentration of 1.5 mg/mL in MHB-II and incubated at 37 °C for 4 h. The discs then were removed and washed using PBS and placed in sterile Falcon tubes containing 2 mL of sterile PBS solution and sonicated in a bath sonicator (60 Hz and 150 W) for 10 min to disrupt any remaining biofilm. The bacterial cell concentration in the resulting suspension was quantified using standard viable cell counts as mentioned in section 7.2.4.1. All measurements were done in triplicate on different days.

7.2.5 Assessment of cellular functions in the presence of AgBG dissolution products

7.2.5.1 Cells culture

The HaCat Human derived keratinocyte cell line (kindly provided by Dr. Anie Philip's group, McGill University) was cultured in T-75 culture flask in DMEM supplemented with 10% fetal bovine serum (FBS) (Hyclone) and 1% penicillin streptomycin (Invitrogen). Cells were incubated at 37 °C under humidified air containing 5% CO_2. At 80% confluency, the cells were washed with sterile PBS, detached with 0.25% trypsin ethylenediaminetetraacetic acid solution (Wisent), and counted using a hemocytometer. Cells between passages 38 and 39 were used for cellular studies.

The NIH/3T3 Mouse derived fibroblastic cell line (ATCC® CRL-1658™) was cultured in T-75 culture flask in DMEM supplemented with 10% fetal calf serum (FCS) (Hyclone) and 1% penicillin streptomycin (Invitrogen). Cells were incubated at 37 °C under humidified air containing 5% CO_2. At 80% confluency, the cells were washed with sterile PBS, detached with 0.25% trypsin ethylenediaminetetraacetic acid solution (Wisent), and counted using a hemocytometer. Cells between passages 9 and 10 were used for cellular studies.

7.2.5.2 Live/dead assay

HaCat cells were plated directly into 96-well assay plates at a density of 4000 cells/well and cultured in the presence of ionic release products generated from the dissolution of AgBGs at three concentrations in DMEM (0.375, 0.75 and 1.5 mg/mL). After 1, 4, or 7 days in culture, cells were stained with 1 μM calcein-AM and 2 μM ethidium homodimer-1 (Live/dead assay; Invitrogen) for 15 min. Images of green fluorescent viable cells and red fluorescent dead cell nuclei were acquired in the same well plates using an Olympus IX81 inverted microscope equipped with a UPlanSApo 10 objective (UIS2 series). All conditions were tested in triplicates.

7.2.5.3 Measurement of cell viability

HaCat and NIH/3T3 cells were plated directly into 96-well assay plates at a density of 4000 cells/well and cultured in the presence of ionic release products generated from the dissolution of the AgBGs in DMEM at three concentrations (0.375, 0.75 and 1.5 mg/mL). After 1, 4, or 7 days in culture, cells were incubated with 2 μM calcein-AM in 100 mL PBS. After 15 min, fluorescence was measured in the Mitras LB 940 microplate reader using a 485/535nm excitation/emission filter pair. All conditions were tested in triplicates.

7.2.5.4 Cell metabolic activity

The AlamarBlue™ assay (Invitrogen) was used to assess the effect of ionic dissolution products on the metabolic activities of HaCat and NIH/3T3 cells. Cells were plated directly into 24-well assay plates at a density of 8000 cells/well and cultured in the presence of ionic release products generated from the dissolution of the AgBGs in DMEM at three concentrations (0.375, 0.75 and 1.5 mg/mL). At days 1, 4, and 7 in culture the AlamarBlue™ reagent (5%) was added to each well and, after 4 h incubation at 37 °C, 100 mL aliquots were collected and transferred to a

96-well plate for analysis. The fluorescent intensity of reduced AlamarBlue was measured using a Mitras LB 940 microplate reader (Berthold Technologies) equipped with a 555 nm excitation filter and a 580 nm emission filter. After measurements had been completed, media in the 24-well plates were replaced for ongoing treatment. All conditions were tested in triplicates.

7.2.5.5 Migration assay

The effect of the AgBG ionic dissolution products on the migration of HaCat cells was assessed using the ibidi^{TM} Culture-Insert 3 Well. Cells at a density of 270000 cells/well were initially cultured in each well for 24 h in DMEM in a humidified incubator at 37 °C and under 5% CO_2. After 24 h, the Culture-Insert was gently removed using sterile tweezers followed by washing the cells with PBS twice. The uniform scratch was observed. Then the culture medium was supplemented with ionic release products generated from the dissolution of the AgBGs in DMEM at two concentrations (0.75 and 1.5 mg/mL) and cultured for a further 24 h. Cells cultured with neat DMEM were used as control. Cell migration was observed with an inverted microscope (Leica DMI 3000B, Germany), and images were taken with a CCD camera (Leica DFC 420C). All conditions were tested in duplicates.

7.2.6 Statistical analysis

Data for each assay time point were analyzed for statistical significance between conditions using a Student's t-test at a significance level of $p < 0.05$.

7.3 Results and discussion

7.3.1 Morphological analysis of glass particles

Figure 7.1 shows the glass particles with well distributed particle sizes in the range of 25-75 μm and defined surfaces after calcination at 400 °C. Higher magnification images (Figures 7.1 d-f), indicated their smooth surfaces.

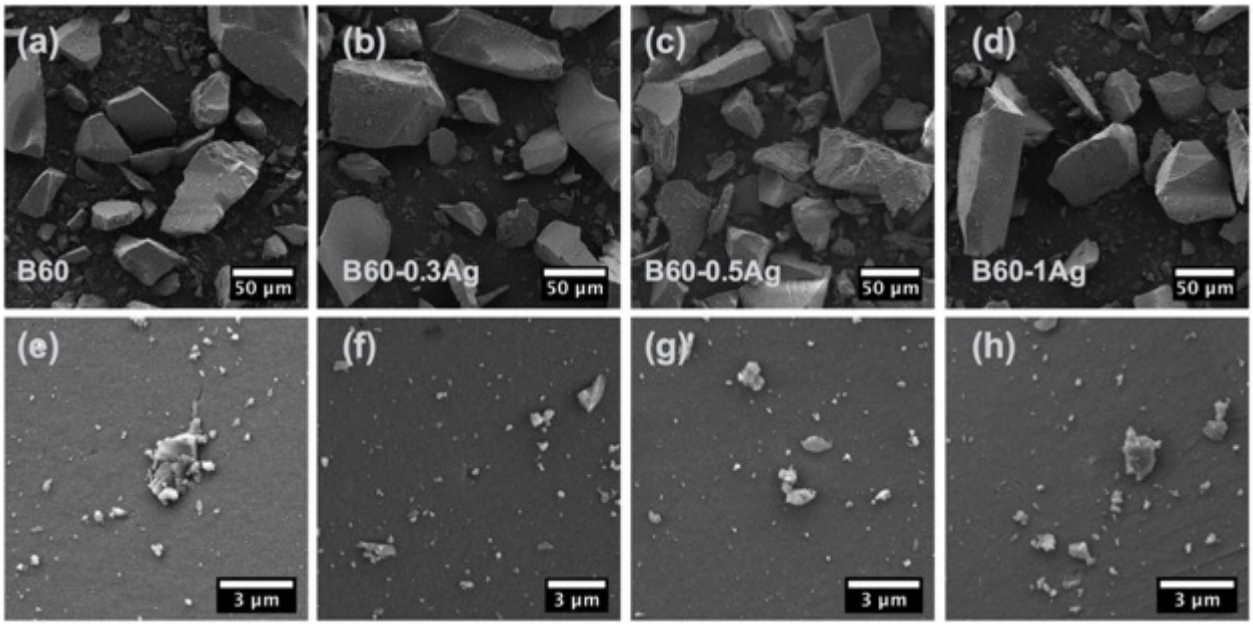

Figure 7. 1: SEM micrographs of the different AgBG glass particle compositions: overview (a, b, c and d for B60, B60-0.3Ag, B60-0.5Ag, and B60-1Ag, respectively) and higher magnification (e, f, g and h for B60, B60-0.3Ag, B60-0.5Ag, and B60-1Ag, respectively).

7.3.2 Glass dissolution and ion release in culture medium

ICP-OES analysis was carried out to examine the ionic release profiles from the dissolution of AgBG particles after immersion in cell culture medium (Figure 7.2). The total boron and calcium ion release in cell culture medium were in agreement with their equivalents in deionized water [24] (Chapter 6). Furthermore, phosphorus and calcium ion release decreased over time which may be due to the the formation of calcium-phosphate precipitates [16]. The extent of silver ion release from the glasses increased with its doping levels in the AgBGs. However, silver ion release in cell culture medium was lower than that observed in deionized water (Figure 6.4b), which can be attributed to the presence of chloride ions as well as organic compounds in the culture medium and the potential formation of silver complexes [262].

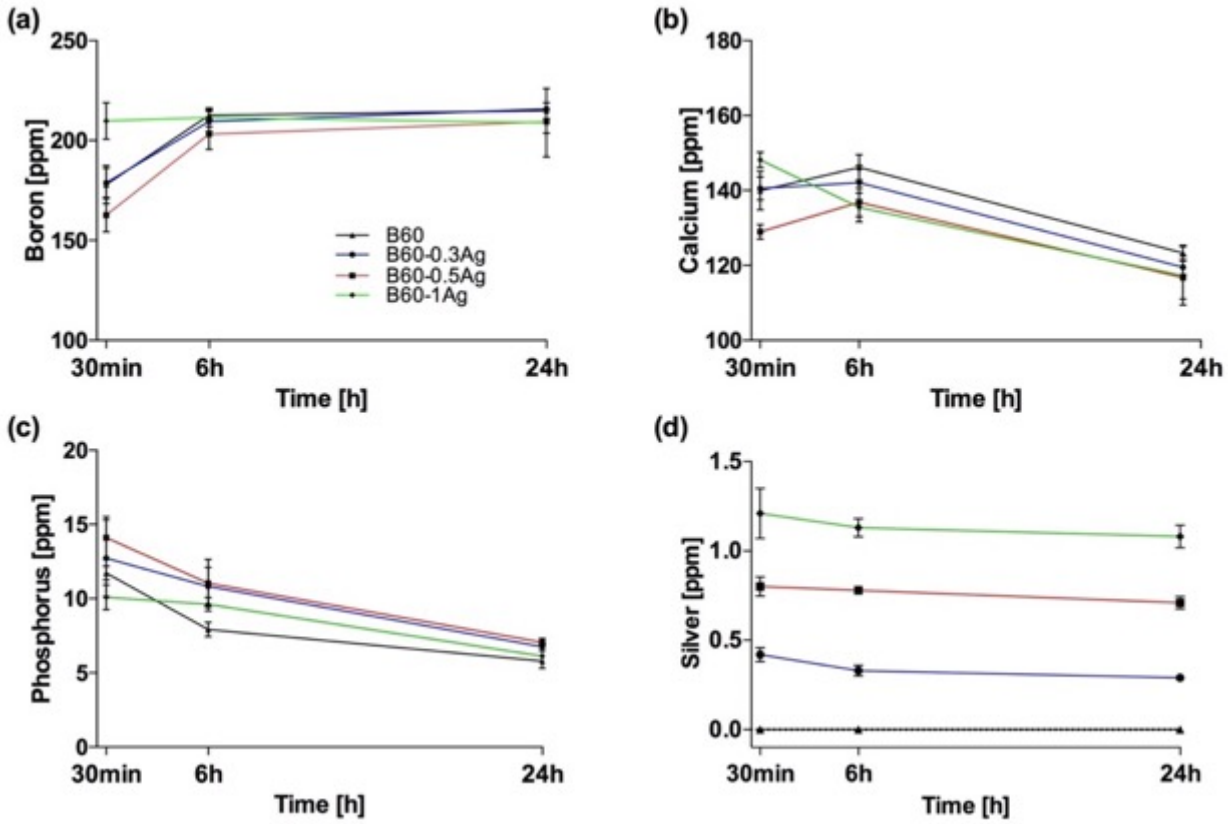

Figure 7. 2: Ionic dissolution products of AgBGs in cell culture medium. (a) boron, (b) calcium, (c) phosphorus, and (d) silver ion release as measured through ICP-OES (Error bars: Standard deviation: SD, n = 3).

7.3.3 Determination of anti-bacterial efficacy of AgBG against *PA14*

Anti-bacterial efficacy of AgBGs at different concentrations was investigated against the viability and growth of a wound-associated pathogen, *PA14*, in both planktonic culture state as well as in biofilm eradication. *PA14* is an opportunistic Gram-negative pathogen causing both acute and chronic infections [263], and has been shown to be difficult to eradicate in skin-related infections since this pathogen has an intrinsic antibiotic resistance, resulting in the formation of chronic wounds [259]. The viable cell count method showed that the ionic dissolution products of AgBGs were effective against *PA14* in a dose dependent manner (Figure 7.3a). For example, AgBGs with 0.5 or 1 mol% silver were 100% effective in killing the bacteria even at the lower concentration of 0.375 mg/mL, while B60-0.3Ag was only effective at the concentration of 1.5 mg/mL. Additionally, the non-silver doped glasses (B60) demonstrated some anti-bacterial

activity at the concentration of 3 mg/mL, where the number of bacteria cell counts underwent a slight decrease. This may be attributed to the increase of local pH [118, 120].

To further evaluate the dose-dependent anti-bacterial efficacy, the growth curve of *PA14* planktonic cells was measured when directly exposed to the AgBG compositional range. Figure 7.3c&b show the growth curves of *PA14* when exposed to 0.375 and 0.75 mg/mL of AgBGs up to 3 days, respectively. It was demonstrated that B60-1Ag glass particles inhibited growth of *PA14* bacteria up to 3 days at both used concentrations, while B60-0.5Ag glass particles were able to inhibit bacteria growth up to day 1 even at the concentration of 0.375 mg/mL. In the case of B60-0.3Ag, the higher concentration of 0.75 mg/mL was required to inhibit bacteria growth and only up to day 1. Non-silver doped glasses, on the other hand, did not inhibit bacterial growth. This result verifies the correlation between anti-bacterial efficacy of AgBGs and silver content in the glass composition in a dose dependent manner. In summary, the anti-bacterial analysis suggested that silver doped AgBG glasses inhibited the growth of *PA14* bacteria in prolonged incubation period.

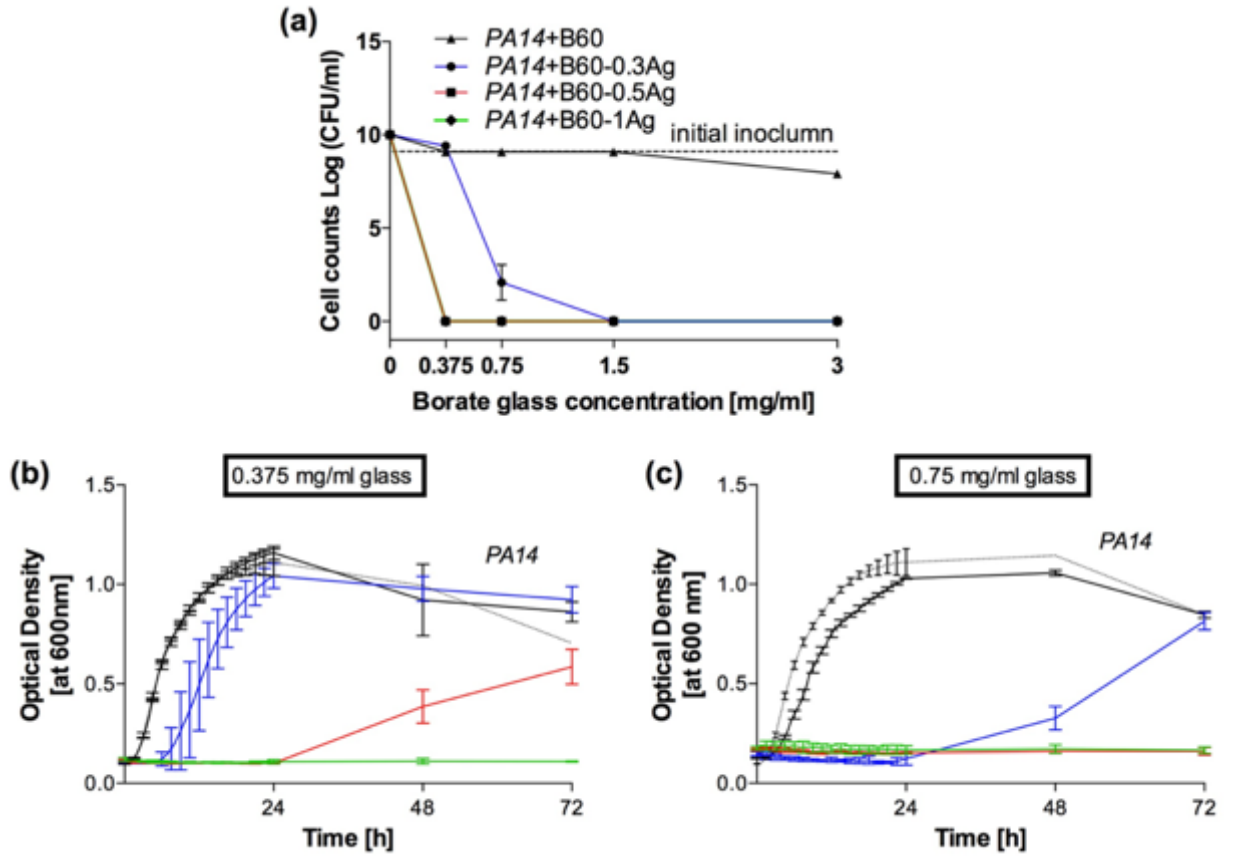

Figure 7. 3: Anti-bacterial efficacy of the AgBG compositional range. (a) Viable cell count of *PA14* as a function of silver content and glass concentration. (b&c) Growth curve of *PA14* at glass concentrations of 0.375 and 0.75 mg/mL, respectively. (Error bars: SD, n = 3).

Figure 7.4 shows the effect of ionic dissolution products from AgBGs at a concentration of 1.5 mg/mL on pre-formed *PA14* biofilms and compared against a control (untreated *PA14* biofilms), where the biofilms were treated only with MHB-II and no utilization of an anti-bacterial agent. It was demonstrated that the bacterial cell counts were reduced by increasing the silver content from 0.3 to 1 mol% in the glass formulation in comparison with the control biofilm (Figure 7.4a). A 99.66% reduction in cell count was achieved when the biofilm was treated with ionic dissolution products from B60-1Ag (Figure 7.4b). Furthermore, it was demonstrated that the non-silver doped glasses reduced the cell counts by 20%, which may be due the increase in the local pH and the osmotic pressure [106, 264, 265].

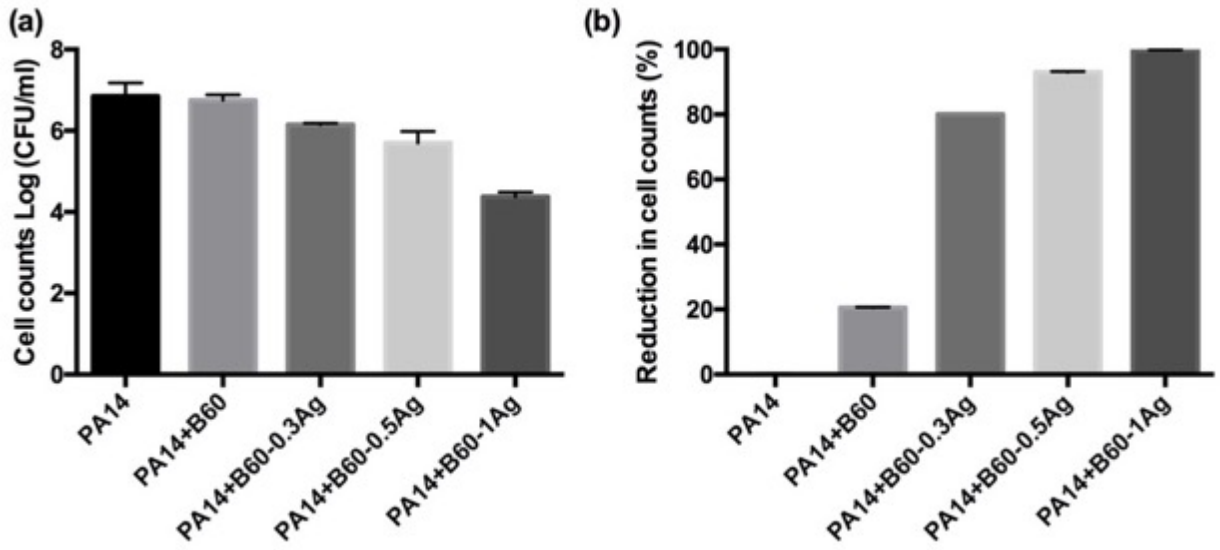

Figure 7. 4: The effect of ionic dissolution products of AgBG on (a) cell counts and (b) equivalent reduction in cell counts of *PA14* bacteria biofilm (Error bars: SD, n = 3).

7.3.4 Effect of AgBG ionic dissolution products on keratinocyte viability and metabolic activity

In order to evaluate the effect of silver ion on HaCat cells, the Live/Dead assay was carried out on cells treated with AgBG ionic dissolution products at concentrations of 0.375, 0.75 and 1.5 mg/mL and visualized up to 7 days in culture (Figures 7.5, 7.6 and 7.7, respectively). In general, under all conditions, there was an increasing trend in the density of viable cells from days 1 to 7. At day 1, predominantly live cells were observed independent of silver content. By day 4, the silver-treated cultures revealed a higher density of viable cells despite the presence of some dead cells. However, at day 7 the presence of viable cells was lower in B60-1Ag when compared to the other conditions. In general, presence of silver ion at lower concentrations did not indicate toxicity against keratinocytes since only a low number of dead cells was observed. It can be summarized that the proliferation rate of cells was slower in the presence of silver ions than those in the control medium.

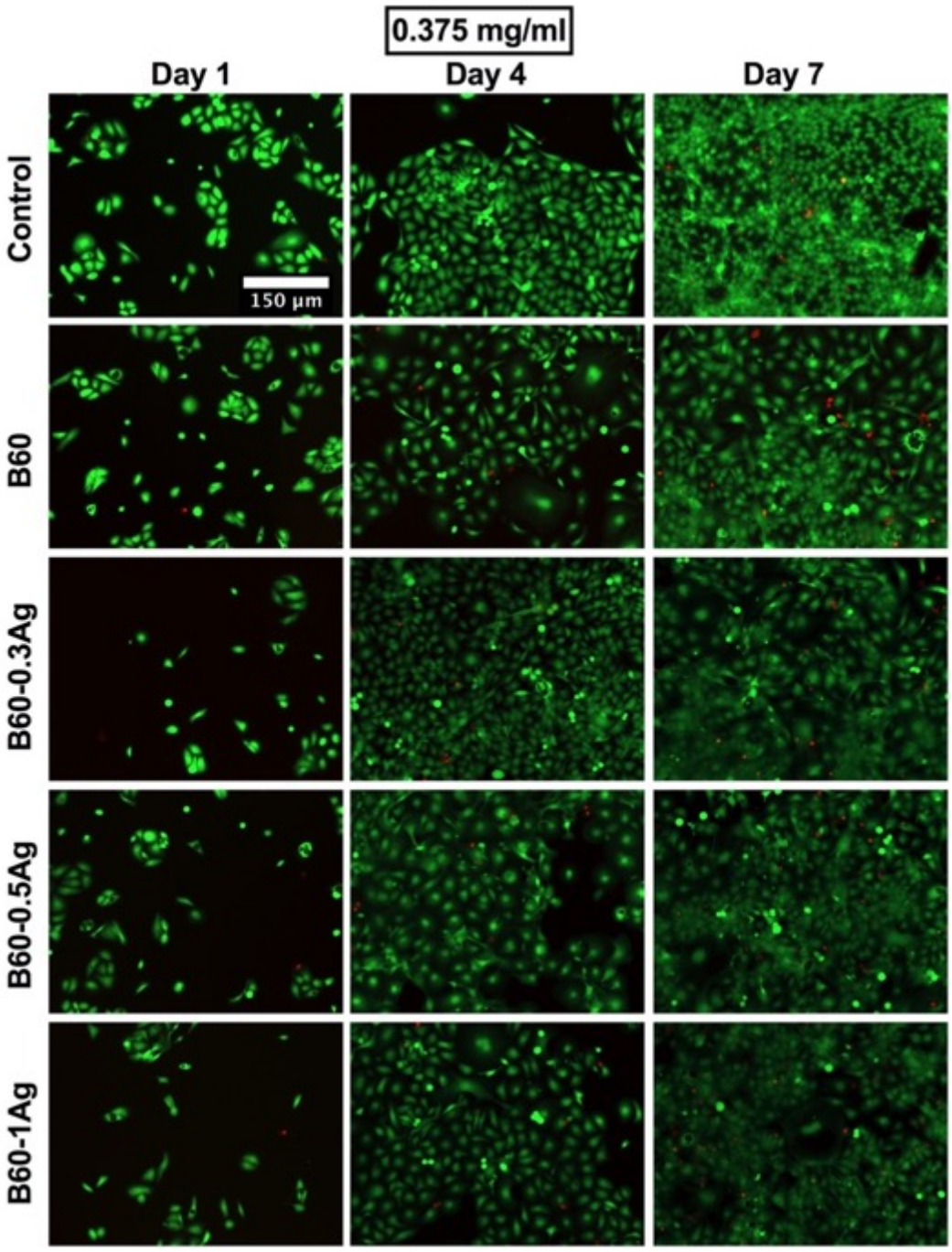

Figure 7. 5: Calcein-AM labeled live HaCat cells (green) and ethidium homodimer-1 binding dead nuclei (red) at days 1, 4 and 7 in culture supplemented with ionic dissolution products of AgBGs at concentration of 0.375 mg/mL, Scale bar = 150 µm.

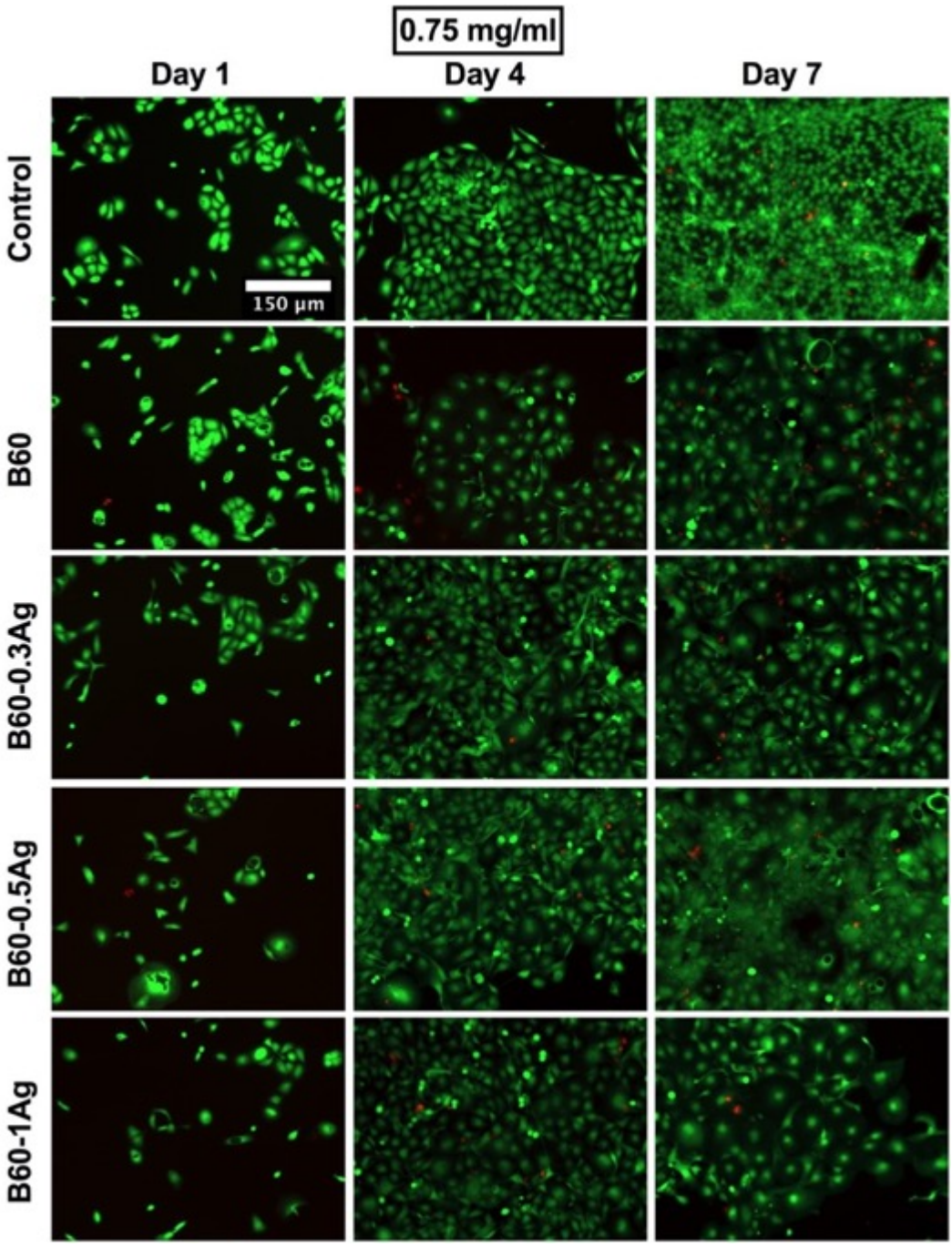

Figure 7. 6: Calcein-AM labeled live HaCat cells (green) and ethidium homodimer-1 binding dead nuclei (red) at days 1, 4 and 7 in culture supplemented with ionic dissolution products of AgBGs at concentration of 0.75 mg/mL, Scale bar = 150 µm.

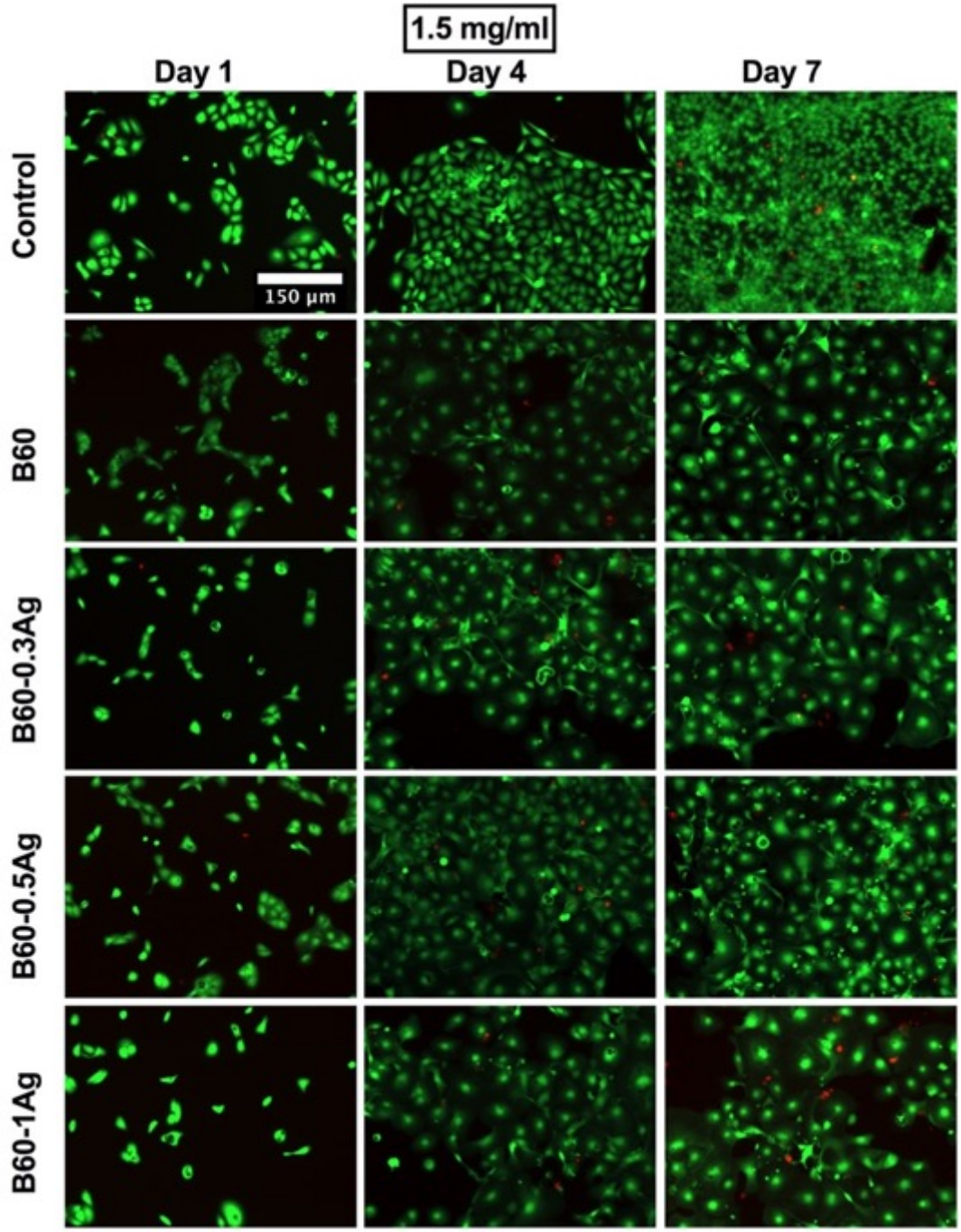

Figure 7. 7: Calcein-AM labeled live HaCat cells (green) and ethidium homodimer-1 binding dead nuclei (red) at days 1, 4 and 7 in culture supplemented with ionic dissolution products of AgBGs at concentration of 1.5 mg/mL, Scale bar = 150 µm.

To better evaluate the effect of ionic release products on HaCat cell viability, the fluorescence of calcein-AM stained live cells was measured (Figure 7.8). In general, there was an increasing trend in the viability of cells from days 1 to 7, independent of conditioning, except for the B60-1Ag when applied at the higher concentrations of 0.75 and 1.5 mg/mL. The non-silver doped glasses (B60) were compared with the control medium (CTR) at all three concentrations to evaluate the effect of boron on cell viability. At 0.375 and 0.75 mg/mL concentrations, there was no significant difference between B60 and control groups indicating that boron did not affect cell viability at lower concentrations (Figures 7.8 a&b). However, in line with the Live/Dead assay, the higher concentration of B60 (*i.e.,* 1.5 mg/mL) showed a significant reduction in cell viability, when compared to those cultured under the control medium (Figure 7.8c).

To better understand the effect of silver on HaCat cell viability, the effect of the ionic dissolution products from the silver doped glasses were compared to that of the baseline formulation (B60). At a concentration of 0.375 mg/mL, cell viability was increased with an increase of up to 0.5 mol% silver. However, a further increase in the silver content up to 1 mol% caused a decrease in keratinocyte cell viability at days 4 and 7 (Figure 7.8a). At a concentration of 0.75 mg/mL, it was observed that cell viability in the presence of B60-1Ag was significantly reduced at day 7 when compared to the B60 group (Figure 7.8b). Figure 7.8c shows the viability of HaCat cells when exposed to the glass ionic dissolution products in cell culture medium at a concentration of 1.5 mg/mL. At day 4, there was an increase in cell viability with an increase in silver content up to 0.5 mol%, which then decreased with a further increase in silver content up to 1 mol%.

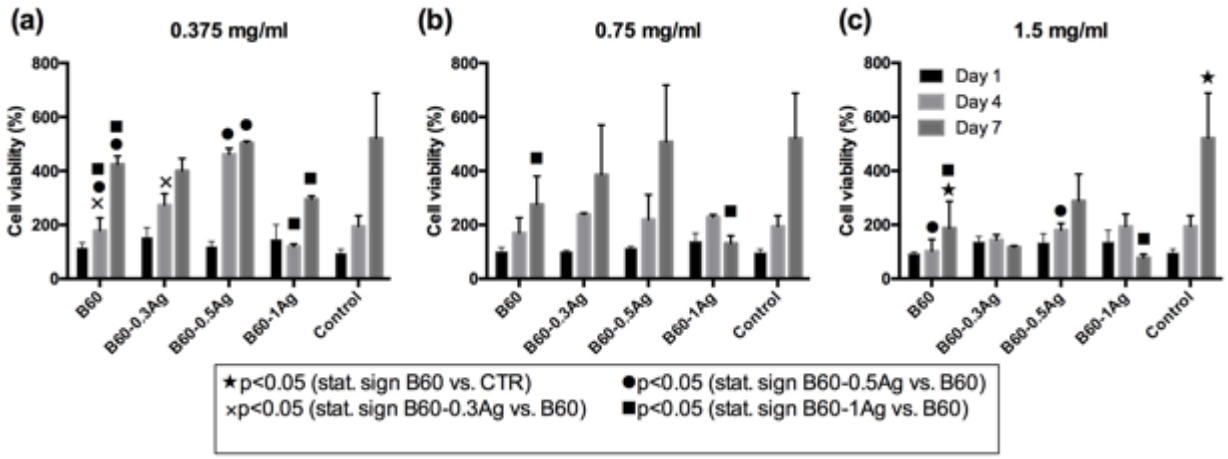

Figure 7. 8: HaCat cell viability (expressed as percentage relative to control at day 1) determined from the fluorescence signal of calcein-AM labeled live cells, treated with ionic dissolution products of AgBGs at concentrations of (a) 0.375, (b) 0.75, and (c) 1.5 mg/mL for up to 7 days in culture (Error bars: SD, n = 3).

Figure 7.9 shows the metabolic activity of HaCat cells cultured over 7 days in media conditioned with ionic dissolution products from AgBGs at concentrations of 0.375, 0.75 and 1.5 mg/mL. In general, there was an increasing trend in the proliferation rates of keratinocyte cells from days 1 to 7, independent of the condition. The non-silver doped glasses (B60) were compared with the control medium (CTR) at all three concentrations to evaluate the effect of boron on metabolic activity. At the concentrations of 0.375 and 0.75 mg/mL, the ionic dissolution products from B60 showed no significant difference on metabolic activity when compared to the control. However, at a higher concentration of 1.5 mg/mL, there was lower metabolic activity in comparison with the control medium at days 4 and 7.

To better understand the effect of silver on HaCat metabolic activity, the effect of the ionic dissolution products from the silver doped glasses were compared to that of the baseline formulation (B60). At concentrations of 0.375 and 0.75 mg/mL silver content in the culture medium did not affect the metabolic activity. However, at day 7 in culture, exposure to ionic dissolution products from B60-0.3Ag at the higher concentration of 1.5 mg/mL caused an increase in the metabolic activity of the HaCat cells relative to those cultured in the presence of B60 ionic products.

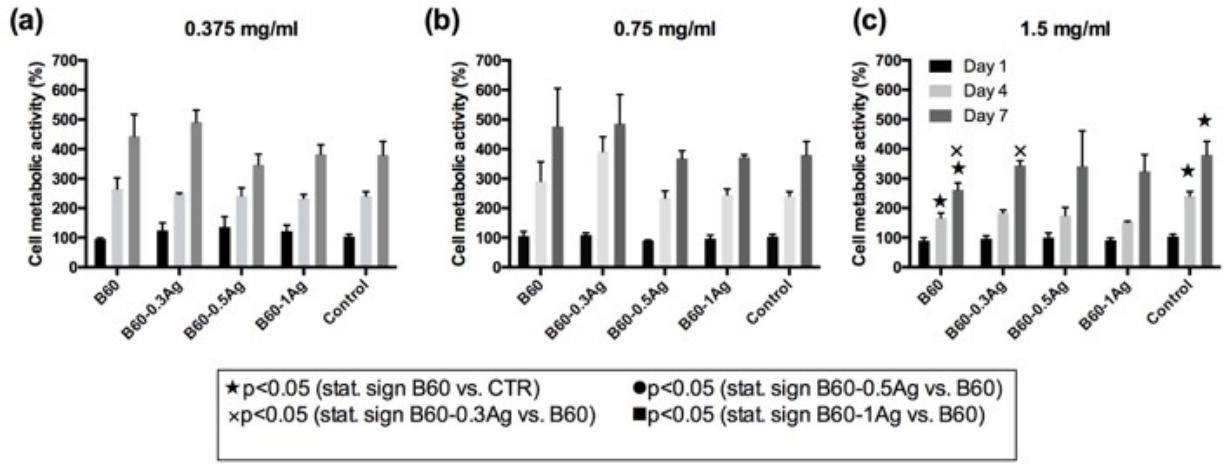

Figure 7. 9: Metabolic activity (expressed as percentage relative to control at day 1) of HaCat cells treated with ionic dissolution products of AgBGs at concentrations of (a) 0.374, (b) 0.75, and (c) 1.5 mg/mL for up to 7 days in culture (Error bars: SD, n = 3).

AlamarBlue® reduction also indicated that the higher concentration of 1.5 mg/mL of non-silver doped glasses led to a lower metabolic activity when compared with the control at days 4 and 7. This reduction in metabolic activity may be due to a high concentration of boron and its potential toxic effect on the HaCat cells, inhibiting both their proliferation and metabolic activity [135]. This finding was in line with the cell viability data and suugested that silver ion up-regulated cell metabolism up to an optimum concentration, effectively extending cell survival. Furthermore, it can be inferred that an optimum sliver ion concentration (less than 1 ppm, B60-0.3Ag and B60-0.5Ag formulations) in the cell culture medium stimulated keratinocyte metabolic activity. Deviation from this concentration may result in an adverse effect on HaCat cell proliferation and viability.

7.3.5 Effect of AgBG ionic dissolution products on fibroblast viability and metabolic activity

In order to evaluate the effect of silver ion on NIH/3T3 cells, the fluorescence of calcein-AM stained live cells was measured (Figure 7.10). The non-silver doped glasses (B60) were compared with the control medium (CTR) at all three concentrations to evaluate the effect of boron release on cell viability. At all concentrations, there was a significant reduction in cell viability when conditioned with ionic dissolution products form B60 when compared to those seeded in the control medium (Figure 7.10a,b&c). To better understand the effect of silver ion on fibroblastic

cell viability, the ionic dissolution products from the silver doped glasses were compared to those released from the baseline formulation (B60). There was no significant difference among the AgBG groups at concentrations of 0.375 and 1.5 mg/mL which suggest that at these concentrations, silver was not toxic to NIH/3T3 cells. Furthermore, the fibroblastic cell viability increased at day 7 by increasing silver content from 0.3 to 1 mol% in comparison with non-doped borate glass formulation at concentration of 0.75 mg/mL. Hence, the toxicity may be due to high concentrations of boron [135].

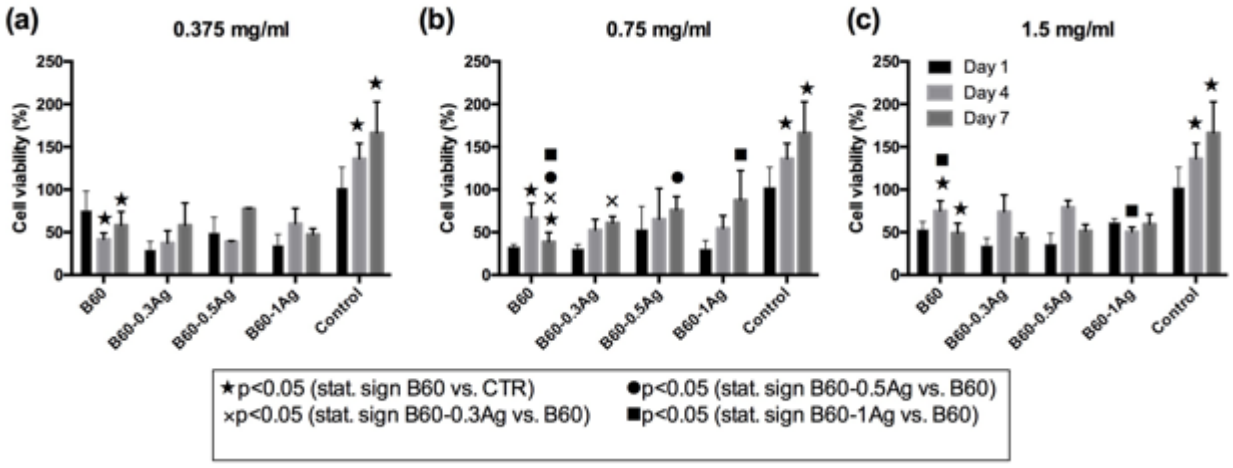

Figure 7. 10: NIH/3T3 cells viability (expressed as percentage relative to control at day 1) determined from the fluorescence signal of calcein-AM labeled live cells, treated with ionic dissolution products of silver doped borate glasses with silver content in the range of (0, 0.3, 0.5 and 1 mol%) and glass concentration of (a) 0.375, (b) 0.75, and (c) 1.5 mg/mL for up to 7 days in culture (Error bars: SD, n = 3).

Figure 7.11 shows the metabolic activity of NIH/3T3 cells cultured over 7 days in media conditioned with ionic dissolution products from AgBGs at concentration of 0.375, 0.75 and 1.5 mg/mL. In general, there was an increasing trend in the metabolic activity of fibroblasts from days 1 to 7, independent of the condition. Compared to the control, there was a lower metabolic activity in NIH/3T3 cells when treated with the B60 ionic dissolution products at days 4 and 7. On the other hand, there was no significant difference between the metabolic activity of NIH/3T3 cells

when conditioned with ionic dissolution products from silver containing glasses and those from the non-doped glass formulation.

Given together, these results suggest that boron has a toxic effect on cell viability at higher concentrations and in line with previous reports [135]. It has also been suggested that the toxic effect of boron can be reduced or eliminated in dynamic flow conditions, which can simulate *in vivo* environment more closely [125, 136]. Brown et al., investigated the *in vitro* biological response of biomaterials for wound healing applications and showed that there is a need for a more reliable method to be able to achieve similar results as *in vivo* [266]. It was proposed that *in vitro* culturing under moderate dynamic conditions may result in a higher cell density and lower toxicity when compared with that under static condition [266]. Furthermore, Yang et al., demonstrated that human skin fibroblast cell viability and proliferation rate can be improved under ideal dynamic flow rate [135]. It was mentioned that under static condition which is in contrast of real wound healing environment, the local increase of boron concentration is highly toxic to cells [135].

It can also be noted that the addition of silver into the glass network can enhance cell viability in comparison with the non-silver doped formulation. For example, it was demonstrated that, glasses containing 0.5 mol% (1.7 wt%) silver were not toxic to keratinocyte and fibroblastic cells. This finding was in line with a previous study [140], which investigated the cytotoxic effect of silver-doped melt-quench derived borate-glasses (doped with 0.75, 1 and 2 wt% Ag_2O) on osteoblastic and fibroblastic cells, *in vitro* [140]. It was found that the ionic dissolution products from glasses with 0.75 and 1 wt.% Ag_2O indicated no toxic effects, whereas glasses with 2 wt% Ag_2O were toxic [140].

These results confirm that the cytotoxic effects of anti-bacterial silver-based biomaterials should be considered for wound care strategies since it was widely shown that both keratinocytes and fibroblasts are susceptible to damage when exposed to high concentrations of silver in spite of its beneficial effect in reducing inflammation and accelerating the early phases of wound healing [179].

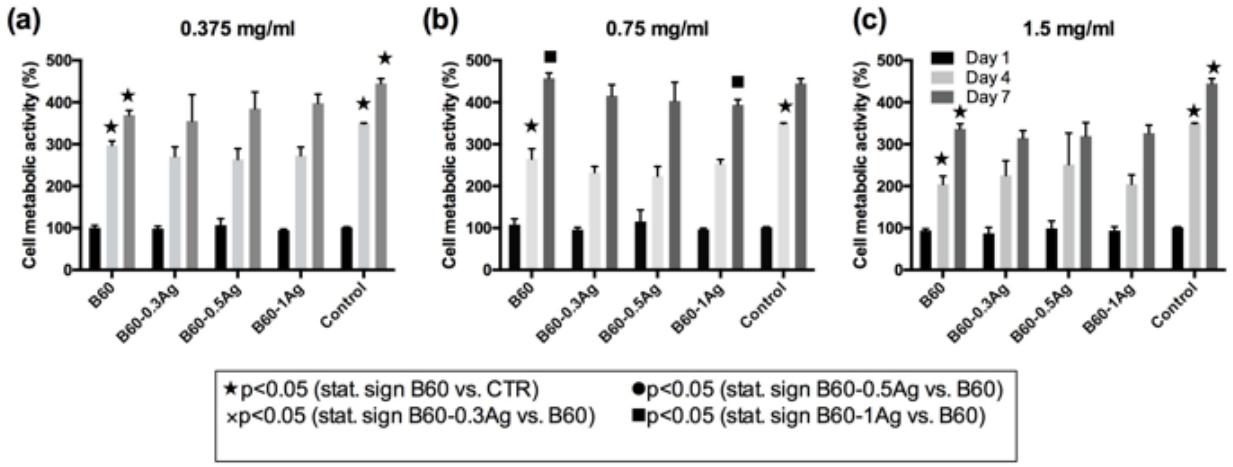

Figure 7. 11: Metabolic activity (expressed as percentage relative to control at day 1) of NIH/3T3 cells treated with ionic dissolution products of silver doped borate glasses with silver content in the range of (0, 0.3, 0.5 and 1 mol%) and glass concentration of (a) 0.375, (b) 0.75, and (c) 1.5 mg/mL for up to 7 days in culture (Error bars: SD, n = 3).

7.3.6 Effects of AgBG ionic dissolution products on the migration of keratinocytes

Ionic dissolution products from glasses dissolved in medium at the concentrations of 0.75 and 1.5 mg/mL were used to investigate the effect of AgBGs on HaCat cell migration (Figure 7.12). At 0 h, scratches of similar width (500 ± 50 μm) were made on the base of each well cultured with HaCat cells using the Culture-Insert^{TM}. After 24 h in culture, qualitatively the scratch in the control and non-doped glasses (B60) group becomes only slightly narrower. However, the width of scratch in the silver doped glasses at the concentration of 0.75 mg/mL decreased in line with an increase in glass silver content, which almost disappeared, indicating that the AgBG ionic dissolution products stimulated HaCat cell migration. By increasing the glass concentration to 1.5 mg/mL, the width of the scratch in the presence of ionic dissolution products of AgBGs containing silver was reduced in the case of 0.5 mol% silver content and increased when B60-1Ag glass composition was utilized. Figure 7.12b shows the statistical analysis of the cell migration assay, which indicated that the percentage of scratch shrinkage in medium conditioned with AgBG ionic dissolution products increased with increasing silver content at the concentration of 0.75 mg/mL. However, at the higher concentration of 1.5 mg/mL, the ionic dissolution products from the B60-1Ag glass formulation demonstrated a lower extent of scratch shrinkage when compared with that of the B60-0.5Ag, though still significantly higher than that of the control and medium exposed to

non-doped glass (B60). These results suggest that silver has the ability to stimulate and accelerate keratinocyte cell migration, which may be replicated in a wound site to potentially accelerate the healing process. However, it should be noted that there appears to be an optimum silver ion concentration, of approximately 1 ppm, which has the highest effect on cell migration, above which the effect may be reversed.

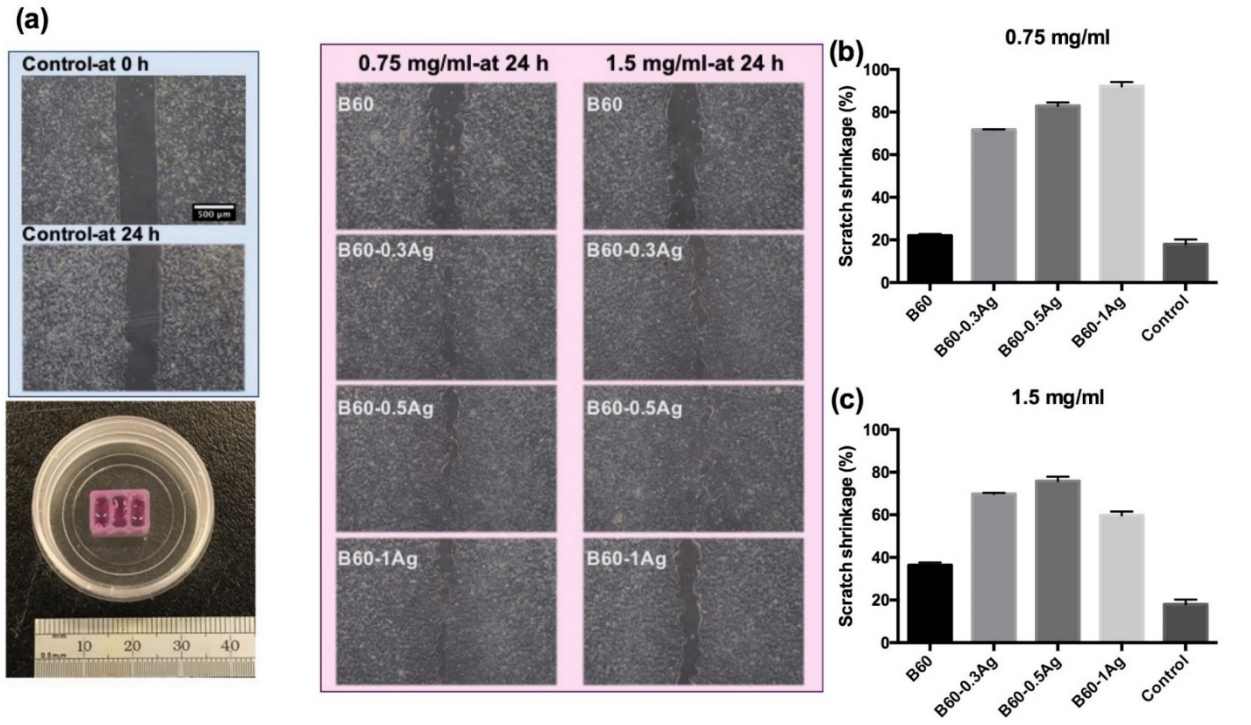

Figure 7. 12: (a) Migration of HaCat cells cultured with ionic dissolution products of AgBGs and concentrations of 0.75 and 1.5 mg/mL. Bar = 500 µm. Statistical analysis of scratch distance shrinkage of glass concentration of (b) 0.75 and (c) 1.5 mg/mL. The original and final width of a scratch were measured to calculate the scratch shrinkage percentage (Error bars: SD, n = 2).

While previous studies have shown that silver ion enhances the migration of fibroblastic cells to a wound area [235, 236, 261], this study focused on evaluating the influence of ionic dissolution products from silver doped borate glasses on the migration of keratinocytes. Keratinocytes have a critical role in stimulating and coordinating the actions of multiple cell types involved in the healing process, such as the maintenance of tissue homeostasis and the recruitment of cells necessary for complete wound closure [267]. Keratinocyte migration is also imperative to wound healing since these cells are able to induce endothelial cell migration and angiogenesis in

the wound site [268, 269] and promote fibroblast proliferation and production of extracellular matrix [270].

7.4 Conclusions

A major issue in chronic wounds is infection, biofilm formation and repeated tissue insults. Therefore, it is crucial to keep infection under control to better overcome wound complications. In this study, a therapeutic borate glass with promising ability to accelerate the healing process was developed. It was shown that AgBG glasses were able to inhibit growth of *PA14* bacteria up to 3 days and eradicate biofilm cells by up to 99.66%. It was demonstrated the AgBG ionic dissolution products, and in particular silver were not toxic to HaCat and NIH/3T3 cells. However, the high boron content in glass formulations may be a source of toxicity. It was also shown that fibroblast cells are more sensitive to boron and silver content than HaCat cells. In sum, the amount of silver dopant and glass concentration can be altered to tune anti-bacterial efficacy and cellular responses such as metabolic activity and migration based on the application needs. Future work will investigate the effect of these glasses on the wound healing process using an *in vivo* model.

Acknowledgements

This study was supported by Canada NSERC, Québec MEIE, CFI and McGill University Faculty of Engineering Hatch Faculty Fellowship for S.N.N. S.N. and G.G. are supported by the McGill Engineering Doctoral Award. The authors would like to thank Professor Anie Philip and Dr. Kenneth Finnson (McGill University) for providing HaCat cells and Dr. Mira Okshevsky for assistance in taking the microscope images.

8 Bioactive Glasses in Wound Healing: Hope or Hype?

The previous two chapters have demonstrated that silver-doped sol-gel derived borate-based glasses have potential in wound repair applications. Chapter 8 reviews the current challenges and approaches in wound repair treatments with bioactive and soluble glasses. This work has been published in *Journal of Materials Chemistry B* and is reproduced below.

Bioactive glasses in wound healing: hope or hype?

Shiva Naseri, William C Lepry, Showan N Nazhat*

Department of Mining and Materials Engineering, McGill University, Montreal, QC, Canada
*corresponding author showan.nazhat@mcgill.ca

Abstract:

Bioactive glasses have long been investigated in mineralized tissue regeneration, but recently their potential applications in soft tissue repair, and in particular wound healing, have demonstrated great promise. Commonly used glasses, such as the silicate-based Bioglass® 45S5 [(46.1)SiO_2-(26.9)CaO-(24.4)Na_2O-(2.6)P_2O_5 (mol %)] and borate-based 13-93B3 [(54)B_2O_3-(22)CaO-(6)Na_2O-(8)K_2O-(8)MgO-(2)P_2O_5 (mol %)] have been implicated in the role of wound healing due to their ability to release ions that can stimulate processes, such as haemostasis, anti-bacterial efficacy, epithelial cell migration, angiogenesis, and fibroblastic cell proliferation amongst others. More recently, a wound dressing composed of a borate-based glass received regulatory approval for use in the treatment of acute and chronic wounds. However, to date, there are no comprehensive reports on their specific mechanism of action in accelerating the wound healing processes. In this highlight, we will provide a brief overview of the wound healing stages, review the bioactive glass formulations that have been investigated for potential applications in wound healing and attempt to summarize the consensus as to why these glasses may be successful in wound healing.

8.1 Introduction

Since their original inception by Dr. Larry Hench in 1969, silicate-based bioactive glasses (BGs) have been considered in the repair and augmentation of mineralized tissues (*e.g.,* bones and teeth) [1]. Two commercially available formulations; Hench's original, Bioglass® 45S5 [(46.1)SiO_2-(26.9)CaO-(24.4)Na_2O-(2.6)P_2O_5 (mol %)] and a second silicate-glass, S53P4 [(53)SiO_2-(20)CaO-(23)Na_2O-(4)P_2O_5 (mol %)] [2, 3] (BonAlive Biomaterials, Finland), have regulatory approvals for clinical applications as filling materials and small implants in bone and dental tissues. While a bioactive material is defined as one that induces a specific biological activity (European Society of Biomaterials Consensus; 1987) [81], Hench's definition specifies BGs as a category of biomaterials that elicit a specific biological response at the interface with host tissues that result in the formation of a chemical bond [3, 129]. In particular, certain compositions of BGs have been extensively shown to form surface hydroxy-carbonate apatite (HCA) when in contact with biological fluid, leading to their bonding to mineralized tissues [1]. This surface HCA layer formation is frequently tested *in vitro* using acellular simulated body fluid [82, 271]. Moreover, a number of reports have documented the interaction and bonding of BGs to the surrounding soft collagenous tissues, also attributable to some extent, to HCA formation (reviewed [129]). This, along with research findings that have strongly implicated the role of inorganics, controllably released from BGs, in soft tissue mechanisms and their cellular functions (reviewed [84, 230]), has contributed to a recent significant increase in exploring the use of BGs in soft tissue repair. Among these, wound healing is increasingly being investigated as it demonstrates promising results. In fact more recently (late 2016), US Food and Drug Administration (FDA) approval was granted on a borate-based glass formulation as a wound dressing (MIRRAGEN™, ETS Wound Care LLC, USA) for applications in acute and chronic wound treatments [10]. However, as also pointed out in a recent review, the exact mechanisms of success of BGs in wound healing are still unknown [272]. Furthermore, since the majority of BGs have been designed for mineralized tissue repair, their success in non-mineralizing sites brings into question the requirements for applications in wound healing. Herein, we will briefly cover the various wound healing stages, discuss the ions implicated in these stages and list the types of BGs that have been investigated for wound healing applications thus far. In addition, a more in depth look at some of the proposed mechanisms as to why BGs may be successful will be highlighted.

8.2 Wound healing

Wound healing encompasses a broad range of clinical applications, including the treatment of oral and skin ulcers, suture sites, burns, extraction sites, surgical, traumatic and chronic wounds, as well as clotting, antimicrobial, angiogenic, and anti-inflammatory uses. Under routine medical conditions, acute wound healing occurs through the body's natural regeneration process, covering four main overlapping stages: haemostasis, inflammation, proliferation and tissue remodeling [176]. Haemostasis is a rapid response to injury where vasoconstriction, platelet aggregation and blood coagulation terminate bleeding. This is followed by inflammation, lasting up to four days in which immune cells are recruited to reduce infection and stimulate capillary growth [176]. Multiple processes take place during the proliferative phase, including re-epithelialization, angiogenesis, fibroblast proliferation, and the production of extracellular matrix (ECM) components, which lead to granulation tissue formation, and wound contraction aided by fibroblast trans-differentiation into myofibroblasts [176]. Tissue remodelling, the latter stage of wound healing, can take several months and is characterized by the continuous low rate of collagen degradation, synthesis and reorganization [176]. However, in compromised patients, numerous factors contribute to wounds with poor healing such as inadequate blood supply, poor glycemic control (*e.g.*, in diabetic patients), immunosuppression (*e.g.,* in transplant recipients), malnutrition, connective tissue disorders, immobility (*e.g.*, stroke or spinal cord injury), heart disease, dementia, cancer, as well as advancing age. In such cases, impaired wound healing results in chronic wounds, *e.g.,* as ulcers in diabetic patients, who are at constant risk of inflammation and often life-threatening infections [76]. Therefore, there is a need to stimulate the healing process by accelerating blood coagulation, preventing infection, and inducing vascularization; all of which are critical in determining the success of healing [76, 273].

Polymeric-based dressings offer one approach for accelerating the healing process [274]. However, these suffer from drawbacks such as the lack of ability to stimulate vascularization and poor integration with the host tissue [26, 78, 275, 276]. These deficiencies have led to the exploration of new materials, such as BGs, for promoting wound [26] healing. In particular, BGs support various ionic doping applications, as numerous modifying metallic oxides can be incorporated into the glass network to adjust their chemical and physical properties. Their subsequent ionic release, as a result of glass dissolution in biological contexts, can offer haemostatic properties (*e.g.,* Ca^{2+} [107, 277]), antimicrobial properties (*e.g.,* Ag^{+} [29, 30, 96, 97,

138-141, 152-156], Cu^{2+} [98, 99, 148], Ga^{3+} [93-95] and Zn^{2+} [142, 146, 170]) against *Escherichia coli*, *Staphylococcus aureus* and *Pseudomonas aeruginosa*, which have been associated with wound infections and biofilm formation[27, 94], anti-inflammatory (*e.g.,* Zn^{2+} [278]), and angiogenic effects (*e.g.,* B^{3+} [103, 134], Cu^{2+} [147]). Table 8.1 provides a list of reported biological responses to ions that can be released through BG dissolution.

Table 8. 1: Reported biological responses to ions that may be released through BG dissolution.

Ion	Biological Response
Si^{4+}	- Induces bone tissue calcination [127].
	- Down regulated TGF-β [114].
	- Ability of neovascularization [279].
	- Down regulated collagen type I and III [114].
	- Stimulates collagen type I formation [128].
Ca^{2+}	- Enhances osteoblast proliferation, differentiation and ECM mineralization [131].
	- Increases the expression of insulin like growth factors [132].
	- Promotes the migration and proliferation of epidermal cells [107].
	- Accelerates blood-clotting [107].
P^{5+}	- Stimulates the expression of matrix Gla protein (MGP) for bone [133].
B^{3+}	- Stimulates vascularization and angiogenesis.[134]
	- Increases RNA synthesis in fibroblasts.[137]
Cu^{2+}	- Stimulates angiogenesis [147].
	- Demonstrates antimicrobial property [148].
	- Increases the differentiation of mesenchymal stem cells (MSCs) [149].
Zn^{2+}	- Stimulates angiogenesis [142].
	- Enhances nerve regeneration.[144]
	- Anti-inflammatory property.[145]

	- Enhances wound healing processes [146].
	- Increases ATP activity [11].
	- Stimulates *in vitro* bone formation [11].
Ag^{+}	- Down regulated TGF-β [280].
	- Anti-inflammatory property [236].
	- Antimicrobial property [27].
Ga^{3+}	- Demonstrates antimicrobial property [94].

ECM: Extracellular Matrix, ATP: Adenosine Tri-Phosphate

TGF- β: Transforming Growth Factor beta

8.3 Bioactive glasses in wound healing

BGs have been widely studied for bone tissue engineering due to their osteo-conductive, -stimulative, and -inductive properties leading to the ability to form HCA, which promotes bone bonding [83]. Outside of bone, certain BG formulations have been considered as biomaterials for wound dressings to help increase the healing rates, a list of which is provided in Table 8.2. BGs have been reported to activate the expression of genes implicated in the healing processes such as vascular endothelial growth factor for angiogenesis, basic fibroblast growth factor, and vascular cell adhesion protein [84]. A number of early studies demonstrating the angiogenic potential of Bioglass® 45S5 were reported by the works of Day and Boccaccini, which highlighted its potential in this area [121, 281]. More recently, Bioglass® 45S5 was shown to protect endothelial cells and enhance gap junction communication, which increases vascularization and consequently accelerates wound healing [282]. Additionally, the increase in local pH through the dissolution of silicate-based glasses have been implicated to have an anti-bacterial effect, thus minimizing tissue loss or death [118]. Indeed, clinical data has demonstrated that S53P4, for example, can be an effective anti-bacterial bone substitute in the treatment of osteomyelitis [283]. *Staphylococcus aureus* bacteria, which are commonly found in wound infections, can also be implicated in osteomyelitis and it has been shown that S53P4 BGs can heal bone infection in a one-step surgical procedure at reduced cost with shorter hospitalization times when compared to calcium-based antibiotic-loaded bone substitutes [283]. It is interesting to note that despite its proven ability to heal bone infections, S53P4 has not been investigated in wound repair applications.

A major ionic component released from silicate-based BGs is Si^{4+}, which has been demonstrated to have a significant role in stimulating ECM/collagen production [128] and neovascularization [279] which are crucial in both regenerating mineralized tissues and in wound healing. However, while the stimulation of collagen production is critical in bone regeneration as it provides the ECM template for osteoblastic induced mineralization [3], in skin repair, the need for modulating collagen production may also be important to prevent scar tissue (fibrosis) formation [176]. Indeed, among the various growth factors implicated in the wound healing process, transforming growth factor-beta (TGF- β) has broad spectrum roles in the inflammation, proliferation and tissue remodelling stages (reviewed [176]). TGF- β has multiple effects on cell proliferation and differentiation, ECM production, and immune modulation. On the other hand, abnormal TGF- β signaling has been implicated in pathological skin disorders, including chronic

Table 8. 2: Bioactive glass compositions that have been investigated for wound healing applications.

Glass Composition	Findings	Ref
SiO_2-CaO-Ag_2O SiO_2-CaO SiO_2	- Ag^+ ion demonstrated antibacterial activity. - Ca^{2+} ion increased blood coagulation rate.	[277]
SiO_2-CaO-P_2O_5	- Stimulate fibroblast cells to secret essential growth factors for vascularization and healing process. - Enhanced wound closure and vascularization *in vivo*.	[115]
90SiO_2-6CaO-4P_2O_5 (mol%)-SG	- Enhance fibroblast cells migration. - Down regulated TGF-β, collagen type I and III resulting in minimal scaring.	[114]
80SiO_2-16CaO-4P_2O_5 (mol%)-SG 60SiO_2-36CaO-4P_2O_5 (mol%)-SG	- Glasses containing 80 SiO_2 increased blood coagulation rate more than glasses contain 60 SiO_2.	[110]
SiO_2-CaO-P_2O_5-0.02Ag_2O (wt%)-SG	- Demonstrated 99% antibacterial rate against *E.coli* bacteria in 12 hrs. - Increased blood coagulation rate.	[138]
60SiO_2-34CaO-4P_2O_5-2Ag_2O (mol%)-SG	- Limited *in vitro* attachment of *Staphylococcus epidermidis*.	[139]
58SiO_2-33CaO-9P_2O_5 (wt%)SG 45SiO_2-24.5Na_2O-24.5CaO-6P_2O_5 (wt%)-MD	- Enhanced wound healing and vascularization processes. - SG glasses showed more rapid wound healing rates compared with MD glasses due to the higher surface area.	[112]
45SiO_2-24.5Na_2O-24.5CaO-6P_2O_5 (wt%)	- Enhanced wound healing rate.	[113]
45SiO_2-24.5Na_2O-24.5CaO-6P_2O_5 (wt%)	- Increased blood coagulation rate.	[117]
45SiO_2-24.5Na_2O-24.5CaO-6P_2O_5 (wt%)-MD	- Enhanced wound closure and vascularization. - Protected endothelial cells from death and Enhanced gap junction communication.	[282]
45SiO_2-24.5Na_2O-24.5CaO-6P_2O_5 -5 and 20.2ZnO (wt%)-MD	- Higher zinc content decreased degradation rate. - Glasses with 20.2 wt% zinc were toxic on endothelial cells.	[143]
45SiO_2-24.5Na_2O-24.5CaO-6P_2O_5 (wt%)-MD 56.6B2O3-18.5CaO-11.1K_2O-5.5Na_2O-4.6MgO-3.7P_2O_5 (wt%)-MD	- Both glass compositions enhanced wound closure and vascularization *in vivo*. - Both glass compositions were not toxic to human umbilical vein endothelial cells *in vitro*. - Borate glass showed higher wound closure and vascularization compared to silicate glass *in vivo*.	[125]
56.6B2O3-18.5CaO-11.1K_2O-5.5Na_2O-4.6MgO-3.7P_2O_5 (wt%)-MD	- Enhanced wound closure and healing rate in diabetic patients with chronic, open wounds.	[174, 258]
56.6B2O3-18.5CaO-11.1K_2O-5.5Na_2O-4.6MgO-3.7P_2O_5 (wt%)-MD 51.6B_2O_3-20CaO-12K_2O-6Na_2O -5MgO-4P_2O_5-0.4CuO-1ZnO (wt%)-MD	- Showed higher proliferation and migration rate of human skin fibroblast cells (HF) than silicate-based glasses. - Under dynamic flow showed higher proliferation rate of HF cells on zinc doped glasses than undoped glasses.	[135]
54B_2O_3-22CaO-8K_2O-6Na_2O-8MgO-2P_2O_5 (mol.%)-MD 54B_2O_3-22CaO-8K_2O-6Na_2O-8MgO-2P_2O_5 (mol.%) -0.5,1 and 3CuO (wt%)- MD	- Showed high proliferation rate of human endothelia cells. - Enhanced wound closure and vascularization. - Cu doped glasses showed higher newly formed blood vessels and wound closure.	[136]

SG: Sol-gel derived glasses, MD: Melt-derived glasses

wounds and excessive scarring [176]. For example, while TGF- β promotes wound closure and resolution through the production of ECM proteins and the inhibition of matrix metalloproteinases, excessive TGF- β production and signaling promotes extensive tissue fibrosis, which can compromise normal tissue function in fibrotic diseases. Therefore, targeting the TGF- β signaling pathway represents a viable strategy for the development of novel therapeutics to improve wound healing. In fact, a recent *in vitro* study reported that the direct exposure of a sol-gel derived silicate-BG, 90S [(90)SiO_2-(6)CaO-(4)P_2O_5 (mol %)] down regulated TGF- β signaling and its downstream molecule Smad2, which suggested that BGs may have a role in modulating the TGF- β pathway (Figure 8.1a) [114]. In addition, 90S supported the proliferation and migration of fibroblasts, regulated the gene expression of collagen types I and III, fibronectin and inhibited fibroblast-to-myofibroblast differentiation, through alpha-smooth muscle actin (α-SMA) down-regulation. It was concluded that the fibroblastic responses were particularly impacted by Si^{4+} ions. However, it is interesting to note that the regulation of collagen I and III contradicts previous findings on the role of Si^{4+} ions, in terms of stimulating collagen type I formation in mineralized tissues [128]. A further study by Yu *et al*., reported on a bioactive skin graft composite of silicate-based BGs and fibroblast derived sheet [115]. Ionic dissolution products were shown to stimulate fibroblasts to secrete essential growth factors for vascularization and healing processes (Figure 8.1b), where significant wound closure and newly formed blood vessels were demonstrated, *in vivo*. It is interesting to note that the expressions of collagen type I and α -SMA in fibroblasts cultured in the presence of glass ionic dissolution products were initially up regulated on day 3 and then down regulated by day 7, which suggests that ionically-mediated gene expression of TGF-β signaling may enhance wound healing.

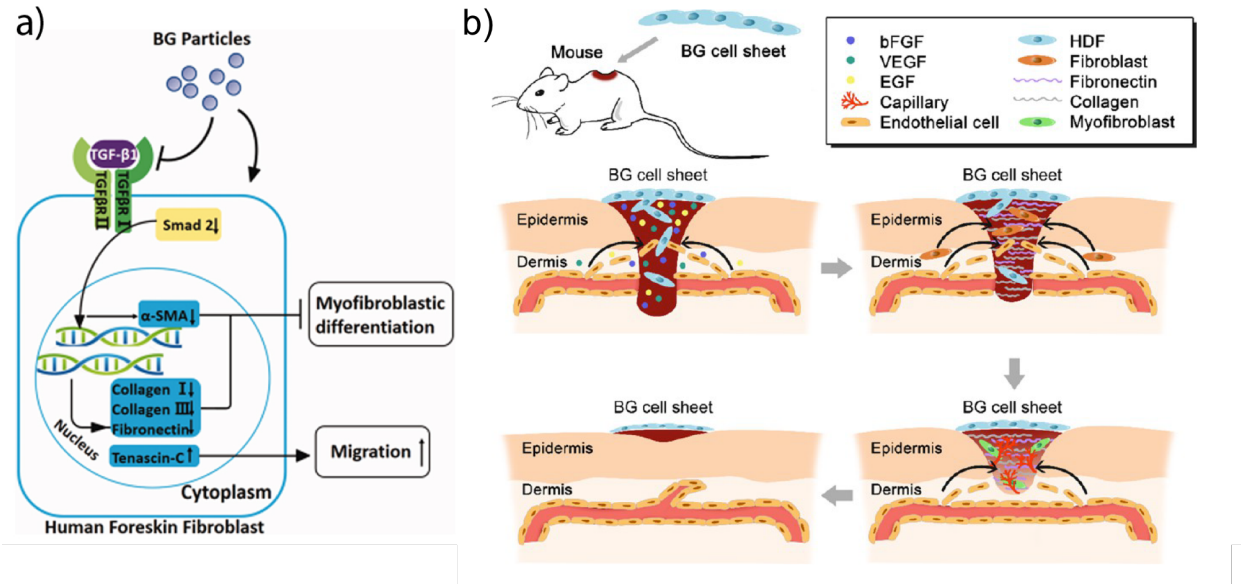

Figure 8. 1: Examples of proposed mechanisms of silicate-based BGs in wound healing. a) Possible mechanism of BGs in wound healing, *in vitro* (Xie et al., 2016 [114]). b) Mechanism of BGs in activating fibroblast cell sheet skin graft to improve wound healing, *in vivo* (Yu et al., 2016 [115]). bFGF: Basic fibroblast growth factor, VEGF: Vascular endothelial growth factor, EGF: Epidermal growth factor, HDF: Human Dermal Fibroblasts.

Interestingly, a number of studies have investigated BGs, including Bioglass® 45S5, with the ability to convert to HCA in accelerating wound healing [110, 112, 113, 115, 135]. However, to the best of our knowledge, there is no specific and comprehensive study to verify the direct role of HCA deposition as a consequence of BG degradation on the wound healing rate. Although a study has demonstrated that the direct addition of hydroxyapatite particles to wounds accelerated healing when compared with a non-treated site and which was attributable to a greater attraction of macrophage and fibroblast cells to the wound site, this study did not explain the direct impact of HCA on the wound healing process [284]. Furthermore, the interplay between the HCA formation ability of BGs with blood clotting activity has been investigated [110]. It has been reported that coagulation rate and the strength of clot decreased when pure hydroxyapatite particles were utilized [111]. Additionally, BG compositions [(60)SiO_2-(36)CaO-(4)P_2O_5 (mol %)], with rapid HCA deposition rates (*i.e.,* low Si/Ca ratio), demonstrated a less overall and a slower rate of clotting activity compared to BGs [(80)SiO_2-(16)CaO-(4)P_2O_5 (mol %)] with lower HCA deposition rates but exhibited more rapid clotting response (*i.e.,* high Si/Ca ratio) [110, 111].

Notwithstanding this, the main question is, why would a mineralizing BG accelerate wound healing in skin? More importantly, will there be long term adverse effects due to HCA formation? For example, we have recently shown that ectopic bone formation is possible by injecting BG incorporated collagen hydrogels into a non-osseous subcutaneous site [285]. Or is it the ionic release from glasses in this dynamically changing environment that leads to more rapid wound healing processes (with HCA formation being a by-product of BG dissolution)? Since BGs generally contain CaO, it has also been shown that Ca^{2+} release can promote blood clot formation along with epidermal cell migration [107, 115]. Furthermore, the direct addition of calcium-based nanoparticles to a wound site, *in vivo*, was shown to enhance wound closure and the healing rate, in which Ca^{2+} accelerated blood coagulation, increased fibroblast proliferation and collagen lattice contraction [108]. More widely, it has also been demonstrated that an ordered mesoporous silica sphere doped with calcium and silver accelerated blood coagulation and antimicrobial properties, respectively [277]. The increase in clotting strength was attributed to Ca^{2+} ion-release, whereas the addition of Ag^{+} was necessary to generate an antimicrobial response.

As a consequence of the slow and incomplete solubility of silicate-based glasses, there is significant interest in developing more soluble BGs based on other network forming oxides, such as phosphates and borates. Borate-based glasses in particular have demonstrated both increased and full conversion rates to HCA when compared to silicate-based glasses due to their lower chemical durability [55, 102, 103]. Lately, they have also shown great promise in wound healing applications attributable to their: (1) high degradation rate, (2) greater increase in local pH compared to silicate-based bioactive glasses, and (3) the ability of boron to stimulate angiogenesis [103, 134]. In a recent study, wound dressings composed of Cu-doped 13-93B3 borate glass microfibers were tested, *in vivo*, using a wound healing mouse model [136]. The Cu-free baseline borate glass composition significantly increased the rate of angiogenesis and healing when compared with a non-treated wound, and this effect was even more enhanced with the Cu-doped BG. It was concluded that the higher healing rate of Cu-doped borate glasses was due to the release of Ca^{2+}, Cu^{2+}, and B^{3+} ions. In a follow up study, wound dressings, composed of the mineralizable melt-derived borate, 13-93B3 [$(54)B_2O_3$-(22)CaO-$(6)Na_2O$-$(8)K_2O$-(8)MgO-$(2)P_2O_5$ (mol %)]) and silicate (45S5) bioactive glass microfibers, were investigated [125]. When tested in an *in vivo* full thickness skin defect rat model, borate-based glasses demonstrated more rapid healing rates when compared with silicate-based glasses. This was attributed to a more rapid release rates of

Ca^{2+} ions (along with the release of B^{3+} ions) from borate-based glasses. Interestingly, this study discussed the rate of HCA formation as a measure of glass degradation and ionic release rates rather than any specific direct role of the HCA formation on the wound healing process. Even though these two studies (Zhao *et al.,* 2015 [136], and Zhou *et al.,* 2016 [125]) have examined the percentage of wound closure *in vivo* using the same protocol, their results contradict each other in the case of the untreated wound (*i.e.,* the controls) and 13-93B3 BG treated wound (Figure 8.2). This discrepancy suggests the need for a reliable standardized method to evaluate the healing effects of BGs more accurately. Nevertheless, neither the role of any potential HCA formation, nor its effect on the healing rate was cited, despite previous studies showing the same glass composition working well in an *in vivo* bone defect model [286, 287]. For example, when 13-93B3 glass scaffolds were examined in a rat calvarial model, there was almost full conversion to HCA within 6 weeks [286]. In addition to animal models, the 13-93B3 borate glass formulation was also clinically tested in diabetic patients with chronic, open wounds [258]. It was reported that after cleaning and debridement of a wound, the glass fibres (13-93B3, DermaFuse, Mo-Sci Corporation, USA) were loosely packed into the cavity, covered with a wrap, and replaced every 2 to 3, or 5 to 7 days. The patients experienced an increase in wound closure rates ranging from 0.3 to 0.8 mm/day and after complete treatment, there was minimal to no scarring. The glass fibres appeared to induce the inflammation phase and the high calcium content was also thought to be desirable since it is suspected to assist in epidermal cell migration [258]. It was concluded that borate glasses have healing effects similar to negative-pressure healing techniques, and at a reduced cost. Follow up clinical studies with more patients and glass compositions were also carried out.[174] While successful with diabetic ulcers, DermaFuse did not indicate positive healing effects on the wounds caused by radiation (such as through cancer treatments). It is also worth noting that, DermaFuse is successfully commercialized for the veterinary market as "RediHeal" which has been used for skin repair for animals [174]. More recently, in late 2016, borate-based glass microfibers (MIRRAGEN™, ETS Wound Care LLC, USA) received FDA approval as a novel wound management for acute and chronic wound healing [10]. It was shown that minimum two-week old wounds that exhibited no healing under conventional treatment can be healed when using MIRRAGEN™ as a wound dressing, which also has to be renewed every 3 to 7 days. It is stated that the "porous structure of MIRRAGEN™… allows it to wick fluid away from the wound bed and control the moisture content…. the dressing facilitates the wound healing response and allows

new tissue to regenerate at the site…" [10]. However, while these recent developments are highly encouraging, the specific mechanisms of BGs on the wound healing process are yet to be fully understood, and this can be a limiting factor in their immediate clinical acceptance.

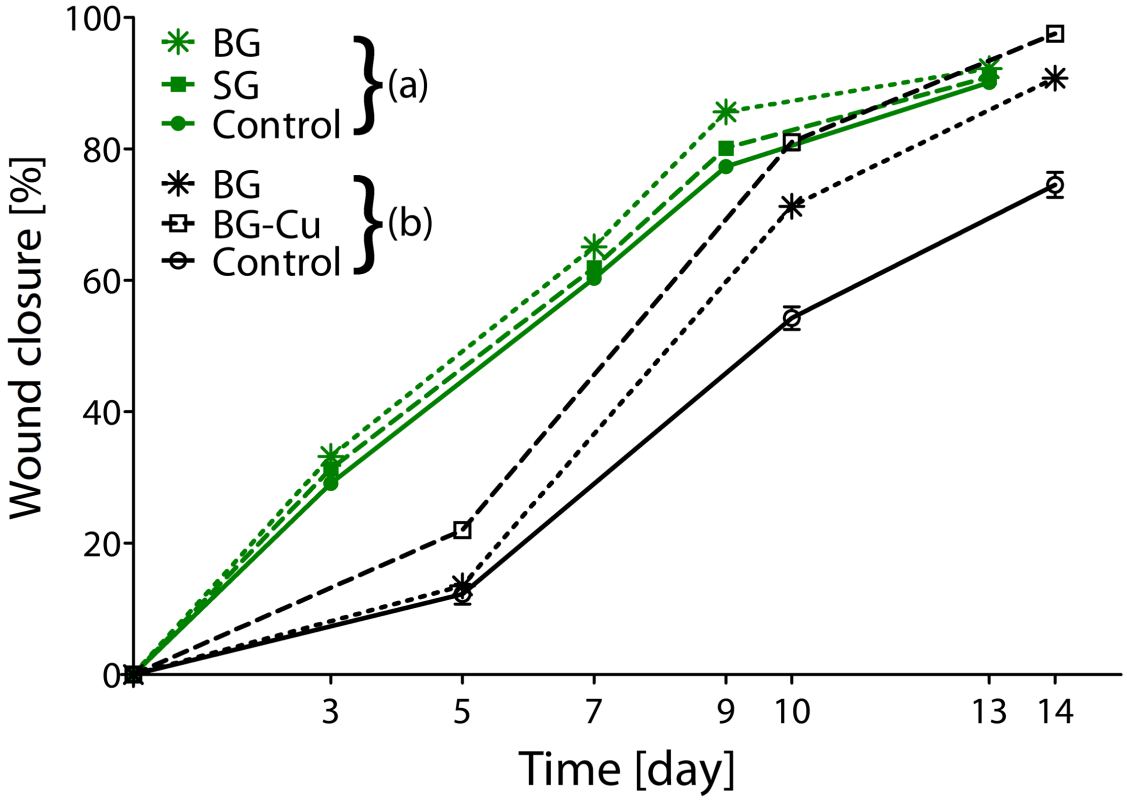

Figure 8. 2: Percentage wound closure of full-thickness skin defects in rats up to 13 days. Graph was generated from data presented in Zhao et al. 2015[136], and Zhou et al. 2016 [125]. Group (a) [Zhou et al., 2016] [125]: Comparison between control (untreated), borate glass "BG" (13-93B3) fibres, and silicate glass "SG" (45S5) fibres. Group (b) [Zhao et al., 2015] [136]: Comparison between control, borate glass "BG" (13-93B3) fibres, and copper-doped borate glass "BG-Cu" (Cu-13-93B3) fibres.

8.4 Summary and future perspectives

BGs have recently stimulated much interest for their use towards wound healing applications since they can accelerate the haemostasis (blood coagulation), inflammation (bacterial prevention and angiogenesis), and cell proliferative stages of wound healing, yet little is known so far about their specific mechanisms in the complex cascade of wound repair. While it is clear that

there is a need for controlled delivery of appropriate, biologically stimulating ions that regulate cellular responses at the various wound healing stages, much of the research undertaken so far in proposing BGs for wound healing has focused on formulations previously applied in mineralized tissues. Indeed, it is not clear if a mineralizing glass is needed or what role the newly formed HCA plays in the healing process. To better understand the impact of BGs, as well as any HCA formation, in wound healing (and other soft tissue) applications, more comprehensive studies are needed to examine the role of mineralizing and non-mineralizing BGs on wound healing. Thus far, we can conclude that the controlled delivery of ions may be the key parameter in the healing efficacy of BGs regardless of their mineralizing ability. However, it is clear that further research is required to decode the role of BGs in wound healing, *via* their angiogenic and antimicrobial ionic release, along with understanding the mechanisms that prevent the potential ectopic calcification of soft tissues.

Acknowledgements

This review was supported by Canada NSERC, CFI and McGill University Faculty of Engineering Hatch Faculty Fellowship for S.N.N. W.C.L. and S.N. are supported by the McGill Engineering Doctoral Award and W.C.L. is also supported by the Fonds de recherche du Québec (FQRNT) – Bourses de doctorat en recherché. The authors would like to thank Professor Anie Philip and Dr. Kenneth Finnson (McGill University) for their discussions on wound healing.

9 General Discussion

9.1 The potential of DVS in the characterizations of bioactive and soluble glasses

There is a lack of standardized and objective approaches to measuring the reactivity of bioactive glasses. To date, aqueous reactivity of bioactive and soluble glasses has been evaluated using traditional methods such as long-term immersion in an aqueous environment [18-20, 56-58]. However, this approach can be time-consuming and may lack accuracy [58, 271]. Therefore, there is interest in exploring potentially rapid, and reliable methods. Recently, the reactivity and aqueous interactions of soluble phosphate-based glasses were characterized using DVS and were correlated with weight loss and ions release rates [188].

In Chapters 4 and 5, DVS was used to further investigate the potential of this technique in correlating the aqueous interactions, as a measure of reactivity, with any bioactivity and ionic release rate in DIW of melt-derived Bioglass® 45S5 (BG) of three different particle sizes (and equivalent specific surface areas) and PGs [21] doped with both SiO_2 and TiO_2 ($(50)P_2O_5$-$(40)CaO$-$(x)SiO_2$-$(10-x)TiO_2$, where x = 7, 5, 3, and 0 mol%). Both glass systems were evaluated through two methods, by measuring the: 1) vapour sorption isotherms of glasses when exposed to systematically increasing and decreasing RH values, and 2) vapour sorption of the glasses when directly exposed to 90% RH for 24 h followed by another 24 h at 0% RH. Using the first method, the sorption phase of all melt-derived silicate- and phosphate-based glasses were characterized by an initial relatively small increase in mass up to a certain % RH value, which was followed by a sudden increase in percentage mass change. This discontinuous change in mass change was termed as the "inflection point", and was explained by a deliquescence phenomenon or the formation of a saturated surface layer of the glass dissolution products [195, 196]. This result was in line with recent work that demonstrated a dramatic increase in mass change in vapour sorption isotherm with Cu-doped phosphate-based glasses [188].

Through the second method, the sorption kinetics of glasses, when directly exposed to 90% RH, were evaluated. Both glass networks demonstrated an immediate increase in mass, when directly exposed to 90% RH. Figure 9.1 shows the initial rate of weight increase calculated from the initial slope of percentage mass change versus time during direct exposure to 90% RH along the specific surface area of glass compositions investigated in Chapters 4 and 5. As it was shown in Chapter 5, there was an increase in the initial rate of weight increase for PGs with the same specific surface area with an increase in silica content (*i.e.,* by replacing Ti with Si). This can be

attributed to the reduction of the strong and stable P-O-Ti bonds within the PG network [225] as well as the formation of surface Si-OH bonds, which contribute to higher aqueous reactivity [21, 224]. In Chapter 4, it was shown that increased surface area lead to greater bioactivity and reactivity of silicate-based glasses with the same composition and processing route. In addition, the sorption phase of silicate-based glasses at 90% RH was characterized by a rapid initial rate of increase in mass, which was followed by a continuous, slower rate of increase up to 24 h (Figure 4.2a). In contrast, the sorption phase of phosphate-based glasses was characterized by linear increase in mass up to 24 h (Figure 5.2c). This may be attributed to the different dissolution mechanisms between silicate and phosphate glasses. In silicate glasses, as described by Hench, the formation of the HCA layer is initiated by the dissolution of glass and rapid ion release from the glass through its aqueous interactions (rapid cation exchange of the Na^+/Ca^{2+} with H^+ or H_3O^+ from solution), which forms Si-OH bonds and consequently a silica rich layer on the glass surface that slows the dissolution rate [3]. Conversely, in phosphate glasses, the dissolution mechanism is based on the hydration and hydrolysis reactions with a continuous dissolution rate [89, 90]. Additionally, for similar surface areas, *i.e.,* particle size range, the extent of weight change at 24 h was higher in phosphates glasses with a silica content of 7 mol% indicating its greater hygroscopicity when compared to silicate glasses [8].

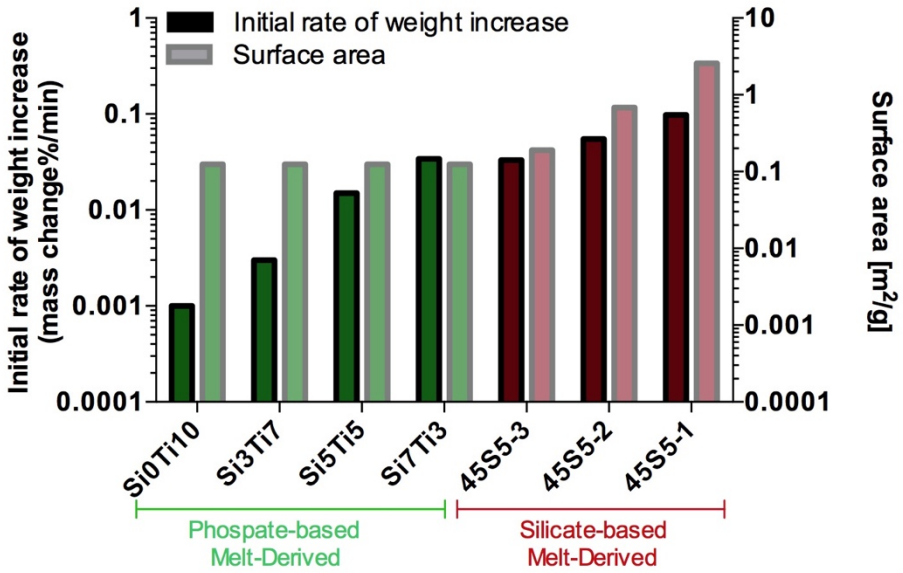

Figure 9. 1: Summary of the rate of weight increase calculated from DVS and surface area of the glass compositions including phosphate- and silicate-based glasses investigated in this thesis.

Figure 9.2 and Table 9.1 compare the effect of the direct substitution of silicate with borate in melt-quench derived borate (45B5) [24] and silicate-based glass (Bioglass® 45S5), respectively. Both glasses, of a similar range of specific surface area were directly exposed to 90% RH for 6 h. It was found that the initial rate of weight increase of 45B5 was approximately 15-fold higher than its silicate glass equivalent, confirming its higher reactivity and lower chemical durability [44, 45]. This is in line with previous findings describing borate-glasses as having lower chemical durability than silicate-glasses, and offering higher rates of dissolution, reactivity and bioactivity [5]. In borate-glasses, the boron ion is typically trigonally coordinated, giving it a pseudo-3D character since the BO_3 network is more planar. However, depending on the amount of modifying oxides present, borate-glasses can also be four coordinated [5]. This combination results in borate-glasses having lower chemical durability than silicate-glasses [5].

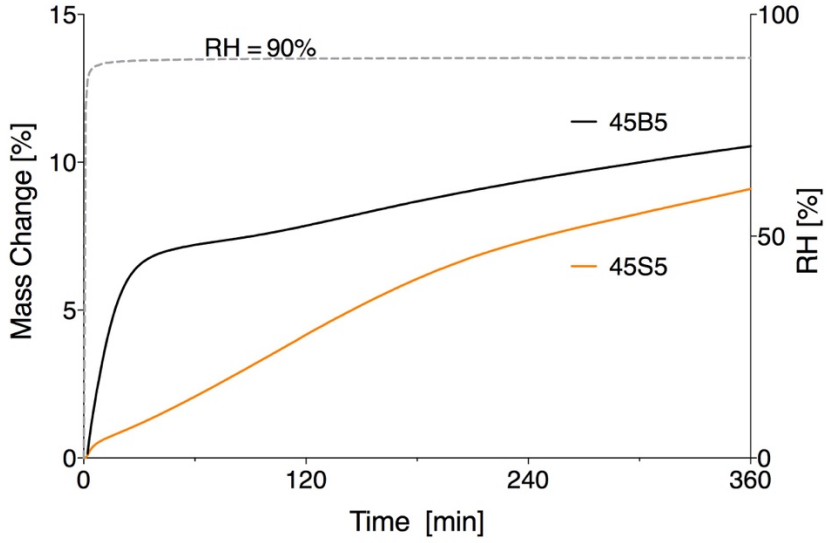

Figure 9. 2: Direct exposure to 90% RH up to 6 h showing higher rate and extent of mass change for melt-derived boron substituted 45S5 glass (45B5) [24] than melt-derived silicate based glass (45S5), suggesting greater extents of reactivity

Table 9. 1: Initial rate of weight increase and surface area of melt-derived borate based glass, 45B5 [24] and melt-derived silicate based glass, 45S5 (Chapter 4).

Glass type / Parameters	45B5	45S5
Initial rate of weight increase (Mass change %/min)	0.44	0.03
Surface area (m^2/g)	0.24	0.19

Chapter 6 examined two different sol-gel derived borate-based glass formulations (B46 and B60) and surface areas *via* DVS through their direct exposure to 90% RH for 2 h followed by desorption for 2 h at 0% RH. Compared to the sodium containing B46, the removal of the highly reactive sodium oxide from the glass formulation (B60), generated a less reactive glass despite its significantly higher surface area, indicating the dominance of composition on the reactivity of multi-component glasses. The significant effect of sodium on the reactivity of AgBGs can be attributed to a greater presence of non-bridging oxygens and OH^- groups in the glass structure resulting in lower chemical durability [26, 250].

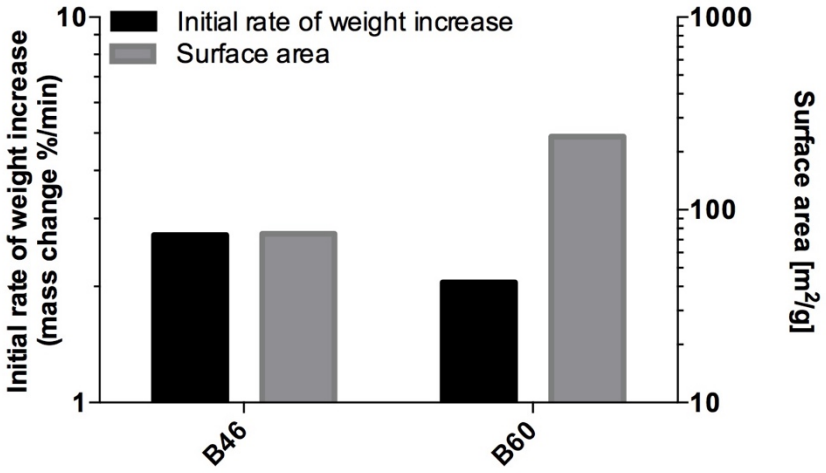

Figure 9. 3: The summary of the rate of weight increase calculated from DVS result and surface area of the glass compositions of borate-based glasses (Chapter 6) investigated in this thesis.

These results verify the ability of DVS in measuring and evaluating the effects of the different glass forming and modifying oxides (composition), processing routes, and surface areas on the reactivity of the glasses.

9.2 The potential of IGC in the characterizations of phosphate-based glasses

To date, the hydrophilicity/hydrophobicity of bioactive and soluble glasses has been evaluated using methods such as contact angle measurements [18-20, 56-58]. However, this technique may not be sensitive enough to measure slight difference in glass surface energies due to differences in chemical composition [22, 205, 288]. This thesis explored the potential of IGC in evaluating the glass solubility and surface energies and correlated these values with their bulk properties such as T_g as well as their dissolution rates in DIW. In Chapter 5, the potential of IGC in characterizing the hydrophilicity/hydrophobicity of glasses was examined by measuring the solubility parameter and surface energy of the PGs doped with both SiO_2 and TiO_2 [21]. Previously, it was shown that the substitution of Ti with Si in the glass network, led to a reduction in T_g and subsequent increase in the dissolution and ion release rates in DIW [21], thereby confirming that glass durability can be linked to its structure [206, 207]. It was found that there was a correlation between polar parts of solubility and surface energy with T_g and dissolution rates [21]. Moreover, there was a good correlation between the polar parts of both the solubility parameter and surface energy (as measured through IGC) and the inflection point (as measured through DVS) values, which suggested that both techniques may be complementary in predicting the dissolution properties of PGs.

9.3 Optimization of composition of silver doped borate glass

Patients with chronic wounds suffer from compromised healing and are at constant risk of inflammation and infection [177]. Therefore, in these cases, there is a need to stimulate and accelerate the healing process, such as through the application of biomaterial-based dressings. One of the promising biomaterial groups for skin repair is bioactive and soluble glasses. Recently, these glasses have gained much interest in soft tissue repair [35, 80]. In 2016, a melt-derived borate glass microfiber-based wound dressing (MIRRAGEN™, ETS Wound Care LLC, USA) obtained FDA approval for acute and chronic wound repairs [10]. However, to date, the development and

characterization of silver doped sol-gel-derived borate glasses (AgBGs) have not been explored for wound healing applications.

Recently, Lepry and Nazhat reported on novel bioactive sol-gel derived borate-based glasses [24]. It was demonstrated that sol-gel derived glasses had higher specific surface areas with nano range porosity resulting in higher degradation rates and reactivity than their melt-derived equivalent. One of the aims of this thesis was to fabricate an anti-bacterial borate-based glass, in which silver was chosen as the anti-bacterial dopant. Since there has not been reports on the processing of sol-gel derived silver doped borate-based glasses, there was a need to systematically optimize the sol-gel process and glass composition to generate an amorphous glass structure with the presence of BO_3 and BO_4 structural units; have a homogeneous formation of the glass structure; and the ability to dope the glasses with silver oxide without the formation of a metallic silver phase.

In Chapter 6, the sol-gel processing was initially adapted to fabricate a silver-doped borate substituted 45S5 bioactive glass composition ("B46") where the silver precursor was added immediately before that of the sodium precursor and the pH was basic (AgBG-1). However, the silver component precipitated during the sol preparation, and after calcination, the presence of a metallic silver phase within the glass network was observed by XRD. In an attempt to solve this issue, the addition order of the silver precursor was modified (AgBG-2). It is well known that in the sol-gel process, the pH of the solution is crucial in determining the final properties of glasses [244, 245]. For this reason, the silver nitrate was added after that of the phosphate source (TEP) where the pH was acidic. The modification of silver nitrate addition order solved the precipitation and formation of a metallic silver phase, however silver ion release was below the detection limit. Furthermore, the XRD pattern of the AgBG-2 glasses after calcination indicated the presence of semi-crystalline sodium nitrate in the glass structure. It was postulated that, the presence of sodium and its reaction with nitrate due to its high reactivity, may be the reason for no silver ion release. This led to the fabrication of the AgBG-3 group, with no sodium in their formulation (B60). The basic structural and chemical characterizations of these glasses satisfied the pre-defined parameters for an optimized glass. As a result, sodium free AgBGs (B60) demonstrated higher levels of silver ion release in DIW, which was in line with glass composition.

9.4 Anti-bacterial efficacy of AgBGs

One of the major problems with infected tissues is the antibiotic resistivity of associated bacteria [259]. For this reason, there is a great interest in finding a new approach to control bacteria more effectively. Silver ion is well-known for its anti-bacterial properties and a good alternative to antibiotics in treating infections [27]. It has been reported that silver ion can kill bacteria through various possible mechanisms, such as by attaching to their DNA and RNA, binding to the tissue proteins [27], and by attaching to cell membranes and inhibiting the respiration process of bacteria [27]. Based on literature, effective concentrations of silver ions against bacteria can vary from 0.1 to 20 ppm depending on the biological condition and bacteria type [151]. This reported range is in line with the concentrations of silver ion released from the B60 AgBG compositional range fabricated in this study. In Chapters 6 and 7, the anti-bacterial efficacy of the AgBG-3 group, $(60)B_2O_3$-$(36)CaO$-$(4-x)P_2O_5$-$(x)Ag_2O$ where x = 0.0, 0.3, 0.5 and 1 (mol%), against wound infection and biofilm associated bacteria, such as the Gram-negative bacteria *E. coli* and *PA14* and the Gram-positive *S. aureus* [152, 153, 289] were evaluated. The viable cell count method was used where post exposure to the glasses, the colony forming unit (CFU) on agar plates were counted. The bacteria growth curves at various glass concentrations also were measured by directly exposing the AgBGs to bacteria suspensions. Furthermore, the efficacy of the ions released from the glasses were tested against pre-formed *PA14* biofilms, which are known to be more resistant than planktonic cultures. The results demonstrated that there was a dose-dependent relationship between the silver content in the AgBGs and anti-bacterial activity which hold promise for chronic and infected wound repairs.

9.5 Cellular function of AgBGs for skin repair

In the case of chronic and infected wounds, the inflammation phase fails to reduce infection through the body's immune cells [73, 76]. Therefore, there is a need to help the body overcome infection, reduce inflammation, and thus accelerate the healing process [76]. Bioactive glasses have earned noticeable attention in potentially accelerating the healing of chronic wounds and diabetic ulcers due to their ability to tune their properties, chemical durability and offer the controlled release of therapeutic ions [80, 84]. In particular, While silver is known for its anti-bacterial efficacy [27], in high doses silver can be toxic to mammalian cells and damage healthy tissues, which highlights the need for controlled delivery [151]. Depending on the biological

environment and cell type, the toxic concentration of silver ion on mammalian cells has been reported to be in the range of 1 to 10 ppm [151]. Therefore, its incorporation into bioactive glasses is a viable strategy since the glass degradation and subsequent silver ion release rates to the target tissue can be controlled [27]. Furthermore, since silver-based biomaterials are not able to selectively distinguish between bacteria and healthy cells involved in wound healing [179], in Chapter 7, it was necessary to examine both the anti-bacterial efficacy and potential cytotoxicity of AgBGs.

To test mammalian cellular responses to the anti-bacterial AgBGs, their ionic dissolution products were exposed to two wound healing associated cell types, keratinocytes (HaCat) and fibroblastic (NIH/3T3) cells. It was shown that at lower concentrations (less than 1 ppm, B60-0.3Ag and B60-0.5Ag formulations in cell culture medium), the release of silver ion was not toxic to these cells. This was in agreement with the above stated toxic concentration range of silver ion(1 to 10 ppm) [151]. However, the high amount of boron in the glass formulation was found to be a possible source of toxicity, which was attributed to the static culturing conditions [290]. In fact, *in vivo*, the dynamic flow conditions prevent the accumulation of high boron in the wound site [291]. The migration assay demonstrated that silver ion has the ability to stimulate the migration of HaCat cells to the wound area and ultimately potentially accelerate the healing process. The results suggested that there is an optimum silver ion concentration of approximately 1 ppm, which has the highest effect on HaCat cell migration. While the effect of silver ion on the migration of fibroblastic cells to a wound area has been demonstrated [235, 236, 261], keratinocytes have a critical role in stimulating and coordinating the actions of multiple cell types involved in the healing process, such as the maintenance of tissue homeostasis and the recruitment of cells necessary for complete wound closure [267]. In fact, the early migration of keratinocyte cells is critical since these cells are also able to induce endothelial cell migration and angiogenesis in the wound site [268, 269] and promote fibroblast proliferation and production of extracellular matrix [270].

10 Conclusions and Future Perspectives

10.1 Conclusions

The following conclusions can be summarized from this dissertation:

- DVS as a novel characterization technique was able to examine the aqueous reactivity of bioactive and soluble glasses based on silicate-, phosphate- and borate- networks. DVS data of melt-derived Bioglass® 45S5 of three different particle sizes (surface areas) correlated with their reactivity, bioactivity, and ionic release rates. Higher surface areas led to higher vapour sorption and reactivity rates. In Si/Ti doped PGs, it was demonstrated that higher silica content led to higher vapour sorption and dissolution rates. Furthermore, based on the aqueous interactions of the borate glasses (AgBG-1, AgBG-2 and AgBG-3 groups) as measured through DVS, it was demonstrated that the extent of vapour sorption was highly related to the presence of sodium in the glass formulation. These results verify the ability of DVS in measuring and evaluating the effects of the different glass forming and modifying oxides (composition), processing routes, and surface areas on the reactivity of the glasses.

- IGC as a novel technique was able to characterize the surface properties of Si/Ti doped phosphate glasses more precisely than traditional contact angle measurements and may be used as a complementary technique in predicting the dissolution properties of PGs. Moreover, there was a good correlation between IGC generated parameters with bulk properties such as T_g and dissolution rates of the PGs as well as DVS generated parameters.

- Silver doped sol-gel derived borate glasses can be processed for potential applications in anti-bacterial needed tissue repair. A four-component glass compositional range, B60: $(60)B_2O_3$-$(36)CaO$-$(4-x)P_2O_5$-$(x)Ag_2O$ where x = 0.0, 0.3, 0.5 and 1 (mol%) was developed using a novel sol-gel processing technique. Addition of a silver precursor (silver nitrate) in acidic condition along with the elimination of a sodium precursor (sodium methoxide) in the glass formulation led to the formation of amorphous glass without a metallic silver phase or semi-crystalline sodium nitrate within the glass

structure. Additionally, the higher specific surface area, and lower pore width and pore volume were achieved when compared to the sodium containing glasses.

- AgBGs demonstrated a dose dependent silver ion release based on the silver content in the glass formulations or glass concentrations. Furthermore, it was shown that there is a dose dependent correlation between silver ion release from the dissolution of AgBGs and their anti-bacterial efficacy against wound infection-associated Gram-negative (*E.coli*) and Gram-positive (*S.aureus*) bacteria, *in vitro*.

- Longer-term anti-bacterial efficacy of AgBG ionic dissolution products against *PA14* bacteria was achieved through glass composition and concentration alterations. Additionally, the efficacy of silver ion released from the dissolution of AgBGs against pre-formed *PA14* biofilms was demonstrated.

- Silver ion released from the dissolution of AgBGs was not toxic to keratinocyte and fibroblastic cells at lower concentrations less than 1 ppm.

- Extent of keratinocyte cell migration was stimulated in a dose dependent manner, *in vitro*.

- The reported compositional range of AgBG: B60 fabricated in this dissertation, holds promise in accelerating the healing process of chronic wounds.

10.2 Future perspectives

The potential of DVS and IGC as novel techniques to characterize aqueous reactivity and solubility properties of bioactive and soluble glasses more precisely has been demonstrated by their good correlation with the surface and bulk properties of glasses. Since there is an extensive need to accurately examine the effects of composition, processing, particle size, and surface area, of bioactive glasses [64], the results reported in this dissertation could serve as a primary study to further develop the utilization of these complementary techniques in their characterization.

The anti-bacterial efficacy of AgBGs has shown great potential in skin tissue repair. The results generated in this dissertation are anticipated to serve as a starting point for development

and optimization of future silver doped borate-based glasses for soft tissue repair applications. However, there is a plenty of room to further examine the composition, sol-gel processing, various precursors, and composite or hybrid scaffold formation.

While the structure of AgBGs was examined using various techniques, advanced X-ray photoelectron spectroscopy studies are needed to investigate and verify the oxidation state of silver in the glass structure to better understand its interaction and integration within the borate network. Additionally, NMR studies are needed in order to better examine the exact amounts of three and four-coordinated boron ions in the glass structure [292], which can help in understanding how the network modifiers influence the glass structure, which is the determining factor for chemical durability of multi-component glasses [26, 250]. There are also numerous sol-gel process parameters that influence the glass properties; these variables have been thoroughly studied for silicate-based glass systems [293]. However, these have not been examined extensively in borate systems, particularly, the role of various dopants and their complications for the sol-gel process. More comprehensive studies are needed to examine the effects of pH, various precursors, sol preparation temperature and calcination temperature.

Since vascularization is a vital process in wound healing, it is important to evaluate the angiogenic potential of the released ions via the analysis of endothelial cell morphogenesis in two dimensions as well as in three dimensions when cultured in an *in vitro* dense collagen gel tissue model [100, 160]. Furthermore, it is necessary to evaluate the collagen production rates of three dimensionally seeded fibroblastic cells using an *in vitro* dense collagen gel tissue model. Also it is significant to evaluate the role of AgBGs on the secretion behavior of growth factors implicated in the wound healing process, such as TGF-β, since it has a broad spectrum roles in the inflammation, proliferation and tissue remodelling stages [176]. All of these analyses will contribute to a greater understanding of the mechanism involved when applying bioactive glasses in wound healing.

In this thesis it was shown that boron itself can be a source of toxicity to mammalian cells, however in order to better evaluate the toxicity of boron, a dynamic cell culture environment is essential. It was previously shown that borate glasses can be toxic when cultured statically [290], while the utilization of dynamic culturing conditions could reduce cytoxicity [291] and better reflect *in vivo* conditions [125, 136]. Thus, key future studies involve more comprehensive cellular studies of keratinocyte, fibroblastic and endothelial cells *in vitro* along with the utilization of *in*

vivo animal models using a full thickness skin defects [125, 136] in both normal and diabetes-impaired skin wounds [113, 229].

11 References

[1] L.L. Hench, Bioceramics - from Concept to Clinic, Journal of the American Ceramic Society, 74 (1991) 1487-1510.
[2] P. Stoor, E. Soderling, R. Grenman, Interactions between the bioactive glass S53P4 and the atrophic rhinitis-associated microorganism klebsiella ozaenae, J Biomed Mater Res, 48 (1999) 869-874.
[3] L.L. Hench, R.J. Splinter, W.C. Allen, T.K. Greenlee, Bonding mechanisms at the interface of ceramic prosthetic materials, Journal of Biomedical Materials Research, 5 (1971) 117-141.
[4] V. Salih, K. Franks, M. James, G.W. Hastings, J.C. Knowles, I. Olsen, Development of soluble glasses for biomedical use Part II: The biological response of human osteoblast cell lines to phosphate-based soluble glasses, Journal of Materials Science: Materials in Medicine, 11 (2000) 615-620.
[5] D.S. Brauer, D. Moncke, Chapter 3 Introduction to the Structure of Silicate, Phosphate and Borate Glasses, in: Bioactive Glasses: Fundamentals, Technology and Applications, The Royal Society of Chemistry, 2017, pp. 61-88.
[6] U. Hoppe, A structural model for phosphate glasses, Journal of Non-Crystalline Solids, 195 (1996) 138-147.
[7] J.C. Knowles, Phosphate based glasses for biomedical applications, Journal of Materials Chemistry, 13 (2003) 2395-2401.
[8] E.A. Abou Neel, D.M. Pickup, S.P. Valappil, R.J. Newport, J.C. Knowles, Bioactive functional materials: a perspective on phosphate-based glasses, Journal of Materials Chemistry, 19 (2009) 690-701.
[9] P. Balasubramanian, T. Büttner, V. Miguez Pacheco, A.R. Boccaccini, Boron-containing bioactive glasses in bone and soft tissue engineering, Journal of the European Ceramic Society, 38 (2018) 855-869.
[10] http://etissuesolutions.com, in, 2017.
[11] A. Hoppe, N.S. Guldal, A.R. Boccaccini, A review of the biological response to ionic dissolution products from bioactive glasses and glass-ceramics, Biomaterials, 32 (2011) 2757-2774.
[12] A. Hoppe, V. Mourino, A.R. Boccaccini, Therapeutic inorganic ions in bioactive glasses to enhance bone formation and beyond, Biomaterials Science, 1 (2013) 254-256.
[13] L. Hupa, M. Hupa, Recent research on composition dependence of the properties of bioactive glasses, in: Ceramic Transactions, 2010, pp. 145-156.
[14] I.K. Jun, Y.H. Koh, H.E. Kim, Fabrication of a highly porous bioactive glass-ceramic scaffold with a high surface area and strength, Journal of the American Ceramic Society, 89 (2006) 391-394.
[15] R. Xin, Q. Zhang, J. Chen, Y. Leng, Effects of porosity and crystallinity of glass ceramics on the in vivo bioactive response, Biomedical Materials, 3 (2008).
[16] M. Cerruti, D. Greenspan, K. Powers, Effect of pH and ionic strength on the reactivity of Bioglass 45S5, Biomaterials, 26 (2005) 1665-1674.
[17] A.J. Garcia, P. Ducheyne, D. Boettiger, Effect of surface reaction stage on fibronectin-mediated adhesion of osteoblast-like cells to bioactive glass, J Biomed Mater Res, 40 (1998) 48-56.
[18] J.J. Blaker, V. Maquet, A.R. Boccaccini, R. Jérôme, A. Bismarck, Wetting of bioactive glass surfaces by poly(α-hydroxyacid) melts: Interaction between Bioglass® and biodegradable polymers, E-Polymers, (2005).

[19] E. Verné, C. Vitale-Brovarone, E. Bui, C.L. Bianchi, A.R. Boccaccini, Surface functionalization of bioactive glasses, Journal of Biomedical Materials Research - Part A, 90 (2009) 981-992.
[20] C. Duée, I. Grattepanche-Lebecq, F. Désanglois, C. Follet-Houttemane, F. Chai, H.F. Hildebrand, Predicting bioactive properties of phosphosilicate glasses using mixture designs, Journal of Non-Crystalline Solids, 362 (2013) 47-55.
[21] M. Shah Mohammadi, F. Chicatun, C. Stahli, N. Muja, M.N. Bureau, S.N. Nazhat, Osteoblastic differentiation under controlled bioactive ion release by silica and titania doped sodium-free calcium phosphate-based glass, Colloids and surfaces. B, Biointerfaces, 121 (2014) 82-91.
[22] E.A. Abou Neel, I. Ahmed, J.J. Blaker, A. Bismarck, A.R. Boccaccini, M.P. Lewis, S.N. Nazhat, J.C. Knowles, Effect of iron on the surface, degradation and ion release properties of phosphate-based glass fibres, Acta Biomaterialia, 1 (2005) 553-563.
[23] C. Stahli, M. Shah Mohammadi, K.E. Waters, S.N. Nazhat, Characterization of aqueous interactions of copper-doped phosphate-based glasses by vapour sorption, Acta Biomater, 10 (2014) 3317-3326.
[24] W.C. Lepry, S.N. Nazhat, Highly Bioactive Sol-Gel-Derived Borate Glasses, Chemistry of Materials, 27 (2015) 4821-4831.
[25] B.B. Hole, D.S. Keller, W.M. Burry, J.A. Schwarz, Surface energetics of bone mineral and synthetic hydroxyapatite using inverse gas chromatography, Journal of Chromatography B: Analytical Technologies in the Biomedical and Life Sciences, 879 (2011) 1847-1850.
[26] J.R. Jones, Review of bioactive glass: From Hench to hybrids, Acta Biomaterialia, 9 (2013) 4457-4486.
[27] M. Rai, A. Yadav, A. Gade, Silver nanoparticles as a new generation of antimicrobials, Biotechnology Advances, 27 (2009) 76-83.
[28] J.H. Fechner, J. Zimmer, Water-insoluble, antimicrobial silicate glass and use thereof, in, Google Patents, 2007.
[29] M. Kawashita, S. Tsuneyama, F. Miyaji, T. Kokubo, H. Kozuka, K. Yamamoto, Antibacterial silver-containing silica glass prepared by sol–gel method, Biomaterials, 21 (2000) 393-398.
[30] M. Bellantone, N.J. Coleman, L.L. Hench, Bacteriostatic action of a novel four-component bioactive glass, Journal of Biomedical Materials Research, 51 (2000) 484-490.
[31] A.S. Halim, T.L. Khoo, S.J. Mohd Yussof, Biologic and synthetic skin substitutes: An overview, Indian J Plast Surg, 43 (2010) S23-28.
[32] J.E. Shelby, Introduction to Glass Science and Technology, Royal Society of Chemistry, 2005.
[33] W.H. Zachariasen, The atomic arrangement in glass, Journal of the American Chemical Society, 54 (1932) 3841-3851.
[34] S. Fagerlund, L. Hupa, Chapter 1 Melt-derived Bioactive Silicate Glasses, in: Bioactive Glasses: Fundamentals, Technology and Applications, The Royal Society of Chemistry, 2017, pp. 1-26.
[35] M.N. Rahaman, D.E. Day, B. Sonny Bal, Q. Fu, S.B. Jung, L.F. Bonewald, A.P. Tomsia, Bioactive glass in tissue engineering, Acta Biomaterialia, 7 (2011) 2355-2373.
[36] M. Vallet-Regi, Ceramics for medical applications, Journal of the Chemical Society-Dalton Transactions, (2001) 97-108.
[37] R.K. Brow, Review: the structure of simple phosphate glasses, Journal of Non-Crystalline Solids, 263 (2000) 1-28.

[38] R.J. Kirkpatrick, R.K. Brow, Nuclear magnetic resonance investigation of the structures of phosphate and phosphate-containing glasses: a review, Solid state nuclear magnetic resonance, 5 (1995) 9-21.
[39] R.K. Brow, T.M. Alam, D.R. Tallant, R.J. Kirkpatrick, Spectroscopic studies on the structures of phosphate sealing glasses, MRS Bulletin, 23 (1998) 63-67.
[40] Y. Peng, D. Day, High thermal expansion phosphate glasses. II, Glass technology, 32 (1991) 200-205.
[41] E.A.A. Neel, D.M. Pickup, S.P. Valappil, R.J. Newport, J.C. Knowles, Bioactive functional materials: a perspective on phosphate-based glasses, Journal of Materials Chemistry, 19 (2008) 690-701.
[42] J. Krogh-Moe, The structure of vitreous and liquid boron oxide, Journal of Non-Crystalline Solids, 1 (1969) 269-284.
[43] A.C. Wright, Borate structures: crystalline and vitreous, Physics and Chemistry of Glasses-European Journal of Glass Science and Technology Part B, 51 (2010) 1-39.
[44] M. Schuch, C. Trott, P. Maass, Network forming units in alkali borate and borophosphate glasses and the mixed glass former effect, Rsc Advances, 1 (2011) 1370-1382.
[45] E.I. Kamitsos, Modifying Role of Alkali-Metal Cations in Borate Glass Networks, Journal of Physical Chemistry, 93 (1989) 1604-1611.
[46] S.A. Feller, A summary of the Second International Conference on Borate Glasses, Crystals and Melts, Physics and Chemistry of Glasses, 41 (2000) 211-215.
[47] H.L. Castricum, A. Sah, M.C. Mittelmeijer-Hazeleger, C. Huiskes, E. Johan, Microporous structure and enhanced hydrophobicity in methylated SiO 2 for molecular separation, Journal of Materials Chemistry, 17 (2007) 1509-1517.
[48] R. Li, A.E. Clark, L.L. Hench, An investigation of bioactive glass powders by sol-gel processing, J Appl Biomater, 2 (1991) 231-239.
[49] W.K. Brinker C, Keefer K, Holupka E, Bray P, Pearson R, Synthesis and Structure of Borate Based Aerogels. Aerogels, Springer, 1986.
[50] C.J. Brinker, G.W. Scherer, Sol-gel science: the physics and chemistry of sol-gel processing, Academic press, 1990.
[51] C. Brinker, K. Ward, K. Keefer, E. Holupka, P. Bray, R. Pearson, Synthesis and Structure of Borate Based Aerogels, in: Aerogels, Springer, 1986, pp. 57-67.
[52] N. Tohge, J. Mackenzie, Preparation of 20Na2O·80B2O3 glasses by sol-gel method, Journal of non-crystalline solids, 68 (1984) 411-418.
[53] W.C. Lepry, S. Naseri, S.N. Nazhat, Effect of processing parameters on textural and bioactive properties of sol-gel-derived borate glasses, Journal of Materials Science, 52 (2017) 8973-8985.
[54] W.C. lepry, Sol-gel-derived bioactive borate glasses for mineralized tissue repair (Doctoral disseration), in, 2017.
[55] Q. Fu, M.N. Rahaman, H. Fu, X. Liu, Silicate, borosilicate, and borate bioactive glass scaffolds with controllable degradation rate for bone tissue engineering applications. I. Preparation and in vitro degradation, J Biomed Mater Res A, 95 (2010) 164-171.
[56] T. Kokubo, Bioactive glass ceramics: properties and applications, Biomaterials, 12 (1991) 155-163.
[57] D.C. Clupper, J.J. Mecholsky, G.P. LaTorre, D.C. Greenspan, Sintering temperature effects on the in vitro bioactive response of tape cast and sintered bioactive glass-ceramic in Tris buffer, Journal of Biomedical Materials Research, 57 (2001) 532-540.

[58] D. Rohanova, A.R. Boccaccini, D. Horkavcova, P. Bozdechova, P. Bezdicka, M. Castoralova, Is non-buffered DMEM solution a suitable medium for in vitro bioactivity tests?, Journal of Materials Chemistry B, 2 (2014) 5068-5076.
[59] D. Rohanová, A.R. Boccaccini, D.M. Yunos, D. Horkavcová, I. Březovská, A. Helebrant, TRIS buffer in simulated body fluid distorts the assessment of glass–ceramic scaffold bioactivity, Acta biomaterialia, 7 (2011) 2623-2630.
[60] M. Bohner, J. Lemaitre, Can bioactivity be tested in vitro with SBF solution?, Biomaterials, 30 (2009) 2175-2179.
[61] R. Hill, An alternative view of the degradation of bioglass, Journal of Materials Science Letters, 15 (1996) 1122-1125.
[62] S.E. Hogan, G. Buckton, The application of near infrared spectroscopy and dynamic vapor sorption to quantify low amorphous contents of crystalline lactose, Pharmaceutical research, 18 (2001) 112-116.
[63] G. Bingol, B. Prakash, Z. Pan, Dynamic vapor sorption isotherms of medium grain rice varieties, LWT-Food Science and Technology, 48 (2012) 156-163.
[64] V. Stanić, Variation in properties of bioactive glasses after surface modification, in: Clinical Applications of Biomaterials: State-of-the-Art Progress, Trends, and Novel Approaches, 2017, pp. 35-63.
[65] S. Faghihi, F. Azari, A.P. Zhilyaev, J.A. Szpunar, H. Vali, M. Tabrizian, Cellular and molecular interactions between MC3T3-E1 pre-osteoblasts and nanostructured titanium produced by high-pressure torsion, Biomaterials, 28 (2007) 3887-3895.
[66] T.J. Webster, C. Ergun, R.H. Doremus, R.W. Siegel, R. Bizios, Specific proteins mediate enhanced osteoblast adhesion on nanophase ceramics, Journal of Biomedical Materials Research, 51 (2000) 475-483.
[67] K. von der Mark, J. Park, S. Bauer, P. Schmuki, Nanoscale engineering of biomimetic surfaces: cues from the extracellular matrix, Cell and Tissue Research, 339 (2010) 131-153.
[68] D. Lehnert, B. Wehrle-Haller, C. David, U. Weiland, C. Ballestrem, B.A. Imhof, M. Bastmeyer, Cell behaviour on micropatterned substrata: limits of extracellular matrix geometry for spreading and adhesion, Journal of Cell Science, 117 (2004) 41-52.
[69] J. Mesquita-Guimaraes, E. Garcia, P. Miranzo, M.I. Osendi, C.V. Cojocaru, R.S. Lima, Mullite-YSZ multilayered environmental barrier coatings tested in cycling conditions under water vapor atmosphere, Surface & Coatings Technology, 209 (2012) 103-109.
[70] S. Mohammadi-Jam, K.E. Waters, Inverse gas chromatography applications: A review, Advances in Colloid and Interface Science, 212 (2014) 21-44.
[71] I.D. Smičiklas, S.K. Milonjić, S. Zec, An inverse gas chromatographic study of the adsorption of alkanes on hydroxyapatite, Journal of Materials Science, 35 (2000) 2825-2828.
[72] J. Fore, A review of skin and the effects of aging on skin structure and function, Ostomy Wound Management, 52 (2006) 24-37.
[73] P. Martin, Wound healing - Aiming for perfect skin regeneration, Science, 276 (1997) 75-81.
[74] N.J. Percival, Classification of Wounds and their Management, Surgery (Oxford), 20 (2002) 114-117.
[75] L. Bolton, L. van Rijswijk, Wound dressings: meeting clinical and biological needs, Dermatology nursing / Dermatology Nurses" Association, 3 (1991) 146-161.
[76] J.S. Boateng, K.H. Matthews, H.N.E. Stevens, G.M. Eccleston, Wound healing dressings and drug delivery systems: A review, Journal of Pharmaceutical Sciences, 97 (2008) 2892-2923.

[77] K.A. Rieger, N.P. Birch, J.D. Schiffman, Designing electrospun nanofiber mats to promote wound healing-a review, Journal of Materials Chemistry B, 1 (2013) 4531-4541.
[78] M. Norouzi, S.M. Boroujeni, N. Omidvarkordshouli, M. Soleimani, Advances in skin regeneration: application of electrospun scaffolds, Adv Healthc Mater, 4 (2015) 1114-1133.
[79] J.-H. Jo, E.-J. Lee, D.-S. Shin, H.-E. Kim, H.-W. Kim, Y.-H. Koh, J.-H. Jang, In vitro/in vivo biocompatibility and mechanical properties of bioactive glass nanofiber and poly(ε-caprolactone) composite materials, Journal of Biomedical Materials Research Part B: Applied Biomaterials, 91B (2009) 213-220.
[80] S. Naseri, W.C. Lepry, S.N. Nazhat, Bioactive glasses in wound healing: hope or hype?, Journal of Materials Chemistry B, 5 (2017) 6167-6174.
[81] D.F. Williams, European Society for Biomaterials., Definitions in biomaterials : proceedings of a consensus conference of the European Society for Biomaterials, Chester, England, March 3-5, 1986, Elsevier, Amsterdam ; New York, 1987.
[82] W.P. Cao, L.L. Hench, Bioactive materials, Ceramics International, 22 (1996) 493-507.
[83] L.L. Hench, The story of Bioglass, J Mater Sci Mater Med, 17 (2006) 967-978.
[84] V. Miguez-Pacheco, L.L. Hench, A.R. Boccaccini, Bioactive glasses beyond bone and teeth: Emerging applications in contact with soft tissues, Acta Biomaterialia, 13 (2015) 1-15.
[85] L.L. Hench, Biomaterials: a forecast for the future, Biomaterials, 19 (1998) 1419-1423.
[86] T. Kokubo, H. Kushitani, S. Sakka, T. Kitsugi, T. Yamamuro, Solutions able to reproduce in vivo surface-structure changes in bioactive glass-ceramic A-W3, Journal of Biomedical Materials Research, 24 (1990) 721-734.
[87] H.S. Gao, T.N. Tan, D.H. Wang, Effect of composition on the release kinetics of phosphate controlled release glasses in aqueous medium, Journal of Controlled Release, 96 (2004) 21-28.
[88] K. Franks, I. Abrahams, J.C. Knowles, Development of soluble glasses for biomedical use Part I: In vitro solubility measurement, Journal of Materials Science-Materials in Medicine, 11 (2000) 609-614.
[89] B.C. Bunker, G.W. Arnold, J.A. Wilder, Phosphate glass dissolution in aqueous solutions, Journal of Non-Crystalline Solids, 64 (1984) 291-316.
[90] H. Gao, T. Tan, D. Wang, Dissolution mechanism and release kinetics of phosphate controlled release glasses in aqueous medium, Journal of Controlled Release, 96 (2004) 29-36.
[91] B. Clarke, Normal bone anatomy and physiology, Clin J Am Soc Nephrol, 3 Suppl 3 (2008) S131-139.
[92] S.P. Valappil, M. Coombes, L. Wright, G.J. Owens, R.J.M. Lynch, C.K. Hope, S.M. Higham, Role of gallium and silver from phosphate-based glasses on in vitro dual species oral biofilm models of Porphyromonas gingivalis and Streptococcus gordonii, Acta Biomaterialia, 8 (2012) 1957-1965.
[93] S.P. Valappil, D. Ready, E.A. Abou Neel, D.M. Pickup, L.A. O'Dell, W. Chrzanowski, J. Pratten, R.J. Newport, M.E. Smith, M. Wilson, J.C. Knowles, Controlled delivery of antimicrobial gallium ions from phosphate-based glasses, Acta Biomater, 5 (2009) 1198-1210.
[94] S.P. Valappil, D. Ready, E.A. Abou Neel, D.M. Pickup, W. Chrzanowski, L.A. O'Dell, R.J. Newport, M.E. Smith, M. Wilson, J.C. Knowles, Antimicrobial gallium-doped phosphate-based glasses, Advanced Functional Materials, 18 (2008) 732-741.
[95] D.M. Pickup, S.P. Valappil, R.M. Moss, H.L. Twyman, P. Guerry, M.E. Smith, M. Wilson, J.C. Knowles, R.J. Newport, Preparation, structural characterisation and antibacterial properties of Ga-doped sol-gel phosphate-based glass, Journal of Materials Science, 44 (2009) 1858-1867.

[96] I. Ahmed, D. Ready, M. Wilson, J.C. Knowles, Antimicrobial effect of silver-doped phosphate-based glasses, J Biomed Mater Res A, 79 (2006) 618-626.
[97] A.M. Mulligan, M. Wilson, J.C. Knowles, Effect of increasing silver content in phosphate-based glasses on biofilms of Streptococcus sanguis, Journal of Biomedical Materials Research Part A, 67 (2003) 401-412.
[98] A.M. Mulligan, M. Wilson, J.C. Knowles, The effect of increasing copper content in phosphate-based glasses on biofilms of Streptococcus sanguis, Biomaterials, 24 (2003) 1797-1807.
[99] E.A. Abou Neel, I. Ahmed, J. Pratten, S.N. Nazhat, J.C. Knowles, Characterisation of antibacterial copper releasing degradable phosphate glass fibres, Biomaterials, 26 (2005) 2247-2254.
[100] C. Stahli, M. James-Bhasin, S.N. Nazhat, Three-dimensional endothelial cell morphogenesis under controlled ion release from copper-doped phosphate glass, Journal of Controlled Release, 200 (2015) 222-232.
[101] Q. Fu, M.N. Rahaman, B.S. Bal, L.F. Bonewald, K. Kuroki, R.F. Brown, Silicate, borosilicate, and borate bioactive glass scaffolds with controllable degradation rate for bone tissue engineering applications. II. In vitro and in vivo biological evaluation, J Biomed Mater Res A, 95 (2010) 172-179.
[102] W. Huang, D.E. Day, K. Kittiratanapiboon, M.N. Rahaman, Kinetics and mechanisms of the conversion of silicate (45S5), borate, and borosilicate glasses to hydroxyapatite in dilute phosphate solutions, J Mater Sci Mater Med, 17 (2006) 583-596.
[103] A.H. Yao, D.P. Wang, W.H. Huang, Q. Fu, M.N. Rahaman, D.E. Day, In vitro bioactive characteristics of borate-based glasses with controllable degradation behavior, Journal of the American Ceramic Society, 90 (2007) 303-306.
[104] D. Carta, J.C. Knowles, P. Guerry, M.E. Smith, R.J. Newport, Sol–gel synthesis and structural characterisation of P2O5–B2O3–Na2O glasses for biomedical applications, Journal of materials chemistry, 19 (2009) 150-158.
[105] D.M. Pickup, R.J. Newport, J.C. Knowles, Sol-gel phosphate-based glass for drug delivery applications, J Biomater Appl, 26 (2012) 613-622.
[106] D. Zhang, O. Leppäranta, E. Munukka, H. Ylänen, M.K. Viljanen, E. Eerola, M. Hupa, L. Hupa, Antibacterial effects and dissolution behavior of six bioactive glasses, Journal of Biomedical Materials Research Part A, 93A (2010) 475-483.
[107] A.B.G. Lansdown, Calcium: a potential central regulator in wound healing in the skin, Wound Repair and Regeneration, 10 (2002) 271-285.
[108] K. Kawai, B.J. Larson, H. Ishise, A.L. Carre, S. Nishimoto, M. Longaker, H.P. Lorenz, Calcium-Based Nanoparticles Accelerate Skin Wound Healing, Plos One, 6 (2011).
[109] R.L. Gillette, S.F. Swaim, E.A. Sartin, D.M. Bradley, S.L. Coolman, Effects of a bioactive glass on healing of closed skin wounds in dogs, American Journal of Veterinary Research, 62 (2001) 1149-1153.
[110] T.A. Ostomel, Q. Shi, C.-K. Tsung, H. Liang, G.D. Stucky, Spherical Bioactive Glass with Enhanced Rates of Hydroxyapatite Deposition and Hemostatic Activity, Small, 2 (2006) 1261-1265.
[111] T.A. Ostomel, Q.H. Shi, G.D. Stucky, Oxide hemostatic activity, Journal of the American Chemical Society, 128 (2006) 8384-8385.
[112] C. Lin, C. Mao, J. Zhang, Y. Li, X. Chen, Healing effect of bioactive glass ointment on full-thickness skin wounds, Biomedical Materials (Bristol), 7 (2012).

[113] C. Mao, C. Lin, X.F. Chen, Enhanced Healing of Full-thickness Diabetic Wounds Using Bioactive Glass and Yunnan Baiyao Ointments, Journal of Wuhan University of Technology-Materials Science Edition, 29 (2014) 1063-1070.
[114] W.H. Xie, X.F. Chen, G.H. Miao, J.Y. Tang, X.L. Fu, Regulation of cellular behaviors of fibroblasts related to wound healing by sol-gel derived bioactive glass particles, Journal of Biomedical Materials Research Part A, 104 (2016) 2420-2429.
[115] H.F. Yu, J.L. Peng, Y.H. Xu, J. Chang, H.Y. Li, Bioglass Activated Skin Tissue Engineering Constructs for Wound Healing, Acs Applied Materials & Interfaces, 8 (2016) 703-715.
[116] Q.Y. Zeng, Y. Han, H.Y. Li, J. Chang, Design of a thermosensitive bioglass/agarose-alginate composite hydrogel for chronic wound healing, Journal of Materials Chemistry B, 3 (2015) 8856-8864.
[117] L. Francis, D.C. Meng, I.C. Locke, J.C. Knowles, N. Mordan, V. Salih, A.R. Boccaccini, I. Roy, Novel poly(3-hydroxybutyrate) composite films containing bioactive glass nanoparticles for wound healing applications, Polymer International, 65 (2016) 661-674.
[118] P. Stoor, E. Soderling, J.I. Salonen, Antibacterial effects of a bioactive glass paste on oral microorganisms, Acta Odontologica Scandinavica, 56 (1998) 161-165.
[119] I. Allan, H. Newman, M. Wilson, Antibacterial activity of particulate bioglass against supra- and subgingival bacteria, Biomaterials, 22 (2001) 1683-1687.
[120] P. Stoor, E. Söderling, R. Grénman, Bioactive glass S53P4 in repair of septal perforations and its interactions with the respiratory infection-associated microorganisms Heamophilus influenzae and Streptococcus pneumoniae, Journal of Biomedical Materials Research, 58 (2001) 113-120.
[121] R.M. Day, Bioactive glass stimulates the secretion of angiogenic growth factors and angiogenesis in vitro, Tissue engineering, 11 (2005) 768-777.
[122] J.K. Leach, D. Kaigler, Z. Wang, P.H. Krebsbach, D.J. Mooney, Coating of VEGF-releasing scaffolds with bioactive glass for angiogenesis and bone regeneration, Biomaterials, 27 (2006) 3249-3255.
[123] A. Leu, J.K. Leach, Proangiogenic potential of a collagen/bioactive glass substrate, Pharmaceutical Research, 25 (2008) 1222-1229.
[124] E.S. Tadjoedin, G.L. de Lange, P.J. Holzmann, L. Kulper, E.H. Burger, Histological observations on biopsies harvested following sinus floor elevation using a bioactive glass material of narrow size range, Clin Oral Implants Res, 11 (2000) 334-344.
[125] J. Zhou, H. Wang, S. Zhao, N. Zhou, L. Li, W. Huang, D. Wang, C. Zhang, In vivo and in vitro studies of borate based glass micro-fibers for dermal repairing, Mater Sci Eng C Mater Biol Appl, 60 (2016) 437-445.
[126] R.J. Fair, Y. Tor, Antibiotics and bacterial resistance in the 21st century, Perspect Medicin Chem, 6 (2014) 25-64.
[127] E.M. Carlisle, Silicon: a possible factor in bone calcification, Science, 167 (1970) 279-280.
[128] D.M. Reffitt, N. Ogston, R. Jugdaohsingh, H.F. Cheung, B.A. Evans, R.P. Thompson, J.J. Powell, G.N. Hampson, Orthosilicic acid stimulates collagen type 1 synthesis and osteoblastic differentiation in human osteoblast-like cells in vitro, Bone, 32 (2003) 127-135.
[129] L.L. Hench, D. Greenspan, Interactions between Bioactive Glass and Collagen: A Review and New Perspectives, Journal of the Australian Ceramic Society, 49 (2013) 1-40.
[130] J.E. Gough, J.R. Jones, L.L. Hench, Nodule formation and mineralisation of human primary osteoblasts cultured on a porous bioactive glass scaffold, Biomaterials, 25 (2004) 2039-2046.

[131] S. Maeno, Y. Niki, H. Matsumoto, H. Morioka, T. Yatabe, A. Funayama, Y. Toyama, T. Taguchi, J. Tanaka, The effect of calcium ion concentration on osteoblast viability, proliferation and differentiation in monolayer and 3D culture, Biomaterials, 26 (2005) 4847-4855.
[132] P. Valerio, M.M. Pereira, A.M. Goes, M.F. Leite, Effects of extracellular calcium concentration on the glutamate release by bioactive glass (BG60S) preincubated osteoblasts, Biomedical Materials, 4 (2009).
[133] M. Julien, S. Khoshniat, A. Lacreusette, M. Gatius, A. Bozec, E.F. Wagner, Y. Wittrant, M. Masson, P. Weiss, L. Beck, D. Magne, J. Guicheux, Phosphate-dependent regulation of MGP in osteoblasts: Role of ERK1/2 and Fra-1, Journal of Bone and Mineral Research, 24 (2009) 1856-1868.
[134] L.A. Haro Durand, A. Gongora, J.M. Porto Lopez, A.R. Boccaccini, M.P. Zago, A. Baldi, A. Gorustovich, In vitro endothelial cell response to ionic dissolution products from boron-doped bioactive glass in the SiO2-CaO-P2O5-Na2O system, Journal of Materials Chemistry B, 2 (2014) 7620-7630.
[135] Q. Yang, S. Chen, H. Shi, H. Xiao, Y. Ma, In vitro study of improved wound-healing effect of bioactive borate-based glass nano-/micro-fibers, Mater Sci Eng C Mater Biol Appl, 55 (2015) 105-117.
[136] S. Zhao, L. Li, H. Wang, Y. Zhang, X. Cheng, N. Zhou, M.N. Rahaman, Z. Liu, W. Huang, C. Zhang, Wound dressings composed of copper-doped borate bioactive glass microfibers stimulate angiogenesis and heal full-thickness skin defects in a rodent model, Biomaterials, 53 (2015) 379-391.
[137] M. Dzondo-Gadet, R. Mayap-Nzietchueng, K. Hess, P. Nabet, F. Belleville, B. Dousset, Action of boron at the molecular level - Effects on transcription and translation in an acellular system, Biological Trace Element Research, 85 (2002) 23-33.
[138] G. Hu, L. Xiao, P. Tong, D. Bi, H. Wang, H. Ma, G. Zhu, H. Liu, Antibacterial hemostatic dressings with nanoporous bioglass containing silver, International Journal of Nanomedicine, 7 (2012) 2613-2620.
[139] J. Pratten, S.N. Nazhat, J.J. Blaker, A.R. Boccaccini, In vitro attachment of staphylococcus epidermidis to surgical sutures with and without Ag-containing bioactive glass coating, Journal of Biomaterials Applications, 19 (2004) 47-57.
[140] S.-H. Luo, W. Xiao, X.-J. Wei, W.-T. Jia, C.-Q. Zhang, W.-H. Huang, D.-X. Jin, M.N. Rahaman, D.E. Day, In vitro evaluation of cytotoxicity of silver-containing borate bioactive glass, Journal of Biomedical Materials Research Part B: Applied Biomaterials, 95B (2010) 441-448.
[141] H. Kamal, Structure and physical properties of silver borate bioactive glasses, Research Journal of Pharmaceutical, Biological and Chemical Sciences, 5 (2014) 822-832.
[142] R. Augustine, E.A. Dominic, I. Reju, B. Kaimal, N. Kalarikkal, S. Thomas, Investigation of angiogenesis and its mechanism using zinc oxide nanoparticle-loaded electrospun tissue engineering scaffolds, RSC Advances, 4 (2014) 51528-51536.
[143] V. Aina, G. Malavasi, A.F. Pla, L. Munaron, C. Morterra, Zinc-containing bioactive glasses: Surface reactivity and behaviour towards endothelial cells, Acta Biomaterialia, 5 (2009) 1211-1222.
[144] Y. Yin, Q. Cui, Y. Li, N. Irwin, D. Fischer, A.R. Harvey, L.I. Benowitz, Macrophage-derived factors stimulate optic nerve regeneration, Journal of Neuroscience, 23 (2003) 2284-2293.
[145] C. Lang, C. Murgia, M. Leong, L.W. Tan, G. Perozzi, D. Knight, R. Ruffin, P. Zalewski, Anti-inflammatory effects of zinc and alterations in zinc transporter mRNA in mouse models of

allergic inflammation, American Journal of Physiology - Lung Cellular and Molecular Physiology, 292 (2007) L577-L584.
[146] A.B.G. Lansdown, U. Mirastschijski, N. Stubbs, E. Scanlon, M.S. Ågren, Zinc in wound healing: Theoretical, experimental, and clinical aspects, Wound Repair and Regeneration, 15 (2007) 2-16.
[147] C. Gérard, L.J. Bordeleau, J. Barralet, C.J. Doillon, The stimulation of angiogenesis and collagen deposition by copper, Biomaterials, 31 (2010) 824-831.
[148] Y.-F. Goh, A.Z. Alshemary, M. Akram, M.R. Abdul Kadir, R. Hussain, Bioactive Glass: An In-Vitro Comparative Study of Doping with Nanoscale Copper and Silver Particles, International Journal of Applied Glass Science, 5 (2014) 255-266.
[149] J. Pablo Rodrguez, S. Ros, M. Gonzlez, Modulation of the proliferation and differentiation of human mesenchymal stem cells by copper, Journal of Cellular Biochemistry, 85 (2002) 92-100.
[150] Q.L. Feng, J. Wu, G.Q. Chen, F.Z. Cui, T.N. Kim, J.O. Kim, A mechanistic study of the antibacterial effect of silver ions on Escherichia coli and Staphylococcus aureus, J Biomed Mater Res, 52 (2000) 662-668.
[151] S. Chernousova, M. Epple, Silver as Antibacterial Agent: Ion, Nanoparticle, and Metal, Angewandte Chemie International Edition, 52 (2013) 1636-1653.
[152] M. Bellantone, H.D. Williams, L.L. Hench, Broad-spectrum bactericidal activity of Ag2O-doped bioactive glass, Antimicrobial Agents and Chemotherapy, 46 (2002) 1940-1945.
[153] M. Catauro, M.G. Raucci, F. de Gaetano, A. Marotta, Antibacterial and bioactive silver-containing Na2O·CaO·2SiO2 glass prepared by sol–gel method, Journal of Materials Science: Materials in Medicine, 15 (2004) 831-837.
[154] J.J. Blaker, S.N. Nazhat, A.R. Boccaccini, Development and characterisation of silver-doped bioactive glass-coated sutures for tissue engineering and wound healing applications, Biomaterials, 25 (2004) 1319-1329.
[155] U. Lohbauer, G. Jell, P. Saravanapavan, J.R. Jones, L.L. Hench, Indirect cytotoxicity evaluation of silver doped bioglass Ag-S70C30 on human primary keratinocytes, in: Key Engineering Materials, 2005, pp. 431-434.
[156] A.W. Wren, A. Coughlan, P. Hassanzadeh, M.R. Towler, Silver coated bioactive glass particles for wound healing applications, Journal of Materials Science: Materials in Medicine, 23 (2012) 1331-1341.
[157] C. Sanchez, M. Lopez-Jurado, P. Aranda, J. Llopis, Plasma levels of copper, manganese and selenium in an adult population in southern Spain: Influence of age, obesity and lifestyle factors, Science of the Total Environment, 408 (2010) 1014-1020.
[158] B. Marelli, D. Le Nihouannen, S.A. Hacking, S. Tran, J. Li, M. Murshed, C.J. Doillon, C.E. Ghezzi, Y.L. Zhang, S.N. Nazhat, J.E. Barralet, Newly identified interfibrillar collagen crosslinking suppresses cell proliferation and remodelling, Biomaterials, 54 (2015) 126-135.
[159] P. Carmeliet, Mechanisms of angiogenesis and arteriogenesis, Nature Medicine, 6 (2000) 389-395.
[160] C. Stahli, M. James-Bhasin, A. Hoppe, A.R. Boccaccini, S.N. Nazhat, Effect of ion release from Cu-doped 45S5 Bioglass(R) on 3D endothelial cell morphogenesis, Acta Biomater, 19 (2015) 15-22.
[161] C. Stahli, N. Muja, S.N. Nazhat, Controlled copper ion release from phosphate-based glasses improves human umbilical vein endothelial cell survival in a reduced nutrient environment, Tissue Eng Part A, 19 (2013) 548-557.

[162] C.K. Sen, S. Khanna, M. Venojarvi, P. Trikha, E.C. Ellison, T.K. Hunt, S. Roy, Copper-induced vascular endothelial growth factor expression and wound healing, American Journal of Physiology-Heart and Circulatory Physiology, 282 (2002) H1821-H1827.
[163] D. Bar-Or, G.W. Thomas, R.L. Yukl, L.T. Rael, R.P. Shimonkevitz, C.G. Curtis, J.V. Winkler, Copper stimulates the synthesis and release of interleukin-8 in human endothelial cells: A possible early role in systemic inflammatory responses, Shock, 20 (2003) 154-158.
[164] B.R. Mcauslan, W. Reilly, Endothelial-Cell Phagokinesis in Response to Specific Metal-Ions, Experimental Cell Research, 130 (1980) 147-157.
[165] G. Borkow, J. Gabbay, R. Dardik, A.I. Eidelman, Y. Lavie, Y. Grunfeld, S. Ikher, M. Huszar, R.C. Zatcoff, M. Marikovsky, Molecular mechanisms of enhanced wound healing by copper oxide-impregnated dressings, Wound Repair and Regeneration, 18 (2010) 266-275.
[166] N. Kong, K.L. Lin, H.Y. Li, J. Chang, Synergy effects of copper and silicon ions on stimulation of vascularization by copper-doped calcium silicate, Journal of Materials Chemistry B, 2 (2014) 1100-1110.
[167] Y. Kaneko, M. Thoendel, O. Olakanmi, B.E. Britigan, P.K. Singh, The transition metal gallium disrupts Pseudomonas aeruginosa iron metabolism and has antimicrobial and antibiofilm activity, Journal of Clinical Investigation, 117 (2007) 877-888.
[168] D.M. Pickup, R.M. Moss, D. Qiu, R.J. Newport, S.P. Valappil, J.C. Knowles, M.E. Smith, Structural characterization by x-ray methods of novel antimicrobial gallium-doped phosphate-based glasses, Journal of Chemical Physics, 130 (2009).
[169] A.S. Prasad, Zinc in human health: An update, The Journal of Trace Elements in Experimental Medicine, 11 (1998) 63-87.
[170] Y.H. Cho, S.J. Lee, J.Y. Lee, S.W. Kim, C.B. Lee, W.Y. Lee, M.S. Yoon, Antibacterial effect of intraprostatic zinc injection in a rat model of chronic bacterial prostatitis, International Journal of Antimicrobial Agents, 19 (2002) 576-582.
[171] L. Cordero-Arias, S. Cabanas-Polo, O.M. Goudouri, S.K. Misra, J. Gilabert, E. Valsami-Jones, E. Sanchez, S. Virtanen, A.R. Boccaccini, Electrophoretic deposition of ZnO/alginate and ZnO-bioactive glass/alginate composite coatings for antimicrobial applications, Materials Science & Engineering C-Materials for Biological Applications, 55 (2015) 137-144.
[172] A. Coughlan, S.M. Breed, C. Ashraf, J.A. Cardinale, M.M. Hall, M.R. Towler, Does elevating silver content in zinc-based glass polyalkenoate cements increase their antibacterial efficacy against two common bacteria using the agar gel diffusion method?, Journal of Biomaterials Applications, 27 (2013) 840-847.
[173] A. Coughlan, M.P. Ryan, N.M. Cummins, M.R. Towler, The response of Pseudomonas aeruginosa biofilm to the presence of a glass polyalkenoate cement formulated from a silver containing glass, Journal of Materials Science, 46 (2011) 285-287.
[174] P. Wray, Wound healing: An update on Mo-Sci's novel borate glass fibers, American Ceramic Society Bulletin, 92 (2013) 30-35.
[175] E. Munthe, J. Aaseth, E. Jellum, Trace elements and rheumatoid arthritis (RA) - Pathogenetic and therapeutic aspects, Acta Pharmacologica et Toxicologica, 59 (1986) 365-373.
[176] K.W. Finnson, S. McLean, G.M. Di Guglielmo, A. Philip, Dynamics of Transforming Growth Factor Beta Signaling in Wound Healing and Scarring, Adv Wound Care (New Rochelle), 2 (2013) 195-214.
[177] A.J. Singer, R.A. Clark, Cutaneous wound healing, N Engl J Med, 341 (1999) 738-746.

[178] X.F. Chen, L.L. Hench, D. Greenspan, J.P. Zhong, X.K. Zhang, Investigation on phase separation, nucleation and crystallization in bioactive glass-ceramics containing fluorophlogopite and fluorapatite, Ceramics International, 24 (1998) 401-410.
[179] V.K.M. Poon, A. Burd, In vitro cytotoxity of silver: implication for clinical wound care, Burns, 30 (2004) 140-147.
[180] L.L. Hench, Chronology of Bioactive Glass Development and Clinical Applications, New Journal of Glass and Ceramics, 3 (2013) 67.
[181] L.L. Hench, Bioceramics, Journal of the American Ceramic Society, 81 (1998) 1705-1727.
[182] A.R. Boccaccini, M. Erol, W.J. Stark, D. Mohn, Z. Hong, J.F. Mano, Polymer/bioactive glass nanocomposites for biomedical applications: A review, Composites Science and Technology, 70 (2010) 1764-1776.
[183] G.E. Vargas, L.A.H. Durand, V. Cadena, M. Romero, R.V. Mesones, M. Mačković, S. Spallek, E. Spiecker, A.R. Boccaccini, A.A. Gorustovich, Effect of nano-sized bioactive glass particles on the angiogenic properties of collagen based composites, Journal of Materials Science: Materials in Medicine, (2013) 1-9.
[184] E. Palin, H. Liu, T.J. Webster, Mimicking the nanofeatures of bone increases bone-forming cell adhesion and proliferation, Nanotechnology, 16 (2005) 1828.
[185] M. Cerruti, Surface characterization of silicate bioceramics, Philosophical Transactions of the Royal Society A: Mathematical, Physical and Engineering Sciences, 370 (2012) 1281-1312.
[186] M. Edén, The split network analysis for exploring composition–structure correlations in multi-component glasses: I. Rationalizing bioactivity-composition trends of bioglasses, Journal of Non-Crystalline Solids, 357 (2011) 1595-1602.
[187] R.G. Hill, D.S. Brauer, Predicting the bioactivity of glasses using the network connectivity or split network models, Journal of Non-Crystalline Solids, 357 (2011) 3884-3887.
[188] C. Stähli, M. Shah Mohammadi, K.E. Waters, S.N. Nazhat, Characterization of aqueous interactions of copper-doped phosphate-based glasses by vapour sorption, Acta biomaterialia, (2014).
[189] S. Brunauer, P.H. Emmett, E. Teller, Adsorption of gases in multimolecular layers, Journal of the American Chemical Society, 60 (1938) 309-319.
[190] E. Ortega-Rivas, P. Juliano, H. Yan, Food powders: physical properties, processing, and functionality, Springer, 2006.
[191] O. Peitl, E. Dutra Zanotto, L.L. Hench, Highly bioactive P2O5-Na2O-CaO-SiO2glass-ceramics, Journal of Non-Crystalline Solids, 292 (2001) 115-126.
[192] B. Marelli, C.E. Ghezzi, J.E. Barralet, A.R. Boccaccini, S.N. Nazhat, Three-dimensional mineralization of dense nanofibrillar collagen-bioglass hybrid scaffolds, Biomacromolecules, 11 (2010) 1470-1479.
[193] S. Koutsopoulos, Synthesis and characterization of hydroxyapatite crystals: a review study on the analytical methods, Journal of Biomedical Materials Research, 62 (2002) 600-612.
[194] I. Rehman, J.C. Knowles, W. Bonfield, Analysis of in vitro reaction layers formed on Bioglass using thin-film X-ray diffraction and ATR-FTIR microspectroscopy, Journal of Biomedical Materials Research, 41 (1998) 162-166.
[195] C.-T. Lee, W.-C. Hsu, The Measurement of LiquidI Water Mass Associated With Collected Hygroscopic Particles, Journal of Aerosol Science, 31 (2000) 189-197.
[196] E. Mikhailov, S. Vlasenko, S.T. Martin, T. Koop, U. Pöschl, Amorphous and crystalline aerosol particles interacting with water vapor: conceptual framework and experimental evidence

for restructuring, phase transitions and kinetic limitations, Atmospheric Chemistry and Physics, 9 (2009) 9491-9522.
[197] M.G. Cerruti, D. Greenspan, K. Powers, An analytical model for the dissolution of different particle size samples of Bioglass® in TRIS-buffered solution, Biomaterials, 26 (2005) 4903-4911.
[198] M. Erol, S. Kucukbayrak, A. Ersoy-Mericboyu, Influence of particle size on the crystallization kinetics of glasses produced from waste materials, Journal of Non-Crystalline Solids, 357 (2011) 211-219.
[199] D.V. Lenihan, A.J. Carter, T. Gilchrist, D.M. Healy, I.A. Miller, L.M. Myles, M.A. Glasby, Biodegradable controlled release glass in the repair of peripheral nerve injuries, Journal of Hand Surgery, 23 B (1998) 588-593.
[200] T. Gilchrist, M.A. Glasby, D.M. Healy, G. Kelly, D.V. Lenihan, K.L. McDowall, I.A. Miller, L.M. Myles, In vitro nerve repair - in vivo. The reconstruction of peripheral nerves by entubulation with biodegradeable glass tubes - a preliminary report, British Journal of Plastic Surgery, 51 (1998) 231-237.
[201] C. Sandino, S. Checa, P.J. Prendergast, D. Lacroix, Simulation of angiogenesis and cell differentiation in a CaP scaffold subjected to compressive strains using a lattice modeling approach, Biomaterials, 31 (2010) 2446-2452.
[202] R. Shah, A.C.M. Sinanan, J.C. Knowles, N.P. Hunt, M.P. Lewis, Craniofacial muscle engineering using a 3-dimensional phosphate glass fibre construct, Biomaterials, 26 (2005) 1497-1505.
[203] A. Patel, J.C. Knowles, Investigation of silica-iron-phosphate glasses for tissue engineering, Journal of Materials Science-Materials in Medicine, 17 (2006) 937-944.
[204] M.S. Mohammadi, I. Ahmed, B. Marelli, C. Rudd, M.N. Bureau, S.N. Nazhat, Modulation of polycaprolactone composite properties through incorporation of mixed phosphate glass formulations, Acta Biomaterialia, 6 (2010) 3157-3168.
[205] M.S. Mohammadi, I. Ahmed, N. Muja, S. Almeida, C.D. Rudd, M.N. Bureau, S.N. Nazhat, Effect of Si and Fe doping on calcium phosphate glass fibre reinforced polycaprolactone bone analogous composites, Acta Biomaterialia, 8 (2012) 1616-1626.
[206] E.A. Abou Neel, W. Chrzanowski, J.C. Knowles, Effect of increasing titanium dioxide content on bulk and surface properties of phosphate-based glasses, Acta Biomaterialia, 4 (2008) 523-534.
[207] E.A. Abou Neel, J.C. Knowles, Physical and biocompatibility studies of novel titanium dioxide doped phosphate-based glasses for bone tissue engineering applications, Journal of Materials Science-Materials in Medicine, 19 (2008) 377-386.
[208] S. Naseri, W.C. Lepry, W. Li, K.E. Waters, A.R. Boccaccini, S.N. Nazhat, 45S5 bioactive glass reactivity by dynamic vapour sorption, Journal of Non-Crystalline Solids, 432, Part A (2016) 47-52.
[209] J. Guillet, Z.Y. Al-Saigh, Inverse gas chromatography in analysis of polymers, Encyclopedia of Analytical Chemistry, (2006) 1-34.
[210] A. Voelkel, B. Strzemiecka, K. Adamska, K. Milczewska, Inverse gas chromatography as a source of physiochemical data, Journal of Chromatography A, 1216 (2009) 1551-1566.
[211] F. Thielmann, D.A. Butler, D.R. Williams, E. Baumgarten, Characterisation of microporous materials by dynamic sorption methods, in: Studies in Surface Science and Catalysis, 2000, pp. 633-638.
[212] D. Benczedi, I. Tomka, F. Escher, Thermodynamics of amorphous starch-water systems. 1. Volume fluctuations, Macromolecules, 31 (1998) 3055-3061.

[213] G. Dipaolabaranyi, J.E. Guillet, Estimation of Polymer Solubility Parameters by Gas-Chromatography, Macromolecules, 11 (1978) 228-235.
[214] M. Lu, F. Wang, Q. Liao, K. Chen, J. Qin, S. Pan, FTIR spectra and thermal properties of TiO2-doped iron phosphate glasses, Journal of Molecular Structure, 1081 (2015) 187-192.
[215] Y.M. Moustafa, K. El-Egili, Infrared spectra of sodium phosphate glasses, Journal of Non-Crystalline Solids, 240 (1998) 144-153.
[216] E.A. Abou Neel, W. Chrzanowski, S.P. Valappil, L.A. O'Dell, D.M. Pickup, M.E. Smith, R.J. Newport, J.C. Knowles, Doping of a high calcium oxide metaphosphate glass with titanium dioxide, Journal of Non-Crystalline Solids, 355 (2009) 991-1000.
[217] E.A. Abou Neel, W. Chrzanowski, D.M. Pickup, L.A. O'Dell, N.J. Mordan, R.J. Newport, M.E. Smith, J.C. Knowles, Structure and properties of strontium-doped phosphate-based glasses, Journal of the Royal Society Interface, 6 (2009) 435-446.
[218] C. Mercier, L. Montagne, H. Sfihi, G. Palavit, Surface alteration of zinc ultraphosphate glass in humid air at 140°C, Journal of Non-Crystalline Solids, 256–257 (1999) 124-129.
[219] I. Ahmed, M. Lewis, I. Olsen, J.C. Knowles, Phosphate glasses for tissue engineering: Part 1. Processing and characterisation of a ternary-based P2O5–CaO–Na2O glass system, Biomaterials, 25 (2004) 491-499.
[220] R.K. Brow, D.R. Tallant, J.J. Hudgens, S.W. Martin, A.D. Irwin, The short-range structure of sodium ultraphosphate glasses, Journal of Non-Crystalline Solids, 177 (1994) 221-228.
[221] A. Kiani, L.S. Cahill, E.A. Abou Neel, J.V. Hanna, M.E. Smith, J.C. Knowles, Physical properties and MAS-NMR studies of titanium phosphate-based glasses, Materials Chemistry and Physics, 120 (2010) 68-74.
[222] P. Hartmann, J. Vogel, B. Schnabel, The Influence of Short-Range Geometry on the 31P Chemical-Shift Tensor in Protonated . Phosphates, Journal of Magnetic Resonance, Series A, 111 (1994) 110-114.
[223] R.M. Wenslow, K.T. Mueller, Structural details of aqueous attack on a phosphate glass by H-1/P-31 cross-polarization NMR, Journal of Physical Chemistry B, 102 (1998) 9033-9038.
[224] J.J. Blaker, A. Bismarck, A.R. Boccaccini, A.M. Young, S.N. Nazhat, Premature degradation of poly(α-hydroxyesters) during thermal processing of Bioglass®-containing composites, Acta Biomaterialia, 6 (2010) 756-762.
[225] M. Navarro, M.-P. Ginebra, J. Clément, M. Salvador, A. Gloria, J.A. Planell, Physicochemical Degradation of Titania-Stabilized Soluble Phosphate Glasses for Medical Applications, Journal of the American Ceramic Society, 86 (2003) 1345-1352.
[226] M. Cerruti, G. Magnacca, V. Bolis, C. Morterra, Characterization of sol-gel bioglasses with the use of simple model systems: a surface-chemistry approach, Journal of Materials Chemistry, 13 (2003) 1279-1286.
[227] F.M. Ernsberger, Molecular Water in Glass, Journal of the American Ceramic Society, 60 (1977) 91-92.
[228] I. Ahmed, M.P. Lewis, S.N. Nazhat, J.C. Knowles, Quantification of anion and cation release from a range of ternary phosphate-based glasses with fixed 45 mol% P2O5, J Biomater Appl, 20 (2005) 65-80.
[229] C. Lin, C. Mao, Y.L. Li, J.J. Zhang, G.H. Miao, X.F. Chen, Structural properties and wound healing effect of the Sol-Gel bioactive glass on diabetic skin wounds, Wuji Cailiao Xuebao/Journal of Inorganic Materials, 28 (2013) 103-108.

[230] F. Baino, G. Novajra, V. Miguez-Pacheco, A.R. Boccaccini, C. Vitale-Brovarone, Bioactive glasses: Special applications outside the skeletal system, Journal of Non-Crystalline Solids, 432 (2016) 15-30.
[231] P. Balasubramanian, T. Büttner, V. Miguez Pacheco, A.R. Boccaccini, Boron-containing bioactive glasses in bone and soft tissue engineering, Journal of the European Ceramic Society, (2017).
[232] X. Liu, M.N. Rahaman, D.E. Day, In Vitro Degradation and Conversion of Melt-Derived Microfibrous Borate (13-93B3) Bioactive Glass Doped with Metal Ions, Journal of the American Ceramic Society, 97 (2014) 3501-3509.
[233] M. Diba, A.R. Boccaccini, Silver-containing bioactive glasses for tissue engineering applications, in: Precious Metals for Biomedical Applications, 2014, pp. 177-211.
[234] K.K.Y. Wong, S.O.F. Cheung, L.M. Huang, J. Niu, C. Tao, C.M. Ho, C.M. Che, P.K.H. Tam, Further Evidence of the Anti-inflammatory Effects of Silver Nanoparticles, Chemmedchem, 4 (2009) 1129-1135.
[235] K. Neibert, V. Gopishetty, A. Grigoryev, I. Tokarev, N. Al-Hajaj, J. Vorstenbosch, A. Philip, S. Minko, D. Maysinger, Wound-healing with mechanically robust and biodegradable hydrogel fibers loaded with silver nanoparticles, Adv Healthc Mater, 1 (2012) 621-630.
[236] K. Chaloupka, Y. Malam, A.M. Seifalian, Nanosilver as a new generation of nanoproduct in biomedical applications, Trends in Biotechnology, 28 (2010) 580-588.
[237] H. Wang, S. Zhao, X. Cui, Y. Pan, W. Huang, S. Ye, S. Luo, M.N. Rahaman, C. Zhang, D. Wang, Evaluation of three-dimensional silver-doped borate bioactive glass scaffolds for bone repair: Biodegradability, biocompatibility, and antibacterial activity, Journal of Materials Research, 30 (2015) 2722-2735.
[238] W. Xiao, S.H. Luo, X.J. Wei, C.Q. Zhang, W.H. Huang, J.K. Chen, Y. Cai, Y. Rui, M.N. Rahaman, Evaluation of Ti implants coated with Ag-containing borate bioactive glass for simultaneous eradication of infection and fracture fixation in a rabbit tibial model, Journal of Materials Research, 27 (2012) 3147-3156.
[239] L.G. Joyner, E.P. Barrett, R. Skold, The Determination of Pore Volume and Area Distributions in Porous Substances. II. Comparison between Nitrogen Isotherm and Mercury Porosimeter Methods, Journal of the American Chemical Society, 73 (1951) 3155-3158.
[240] V. Simon, C. Albon, S. Simon, Silver release from hydroxyapatite self-assembling calcium-phosphate glasses, Journal of Non-Crystalline Solids, 354 (2008) 1751-1755.
[241] J.R.J. Delben, O.M. Pimentel, M.B. Coelho, P.D. Candelorio, L.N. Furini, F.A. dos Santos, F.S. de Vicente, A.A.S.T. Delben, Synthesis and thermal properties of nanoparticles of bioactive glasses containing silver, Journal of Thermal Analysis and Calorimetry, 97 (2009) 433-436.
[242] A. Vulpoi, L. Baia, S. Simon, V. Simon, Silver effect on the structure of SiO2-CaO-P2O5 ternary system, Materials Science & Engineering C-Materials for Biological Applications, 32 (2012) 178-183.
[243] C. Gautam, A.K. Yadav, A.K. Singh, A Review on Infrared Spectroscopy of Borate Glasses with Effects of Different Additives, ISRN Ceramics, 2012 (2012) 17.
[244] R.L. Siqueira, O. Peitl, E.D. Zanotto, Gel-derived SiO2-CaO-Na2O-P2O5 bioactive powders: Synthesis and in vitro bioactivity, Materials Science & Engineering C-Materials for Biological Applications, 31 (2011) 983-991.
[245] A. Lucas-Girot, F.Z. Mezahi, M. Mami, H. Oudadesse, A. Harabi, M. Le Floch, Sol-gel synthesis of a new composition of bioactive glass in the quaternary system SiO2-CaO-Na2O-P2O5 Comparison with melting method, Journal of Non-Crystalline Solids, 357 (2011) 3322-3327.

[246] X. Chatzistavrou, E. Kontonasaki, A. Bakopoulou, A. Theocharidou, A. Sivropoulou, K.M. Paraskevopoulos, P. Koidis, A.R. Boccaccini, T. Kasuga, Development of new sol-gel derived Ag-doped biomaterials for dental applications, in: Materials Research Society Symposium Proceedings, 2012, pp. 41-46.
[247] Q.Z. Chen, Y.A. Li, L.Y. Jin, J.M.W. Quinn, P.A. Komesaroff, A new sol-gel process for producing Na2O-containing bioactive glass ceramics, Acta Biomaterialia, 6 (2010) 4143-4153.
[248] A.N. Cormack, The Structure of Bioactive Glasses and Their Surfaces, in: Bio-Glasses, John Wiley & Sons, Ltd, 2012, pp. 65-74.
[249] A. Tilocca, Structural models of bioactive glasses from molecular dynamics simulations, Proceedings of the Royal Society a-Mathematical Physical and Engineering Sciences, 465 (2009) 1003-1027.
[250] A. Tilocca, Structural models of bioactive glasses from molecular dynamics simulations, Proceedings of the Royal Society A: Mathematical, Physical and Engineering Science, 465 (2009) 1003-1027.
[251] W.K. Jung, H.C. Koo, K.W. Kim, S. Shin, S.H. Kim, Y.H. Park, Antibacterial activity and mechanism of action of the silver ion in Staphylococcus aureus and Escherichia coli, Applied and Environmental Microbiology, 74 (2008) 2171-2178.
[252] G. Zhao, M.L. Usui, S.I. Lippman, G.A. James, P.S. Stewart, P. Fleckman, J.E. Olerud, Biofilms and Inflammation in Chronic Wounds, Advances in Wound Care, 2 (2013) 389-399.
[253] W.K. Stadelmann, A.G. Digenis, G.R. Tobin, Physiology and healing dynamics of chronic cutaneous wounds, American Journal of Surgery, 176 (1998) 26s-38s.
[254] L. Ma, C. Gao, Z. Mao, J. Zhou, J. Shen, X. Hu, C. Han, Collagen/chitosan porous scaffolds with improved biostability for skin tissue engineering, Biomaterials, 24 (2003) 4833-4841.
[255] A.D. Metcalfe, M.W.J. Ferguson, Bioengineering skin using mechanisms of regeneration and repair, Biomaterials, 28 (2007) 5100-5113.
[256] I.D. Xynos, A.J. Edgar, L.D.K. Buttery, L.L. Hench, J.M. Polak, Ionic products of bioactive glass dissolution increase proliferation of human osteoblasts and induce insulin-like growth factor II mRNA expression and protein synthesis, Biochemical and Biophysical Research Communications, 276 (2000) 461-465.
[257] S.Q. Yang, Q.Y. Guo, L.S. Shores, A. Aly, M. Ramakrishnan, G.H. Kim, Q.Z. Lu, L.X. Su, J.H. Elisseeff, Use of a chondroitin sulfate bioadhesive to enhance integration of bioglass particles for repairing critical-size bone defects, Journal of Biomedical Materials Research Part A, 103 (2015) 235-242.
[258] P. Wray, Cotton candy' that heals? Borate glass nanofibers look promising, American Ceramic Society Bulletin, 90 (2011) 25-29.
[259] R. Serra, R. Grande, L. Butrico, A. Rossi, U.F. Settimio, B. Caroleo, B. Amato, L. Gallelli, S. de Franciscis, Chronic wound infections: the role of Pseudomonas aeruginosa and Staphylococcus aureus, Expert Review of Anti-Infective Therapy, 13 (2015) 605-613.
[260] P.L. Nadworny, J.F. Wang, E.E. Tredget, R.E. Burrell, Anti-inflammatory activity of nanocrystalline silver in a porcine contact dermatitis model, Nanomedicine-Nanotechnology Biology and Medicine, 4 (2008) 241-251.
[261] C. You, Q. Li, X. Wang, P. Wu, J.K. Ho, R. Jin, L. Zhang, H. Shao, C. Han, Silver nanoparticle loaded collagen/chitosan scaffolds promote wound healing via regulating fibroblast migration and macrophage activation, Scientific Reports, 7 (2017).

[262] J.P. Kaiser, M. Roesslein, L. Diener, A. Wichser, B. Nowack, P. Wick, Cytotoxic effects of nanosilver are highly dependent on the chloride concentration and the presence of organic compounds in the cell culture media, Journal of Nanobiotechnology, 15 (2017).
[263] H. Mikkelsen, R. McMullan, A. Filloux, The Pseudomonas aeruginosa Reference Strain PA14 Displays Increased Virulence Due to a Mutation in ladS, Plos One, 6 (2011).
[264] M. Gubler, T.J. Brunner, M. Zehnder, T. Waltimo, B. Sener, W.J. Stark, Do bioactive glasses convey a disinfecting mechanism beyond a mere increase in pH?, International Endodontic Journal, 41 (2008) 670-678.
[265] M. Zehnder, G. Baumgartner, K. Marquardt, F. Paque, Prevention of bacterial leakage through instrumented root canals by bioactive glass S53P4 and calcium hydroxide suspensions in vitro, Oral Surgery Oral Medicine Oral Pathology Oral Radiology and Endodontology, 103 (2007) 423-428.
[266] R.F. Brown, M.N. Rahaman, A.B. Dwilewicz, W. Huang, D.E. Day, Y. Li, B.S. Bal, Effect of borate glass composition on its conversion to hydroxyapatite and on the proliferation of MC3T3-E1 cells, Journal of Biomedical Materials Research Part A, 88a (2009) 392-400.
[267] A.M. Wojtowicz, S. Oliveira, M.W. Carlson, A. Zawadzka, C.F. Rousseau, D. Baksh, The importance of both fibroblasts and keratinocytes in a bilayered living cellular construct used in wound healing, Wound Repair and Regeneration, 22 (2014) 246-255.
[268] K. Park, H. Amano, S. Kashiwagi, M. Shibuya, M. Majima, A. Takeda, The Role of Vascular Endothelial Growth Factor Receptor 1 (Vegfr-1) Signalling in Wound Healing, Wound Repair and Regeneration, 24 (2016) A4-A4.
[269] P. Bao, A. Kodra, M. Tomic-Canic, M.S. Golinko, H.P. Ehrlich, H. Brem, The Role of Vascular Endothelial Growth Factor in Wound Healing, Journal of Surgical Research, 153 (2009) 347-358.
[270] S. Barrientos, O. Stojadinovic, M.S. Golinko, H. Brem, M. Tomic-Canic, Growth factors and cytokines in wound healing, Wound Repair and Regeneration, 16 (2008) 585-601.
[271] T. Kokubo, H. Takadama, How useful is SBF in predicting in vivo bone bioactivity?, Biomaterials, 27 (2006) 2907-2915.
[272] J.R. Jones, D.S. Brauer, L. Hupa, D.C. Greenspan, Bioglass and Bioactive Glasses and Their Impact on Healthcare, International Journal of Applied Glass Science, 7 (2016) 423-434.
[273] J. Boateng, O. Catanzano, Advanced Therapeutic Dressings for Effective Wound Healing--A Review, J Pharm Sci, 104 (2015) 3653-3680.
[274] R. Jayakumar, M. Prabaharan, P.T.S. Kumar, S.V. Nair, H. Tamura, Biomaterials based on chitin and chitosan in wound dressing applications, Biotechnology Advances, 29 (2011) 322-337.
[275] V.J. Reddy, S. Radhakrishnan, R. Ravichandran, S. Mukherjee, R. Balamurugan, S. Sundarrajan, S. Ramakrishna, Nanofibrous structured biomimetic strategies for skin tissue regeneration, Wound Repair and Regeneration, 21 (2013) 1-16.
[276] J.S. Choi, K.W. Leong, H.S. Yoo, In vivo wound healing of diabetic ulcers using electrospun nanofibers immobilized with human epidermal growth factor (EGF), Biomaterials, 29 (2008) 587-596.
[277] C.L. Dai, Y. Yuan, C.S. Liu, J. Wei, H. Hong, X.S. Li, X.H. Pan, Degradable, antibacterial silver exchanged mesoporous silica spheres for hemorrhage control, Biomaterials, 30 (2009) 5364-5375.
[278] A.K. Barui, V. Veeriah, S. Mukherjee, J. Manna, A.K. Patel, S. Patra, K. Pal, S. Murali, R.K. Rana, S. Chatterjee, C.R. Patra, Zinc oxide nanoflowers make new blood vessels, Nanoscale, 4 (2012) 7861-7869.

[279] L.C. Gerhardt, K.L. Widdows, M.M. Erol, A. Nandakumar, I.S. Roqan, T. Ansari, A.R. Boccaccini, Neocellularization and neovascularization of nanosized bioactive glass-coated decellularized trabecular bone scaffolds, J Biomed Mater Res A, 101 (2013) 827-841.
[280] P.L. Nadworny, J. Wang, E.E. Tredget, R.E. Burrell, Anti-inflammatory activity of nanocrystalline silver in a porcine contact dermatitis model, Nanomedicine, 4 (2008) 241-251.
[281] R.M. Day, A.R. Boccaccini, Effect of particulate bioactive glasses on human macrophages and monocytes in vitro, Journal of Biomedical Materials Research Part A, 73a (2005) 73-79.
[282] H. Li, J. He, H. Yu, C.R. Green, J. Chang, Bioglass promotes wound healing by affecting gap junction connexin 43 mediated endothelial cell behavior, Biomaterials, 84 (2016) 64-75.
[283] N. Lindfors, J. Geurts, L. Drago, J.J. Arts, V. Juutilainen, P. Hyvonen, A.J. Suda, A. Domenico, S. Artiaco, C. Alizadeh, A. Brychcy, J. Bialecki, C.L. Romano, Erratum to: Antibacterial Bioactive Glass, S53P4, for Chronic Bone Infections - A Multinational Study, Adv Exp Med Biol, (2017).
[284] A.A.M.a.R.A.A. Naimi, Role of hydroxyapatite in healing of experimentally induced cutaneous wound in rabbits, Journal of Veterinary Science, 5 (2012) 74-81.
[285] A.K. Miri, N. Muja, N.O. Kamranpour, W.C. Lepry, A.R. Boccaccini, S.A. Clarke, S.N. Nazhat, Ectopic bone formation in rapidly fabricated acellular injectable dense collagen-Bioglass hybrid scaffolds via gel aspiration-ejection, Biomaterials, 85 (2016) 128-141.
[286] Y. Gu, W. Huang, M.N. Rahaman, In vivo evaluation of scaffolds with a grid-like microstructure composed of a mixture of silicate (13-93) and borate (13-93B3) bioactive glasses, in: Ceramic Engineering and Science Proceedings, 2014, pp. 53-64.
[287] L. Bi, B. Zobell, X. Liu, M.N. Rahaman, L.F. Bonewald, Healing of critical-size segmental defects in rat femora using strong porous bioactive glass scaffolds, Materials Science and Engineering C, 42 (2014) 816-824.
[288] Y. Yuan, T.R. Lee, Contact angle and wetting properties, in: Surface science techniques, Springer, 2013, pp. 3-34.
[289] P.G. Bowler, B.I. Duerden, D.G. Armstrong, Wound microbiology and associated approaches to wound management, Clin Microbiol Rev, 14 (2001) 244-269.
[290] V.C. Modglin, R.F. Brown, S.B. Jung, D.E. Day, Cytotoxicity assessment of modified bioactive glasses with MLO-A5 osteogenic cells in vitro, Journal of Materials Science: Materials in Medicine, 24 (2013) 1191-1199.
[291] R.F. Brown, M.N. Rahaman, A.B. Dwilewicz, W. Huang, D.E. Day, Y. Li, B.S. Bal, Effect of borate glass composition on its conversion to hydroxyapatite and on the proliferation of MC3T3-E1 cells, Journal of Biomedical Materials Research Part A, 88 (2008) 392-400.
[292] M.D. O'Donnell, S.J. Watts, R.V. Law, R.G. Hill, Effect of P2O5 content in two series of soda lime phosphosilicate glasses on structure and properties – Part I: NMR, Journal of Non-Crystalline Solids, 354 (2008) 3554-3560.
[293] G. Kaur, G. Pickrell, N. Sriranganathan, V. Kumar, D. Homa, Review and the state of the art: Sol–gel and melt quenched bioactive glasses for tissue engineering, Journal of Biomedical Materials Research Part B: Applied Biomaterials, (2015).